Bitopic Ligands and their molecular fragments for the study of the M1 Muscarinic Receptor

Bitopische Liganden und ihre Molekülfragmente für die Untersuchung des M1 Muskarinischer Rezeptor

Doctoral thesis for a doctoral degree

at the Graduate School of Life Sciences,

Julius-Maximilians-Universität Würzburg,

Section Infection and Immunity

submitted by

Daniela Volpato
from
Milan

Würzburg 2021

Submitted on: ……..……..

Members of the *Promotionskomitee*:

Chairperson: Prof. Dr. Christoph Sotriffer

Primary Supervisor: Prof. Dr. Ulrike Holzgrabe

Supervisor (Second): Prof. Dr. Carsten Hoffmann

Supervisor (Third): Prof. Dr. Marco De Amici

Supervisor (Fourth): …….

(If applicable)

Date of Public Defence: ……..……

Date of Receipt of Certificates: ……..

Acknowledgments

The experimental part of this work was carried out between December 2014 and December 2018 under the supervision of Prof. Dr. Ulrike Holzgrabe at the Institute of Pharmacy and Food Chemistry, Julius Maximilians Universität Würzburg. This thesis was founded by Elite Network of Bavaria within the framework of the International Graduate Program “Receptor Dynamics: Emerging Paradigms for Novel Drugs” and was supported by the Graduate School of Life Science.

I would like to thank my supervisor Professor Ulrike Holzgrabe for giving me the opportunity to work in her research group and gave me such an interesting project to explore and the admission of the “Receptor Dynamics: Emerging Paradigms for Novel Drugs” International Program. I thank her for the supervision that he provided me during my period in her department and for her help in my scientific development.

I would like to express my since gratitude

to Professor Marco De Amici from the University of Milan who introduced me to the interesting research topic, for the cooperation and for his contributions to a successful doctoral study;

to Professor Carsten Hoffmann from the University of Jena and Dr. Micheal Kauk for the cooperation in this research project;

to thank Professor Lohse from Max-Delbrück-Centrum für Molekulare Medizin for accommodating me in his group during my research stay and for the successfull collaboration. I had a wonderful and inspiring time in his group;

to Dr. Andreas Bock from Max-Delbrück-Centrum für Molekulare Medizin for introducing me to the binding experiments, which completed my research. I am very grateful for the exciting insights and explanations in his field of research and for the incredible final help in concluding my PhD project;

to Professor Gerhard Wolber and Dr. Marcel Bermudez from the Freie Universität in Berlin for the molecular docking of the target compounds, which essentially contributed to the quality of my project;

to Professor Dr. Christoph Sotriffer and Natalia Yuan Chen from the University of Würzburg for the nice collaboration and contribution with docking studies on the Cholinesterase inhibitors;

to Dr. Clelia DallaNoce and to the exchange students from the University of Milan Davide Cirillo, Marco Maspero and Alessandro Mussida for the enthusiasm, the sucesfull collaboration and contibutions to the projects;

to Professor Armin Buschauer and especially to Dr. Timo Littmann from the University of Regensburg who shared the split luciferase complementation assay with our research group and for the excellent technical assistance and the patient explenations of assay;

to Dr. Valerie Jahns, Claudia Schütz and Nadine Groß for the incredibly great help in establishing the IP-one accumulation assay and for a nice welcome in their lab.

I would like to thank all the colleagues and friends for the good cooperation, the great working atmosphere and of course for the time we had together: Alessandro, Alex, Andi, Anja, Anna, Antonio, Christiane, Christine E. , Christine H., David, Davide, Edgar, Florian, Jogi, Klaus, Lu, Marco, Markus, Michi, Miri, Niclas, Nils, Nina, Olli, Patrick , Paul, Raphael, Maike, Stoyan, Melli, Diego, Simon, Luca, Sandra, Jonas and Jonas, Joshua, Linda, Simon und Andreas, Matthias, Paul, Rasmus, Kerstin, Theresa, Selma, Katarina, Joseph, Patrick, Lina, Lieselotte Möhler and Christine Ebner from the secretariat, Georg Walter, Matthias Völker and Karl Vollmuth from the technical service team and Curd, Jens and Lu. All the members of the Elite Network of Bavaria.

Finally, I would like to thank my family, Stefano and my friends for the immense support that they gave me during these years abroad. This wouldn’t have been possible without your love and encouragement.

Index

A. Introduction

The past decades have witnessed the development of new pharmaceutical compounds that modulate receptor function by targeting allosteric sites. Allosteric sites are, by definition, domains topographically distinct from the orthosteric binding pocket[1] where the natural ligand binds. Exploring the possibilities of linking orthosteric and allosteric pharmacophores in one compound to yield 'bitopic' compounds[2,3] is a strategy derived from the "message-address" concept by Schwyzer[4], first applied to GPCRs by Portoghese et al.[5] This concept explicitly underlines the orthosteric/allosteric combination, in opposite to the more general umbrella term bivalent. The broad possibilities of bitopic ligands in the pharmaceutical field are under continuous study. Bitopic compounds are promising pharmaceutical tools for taking advantage of the allosteric binding to achieve subtype selectivity while preserving high affinity at the receptor. The development of bitopic ligands, based on the idea of combining high affinity (via orthosteric sites) with high selectivity (via allosteric sites), have led to the development of highly selective bivalent ligands for GPCRs[6], such as for the opioid receptors[7–9], muscarinic acetylcholine receptors (mAChRs) [10–13], serotonin receptors[14,15], cannabinoid receptors[16], and gonadotropin-releasing hormone receptors[17]. This concept has even been extended to other receptors, for examples nicotinic receptors[18–21] and other proteins, such as acetylcholinesterases[22,23] and the tyrosine kinase receptors TrkA[24] and TrkC[16].

The reasons to pursue a bitopic ligand approach are various. An improved affinity for the target GPCR and/or an improved selectivity either at the level of receptor subtype, or at the level of signaling pathway. Another advantage of bitopic ligands over purely allosteric ligands is that the former rely on the appropriate presence of endogenous agonist tone to mediate their effects, whereas a bitopic ligand would engage the orthosteric site irrespective of the presence or absence of endogenous tone[25].

By way of introduction to the hybrid approach, a review of the concept of hybrids compounds targeting the cholinergic system is presented in section A of this thesis. Recent updates in hybrid molecule design as a strategy for selectively addressing multiple target proteins involved in Alzheimer's disease (AD) is here reported[26]. This represents the potential and the growing interest in hybrid compound as pharmacological tools to achieve receptor subtype selectivity and/or, to study the overall functional

activity of the receptor. Until now, muscarinic acetylcholine receptors (mAChRs) have proved to be a particularly fruitful receptor model for the development and characterization of bitopic ligands.

In this thesis, several examples of new muscarinic bitopic approach are reported in the results section. A study of bipharmacophoric ligands composed of the muscarinic positive allosteric modulators (BQCA-derived compounds) linked with chain of various lengths to different orthosteric building blocks[27] is reported in the result part 1. Synthesis and examination of the potential pharmacological characteristic of Oxotremorine-BQCAd compounds and Xanomeline-BQCAd hybrid derivatives are described in results parts 2 and 4, respectively. Moreover, the bitopic concept has even been extended to other proteins, such as acetylcholinesterase. In the result part 5 an overview of the new Tacrine-Xanomeline hybrids[22] aiming to improve the inhibitory potency of the acetylcholinesterase and simultaneously to increase the cholinergic tone, via the xanomelinic portion acting on the M1 receptor is given. A new trivalent approach is presented for the first time to deepen the study of the M1 muscarinic receptor in the result part 6. Moreover, the synthesis of a new series of iperoxo-derived alkane, bis(ammonio)alkane-type and rigidified chain ligands is given in the result part 7 together with some prospects for further research.

The results of the thesis are summarized in English and German in section E and F.

Review

Designing hybrids targeting the Cholinergic system by Modulating the muscarinic and Nicotinic receptors: A Concept to treat Alzheimer's Disease

Daniela Volpato [1], Ulrike Holzgrabe [1,*]

[1] Department of Pharmaceutical and Medicinal Chemistry, Institute of Pharmacy, University of Würzburg, Am Hubland, 97074 Würzburg, Germany
* Correspondence: ulrike.holzgrabe@uni-wuerzburg.de; Tel.: +49-931-31-85460

Received: 22 November 2018; Accepted: 5 December 2018; Published: 7 December 2018.

Abstract: The cholinergic hypothesis has been reported first being the cause of memory dysfunction in the Alzheimer's disease. Researchers around the globe have focused their attention on understanding the mechanisms of how this complicated system contributes to processes such as learning, memory, disorientation, linguistic problems, and behavioral issues in the indicated chronic neurodegenerative disease. The present review reports recent updates in hybrid molecule design as a strategy for selectively addressing multiple target proteins involved in Alzheimer's disease (AD) and the study of their therapeutic relevance. The rationale and the design of the bifunctional compounds will be discussed in order to understand their potential as tools to investigate the role of the cholinergic system in AD.

Keywords: AChE inhibitor; Alzheimer's disease; bitopic ligand; Cholinergic system; hybrid molecules; muscarinic receptors; nicotinic receptors.

---

1. Introduction

Alzheimer's disease (AD) is the most common form of dementia among geriatric people since the beginning of the 21st century. In 2016, over 47.5 million people around the world suffered from dementia. The World Health Organization hypothesizes that the number may rise to 75.6 million by 2030. The clinical condition of AD is characterized by a progressive loss of memory and other intellectual abilities

up to serious levels where the daily life is severely affected [28]. Of note, no definitive cause and no known cure have been found yet.

The characteristic features of the neurodegenerative decline include a decrease in levels of acetylcholine (ACh) followed by dysfunction and eventual death of cholinergic neurons. Furthermore, soluble β-amyloid oligomers (sAβ), β-amyloid fibrils (fAβ) misfolding and aggregation as well as formation of tau protein tangles in the nervous tissue of brain occur as a result of tau-protein hyperphosphorylation[28–30]. Water-soluble Aβ aggregates, detected in human brain lysates from AD patients, were found to be more toxic than their insoluble fibrillar counterparts by Li et al. [31]. Several other co-factors were hypothesized, such as oxidative stress and heavy metal dyshomeostasis[32].

Etiologic evidence exists between AD, cholinergic, and glutamatergic neurochemical systems. ACh is a crucial neurotransmitter responsible for mental and learning abilities. In AD patients, a dramatic decrease in cholinergic innervation in the cortex and the hippocampus is related to the loss of neurons in the basal forebrain [33]. Presynaptic cholinergic dysfunctions, loss of the cholinergic neural network, and overactivation of acetylcholinesterase (AChE), which leads to weakened neurotransmission, support the cholinergic hypothesis of the disease. This assumption suggests that cholinergic restoration therapy could be useful for alleviating the cognitive symptoms[34]. Another neurochemical hypothesis is mediated by *N*-methyl-D-aspartate (NMDA). Glutamate is an excitatory neurotransmitter for NMDA receptors which are essential in cognitive processes. However, in addition to the physiological stimulation, glutamate receptors cause neuronal damage due to excitotoxicity under certain circumstances[35].

The conventional pharmacotherapy of AD makes use of compounds which inhibit the enzyme AChE (donepezil, rivastigmine, and galantamine) in order to increase the levels of acetylcholine in the nervous tissue of the brain ((1-3), Figure 1). However, these compounds can improve the cognitive deficits of the disease only for a couple of months before losing activity. The shortness of the effect could be due to a decrease of the AChE itself in the relevant regions of the brain [36]. Later in time, another drug was introduced for the treatment of AD, i.e. memantine ((4), Figure 1) being a glutamatergic antagonist which protects nerve tissue against glutamate-mediated excitotoxicity. Unfortunately, both classes of drugs only provide a symptomatic relief without preventing the progression of the disease, a fact which is not

surprising given the intricacy of the pathology. Thus, there is a desperate need to find selective and powerful drugs to improve the treatment of AD[28].

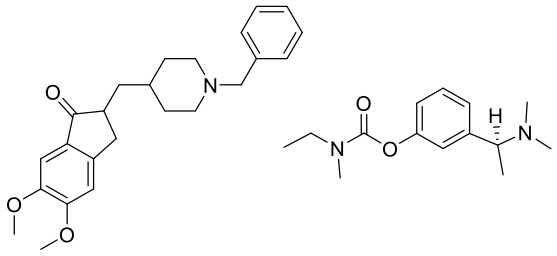

Donepezil **(1)** Rivastigmine **(2)**

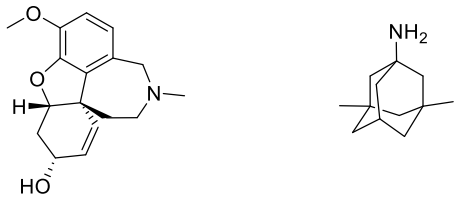

Galantamine **(3)** Memantine **(4)**

Figure 1. Structures of donepezil, rivastigmine, galantamine and memantine.

So far, developing new leading compounds with a lower risk-to-benefit ratio where benefits clearly overcome the side effects has not been accomplished yet due to the complexity and incomplete understanding of the pathophysiological processes in AD. Progress through clinical trials is limited by poor selectivity of candidate molecules and a lack of knowledge of the exact role of proteins considered as crucial targets. To combat this complex multifactorial disease, the challenge is to discover which and how many biological targets have to be modulated by developing powerful and selective drugs. Hence, the idea of creating hybrid molecules containing two discrete recognition units linked through a spacer, resulting in the so-called hybridization approach, is followed. A supplemental molecular segment next to the first standard pharmacophore could serve to address different molecular targets or distinct domains of the same protein. In addition to traditional methods, various modern drug discovery approaches must be investigated in parallel and complementarily to bring new hopes in this therapeutic field. The resulting hybrid molecules can serve as tools for opening new interesting perspectives in medicinal chemistry with more promising therapeutic opportunities to fight AD (for discussions on the further potential of the multifunctional approach see ref. 10).[37]

2. The cholinergic hypothesis of memory dysfunction

The substantial loss of presynaptic cholinergic neurons in human postmortem Alzheimer's-diseased brains, the dysfunction of cholinergic markers such as ACh, choline, and choline acetyl transferase (ChAT, an enzyme responsible for ACh production) as well as the consequent loss of cognitive skills and the mental improvement observed in patients upon artificial restoration of cholinergic activity unequivocally confirm the validity of the cholinergic hypothesis in AD[29]. Acetylcholine receptors (AChRs) propagate the cognitive ability and consist of two primary members namely muscarinic (mAChRs) and nicotinic receptors (nAChRs). While mAChRs are G-protein coupled receptors (GPCRs), nAChRs are ligand gated ion channels. After release, ACh is hydrolyzed to choline and acetate in the synaptic cleft by two cholinesterases, i.e. the AChE and the butyrylcholinesterase (BChE) (see Figure 2). Over the course of the disease, the concentration of AChE decreases by 85%, whereas high levels of BChE were found to influence the aggregation of Aβ, the main component of the amyloid plaques found in the brains of Alzheimer patients[38,39]. Furthermore, synaptic dysfunction and neuronal cell death *in vitro* [40–43] as well as impaired behavioral performance in animal models[44–46] seem to be directly correlated with sAβ aggregates [47]. For this reason, mAChRs, nAChRs, as well as the hydrolases AChE and BChE are important targets in the treatment of AD[48–50].

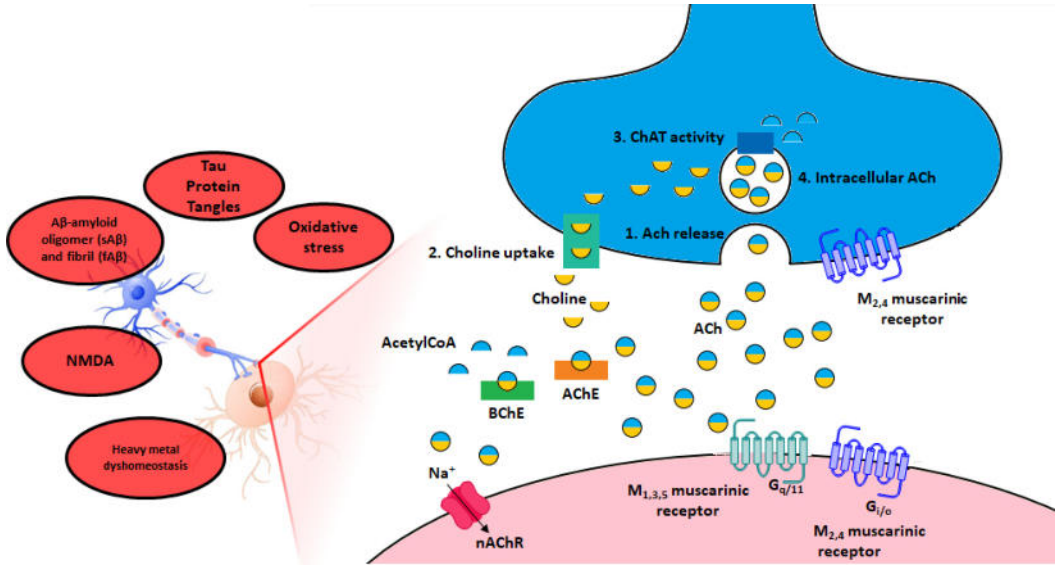

Figure 2. In the red circles some hallmarks of Alzheimer's disease are reported, the cholinergic hypothesis is emphasized through the schematic representation of a pre and postsynaptic neuron. Zoom in on the cholinergic synapse in particular biosynthesis, storage, release, hydrolysis of ACh and AChR locations are illustrated (modified from Auld et al. [51]).

3. Hybrid compounds as drug discovery tools in AD

Due to the absolute relevance of the cholinergic system in AD it may be desirable to address the involved cholinergic receptors and enzymes simultaneously by means of a multi-target strategy and/or selectively through a dualsteric approach. This can be realized by addressing different binding pockets of the same protein's surface with one hybrid molecule or different proteins involved in the same pathology. “Bivalent ligand” and “hybrid” are the general terms defining compounds which are composed of two functional pharmacophores linked by a spacer[52].

3.1. One single molecule - Different targets

Because of the multifactorial dimension of AD and the difficulty to apply the classical “one target - one disease” concept [53], the multitarget compounds approach has often been considered in recent years[54]. In this review, only hybrids intended to activate the cholinergic system will be described. The advantages of the multipotent strategy are obvious, but it remains absolutely challenging. In fact, molecular hybridization involves integration of the structure-activity relationships of two individual chemical species into a single molecular entity which should result in a balance of potency, efficacy, and selectivity for all the targets. The new hybrids can be designed with different degrees of pharmacophore overlapping, with linking or merging techniques, and using distinct connection positions of the active moieties. Furthermore, the combination of several pharmacophoric units usually results in large molecules which have limits in terms of molecular weight, lipophilicity, permeability of membranes, and hydrogen bonds acceptance and donation[54]. The technique lends itself well to address the cholinergic system in AD by concomitant inhibition of AChE and direct muscarinic and nicotinic activation.

3.2. One single molecule - Different binding pockets of a protein's surface

As already mentioned, the hybridization strategy can be used to obtain molecules containing two pharmacophoric entities able to bind topographically different binding sites of the same target protein, e.g. the endogenous orthosteric site and the allosteric one. Allosterism, first defined to describe the modification of any enzyme activity by the binding of ligands to sites that were different from the substrate-binding site itself [55], is widely explored for GPCRs, representing the largest class of drug targets in the human genome[52]. It provides the great opportunity of selectively affecting one GPCR subtype and simultaneously avoiding the problem of targeting the structurally conserved orthosteric

binding site[56]. Novel drugs targeting GPCRs do not enter the market as frequent as expected due to unwanted off-target effects resulting from the lack of selectivity within a distinct receptor family [57].

3.2.1. Allosteric modulation

GPCRs constitute a superfamily of integral membrane proteins characterized by seven transmembrane domains being connected by three extracellular (EL) and intracellular (IL) loops[58]. Allosteric modulators do not bind to the orthosteric binding site but act at a distinct binding site (i.e., an allosteric site) to either potentiate or inhibit activation of the receptor by its endogenous ligand[59]. An innovative perspective in drug development takes advantage of allosteric binding sites which usually altered between the different receptor subtype throughout the evolutionary processes. Conformational changes of the receptor upon allosteric ligand binding can modify the activity of an orthosteric agent in terms of the binding affinity and/or the downstream efficacy. This means emphasizing signals to some pathways over others among the various possible combinations which are associated with receptor activation, a phenomenon known as bias signaling (cf. Figure 3)[60,61].

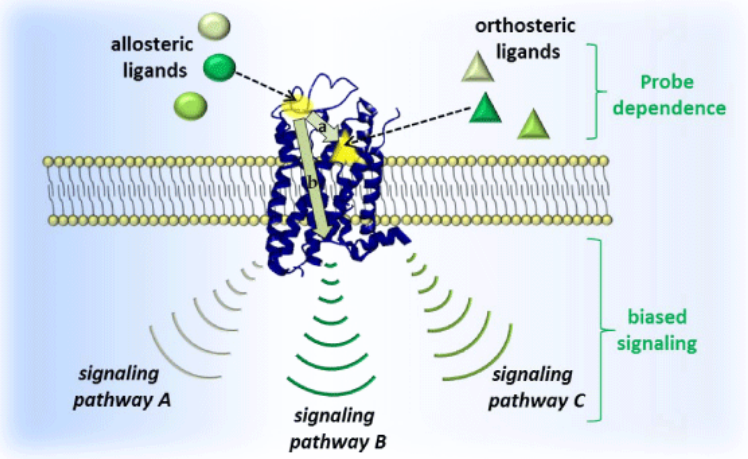

Figure 3. Schematic of GPCR signal transduction: allosteric modulators (spheres) bind to a topographically different site (yellow sphere) than the orthosteric site (yellow triangle) which hosts an orthosteric ligand (triangles). Reproduced with permission from[62].

Besides subtype selectivity, allosteric modulators offer the advantage of saturable effects. Since most of them lack agonistic activity, they can perfectly “fine-tune” any orthosteric ligand activity to a ceiling level above which no further modulation occurs; this means they can be administered with higher doses and lower propensity to toxicity compared to classic agonists or antagonists[52].

Since the discovery of allosterism, several theories were postulated in order to identify and quantify this phenomenon: Ehlert's ternary complex model is one of the most significant methods describing how two distinct ligands, orthosteric and allosteric, may influence the binding and functioning of each other [63]. The cooperativity level, indicated by the cooperativity factor α, distinguishes between positive and negative allosteric modulators (PAMs and NAMs) and neutral allosteric ligands (NALs). It is important to keep in mind that the obtained cooperativity is always referred to a single allosteric modulator for a specific orthosteric probe and that an accurate interpretation of a combination of functional and binding assays is necessary to understand the actual kind of modulation. Probe dependency and cooperativity reveal a new level of subtype selectivity rather than affinity, a phenomenon which was termed “absolute subtype selectivity”. For example, the binding of ACh is selectively enhanced at the M4 muscarinic receptor by thiochrome binding to the allosteric site, even though this allosteric modulator shows almost equal affinity for all muscarinic subtypes[64].

A particular beneficial therapeutic meaning may be associated with allosteric agonist compounds which differ from pure allosteric modulators. They are able to directly activate a receptor by binding to an allosteric binding site even in the absence of an orthosteric ligand. These allosteric agonists might be more suitable for the treatment of AD, either because of the reduced endogenous tone of neurotransmitters or even their complete lack[65].

3.2.2. Bitopic ligand principle

The structural diversity among the extracellular vestibules allowed an innovative medicinal chemistry strategy for the design of novel ligands, i.e. hybrid compounds. They are characterized by chemical fragments which allow an interaction with both orthosteric and allosteric recognition sites.

Merging the best of both allosteric and orthosteric worlds in one ligand launches the bitopic or dualsteric compounds[2,3], a strategy derived from the “message-address” concept by Schwyzer[4] which was first applied to GPCRs by Portoghese et al.[5]. This concept explicitly underlines the orthosteric/allosteric combination, in opposite to the more general umbrella term bivalent [52]. The orthosteric interaction provides high affinity binding and activation/inhibition of a receptor (message), whereas the allosteric

interaction yields receptor subtype-selectivity (address) and may modulate both efficacy and intracellular signaling pathway activation[66].

In fact, the transduction pathway of GPCRs include a large set of intracellular signaling proteins like different G proteins, GRKs (protein coupled receptor kinase), and arrestins[67]. Such hybrid molecules would allow to selectively identify therapeutically relevant signaling pathways, attenuate harmful signals, or selectively block the ability of the agonist to produce unselective signals resulting in side effects[68]. The recent functional screening of biased ligands using multiple assay formats suggest that the phenomenon represents an existing and relevant therapeutic opportunity for the treatment of different disorders[66]. The dualsteric principle was validated through numerous bitopic ligands examples:

Iper-6-phth ((**5a-C6**), Figure 4) and iper-6-naph ((**5b-C6**), Figure 4) are derived from the M2 allosteric hexamethonium compounds W84 and naphmethonium (NAM regarding orthosteric agonists) linked with the non-selective orthosteric superagonist iperoxo. The dualsteric compounds possess relatively good selectivity for the M2 receptor regarding potency and affinity. Agonistic activation and unexpected selectivity in the intracellular G protein pathway were observed: activation of G_i signaling at the expense of the G_s.

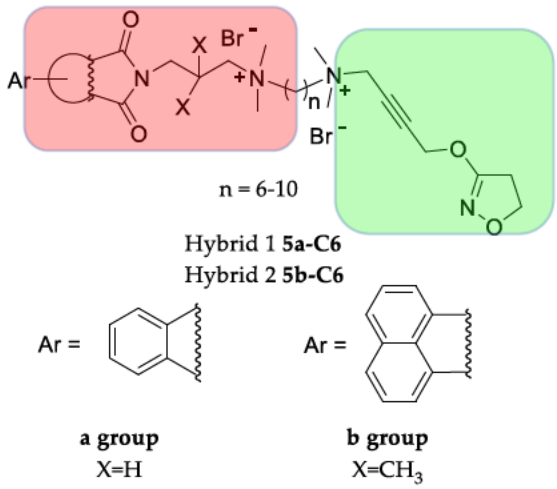

Figure 4. Structures of bitopic hybrids. **5a-C6,5b-C6** M2 muscarinic hybrid. Green: orthosteric building block, red: allosteric building block.

Starting from the structure of the M2 preferring antagonist DIBA ((**6**), Figure 5), the homo-dimeric dibenzodiazepinone derivatives UNSW-MK250 ((**7**), Figure 5) and UNSW-MK262 ((**8**), Figure 5) as well

as the heterodimeric UR-SK75 ((**9**), Figure 5) compounds were prepared. All molecules exhibited high M2 receptor affinities and were capable of retarding [3H]NMS dissociation, indicating an allosteric interaction[69]. Saturation binding experiments in the presence of M2 allosteric modulators and some radiolabeled dibenzodiazepinone compounds highlighted a competitive mechanism suggesting a dualsteric binding mode[70,71].

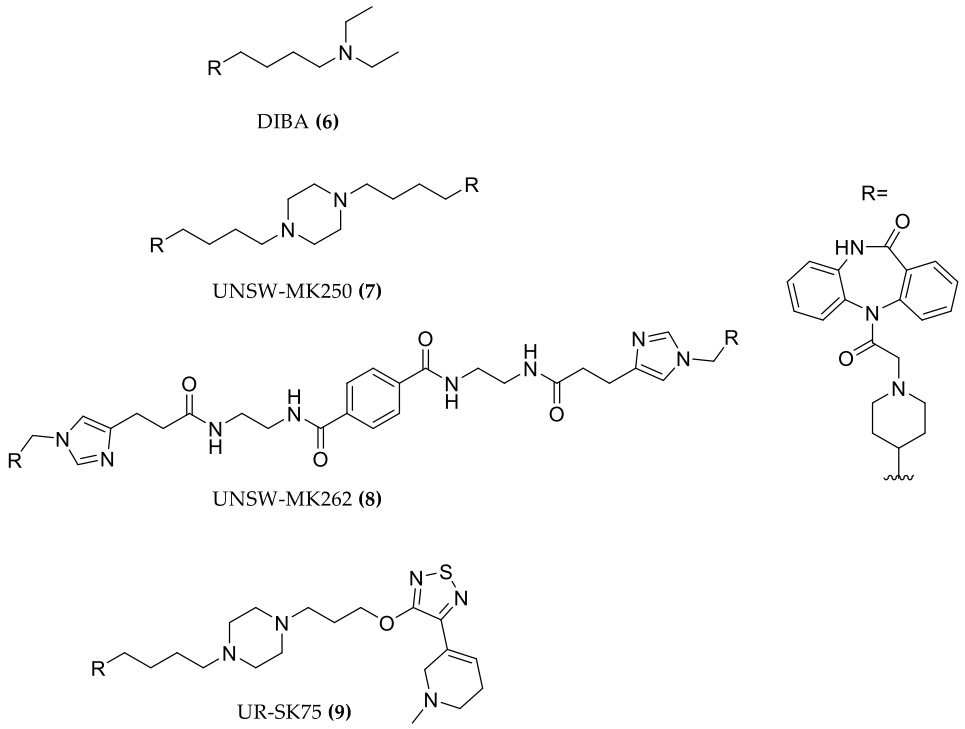

Figure 5. Structures of homo-hetero dimeric dibenzodiazepinone M2 derivatives.

Extending the approach to other GPCRs includes the adenosine A1 receptor with the dualsteric ligands LUF6258, VCP746 and VCP171 ((**10**, **11**), Figure 6; VCP171, structure not disclosed). An orthosteric adenosine agonist was connected through an alkyl chain linker to a PAM of the PD81,723 type. The resulting bitopic ligands were evaluated pharmacologically in radioligand displacement studies suggesting a dualsteric receptor interaction of LUF6258[72]. VCP746 was subsequently developed by Valant et al.[73] by inclusion of the PAM (2-amino-4-(2-(trifluoromethyl)phenyl)thiophen-3-yl)(phenyl)-methanone) in the dualsteric structure. The bitopic ligand **11** was found to induce significant biased cellular signaling in favor of cytoprotection and to the detriment of bradycardia side effects.

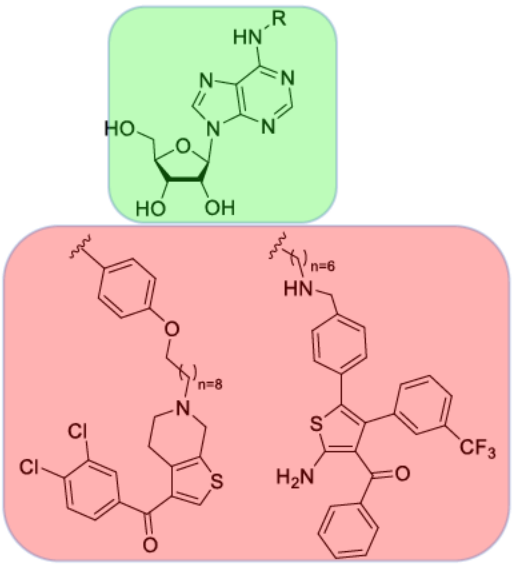

Figure 6. Structures of bitopic ligands **10**, **11** at A1 adenosine receptor. Green: orthosteric building block, red: allosteric building block.

The compound THR-160209 ((**12**), Figure 7) was obtained by Steinfeld et al. [74] by connection of an orthosteric 3-benzylhydrylpyrrolinyl building block to an allosteric 4-aminobenzylpiperidine motif using a heptane chain. A significant increase in affinity was noted for the bitopic ligand (**12**), exhibiting a certain preference for the M2 AChR compared with its orthosteric or allosteric fragments[52,58].

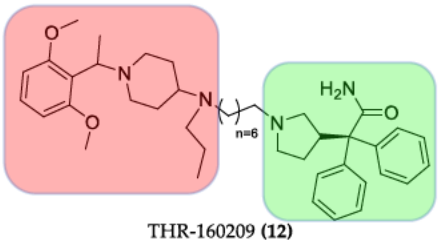

Figure 7. Structures of bitopic hybrids.**12** M2 acetylcholine receptor antagonist. Green: orthosteric building block, red: allosteric building block.

The dopamine D2-like receptor is object of research as drug target for neuropsychiatric disorders. The bitopic mode of action with D2 and D3 receptors was demonstrated for the dopaminergic ligand SB269652 ((**13**), Figure 8). Only a few years after its publication by Stemp et al.[75,76], SB269652 was described as an atypical bitopic ligand. It behaves like a competitive antagonist with receptor monomers

and allosterically across receptor dimers by changing the ability of ligands to bind the orthosteric binding pocket on the other protomer of the dimer [77,78].

A new and potent bitopic sphingosine-1-phosphate subtype 3 receptor (S1P3) antagonist, SPM-354 ((**15**), Figure 8), with *in vivo* activity was a useful tool to define the spatial and functional properties of S1P3 in regulating cardiac conduction. SPM-354 can compete with both the allosteric S1P3 selective agonist CYM-5541 as well as the orthosteric agonist S1P, showing bitopic properties. SPM-354, a 2-propyl derivative of the previously described SPM242, was chosen for *in vivo* studies ((**14**) Figure 8) because of its improved potency and *in vivo* efficacy[79,80].

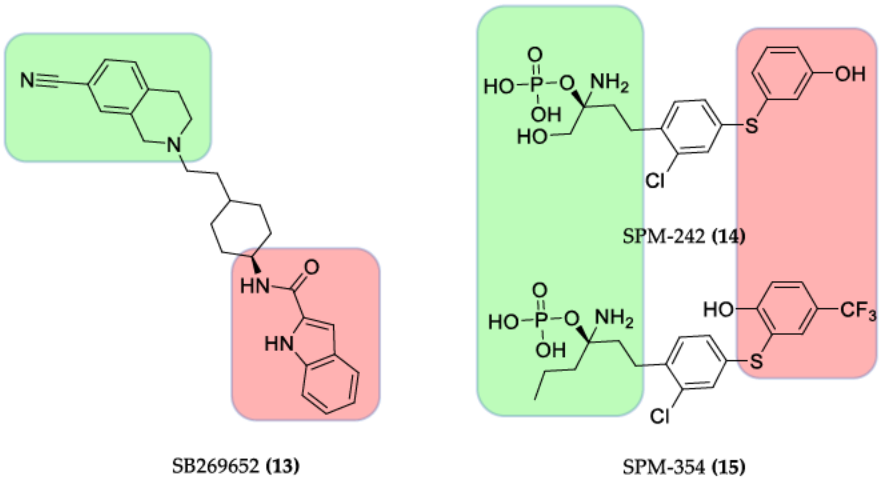

Figure 8. Structures of bitopic hybrids. **13** D3 dopaminergic ligand SB269652; **14**, **15** bitopic S1P3 antagonist. Orthosteric building block in green allosteric building block in red.

All these examples illustrate that this principle is applicable across the GPCR landscape. Additionally, thanks to the progress in understanding dualsteric ligands, several ligands which were thought to be allosteric modulators were re-classified later as dualsteric ligands (e.g. 77-LH-28-1 and AC-42 at M1 receptor described below see par. 4.1.4). Hence, one can be optimistic that in the future, more dualsteric ligands at different GPCRs will be discovered and designed using rational structure-based drug discovery.

3.2.3. Hybrid Strategies Design

Both orthosteric and allosteric fragments and the linker play an important role in the interaction with the target protein, thus an optimization process considering these moieties is indispensable. Both pharmacophores have to be enhanced separately in a kind of fragment-based design approach, investigating the chemical environment of the two binding pockets. However, one should remember that the binding of one pharmacophore is influencing the binding of the other moiety. For example, it is possible that upon binding of the ligand the receptor goes through conformational changes causing negative cooperativity for the complementary moiety. Therefore, it is difficult to predict the pharmacological outcome of such bitopic molecules. Furthermore, the linker must fit perfectly, allowing the allosteric and orthosteric fragments to reach their target pockets. Length, flexibility, connection position, and chemical characteristics of the linker play a fundamental role in the bitopic interaction.

Bitopic ligands range from the first combination of agonist-NAM (e.g. iperoxo-6-phth)[81] to agonist-PAM (e.g. iperoxo-BQCAd)[72,73,82,83] and antagonist-NAM (e.g. atr-6-naph)[84] for the M2 and M1 muscarinic receptors. All possible combinations easily widen the spectrum of opportunities.

Alternative approaches may also include the use of bitopic ligands to study the low-affinity and transient binding sites which are defined as metastable sites[85]. Several research groups have hypothesized the existence of such a binding site at the entrance of the receptor to which ligands bind transiently [86–91]. If an energetically favorable conformation change of the complex ligand-receptor occurs, the ligand continues its path down to the orthosteric site whereas otherwise, its route is prevented through dissociation. This metastable site acts as a selectivity filter: access is denied to molecules that do not have the required physico-chemical characteristics for the binding site. Metastable binding sites offer new receptor sections that can be explored, opening new strategic opportunities in the field of bitopic ligands.

Since several GPCRs are organized in dimeric or oligomeric complexes, respectively, bivalent ligands intended to target an allosteric and orthosteric binding sites or even two orthosteric sites of two different protomers in a receptor dimer. This will constitute a new design prospective. Rather than promoting a ligand-induced dimerization, the bivalent ligands tend to stabilize the pre-existing dimers. Unique pharmacological properties including receptor selectivity could be achieved as bivalent ligands are able to bridge different receptor units. Heterodimers can be highly selective compounds targeting only those

tissues in which both receptors are co-expressed. Apart from the opioid receptor field, the potential of these ligands has been poorly explored up to now[7].

The bitopic approach used for the first time in 2006 by De Amici et al.[92] on the M2 muscarinic receptor was recently extended in the research field of AD on M1 receptor.

4. Muscarinic receptor

The muscarinic receptors are involved in diverse functions throughout the body with particular focus on the bladder, gastrointestinal tract, eye, heart, brain, and salivary glands[93]. Physiologically, these functions are activated and deactivated selectively thanks to the specific tissue distribution of receptors and the existence of five different receptor subtypes (M1-M5). The M1-type muscarinic AChRs, predominantly expressed in the hippocampus and cerebral cortex, play a central role in cognitive processing, memory, and learning. Since structure and density of these AChRs remain almost unchanged in the disease state, the M1 receptor is considered a very promising target to increase the cholinergic tone[94].

Highly subtype selective drugs are needed in order to avoid side effects originating from unwanted receptor activation or inhibition[65]. A number of M1 muscarinic agonists was developed to treat AD. These are promising agents as they display significant neurotrophic effect, decrease β-amyloid plaque deposition, and improve oxidative stress-induced damage. Several compounds have shown an efficacy on the M1 as a therapeutic target for the AD as they not only enhance the cholinergic functions but can also shift the APP (amyloid precursor protein) processing towards the nonamyloidogenic pathway through activation of protein kinase C, the metalloproteinase domain 17 (ADAM17), and a disintegrin[30]. Activation of M1 muscarinic receptors attenuates tau hyperphosphorylation via glycogen synthase kinase-3b (GSK-3b) inhibition, reduces β amyloid peptide levels, and increases ERK activation and potentiation of NMDA receptors[65,95,96].

Considerable efforts were made to obtain agonists for M1 but their off-target effects preclude the therapeutic use. Various agonists for M1 muscarinic receptor including arecoline ((**16**), Figure 9) CI-1017 ((**17**), Figure 9), xanomeline ((**18**), Figure 9), tazomeline ((**19**), Figure 9), talsaclidine ((**20**), Figure 9) and milameline ((**21**), Figure 9) do not show sufficient selectivity for the M1 subtype. The most prominent candidates in the past few years were the M1 muscarinic agonists AF102B ((**22**), Figure 9)

(cevimeline; approved in the USA and Japan for Sjogren's Syndrome and having excellent pharmacokinetic properties), AF150(S) ((**23**), Figure 9) and AF267B ((**24**), Figure 9) which additionally show a significant neurotrophic effect, inhibit Aβ and oxidative stress induced cell death as well as apoptosis in PC12 cells transfected with the M1 muscarinic receptor [32,97].

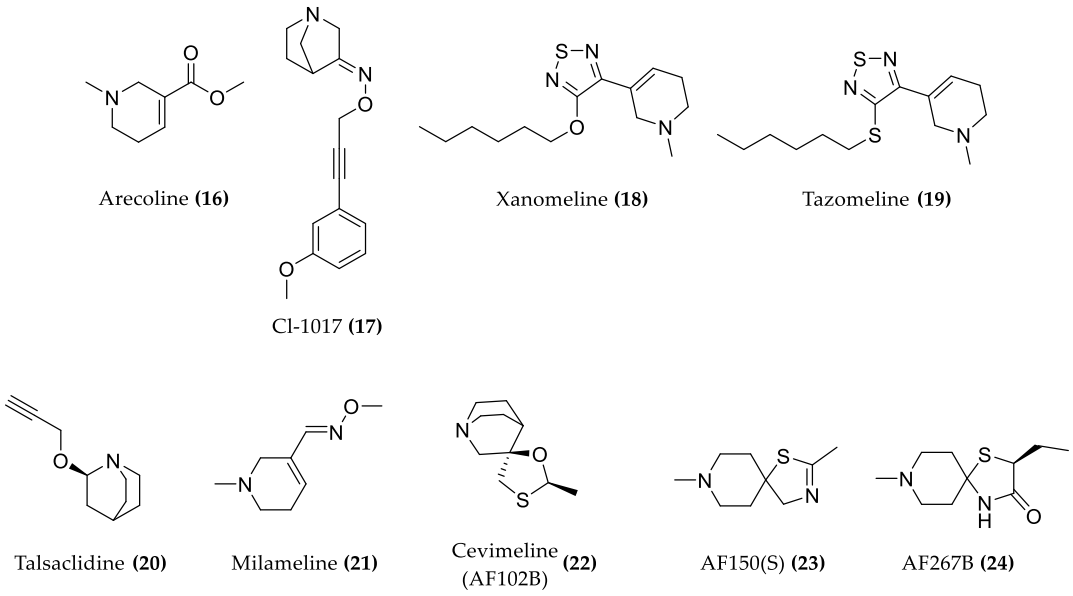

Figure 9. Structures of moderately active and selective orthosteric M1 agonists.

Furthermore, the M1 selective agonist lead candidates VU0364572 ((**25**), Figure 10) and VU0357017 ((**26**), Figure 10) were tested on cell lines as well as animal models and exhibited encouraging as well as effective properties on various parameters. The compound VU0357017 not only showed excellent M1 subtype selectivity but also a good blood brain barrier (BBB) penetration and *in vivo* efficacy[65]. EVP-6124 (enceniclin) ((**27**), Figure 10) was the last cholinergic receptor agonist which entered phase 3 trials but it was withdrawn due to severe gastrointestinal adverse effects[30].

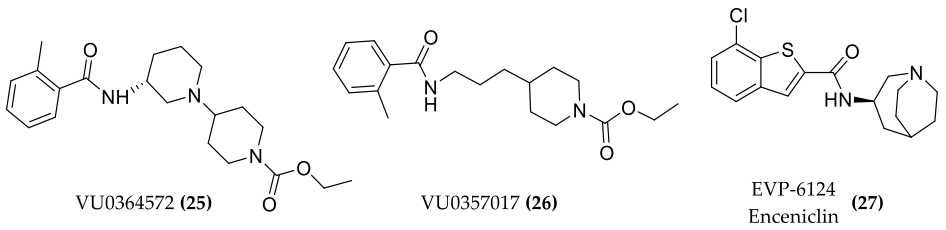

Figure 10. Structures of M1 lead candidates

Some highly M1-selective allosteric agonists must also be mentioned here which do not require an orthoster bound to the receptor for activation. For example, the TBPB allosteric agonist ((**28**), Figure 11) interacts with slightly different binding domains of the M1 receptor which are all adjacent to the orthosteric site. LuAE51090 ((**29**), Figure 11) displayed a high degree of selectivity when tested in a broad panel of GPCRs, ion channels, transporters, and enzymes, and showed an acceptable pharmacokinetic profile and BBB penetration properties *in vivo*[98]. Compound **30** (Figure 11) was identified by high throughput screening (HTS) and virtual screening at GlaxoSmithKline, unraveling a molecule with improved binding and pharmacokinetic parameters. For **30**, good M1 agonist potency, intrinsic activity, and subtype selectivity for M1 are reported[99,100].

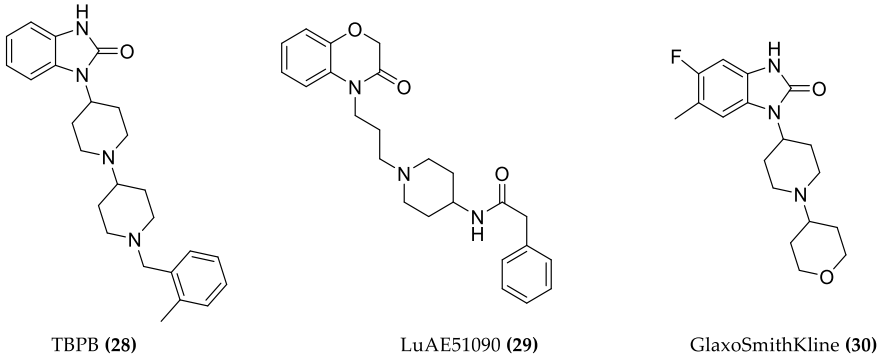

Figure 11. Structures of M1 allosteric agonists

Both the comparison of the allosteric agonists among each other and even with M1-PAMs reveals structural similarities. They all consist of an heterobicycle system with at least one nitrogen atom and a carbonyl group close to the nitrogen. Furthermore, the heterocycle is connected to piperidine rings which are linked to another cyclic moiety.

4.1. Design of hybrid compounds to investigate the muscarinic receptor

The allosterically less conserved site of the mAChR which is located in the extracellular vestibule (ECV) and separated from the orthosteric pocket by a tyrosine lid[101] lends itself well as binding site for new dualsteric ligands. The close proximity of the orthosteric and the allosteric subdomains, a typical feature of the Class A GPCRs, allows the dualsteric compounds to simultaneously interact with the two binding sites.

The chemical space between the orthosteric and allosteric portions of the M2 receptor was investigated thanks to the pharmacological analysis of Iper-8-naph ((**5b-C8**), Figure 4) [102,103], McN-A-343 ((**31**), Figure 12), and its fragments and analogues[104].

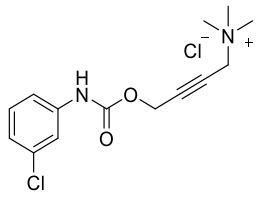

McN-A-343 **(31)**

Figure 12. Structures of McN-A-343

The long-known partial agonist McN-A-343 interacts with the allosteric EL2 vestibule through its 3-chlorphenylcarbamate. The binding to the orthosteric sites is guaranteed by the tetramethylammonium cation. The two parts are linked via a rigid butynyl chain. However, this molecule is probably too small to entirely occupy the allosteric pocket and thereby achieves no subtype selectivity. It binds to both M2 and M4 receptors[58].

Iper-8-naph is a partial agonist at the M2 receptor. The partial agonism of most of the dualsteric agonists depends on both the dualsteric binding mode itself and on the dynamic equilibrium of multiple inactive and active states, i.e. the ligand binding ensemble. In the “dualsteric binding mode”, iperoxo is bound to the orthosteric pocket while the allosteric naphthalimide moiety protrudes towards the extracellular part of the receptor. This pose is responsible for a functionally selective activation of the G proteins and cellular signaling[103,105]. In the alternative pose, which is a “purely allosteric binding mode”, the entire bitopic ligand (both the orthosteric and the allosteric moieties) is in the allosteric vestibule. In this case, the inactive receptor conformation is stabilized. It would be difficult to pharmacologically distinguish the “flip-flop” mechanism from a ligand with a purely bitopic binding mode. In case of the iperoxo-dualsteric derivatives at the M2R, the bitopic mode of interaction was validated by the following experiments: radioligand binding analysis, in wild-type and mutant receptors, and downstream signaling assays in addition to receptor docking simulations[61]. Partial agonism is the direct consequence of this dynamic balance. Measuring the partial agonism depends on the affinity of the two pharmacophores and of the dualsteric ligand itself for the respective binding sites[57].

4.1.1. BQCAd hybrid derivatives

The same approach was applied for exploring the M1 receptor binding pockets. Among several selective M1 allosteric modulators known, the promising group of *N*-benzyl quinolone carboxylic acids (BQCAs) was selected as positive allosteric moieties of these dualsteric M1 hybrids[82,83]. The BQCA allosteric modulator ((**32a**), Figure 13) was first described by the Merck laboratory. The compound is a positive allosteric modulator, an allosteric agonist, and exhibits pure subtype selectivity for the M1 receptor: no agonism, antagonism, nor potentiation activity was observed at other mAChRs up to 100 μM. The concentration of ACh which needed to activate the receptor decreased up to 129-fold in the presence of BQCA and an inflection point of 845 nM is reported in the presence of 3 nM ACh. Its allosteric modulation is mediated by the interaction with the residues Y179 and W400, suggesting the binding of BQCA to the "common" allosteric site[106,107]. As an orthosteric fragment, the non-selective superagonist iperoxo ((**33**), Figure 13)[82] and the endogenous ligand ACh were linked to the BQCA derivative (BQCAd ((**32b**), Figure 13))[83]. The two parts were connected by alkylene chains of different lengths (C4, C6, C8, C10) ((**34a, b, c, d**), Figure 13).

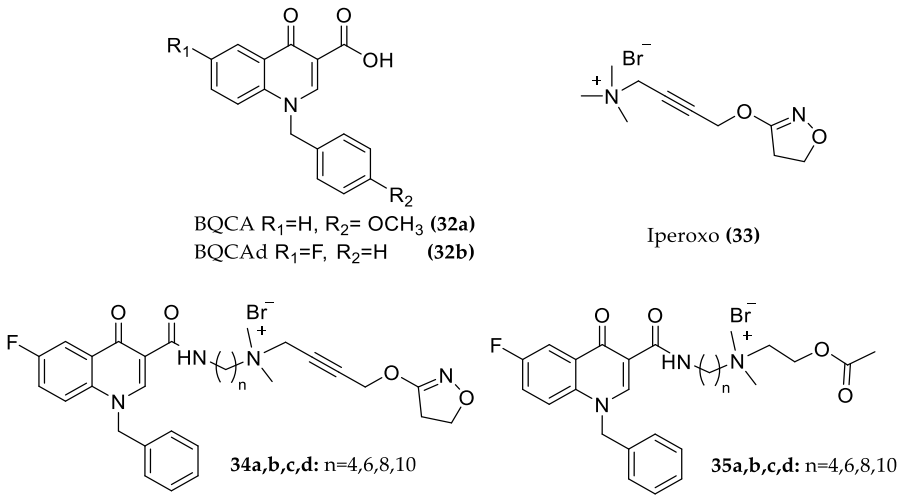

Figure 13. Structures of BQCAd/Iperoxo-ACh hybrids

The compounds showed

[1] subtype selectivity: receptor activation and signaling pathway studies performed with (dynamic mass redistribution) DMR in the presence and absence of specific G_i and G_q signaling blockers indicate a preferentially Gq mediated signal of the hybrids.

[2] partial agonism which may provide controlled activation without overdriving the M1 signaling and with possible improved side effect profile over the control of cognition[108].

[3] potency and efficacy dependency on the length of the chain and on the substitution pattern of the allosteric fragment. Elongating the chain from C4 to C6 switches the receptor fractional occupancy from the inactive, purely allosteric pose to the active binding pose which defines the efficacy of the dualsteric ligands[109].

The interaction of these compounds with the M1 muscarinic receptor was further investigated by Fluorescence Resonance Energy Transfer (FRET) measurements in a living cell system for a closer understanding of the receptor movement. Here, some other ligands were added to the hybrid series including longer chained (C8, C10) compounds and ACh hybrids ((**35a,b,c,d**)**,** Figure 13)[83]. The optimal linker length for the activation of the receptor was confirmed to be a C6 chain, e.g. in the case of iperoxo-C6-BQCA with a maximal detected signal of about 24% compared to 100 µM of the iperoxo reference. Surprisingly, a new receptor conformation was observed: a FRET signal with opposite direction to the typical agonist signal occurred for the longer chain hybrids. How this unknown receptor activation process at a molecular level is connected with the bitopic compound interaction mode, the different G-protein activation, β-arrestin recruitment, or further downstream signaling must be investigated to completely understand this unexpected M1 receptor arrangement. The distinct receptor movement that occurs upon binding of dualster ligands may help to illuminate the interplay between G proteins and β-arrestins preferentially coupling to different receptor conformations[110]. Particularly within the M1 pharmacology, functionally selective properties can be exploited to characterize which signaling outcomes would address neuropsychiatric illnesses [12]. Of note, replacing the flexible alkyl chain with a rigid alkynylbenzene linker (**(36)**, Figure 14) leads to a delayed FRET signal, indicating slower receptor

kinetics. The compound with a flexible chain of corresponding length afforded a sharper FRET signal, indicating the responsibility of the rigidification in the kinetic modification [83,111].

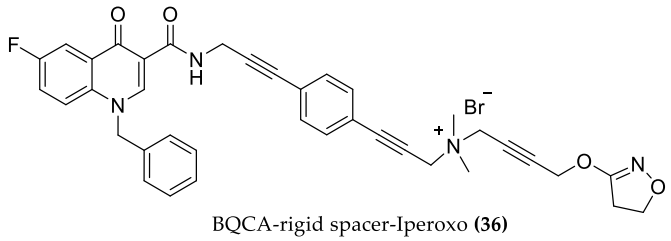

BQCA-rigid spacer-Iperoxo **(36)**

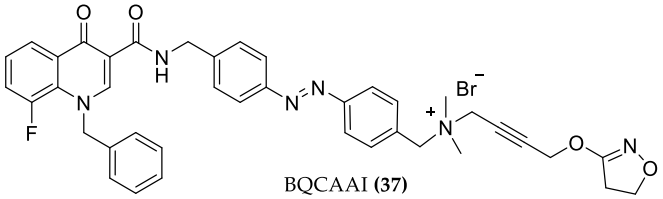

BQCAAI **(37)**

Figure 14. Structures of BQCAd/Iperoxo hybrids connected by a rigid linker and a photo-switchable moiety

Probably, a cation-π interaction between the three tyrosines Y104$^{3.33}$, Y403$^{6.51}$ and Y426$^{7.39}$ of the so-called tyrosine lid with the rigid linker contributes to the delayed FRET signal. (Remodeling of the tyrosine lid. in figure 15).

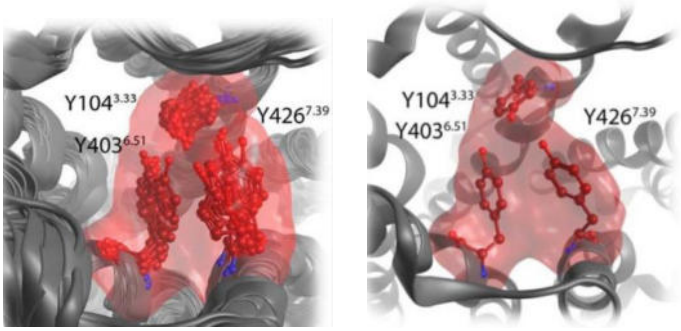

Figure 15. Left: top view snapshots from a molecular dynamics simulation of the iperoxo-bound crystal structure unveil the conformational flexibility of the tyrosine lid, especially Tyr-426$^{7.39}$. Right: based on the sampling of side chain conformations, the tyrosine lid was remodeled for binding mode investigations on dualsteric agonist. Reproduced with permission from [105].

A further step in the study of M1 activation processes was performed with the synthesis and pharmacological investigation of the first new photo-switchable dualsteric ligand. Agnetta et al. [111]

designed a pharmacological tool in which the photochromic azobenzene moiety was inserted as a spacer in the hybrid compound. Regarding the time course of M1 activation, compound **37** was found to be as slow as with the rigid compound, underlining the fundamental role of the chain structure of the dualsteric hybrids in the M1 receptor kinetic. More interestingly, with the BQCAAI ((**37**), Figure 14) compound, the drastic influence of the iperoxo-BQCA hybrid geometry on the activity of the compound was demonstrated. A simple light-induced isomerization from the *cis* to the less stable *trans* BQCAAI isomer turns the antagonist compound into an agonist.

4.1.2. LY593093

Another allo/ortho partial agonist hybrid was designed at Eli Lilly: LY593093 ((**38**), Figure 16). The molecule displaced the [^{3}H]NMS antagonist from M1 muscarinic receptor (pK_i of 6.21) without any effect on [^{3}H]NMS binding at the M3-M5AChR and stimulating β-arrestin recruitment. Additionally, LY593093 had no modulatory role in potentiating ACh functional activity and the binding was not affected by an increasing concentration of the PAM BQCA, indicating that the interaction between LY593093 and M1AChR is different from the interaction of the receptor with the endogenous ligand ACh. High subtype selectivity is achieved through multiple points of binding pocket interactions which was shown in the docking model [108]. Binding was also observed for the M2 receptor, but in terms of functional activity the Eli Lilly compound is 5 and 120 times more potent on M1 AChR than on other muscarinic receptor subtypes and shows an E_{max} at least 2-fold higher [112]. Progression through clinical trials was however interrupted due to its modest brain penetration.

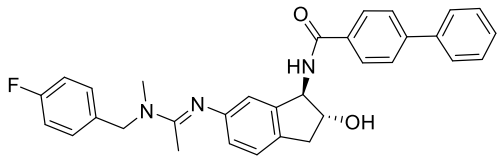

LY593090 **(38)**

Figure 16. Structure of LY593093

4.1.3. AC-42 and AC-260584

The allosteric and orthosteric mode of action was also demonstrated by means of a combination of functional and binding assays for the AC-42 compound ((**39**), Figure 17). The compound slows down the dissociation of [^{3}H]NMS from the M1 muscarinic receptor, indicating its allosteric capabilities;

moreover, in equilibrium binding studies, AC-42 almost completely inhibits the binding of the [^{3}H]NMS orthosteric probe and, in the functional test IP1, the antagonist atropine decreases the potency of the ligand in a concentration-dependent manner. Later findings indicated an additional orthosteric binding pose of the ligand [29,113,114]. AC-42, unlike oxo-M, arecoline, and pilocarpine, is unable to promote M1-$G_{\alpha i1/2}$ protein coupling, proving the ability of bitopic ligands to activate different down streaming effectors [115]. AC-260584 ((**40**), Figure 17), the orally bioavailable and structurally related compound with greater potency and efficacy than AC-42, was initially defined as an allosteric agonist. Mutation of amino acids in the TM3 of the M1 receptor (ACh binding site) affects the binding of the compound and hence supports the hypothesis of the bitopic behavior [116].

4.1.4. 77-LH-28-1

77-LH-28-1 ((**41**), Figure 17), a close structural analogue of AC-42, was initially described as an allosteric agonist. However, it might have a bitopic binding mode because the antagonist scopolamine is able to shift its dose-response curve rightward indicating an orthosteric binding mode. Further evidence supporting this theory is the competition at the NMS-occupied receptor with a prototypical muscarinic negative allosteric bis-quaternary phthalimidopropyl modulator (heptane- 1,7-bis(dimethyl-3'-phthalimidopropylammonium bromide, abbreviated as C7/3-phth) [113].

77-LH-28-1 was, however, used as an allosteric fragment of the bitopic hybrids synthesized by Piergentili et al. [12] The compounds containing xanomeline as orthosteric fragment were pharmacologically investigated as described below (See par. 5.1.4).

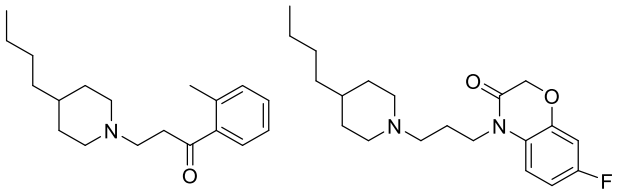

Figure 17. Structures of AC-42, AC-260584 and 77-LH-28-1

5. Acetylcholinesterase (AChE)

The decreasing cholinergic tone is one of the physiological reasons of the debilitating AD. To switch off a cholinergic signal, ACh is catabolized by the acetylcholinesterase (AChE) which hydrolyzes the ester of the neurotransmitter to acetic acid and choline. The enzyme also appears to be involved in the aggregation of Aβ by a peripheral anionic site (PAS) in addition to its classical enzymatic hydrolysis of ACh [117,118]. AChE inhibitors compensate the cholinergic tone in the synaptic transmission and thus, because of an augmenting ACh concentration, usually relieve the symptoms and can decrease the rate of cognitive decline for some months. However, they are not able to arrest disease progression and inexorable neurodegeneration [54]. Already in 1991, Sussman et al. described the enzyme as a narrow cavity that drives the substrate through a peripheral anionic site (PAS) to the catalytic site (CAS), where the catalytic triad Glu-His-Ser is located [119]. (Figure 18).

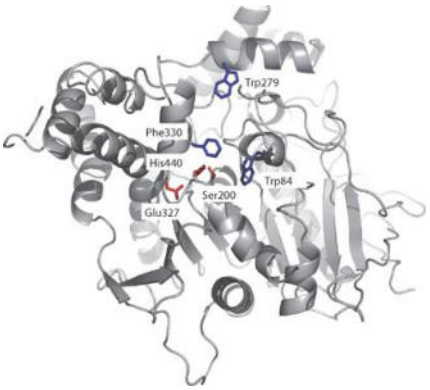

Figure 18. 3D structure of native *torpedo californica* AChE. The catalytic triad in red, Trp84 in the CAS, Trp279 at the PAS, and the bottleneck residue Phe330 in blue. Reproduced with permission from [120].

The knowledge of the active site and of the exact function of each amino acid of the catalytic triad allowed the discovery of enzymatic inhibitors. The AChE inhibitors (AChEIs) donepezil, galantamine, rivastigmine ((**1-3**), Figure 1), and tacrine ((**42**), Figure 19) were successfully developed and approved by international authorities. Later, tacrine was withdrawn from the market due to a significant hepatic toxicity.

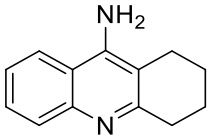

Tacrine **(42)**

Figure 19. Structure of tacrine

These compounds inhibit the enzyme differently: several ligands, e.g. galantamine, covalently bind to the serine residue and form a bond that is stable for about 15-20 minutes; during this time, the enzyme is inhibited. Tacrine blocks the passage of the neurotransmitter due to a strong π-stacking interaction with Trp84 (Figure 20)[121].

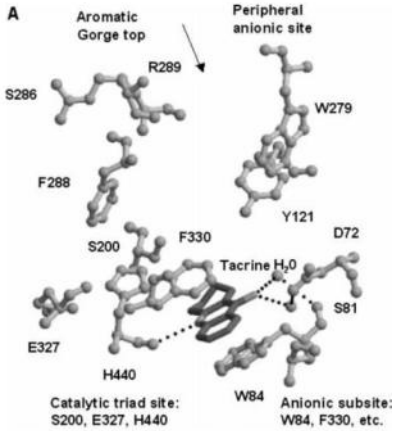

Figure 20. Overlay of the trigonal crystal structure of tacrine (black) and Tc AChE (gray) complex: showing the catalytic anionic site, aromatic gorge, and peripheral anionic site. Reproduced with permission from[121].

Rivastigmine is a pseudo-irreversible arylcarbamate inhibitor of both AChE and BChE. Clinical studies comparing the effect of the two approved drugs donepezil (only AChE inhibition) and rivastigmine (AChE and BChE inhibition) revealed an additional benefit in daily living, global function, and behavior for rivastigmine in patients with wild-type BuChE allele due to the dual inhibition of AChE and BChE [122–124]. Anyway, the use of AChEIs for AD is considered a suboptimal therapy and is still under discussion [125]. This review will not give details about all AChEIs because they were already summarized excellently in ref. 105-108 [126–129].

5.1. Design of hybrid compounds inhibiting the cholinesterase

5.1.1. Tacrine hybrids

In order to investigate the potency of tacrine for the inhibition of AChE with simultaneously reduced hepatotoxicity, tacrine was intensively used for the development of hybrid molecules. Pang et al. found a bis-C7-tacrine homodimer ((**43-C7**), Figure 21) exhibiting a 1000-fold higher AChE inhibitory potency in rats than the monomer, indicating the absence of steric interaction problems in the narrow cavity preceding the catalytic site of the enzyme. The tacrine dimers are able to establish interactions with both the catalytic and the peripheral site. A shorter tether (< 5 methylene units) hampers the simultaneous binding to both interaction sites of AChE (dual-site binding). In addition, the lipophilicity of the hybrid was found to be increased compared to tacrine itself[130,131].

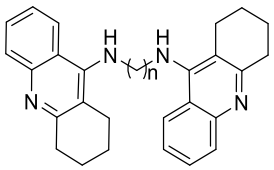

(43) n=7,9

Figure 21. Bis tacrine homodimers

5.1.2. Tacrine/Iperoxo hybrids

Some bitopic ligands combining the M2 allosteric structure of the allosteric modulator W84 and naphmethonium and the non-selective superagonist iperoxo, rationally developed as M2 subtype-selective ligands ((**5a,b**-**C7,8,9,10**), Figure 4), were tested for the inhibitory activity of the AChE and found to have modest activity. The potency is influenced by the length of the linker chain connecting the orthosteric and allosteric sites. The longest chains result in a higher activity: the decamethylene chain seems to span the AChE binding gorge, allowing the quaternary ammonium head of iperoxo to be localized in the PAS region. Compounds containing the naphthalimide portion ((**5b-C7,8,9,10**), Figure 4) show stronger inhibition than those containing the phthalimide part ((**5a-C7,8,9,10**), Figure 4). When replacing the iperoxo moiety with an isoxazole ring, almost no AChE/BuChE inhibition was observed ((**44-C4,6,8**), Figure 22; Tab. 1)[102].

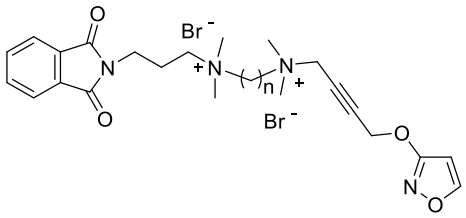

(44) n=4,6,8

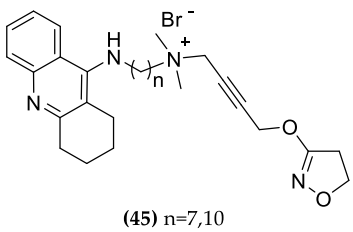

(45) n=7,10

Figure 22. AChE inhibitor/ mAchR agonist compounds

Table 1. Cholinesterase activity and cytotoxicity of the M2 bitopic compounds and tacrine hybrids. BChE from equine serum, AChE from electric eel.[131]

Compound	BChE pIC_{50} [M]	AChE pIC_{50} [M]	Cytotoxicity HEP G2 IC_{50} [µM]
Tacrine (**42**)	8.57	7.60	111 (±2.28)
Phth-7-iper (**5a-C7**)	5.19	4.83	n.d. [1]
Phth-8-iper (**5a-C8**)	5.13	4.89	n.d. [1]
Phth-9-iper (**5a-C9**)	4.88	4.80	n.d. [1]
Phth-10-iper (**5a-C10**)	5.37	5.26	n.d. [1]
Naph-7-iper (**5b-C7**)	6.69	6.04	n.d. [1]
Naph-8-iper (**5b-C8**)	6.46	6.10	n.d. [1]
Naph-9-iper (**5b-C9**)	6.49	6.44	n.d. [1]
Naph-10-iper (**5b-C10**)	6.99	6.50	n.d. [1]
Tac-7-Tac (**43-C7**)	9.14	10.48	<1.38 (±0.08)
Tac-10-Tac (**43-C10**)	9.34	9.00	<1.25 (±0.00)
Phth-4-isoxo (**44-C4**)	4.07	19.12% inhib. at 100 µM	n.d. [1]
Phth-6-isoxo (**44-C6**)	4.41	32.91% inhib. at 100 µM	n.d. [1]
Phtal-8-isoxo (**44-C8**)	5.10	4.17	n.d. [1]
Tac-7-iper (**45-C7**)	8.29	8.76	>160 (±0.00)
Tac-10-iper (**45-C10**)	8.75	9.81	32.2 (±0.41)

[1] n.d.: not determined.

Starting from this finding, new hybrids with multitarget potential ((**45**), Figure 22) were synthesized consisting of a tacrine and an iperoxo moiety, aiming at higher inhibitory activity for the AChE and BChE [132]. The idea was to combine the iperoxo affinity for the M1 and M2 receptor with the AChE inhibitory activity. Tacrine can serve as both an allosteric modulator for M receptor and as inhibitor of AChE [133–135]. In particular, Tac-10-iper ((**45-C10**), Figure 22) was an extremely potent inhibitor with an IC_{50} value of 9.81 (AChE from electric eel; tacrine IC_{50} 7.60) and 8.75 (BChE from equine serum; tacrine IC_{50} 8.57) which is even better than tacrine itself. Moreover, it shows less cytotoxicity.

Docking studies show a similar binding mode of compounds **5a-C10** and **5b-C10** to Tac-10-iper ((**45-C10**) in the CAS and PAS regions of AChE (Figure 23). The remarkably lower affinity of **45-C10** is probably due to the additional quaternary ammonium group of the Phtal- and Naph-compounds which causes a much higher desolvation penalty in comparison to the uncharged alkylene chain.

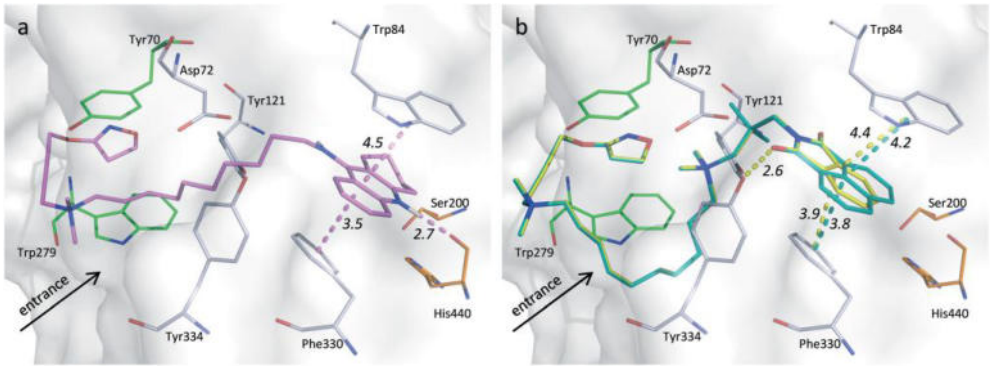

Figure 23. (a) Docking pose of **45-C10** (pink), with the interaction distances shown in the CAS (orange) and in the PAS (green). (b) Docking representation of **5b-C10** (blue) and **5a-C10** with their interaction distances shown in yellow. Reproduced with permission from[131].

A dual mechanism of action which appears to be the right innovation to fight the AD pathology may also be possible due to the high affinity for M1 and M2 receptors. Furthermore, functional studies (investigation of Ga and PLC-b3 proteins interaction through Split-Luciferase assays) demonstrated the ability of Tac-7-Iper and Tac-10-Iper ((**45-C7**, **45-C10**, Figure 22) to activate the M1 muscarinic receptor in a nanomolar range (Volpato et al., unpublished results). Further studies are necessary for developing uncharged molecules that could cross the BBB; so far, it is promising to see that compounds with a single positive charge are associated with better activity than compounds with two charges[131,132].

5.1.3. Tacrine/Xanomeline hybrids

A similar dualsteric strategy was previously employed by the Decker group[135]. They designed and synthesized tacrine and xanomeline hybrid compounds ((**46a**), Figure 24). The rational design of these hybrids was aimed at a triple mechanism of cooperative action: activation of the M1 receptor through the xanomelinic molecular portion ((**18**), Figure 9), positive allosteric modulation regarding orthosteric agonists at the M1 receptor subtype thanks to the allosteric properties of tacrine, and increasing the amount of ACh in cholinergic synapses due to the AChE inhibiting activity[135]. Xanomeline is an M1 agonist but unfortunately also shows some affinity to the M4 receptor. Therefore, parasympathetic side effects including bradycardia, increased gut motility, and salivation occur. Binding studies on cloned human muscarinic receptors did not detect the selective binding capacity between M1 and M4. Xanomeline is well-known for its anti-dementia properties *in vivo*, and the attenuation of cognitive decline

in 6 months clinical trial human patients proved its activity against AD[136]. The metabolic instability due to an extensive first-pass metabolism, the well-known cholinomimetic side effects, and its undesirable activity for the dopaminergic and 5-TH receptors (serotonin receptors) rendered the compound an insufficient clinical candidate[137,138]. Xanomeline induces a specific mode of M1 receptor activation by interacting with a site that does not fully overlap with the endogenous, orthosteric binding site. Differences in binding kinetics[139] and a wash-persistent binding, probably arising from a hydrophobic interaction of xanomeline's O-hexyl chain with the membrane lipids surrounding the receptor[140,141], may explain its functional selectivity[142].

The xanomeline portion was connected to the tacrine with amide bridges of different length (10-17 atoms spacer). A clear increase of AChE inhibition was observed by increasing the spacer chain from pIC_{50} of 7.20 to 8.21. The hybrids inhibited the AChE with similar or higher potency compared to tacrine but did not activate the M1 receptor. Instead of a simultaneous allosteric/orthosteric binding, the ligands seem to prefer a purely allosteric binding even in the orthosterically free receptor. These findings were supported by *in vivo* studies in rats with a representative compound ((**46a**), Figure 24). The cognitive deficits induced by administration of scopolamine were enhanced by the purely M1 allosteric interaction of the hybrid **46a** counterbalancing its high ChE-inhibitor properties. The desired triple mechanism of action unfortunately did not take place with these compounds. This demonstrates the difficulty of predicting the intrinsic activities of the chosen component molecules and the importance of their cooperativity, which must lead to a balanced compromise.

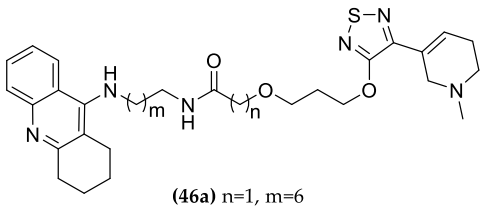

(46a) n=1, m=6

Figure 24. Dual-active AChE inhibitor/ mAChR agonist compounds

5.1.4. 77-LH-28-1/Xanomeline hybrids

As already mentioned above, compound 77-LH-28-1 ((**47**), Figure 25) displaying mixed modes of orthosteric or allosteric pharmacology depending on the experimental assay conditions [143], was

incorporated into a series of allo/ortho hybrid ligands, hypothesizing a shared function of the common chain ligand structures of xanomeline and 77-LH-28-1 ((**48a,b**), Figure 25). With a merging approach, the two scaffolds were fused into the new hybrids, aiming for a better understanding of the allosteric pocket and of the bitopic binding pose of 77-LH-28-1 itself.

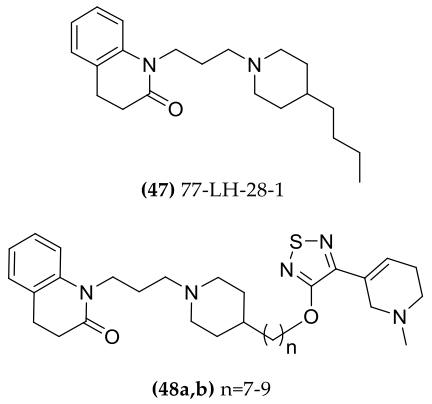

Figure 25. Dual-active AChE inhibitor/ mAChR agonist compounds

The pharmacological investigation of these hybrid derivatives evidenced an affinity at the M1 receptor higher than 77-LH-28-1 and lower than xanomeline. In general, hybrid compounds showed either a weak agonistic or an antagonistic activity profile (M1 and M4) in all the functional assays and the activity/selectivity was related to the length of the spacer. The highest affinity values are associated with a seven- or nine-atom length carbon chain, indicating that the two pharmacophores probably interact with two distinct sites located at a distance of 7 to 9 methylene moieties. Xano-9-77-LH-28-1 exhibited higher efficacy for the β-arrestin2 engagement in M1. In line with the reported functional properties of the aliphatic chain moiety in 77-LH-28-1, these results indicate that the linker extension affects the orthosteric binding site [12].

6. Nicotinic receptor

Nicotinic receptors are transmembrane pentameric proteins that belong to the superfamily of ligand-gated ion channels, composed of α and β subunits assembled around a central hydrophilic pore that mediates the flow of the cations K^+, Na^+, and Ca^{2+}. Different combinations of subunits generate a variety of nAChR subtypes with distinct electrophysiological properties and brain localization [144,145]. nAChRs are considered to play an important role in neuroprotection due to a concentration dependent interaction

with the β-amyloid peptide. In particular, the physiological concentration of Aβ may directly stimulate the α_7 nicotinic receptors while an increasing pathological concentration of Aβ damages the cholinergic responses mediated by α_7 and $\alpha_4\beta_2$ receptors.

6.1. Design of hybrid compounds to investigate the nicotinic receptor

6.1.1. 1-(2-Methoxybenzyl)-piperazine- carbazole hybrids

The mutual interaction between Aβ and cholinergic transmission was investigated. Following a ligand-based approach, hybrid compounds addressing both systems were synthetized and subsequently pharmacologically studied. The molecules combine an α_7 agonist and a carbazole moiety having AChE inhibition properties ((**49a,b**), Fig 26)[18]. Substituted carbazoles are able to interact with the narrow inner part of the AChE enzyme gorge and also present anti-amyloidogenic activity. This moiety was connected with the α_7 agonistic activity of 1-(2-methoxybenzyl)-piperazine[19]. It was selected because of the structural similarity with the ethyl-(2-methoxybenzyl)-amine group recognizing the AChE catalytic site [20,146].

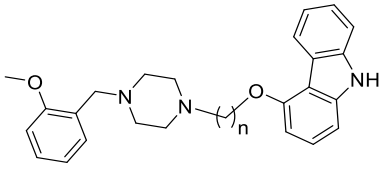

(49a,b) n=5-6

Figure 26. Dual-active AChE inhibitor/ nAChR agonist compounds

The resulting multitarget compounds, in particular compound ((**49b**), Figure 26), presented AChE inhibition activity in a micromolar concentration range (compound with six methylene unit spacer IC_{50} = 0.773 μM). AChE inhibition was strongly dependent on the linker elongation. In particular, compounds with a shorter chain in the series had lower IC_{50} values. In radioligand binding assays, the compounds exhibited a micromolar affinity profile with K_i values ranging from 15 to 120 μM in the displacement of [^{3}H]-epibatidine and [^{125}I]-α-bungarotoxin from $\alpha_4\beta_2$ and α_7 receptor subtypes in rat cortex, without discrimination in the receptor subtype. The action towards nAChRs was tested by using two-electro voltage clamps. Unfortunately, the compounds only reached 15-22% of the response (reference 100 μM Ach) at $\alpha_4\beta_2$ receptors. No response was observed at the α_7 receptor, possibly due to its lower sensibility

to ACh or its faster desensitization. Interestingly, their inhibition ability at 10 μM of Aβ fibril formation, proved with a ThT-based fluorimetric assay, is similar to the anti-aggregating and blocking fibril formation activity of curcumin [147] (28-36% compared to 34.4% of curcumin). Synergistically, a weak perturbation of one of the systems involved in the cholinergic neurotransmission (AChE, nAChRs) and amyloid aggregation could be sufficient to modify the entire scenario. Therefore, the compounds are a suitable starting point for further optimization.

7. Looking to the future for AD hybrids tools

The hybrid compounds targeting different biological proteins and dualsteric ligands addressing distinct parts of the same target or a combination of both strategies provide pharmacological tools that could expand horizons in medicinal chemistry. All the hybrid examples reported provide additional useful and important information regarding their target, showing that the development of bivalent compounds is not only possible but also promising in offering new pharmacological instrumentation. Poor drugability is the direct consequence of the relatively high molecular weight of bitopic ligands which prevents their progression in drug development. The bivalent compounds can provide new useful information regarding protein-ligand interactions anyway, understanding the intricate relationship between receptor activation, conformational dynamics, signaling profile in the cholinergic system, and the connection between different hallmarks of AD. Advantages such as better selectivity, signaling bias, or reduced toxicity of some hybrids can be further exploited through a subsequent fragment based process trying to reduce physicochemical issues but keeping the precious improvement obtained. The simultaneous attack on several fronts seems to provide insights that may be the key to opening new glimpses in the cholinergic field of the AD.

Funding: D.V. received financial support by the international doctoral college “Receptor Dynamics: Emerging Paradigms for Novel Drugs” funded within the framework of the Elite Network of Bavaria (ENB). (Grant number K-BM-2013-247).

Conflict of Interest: The authors declare no conflict of interest.

Sample Availability: Samples of the compounds are not available from the authors.

B. Aim of the Work

The brain's cholinergic system has a central role in ongoing research related to cognition processes and age-related cognitive decline, including dementias such as Alzheimer's disease (AD). The cholinergic hypothesis of AD centered on the progressive loss of limbic and neocortical cholinergic innervation[148] led to the emergence of a large number of potential therapeutic interventions designed to restore cholinergic function. Several approaches are focused on the use of AChE inhibitors that reduce the hydrolysis of ACh. More recent investigational compounds include specific M1 mAChR or nAChR agonists.[149] Despite intense research efforts, the causes of AD and biological pathways of its pathogenesis are still not fully understood. Several common features in AD's patients were found such as formation of senile plaques with β-amyloid (Aβ), misfolding and aggregation of hyperphosphorylated tau-protein, mitochondrial dysfunction, inflammatory processes, oxidative stress and genetic prerequisites.[28–31,150,151] The resulting complex pathological network makes drug therapy a real challenge, in particular the discovery of structural requirements for powerful and selective ligands which avoid site effects. Hence, the idea of multifunctional drugs composed of two drug entities connected by a linker arose. In particular, in the field of muscarinic agonists, the difficulty lies in the achievement of subtype-selectivity among the 5 different muscarinic receptors. With the hybrid approach an additional pharmacophore scaffold is linked to the first one, targeting a further pathological pathway or an accessory protein recognition site, conferring selectivity. Thus, it addresses different involved cholinergic receptors and enzymes simultaneously and enhances the target affinity and/or selectivity. Such hybrid molecular tools are necessary to elucidate numerous molecular basis details of the AD target proteins which are still unclear. Hence, the aim of the first project is the synthesis and pharmacological investigation of newly designed dualsteric compounds for the M1 muscarinic acetylcholine receptor. Starting from bitopic compounds previously synthesized in our research group,[82,83] while maintaining the same allosteric BQCAd allosteric modulator the orthosteric fragment is modified, replacing the heterocyclus of the superagonist iperoxo with ACh, the isoxazole ring, Oxotremorine, Oxotremorine-M or Xanomeline non-selective agonists. With such hybrid ligands the influence of the orthosteric

fragments and different chain lengths can be evaluated with regard to ligand-dependent receptor activation, subtype-selectivity as well as pathway-biased signaling.

In a second project the structural elements of tacrine and xanomeline are linked via alkyl chains of different length in a multitarget approach addressing both the M1 receptor and the AChE, providing new and important drug design contribution regarding these important AD targets. Moreover, the exploration of new medicinal chemistry strategies and pharmacological instrumentation for the study of receptor activation will lead to the synthesis of a new trifunctional ligand, composed of two orthosteric units connected with an allosteric fragment with two hexamethylene chains. The tritopic ligand will serve for the study of the receptor conformational movement, investigation of metastable binding sites as well as for receptor dimerization process analysis.

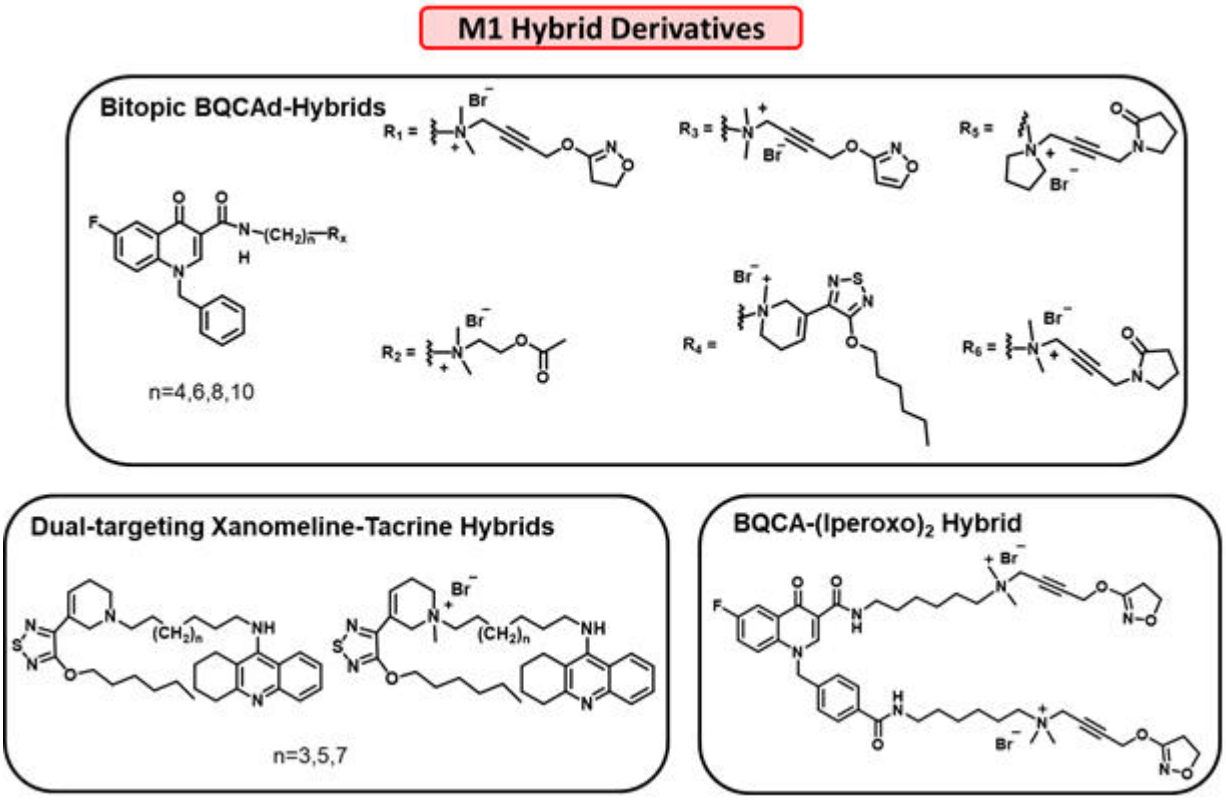

Figure 1. Overview of the M1-Hybrid derivative projects.

Muscarinic acetylcholine receptors belonging to the hepta-helical family proteins transferring information across the membrane and triggering multiple intracellular signaling cascades are identified as target systems for several pathophysiological conditions. Nevertheless, the choice of muscarinic receptors as

therapeutic target is still a challenge due to the lack of subtype-selectivity which lead to side effects. The synthesis of new allosteric and orthosteric molecular fragment aims at the elucidation of structural characteristics responsible for receptor function and structural elements able to distinguish between the five mAChR subtypes. Therefore, the optimization of the two pharmacophoric portions, the orthosteric and the allosteric scaffolds will be done simultaneously. In this way we are going to “measure” the space around the two orthosteric and allosteric portions in term of length, flexibility and chemical characteristics for a detailed pharmacological investigation of the influence of each chemical fragment on the receptor binding and activation. Thus, some BQCAd allosteric derivatives with different chain lengths and a positively charged terminal amine are synthesized and pharmacologically evaluated. Applying a similar approach, the iperoxo pharmacophore is elongated with a spacer up to twelve methylenic units long. Moreover, a quaternary ammonium head, resembling the muscarinic agonist tetramethylammonium (TMA)[152,153] is introduced by the end of the spacer. Additionally, the flexible alkyl chain linker is exchanged by a rigidified linker, to understand the consequences of a reduced suppleness in the receptor activation process.

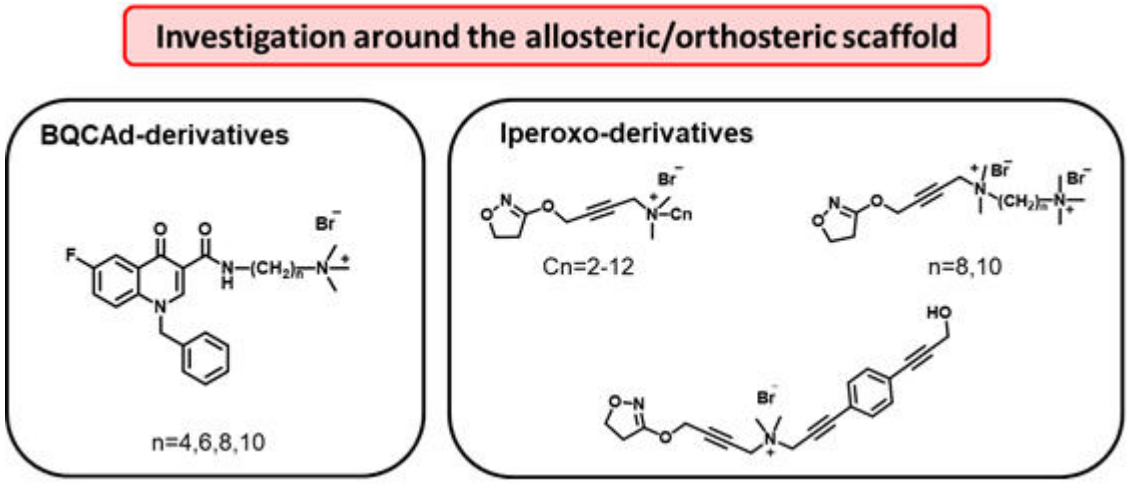

Figure 2. Overview of the allosteric/orthosteric modified compounds.

C. Results

1. The role of orthosteric building blocks of bitopic ligands for muscarinic M1 receptors

Daniela Volpato[a], Michael Kauk[b], Regina Messerer[a], Marcel Bermudez[c], Gerhard Wolber[c], Andreas Bock[d], Carsten Hoffmann[b] and Ulrike Holzgrabe[a*]

[a]Department of Pharmaceutical and Medical Chemistry, Institute of Pharmacy, University of Würzburg, Am Hubland, 97074 Würzburg, Germany

[b]Institute for Molecular Cell Biology, CMB-Center for Molecular Biomedicine, University Hospital Jena, Friedrich-Schiller University Jena, Hans-Knöll-Straße 2, 07745 Jena, Germany

[c]Institute of Pharmacy, Freie Universitaet Berlin, Königin-Luise-Str. 2-4 in 14195 Berlin-Dahlem

[d]Max Delbrück Center for Molecular Medicine, Robert-Rössle-Str. 10, 13125 Berlin, Germany

ACS Omega., • Publication Date: Dec 2020

Reprinted/adapted with permission from Volpato, D.; Kauk, M.; Messerer, R.; Bermudez, M.; Wolber, G.; Bock, A.; Hoffmann, C.; Holzgrabe, U. The Role of Orthosteric Building Blocks of Bitopic Ligands for Muscarinic M1 Receptors. ACS Omega. DOI: 10.1021/acsomega.0c04220. Copyright (2020) American Chemical Society

KEYWORDS: M1 muscarinic acetylcholine receptor, bitopic ligands, BQCAd scaffold, G protein-activation, b-arrestin recruitment

Abstract: The muscarinic M_1 acetylcholine receptor is an important drug target for the treatment of various neurological disorders. Designing M_1 receptor-selective drugs has proven challenging, mainly due to the high conservation of the acetylcholine binding site among muscarinic receptor subtypes. Therefore, less conserved and topographically distinct allosteric binding sites have been explored to increase M_1 receptor selectivity. In this line, bitopic ligands, which target orthosteric and allosteric binding sites simultaneously, may provide a promising strategy. Here, we explore the allosteric, M_1-selective BQCAd scaffold derived from BQCA as starting point for the design, synthesis, and pharmacological evaluation of a series of novel bitopic ligands in which the orthosteric moieties and linker lengths are systematically varied. Since b-arrestin recruitment seems to be favorable to therapeutic implication, all the compounds were investigated by G protein and b-arrestin assays. Some bitopic ligands are partial to full agonists for G protein-activation, some activate b-arrestin recruitment, and the degree of b-arrestin recruitment varies according to the respective modification. The allosteric BQCAd scaffold controls the positioning of the orthosteric ammonium group of all ligands, suggesting that this interaction is essential for stimulating G protein-activation. However, b-arrestin recruitment is not affected. The novel set of bitopic ligands may constitute a toolbox to study the requirements of b-arrestin recruitment during ligand design for therapeutic usage

Introduction

Muscarinic acetylcholine receptors belong to the superfamily of G protein-coupled receptors. Five muscarinic receptors subtypes (M1-M5) are expressed in humans and mediate a variety of physiological functions.[154,155] The binding site for the endogenous neurotransmitter acetylcholine, classical synthetic orthosteric agonists (e.g. carbachol, oxotremorine, oxotremorine-M, and iperoxo), and antagonists (e.g. atropine, N-methylscopolamine, and ipratropium) is located deeply inside the seven-fold transmembrane helical bundle.[156,157] All muscarinic receptor subtypes share a high sequence similarity in their orthosteric binding pockets which has entailed severe difficulties in the discovery of subtype-selective ligands for this receptor family.[157–159] Moreover, all muscarinic receptors possess at least one allosteric binding site which is located on top of the orthosteric binding site comprising the upper parts of transmembrane helices and extracellular loops.[160–163]

M1 muscarinic receptors are predominantly expressed in the central nervous system (CNS), especially in the amygdala, hippocampus, cerebral cortex, and striatum[164,165] where they contribute to essential cognitive functions such as memory and learning. The M1 muscarinic receptor has been identified as an important drug target which may be addressed for the treatment of Alzheimer's disease (AD) and schizophrenia.[143,166] Although activation of M1 receptors with synthetic orthosteric agonists has been shown to be effective in a variety of CNS diseases,[167–169] all ligands exhibited severe adverse effects which have eventually led to withdrawal from drug discovery programs, likely due to missing subtype-selectivity of these drug candidates.[32,170]

New strategies for obtaining more selective ligands have been explored by either using positive allosteric modulators (PAMs)[57,94,171–175] or by structural hybrids of orthosteric and allosteric moieties. These latter so-called bitopic ligands have been originally developed based upon the hypothesis of combining the activation properties of orthosteric ligands with the better selectivity profile of allosteric ligands.[57,25,176,177] Number of studies have lately shown that through the design of bitopic ligand series a differential engagement of all possible GPCR signaling pathways can be studied.[178,179] We have previously synthesized bitopic agonists for the M1 receptor (Scheme 1, 1-Cn) which consist of the orthosteric agonists iperoxo or acetylcholine and the M1R-selective positive allosteric modulators (PAM) BQCAd.[106,180,181,182,183] Benzyl quinolone carboxylic acid (BQCA) and its derivatives were reported being positive allosteric modulators (PAMs). Compared to their orthosteric counterparts, they confer a high selectivity

in terms of binding and function at M1 receptors.[83,181] Underlying structure-activity-relationship studies suggested that the potency and efficacy of bitopic agonists basically depend on three substantial factors, i.e. linker length, geometry of the position of orthosteric and allosteric moieties, as well as the substitution pattern of the allosteric moiety.[82,83,111]

Here, we introduce a systematic set of novel bitopic ligands for the M1 receptor which were designed by connecting the allosteric moiety BQCAd to orthosteric muscarinic agonists using methylene linkers of varying length (Scheme 1). The allosteric interaction of BQCAd is shown in the supplementary information (Table S4, Figure S1 (panel F)). Classical orthosteric agonists were chosen as building blocks of the bitopic ligands aiming at a comparison of a myriad of study results from the literature and obtaining a deepened understanding of previously published works.[82,83] In order to derive structure-activity-relationships, the set of compounds was tested for the ability to activate G protein-signaling and b-arrestin recruitment. Our data shows that efficacy and potency of bitopic ligands strongly depends on the structure of the orthosteric moiety which is supported by respective docking studies. The smallest known muscarinic agonist, tetramethylammonium (TMA)[152,153,] has a sufficient efficacy to activate G proteins but is not suitable for recruiting b-arrestin. Interestingly, the iperoxo hybrids 1-C6, 1-C8 as well as the isoxo ligand 3-C8 were able to recruit β-arrestin2. Of note, our data demonstrates how subtle differences in ligand structure can impact receptor activation and simultaneously suggests that different regions of the orthosteric binding site can be explored in order to investigate M1 receptor signaling.

Result and Discussion

Chemistry

Compounds 1-Cn, 2-Cn, and 5-Cn were prepared according to previously reported procedures.[82,83] Compound series 3-Cn and 4-Cn and their overall synthetic pathways are displayed in Scheme 1 (for further details see Supporting Information Data S1). The 4-oxo-quinoline skeleton was built up using the Gould-Jacobs synthetic procedure using diethyl 2-(ethoxymethylene)-malonate for condensation with 4-fluoroaniline followed by cyclization in diphenyl ether.[184–186] Both synthetic procedures were carried out under microwave assistance to promote conversion and to achieve better yields. The quinolone nitrogen was benzylated followed by amidation of the ester function utilizing an aminoalkyl alcohol of the respective spacer length. Finally, the hydroxyl function was replaced by a bromine atom using hydrobromic acid and sulfuric acid.[82]

All orthosteric fragments were synthesized according to the literature[92,187–189] to obtain the tertiary base which was subsequently used within the final synthesis step yielding the desired bitopic compounds. In brief, the synthesis of the isoxazole moiety[92] starts with treating methyl propiolate with commercial hydroxylamine hydrochloride followed by subsequent reaction with 1,4-dichloro-2-butyne. The tertiary base was finally obtained by adding a two-fold excess of a solution of dimethylamine in DMF at room temperature requiring a three-step synthesis. Oxotremorine-M was obtained by starting from the commercially available 2-pyrrolidinone and propargyl bromide followed by a CuCl-catalyzed Mannich reaction using dimethylamine and paraformaldehyde to obtain the corresponding tertiary bases.[92,188]

The final compounds were obtained by reaction of the allosteric moiety equipped with the brominated spacer and the corresponding tertiary orthosteric bases as shown in Scheme 1. All reactions were conducted using microwave assistance to shorten reaction times up to 8-48 h. The final compounds were purified by recrystallization or, in cases where crystallization was not feasible, by column chromatography using basic aluminum oxide.

Pharmacology

Recent findings correlate pronounced cholinergic adverse responses with G protein activation coupling and phosphorylation-dependent signaling with maximal clinical efficacy across various AD symptoms.[190,191] In order to evaluate the impact of the orthosteric moieties on overall ligand activity and to compare the activity of the novel bitopic compounds with previously studied ones, all ligands were tested in both G protein-signaling and b-arrestin recruitment assays. As a read-out for G protein-signaling we applied a luminescence-based complementation assay: in intact cells, the interaction of Gaq with phospholipase Cb3 being fused to parts of a luciferase[192] can be observed. Upon stimulation of Gq-coupled receptors, spatial proximity between Gaq and PLC-b3 allows complementation of the split luciferase, thus the luminescence derived from a luciferase substrate is detected. b-arrestin recruitment was measured by BRET between a NanoLuc-tagged M1 receptor and b-arrestin2, N-terminally fused to a Halo tag[83]. Moreover, the ability of the novel ligands to interact with both the orthosteric and allosteric binding sites was tested in equilibrium and by applying dissociation binding experiments, respectively (Supporting Information Data S3).

Iperoxo-derived bitopic ligands.

Iperoxo is the most potent and efficacious muscarinic agonist which has served as orthosteric moiety of other bitopic ligands.[82,83,103] We characterized iperoxo-based bitopic ligands with aliphatic linkers spanning 6 to 10 methylene groups (Scheme 1). Gq/PLC-b3 complementation assays (Figure 1a) reveal that all compounds are agonists. 1-C6 and 1-C10 are partial agonists whereas 1-C8 behaves as full agonist for Gq activation. Increasing the linker length from 6 to 8 methylene groups increases both potency and efficacy, whereas a further increase in linker length to 10 methylene groups decreases both potency and efficacy. The bitopic ligands were tested for their ability to stimulate b-arrestin recruitment. 1-C6 and 1-C8 are partial agonists with 1-C6 displaying a slightly higher potency than 1-C8. 1-C10 fails to stimulate b-arrestin recruitment. Interestingly, we find that 1-C8 is much more potent and efficacious than 1-C6 regarding G protein-activation (Figure 1a), however, 1-C6 is more potent in recruiting b-arrestin than 1-C8 (Figure 2a).

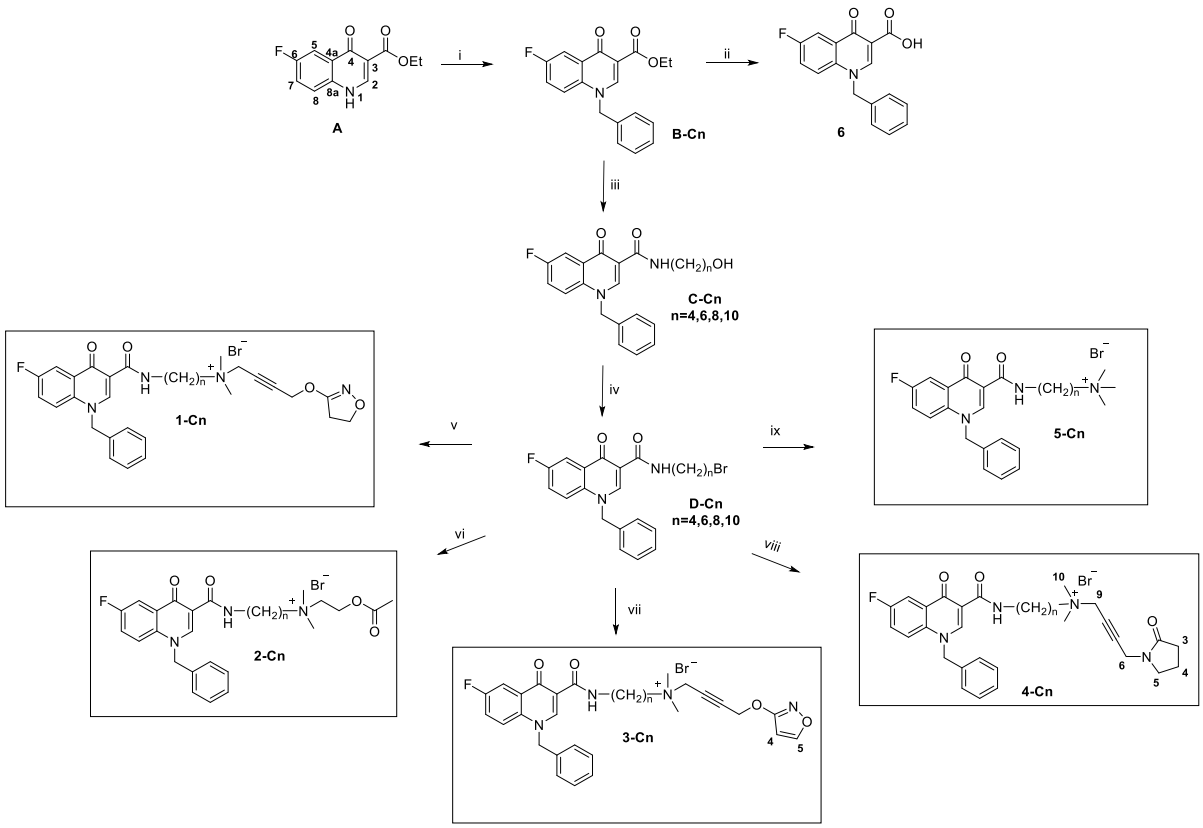

Scheme 1. Synthetic pathway of the bitopic M1 receptor ligands composed of the PAM benzyl quinolone carboxylic acid derivative (BQCAd 6) covalently linked to non-selective muscarinic orthosteric agonist fragments (iperoxo 1, acetylcholine 2, isoxo 3, oxotremorine-M 4, TMA (tetramethylammonium) head 5). Reagents and conditions: (i) benzyl chloride, K2CO3, DMF, 80 °C; (ii) 6 N HCl, MeOH, reflux; (iii) H2N(CH2)nOH, 150 °C; (iv) HBr (48%), H2SO4, reflux; (v) iperoxo base, KI/K2CO3, CH3CN, 80 °C MW; (vi) acetylcholine, KI/K2CO3, CH3CN, 80 °C MW; (vii) isoxo base, KI/K2CO3, CH3CN, 80 °C MW; (viii) oxotremorine-M base, KI/K2CO3, CH3CN, 80 °C MW; (ix) trimethylamine, CH3CN, 40 °C.

ACh-derived bitopic ligands

In analogy to the iperoxo-based compounds we characterized a set of ACh-derived bitopic ligands with varying linker lengths ranging from 6-10 methylene groups (Scheme 1). All bitopic ligands (2-C6, 2-C8, and 2-C10) are partial agonists for G protein-activation (Figure 1b) and hardly induce any b-arrestin recruitment (Figure 2b). Only at very high concentrations, i.e. 100 µM, b-arrestin recruitment can be observed with all three compounds. In line with iperoxo-derived bitopic ligands (Figure 1a), potency and efficacy of ACh-based ligands are dependent on linker length. Increasing the linker length from 6 to 8 (and 10) methylene groups significantly increases the potency of 1-C8 (and 1-C10), whereas 1-C10 displays the weakest efficacy of this series of compounds. The overall efficacy of ACh-derived ligands appears to be reduced compared to the iperoxo-derived ligands, however, the structure-activity-relationships seem to be rather similar.

Isoxazole-derived bitopic ligands

Next, we used an orthosteric agonist, isoxo[187], which is structurally very similar to iperoxo. The molecule differs by a double bond which was introduced into the iperoxo ring system, resulting in an aromatic isoxazole ring whose influence on the ligand-receptor interaction were studied. We used isoxo as an orthosteric fragment to synthesize the bitopic ligands 3-C6, 3-C8, and 3-C10 (Scheme 1). In line with the results obtained with iperoxo- and ACh-derived bitopic ligands, all isoxo-based bitopic ligands stimulated G protein activation (Figure 1c). However, they hardly induced any b-arrestin recruitment (Figure 2c) which is in line with ACh-based ligands. 3-C8 (a full agonist) displayed a higher efficacy than 3-C6 (a partial agonist), whereas 3-C10, in line with aforementioned observations (Figures 1a, 1b), demonstrated the weakest potency and efficacy, respectively, of the entire series. Full concentrations response curves for b-arrestin recruitment could not be obtained. Nevertheless, the data suggest that the activation profile of the ligands follows that for G protein activation with 3-C8 and 3-C10 being the most and least efficacious ligands, respectively (Figure 2c).

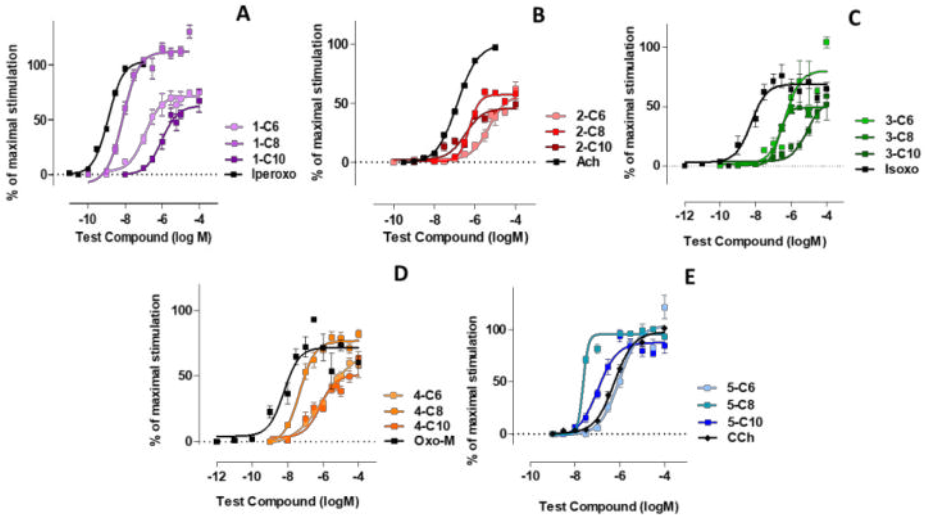

Figure 1. Concentration-response curves in Gα/PLC-β3 split-luciferase interaction assays in HEK293T cells expressing the human muscarinic M1 receptors (hM1) which were stimulated utilizing varying concentrations of indicated compounds. Data is expressed as the means ± S.E.M. of 3-6 independent experiments performed in triplicate. The data were normalized to iperoxo (panel A), ACh (panel B), Isoxo (panel C), Oxo-M (panel D), and Carbachol (CCh) (panel E) as reference (maximum stimulation set to 100%).

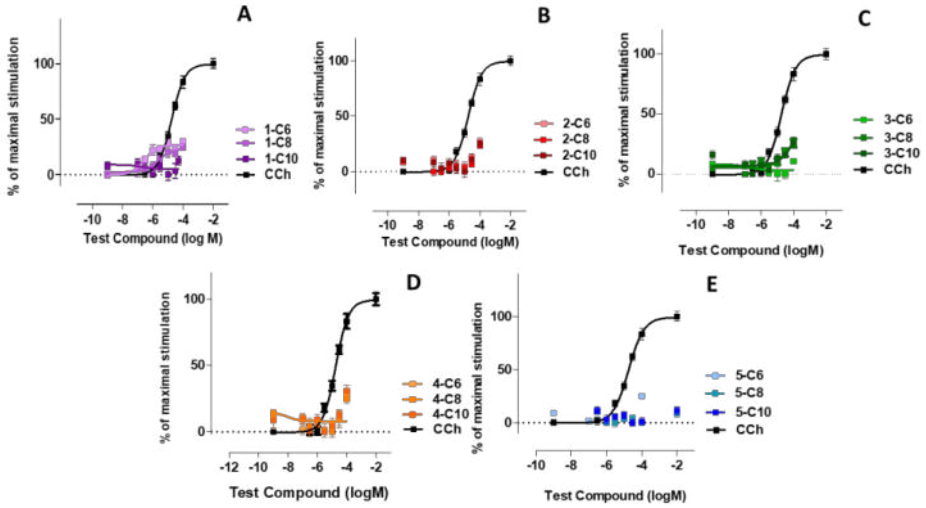

Figure 2. Concentration-response curves obtained with a BRET-based assay reporting the recruitment of b-arrestin to M1 receptors stimulated with various concentrations of indicated compounds (Iperoxo-derived bitopic ligands (panel A), ACh-compounds (panel B), Isoxazole-bitopic ligands (panel C), Oxotremorine-M based ligands (panel D), TMA-derived bitopic compounds (panel E)). b-arrestin recruitment upon stimulation with saturating concentrations of carbachol (CCh) was set to 100%. Data are normalized to CCh and expressed as the means ± S.E.M. of 3-6 independent experiments performed in triplicate

Oxotremorine-M-derived bitopic ligands

In the next set of compounds, another classical non-selective muscarinic agonist, oxotremorine-M, was used as an orthosteric moiety giving rise to the series of bitopic ligands 4-C6, 4-C8, and 4-C10 (Scheme 1). As seen with previous series of bitopic ligands, increasing the linker length from six to eight methylene groups seems to yield better agonists. 4-C8 displays a higher potency and a higher efficacy than 4-C6, whereas further increase of the linker length decreases the potency and efficacy of 4-C10 (Figure 1d). All compounds only weakly stimulate b-arrestin recruitment at 100 µM and appear to behave similar (Figure 2d).

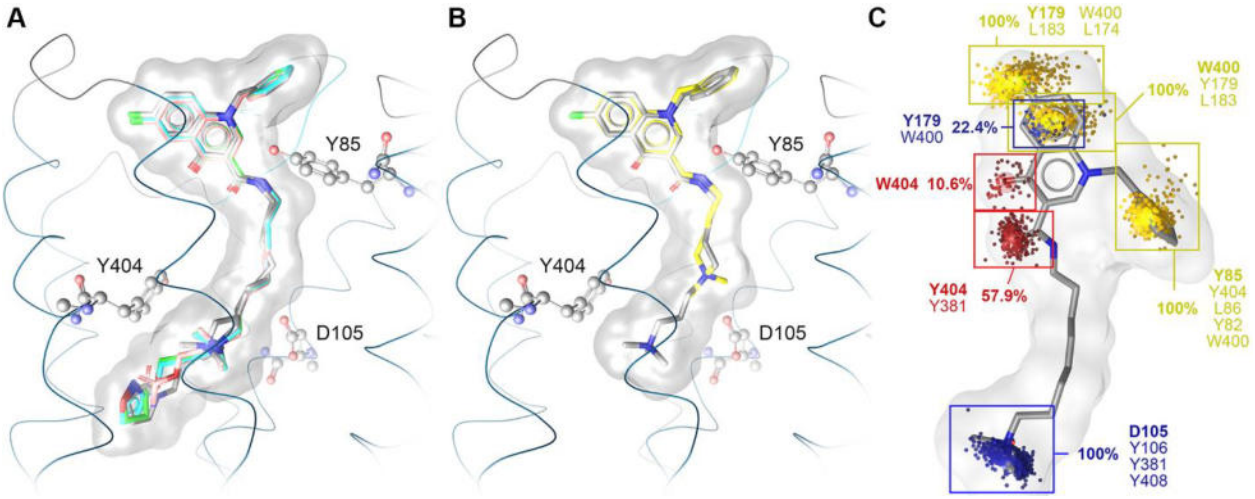

Figure 3. Proposed binding modes for BQCAd-derived bitopic ligands at the M_1 receptor indicate a distinct position of the allosteric BQCAd moiety, whereas the positioning of the orthosteric building block is more diverse. **A:** Superimposition of 1-C8 (green), 2-C8 (salmon), 3-C8 (blue), 4-C8 (dark grey), and 5-C8 (light grey) bound to the M1 receptor. **B:** Superimposition of 5-C8 (light grey) and 5-C4 (yellow) bound to the M1 receptor. **C:** Dynamic interaction pattern of 5-C8, the most potent compound from the series with the minimal orthosteric building block, derived from a 250 ns MD simulation. Yellow point clouds indicate non-polar contacts, the blue point cloud show positive ionizable centers, the purple point cloud shows aromatic interactions and the red point clouds indicate hydrogen bond acceptors. Next to the point clouds, the occurrence frequency and the involved residues are indicated

TMA-derived bitopic ligands

Lastly, we used the smallest muscarinic agonist described in the literature, i.e. TMA, as a building block for bitopic ligands. We synthesized the minimal-size bitopic ligands 5-C6, 5-C8, and 5-C10 (Scheme 1). In line with all previous data, TMA-based ligands stimulated G protein activation (Figure 1e) in a linker-length dependent manner. Again, the octamethylene linker (5-C8) seems to be more favorable for G protein activation than the hexamethylene linker (5-C6). In contrast to the other series of bitopic ligands

described above, the 5-C10 compound shows a higher potency than 5-C6 (Figure1e). Interestingly, all TMA-based ligands behave as full agonists. The ligand-induced b-arrestin2-recruitment, determined by a BRET based assay[192], was very weak for the entire series of ligands, and could only be detected for the highest ligand concentration tested throughout the experiments (100 µM; Figure 2e). Overall, based on the experimental data, three general observations can be made: First, the majority of bitopic ligands of the series 1-Cn to 4-Cn are weaker agonists than their parent orthosteric agonists; second, all bitopic ligands show negligible to little efficacy in recruiting b-arrestin; and third, a linker length of eight methylene groups appears to be optimal for G protein activation by all bitopic ligands. This is in line with the recent finding regarding the bitopic agonist iper-8-phth capable of binding to and activating the M1 receptor as a full agonist.[193] Noteworthy, shortening of the linker to four methylene groups did not lead to improved G protein activation for the TMA bitopic ligands neither in terms of maximum response nor in potency. (Supporting Information Figure S4).

Binding modes of BQCAd-based bitopic ligands

In order to gain structural insight into binding poses and to link them to the observed activities, we performed computational analysis of selected bitopic ligands with focus on the n-C8 series. Docking to the active M1 receptor resulted in plausible poses for all bitopic ligands. Due to the spatial requirements and the rigidity of the BQCAd building block, the orientation of its bitopic derivatives is highly similar (Figure 3A). In case of the M2 receptor, bitopic ligands exhibit a fixed position of the orthosteric moiety which directs the positioning of the allosteric building blocks. Interestingly, our data strongly suggests the opposite for the M1 receptor (Supporting Information Figure S5).[194] Since BQCAd is very specific for the M1 allosteric vestibule, it serves as an anchoring point which controls the positioning of the linker and thereby the position of the orthosteric moiety in the orthosteric binding site.

With regard to the orthosteric binding pocket, the essential interaction responsible for receptor activation is the charge interaction with D1053.32.[195] The positive charge is additionally surrounded by aromatic residues of the tyrosine lid (Y7.39 and Y7.43), forming cation-π interactions. Since the tyrosine lid is flexible to a certain extent and the charge interaction with D1053.32 is not restricted to a distinct geometric position, the position of the positive charge of the ammonium group shows some variance (Figure 3B). Due to the flexibility of the alkyl linker, this essential charge interaction can be observed for

all studied bitopic ligands. Both, the alkyl linker length and the type of the orthosteric building block are controlling the location of the ammonium group. This might also explain why there is no direct pharmacological correlation between bitopic ligands and their purely orthosteric building blocks (Figures 1 and 2). Since the binding mode is mainly determined by the BQCAd moiety and the linker length, the orthosteric building block cannot necessarily build the same interactions as the purely orthosteric ligands themselves. Interestingly, the compound series with the smallest known orthostere (TMA) shows robust G protein activation which suggests that only the charge interaction is crucial for G protein activation. Given that 5-C8 shows the highest potency with regard to G protein activation, we analyzed its receptor-ligand interaction by using dynamic pharmacophores.[105] The initial binding mode of 5-C8 and the respective interaction pattern was conserved over 250 ns of MD simulation (Figure 3C). The largest movement was observed for the benzyl ring which shows a more frayed distribution of its non-polar contacts, but this movement occurred at the very beginning of the trajectory. The dynamic interaction pattern indicates a key role of Y179 in the second extracellular loop (ECL2) and W4007.35 for hosting the BQCAd moiety in the allosteric vestibule of the M1 receptor. This result is in accordance with previous mutational studies that highlight key residues for allosteric modulation at the M1 receptor.[196–198] Interestingly, the same epitopes have also been shown to control shape and ligand binding properties of the extracellular binding site of the M2 receptor.[105,199] Since we observed a surprisingly high potency (e.g. 4-C4) or high efficacy (e.g. 1-C4) for some compounds of the C4 series, we hypothesize that these bitopic ligands might show multiple binding modes as previously reported for some bitopic muscarinic agonists.[200]

In conclusion, we have presented a novel set of BQCAd-based bitopic M1 receptor agonists comprising five different orthosteric agonists and alkyl linkers of varying length. All bitopic ligands are agonists with regard to G protein activation with efficacies ranging from partial to full agonism. On the other hand, only 3 ligands, i.e. 1-C6, 1-C8, and 3-C8, were able to efficiently recruit β-arrestin in the concentration range sufficient for G protein activation. Molecular modeling studies demonstrate that the overall binding mode of the bitopic ligands is mainly determined by the position of the allosteric BQCAd moiety. Hence, the ligands are ‘hung up’ in the allosteric vestibule of the receptor and the orthosteric moieties ‘dangle’ into the orthosteric binding site. This may result in a situation where the orthosteric moieties of the bitopic

ligands adopt different binding poses as their parent orthosteres alone. This would be in line with our experimental data showing that several bitopic ligands are less potent and efficacious than their respective orthosteric agonists. Moreover, shrinking the orthosteric moiety down to the essential ammonium ion (as in TMA, 5-Cn series) is sufficient to induce a potent and efficacious G protein response; however, these bitopic ligands fail to stimulate b-arrestin recruitment. It seems that a quite voluminous molecular portion having a higher molecular weight than originating from the quaternary ammonium head at the orthosteric site is one of the prerequisite for β2-arrestin recruitment. The finding that the ligands' binding poses are determined by their allosteric building block may point towards a higher receptor subtype selectivity than that of other bitopic ligands.[201] Therefore, the whole set of bitopic ligands represents a useful toolbox of compounds to outline the chemical requirements for modulating the degree of β-arrestin recruitment and G protein activation and thus, facilitating the development of efficacious and selective drug candidates for the treatment of diseases such as Alzheimer and schizophrenia.

Material and Methods

Materials

A Chinese hamster ovary (CHO) cell line stably expressing hM1 was obtained from Wyeth Research (Princeton, NJ). 96 well round bottom and white 96 well plates were purchased from Thermo Fisher and from Greiner Bio One, Germany. Dulbecco's modified Eagle's medium (DMEM) and phosphate-buffered saline (PBS) were from Sigma (Schnelldorf, Germany). Leibovitz' L-15 medium (L-15) and Hank's balanced salt solution (HBSS) were from ThermoFisher (Dreieich Germany). Fetal calf serum (FCS), trypsin, and geneticin (G418) were from Merck Biochrom (Berlin, Germany). D-Luciferin was purchased as potassium salt from Pierce (ThermoFisher, Dreieich, Germany) and was dissolved in HBSS at a concentration of 400 mM. Puromycin was obtained from Invivogen (Toulouse, France). [3H]N-Methylscopolaime], 250 µCi (9.25 MBq) was purchased from PerkinElmer (Rodgau, Germany) and Polyethylenimine solution (1%, PEI) from Sigma (Schnelldorf, Germany). For chromatographic applications (HPLC, LC-MS), deionized water produced by means of a Milli-Q® system (Merck, Darmstadt, Germany) was used. HPLC grade and LC-MS grade solvents were from Sigma-Aldrich (Munich, Germany). Unless stated otherwise, all chemicals were purchased from Sigma-Aldrich

(Schnelldorf, Germany), VWR (Darmstadt, Germany), and TCI (Eschborn, Germany), and were used without prior purification.

General Medicinal Chemistry Methods

1H (400.132 MHz) and 13C (100.613 MHz) NMR spectra were recorded using a Bruker AV 400 NMR spectrometer (Bruker Biospin, Ettlingen, Germany). As an internal standard, the signals of the deuterated solvents were used (DMSO-d6: 1H 2.5 ppm, 13C 39.52 ppm; CDCl3: 1H 7.26 ppm, 13C 77.16 ppm). Abbreviations for data quoted are s, singlet; d, doublet; t, triplet; q, quartet; m, multiplet; b, broad; dd, doublet of doublets; dt, doublet of triplets; tt, triplet of triplets; and tq, triplet of quartets. Coupling constants (J) are given in Hz. The NMR signals were assigned polarization transfer experiments (DEPT) and two-dimensional experiments, such as 1H-1H correlation (COSY) and 1H-13C-proton-carbon heteronuclear correlation (HMQC, HMBC). TLC analyses were performed on silica gel 60 F254, C18 silica-coated aluminum panels ALUGRAM® RP-18W / UV254 and on pre-coated TLC-plates Alox-25/UV254 (Macherey-Nagel, Düren, Germany); the detection was made using UV light at 254 nm, intrinsic fluorescence at 366 nm or with ethanolic KMnO4, Dragendorff reagent, or phosphomolybdic acid ethanolic solution. For classical purification, column chromatography using silica gel with a grain size of 63-200 µm (Merck, Darmstadt, Germany). Flash chromatography on a puriFlash®430 system (Interchim, Montluçon, France) was performed using prepacked columns (Interchim, Montluçon, France) with silica gel filling (Particle size 30 microns or 50 microns) for normal phase or with C18-silica gel filling (Particle size 15 µm) for the reverse phase. The detection was carried out by means of a UV detector and Evaporative Light Scattering Detector (ELSD). Microwave assisted reactions were carried out using an MLS-rota PREP or synthWAVE instruments (Milestone). The LC-MS analyses of all the test compounds were performed using a Shimadzu LC-MS-2020 mass spectrometer (Shimadzu Deutschland GmbH, Duisburg, Germany) containing a DGU-20A3R degassing unit, an LC20AB liquid chromatograph and a SPD-20A UV/Vis detector and, an LC / MSD ion trap (Agilent Technologies, Waldbronn, Germany) connected to an Agilent 1100 modular system. A Synergi Fusion-RP (150 mm x 4.6 mm i.d., 4 µm; Phenomenex Ltd., Aschaffenburg, Germany) column and a gradient consisting of solvent A, water with 0.1% formic acid; solvent B, MeOH with 0.1% formic acid.

Solvent B was increased from 0% to 90% in 13 min, then decreased from to 5% in 1 min, and 5% for 4 min. The method was run with a flow rate of 1.0 mL/min, UV detection at 254 nm. All compounds were found to have a purity ≥ 95%. Mass spectra were recorded in ESI-positive mode and the data are reported as mass-to-charge ratio (m/z) of the corresponding positively charged molecular ions. Detailed syntheses and spectral data of intermediate and target compounds are reported in the supporting information (Data S1).

Cell culture

Chinese hamster ovary cells (CHO) stably expressing the hM1 receptor (CHO-hM1 cells) were cultured in Ham's nutrient mixture F-12 (HAM- F12) supplemented with 10 % (v/v) FCS (FCS), 100 U/ml penicillin, 100 µg/ml streptomycin, 0.2 mg/ml G418, and 2 mM L-glutamine at 37 °C in a 5 % CO2 humidified atmosphere. HEK293T cells stably co-transfected with the human M1 receptor and the Gαq-PLC-β3 sensor[192] were kindly provided by Timo Littmann (University of Regensburg). Cells were cultured in DMEM containing 10% FCS (full medium) at 37 °C in a water-saturated atmosphere containing 5% CO2 as reported previously.[192] HEK293T cells for BRET assays were cultured in DMEM high glucose medium containing 10% FCS, 2 mM glutamine, 500 units * ml-1 Penicillin and 0,5 mg *ml-1 Streptomycin.

Split-Luciferase Bioluminescence Assay

HEK293T cells stably co-transfected with the human M1 receptor and the Gαq-PLC-β3 sensor[192] were detached from a 75-cm2 flask by trypsinization and centrifuged (700 g for 5 min). The pellet was resuspended in assay medium consisting of L-15 with 5% FCS and the density of the suspension was adjusted to 1.25 · 106 cells/mL. Then, 80 µL of this suspension was seeded into each well of a 96 well plate, and the plate was subsequently incubated at 37 °C in a humidified atmosphere (without additional CO2) overnight. On the next day, 10 µL of a 10 mM D-Luciferin (Pierce) was added to the cells, and the plate was transferred into a pre-warmed microplate luminescence reader (Mithras LB 940 Multimode Microplate Reader, Berthold Technologies, Bad Wildbad, Germany). The cells were allowed to equilibrate inside the reader for 10 min before the basal luminescence was determined by recording the luminescence for the entire plate ten times with an integration time of 0.5 s per well. In the meantime, serial dilutions of agonists were prepared. The resulting solutions were also pre-warmed to 37 °C and subsequently added to the cells. Thereafter, luminescence was recorded for 15 plate repeats amounting

to a time period of 20 min. Negative controls (solvent) and positive controls (reference full agonist, carbachol (hM1R), eliciting a maximal response (100%) were included for subsequent normalization of the data. After acquisition of the data, the peak luminescence intensities obtained after stimulation were used for quantitative analysis using GraphPad Software (San Diego, CA, USA)

β-arrestin2-recruitment Assay

β-arrestin2-recruitment was determined by measuring BRET by using the NanoBRETTM system.[202] BRET was measured between a full length human M1 receptor N-terminally carrying a FLAG-tag and C-terminally carrying a Nano Luciferase. The β-arrestin2 was N-terminally modified with a HALO-tag and labeled with a HALO-618 fluorescent ligand (Promega, Mannheim, Germany). Therefore, 1*106 HEK293T cells were seeded in a 6 cm dish and after 20 hours transiently transfected with 1 µg receptor, 2 µg β-arrestin2 and 1 µg human GRK2 with the Effectene® transfection reagent in accordance to the user manual. 20 hours after transfection cells were transferred from 6 well plates to 96 well plates. Cells were counted and 20000 cells per well were seeded into white 96-well plates (Brand GmbH & Co KG, Wertheim, Germany). The next day BRET was measured using the Synergy Neo2 Hybrid Multi-Mode Reader (BioTek Instruments GmbH, Bad Friedrichshall, Germany), and the BRET ratio was corrected against buffer conditions. The highest ligand concentration tested was 100 µM due to limited solubility in the buffer used for BRET assays.

Computational analysis methods

All receptor-ligand docking experiments were carried out with the CCDCs software GOLD version 5.1.[203] A previously reported active homology model of M1 receptor, which is in accordance with the available active M1 receptor cryo-EM structure was used for docking[199]. All residues of the receptor core region and the extracellular loop regions were defined as potential binding site. Default settings were applied for receptor-ligand docking using GoldScore as primary scoring function. All docking poses and receptor-ligand interactions were analyzed with LigandScout 4.2[204], using a 3D-pharmacophore approach. The molecular dynamics simulations were carried out on GPUs (Nvidia RTX 2080 Ti) at the Freie Universität Berlin with Desmond 2018-3 following the previously published procedure[105]. Subsequently, the MD trajectories were analyzed with the software VMD[205], and a dynamic pharmacophore approach (dynophores) implemented in the LigandScout framework.[105,204,206]

Data Treatment

The binding data from individual experiments were analyzed by computer-aided nonlinear regression analysis using Prism 5 (GraphPad Software, San Diego, CA, USA). All sigmoidal concentration-response curves were obtained by fitting three-parameter (Hill slope constrained to 1) nonlinear regression curves (GraphPad Prism, San Diego, CA, USA). The BRET raw data were analyzed and corrected in Excel (Microsoft Corporation, WA, USA) and plotted in GraphPad Prism 7 (GraphPad Software, San Diego, CA, USA).

ASSOCIATED CONTENT

Supporting Information

The Supporting Information is available free of charge on the ACS Publications website. Synthesis and experimental data of target compounds, maximum agonist effect (Emax) and potency (pEC50) of bitopic compounds in Gα/PLC-β3 split-luciferase complementation assays, radioligand binding experiments, additional G protein-activation experiments for n-C4 compounds and a comparison of binding modes of bitopic ligands at the M1 and the M2 receptor are reported in the Supplemental Materials (PDF)

AUTHOR INFORMATION

Corresponding Author

* Address correspondence to Prof. Dr. Ulrike Holzgrabe, Department of Pharmaceutical and Medical Chemistry, Institute of Pharmacy, University of Würzburg, Am Hubland, 97074 Würzburg, Germany. E-mail address; ulrike.holzgrabe@uni-wuerzburg.de. Tel.: +49 931 31-85460

Author

Daniela Volpato - daniela.volpato@uni-wuerzburg.de; Michael Kauk - Michael.Kauk@med.uni-jena.de; Regina Messerer - regina.messerer@uni-wuerzburg.de; Marcel Bermudez - m.bermudez@fu-berlin.de; Gerhard Wolber - gerhard.wolber@fu-berlin.de ; Andreas Bock - Andreas.Bock@mdc-berlin.de; Carsten Hoffmann - c.hoffmann@toxi.uni-wuerzburg.de; Ulrike Holzgrabe - ulrike.holzgrabe@uni-wuerzburg.de.

Author Contributions

D.V., M.K., A.B., M.B., G.W., C.H., U.H. participated in research design. D.V., M.K., R.M., M.B. conducted experiments. D.V., M.K. contributed to new reagents or analytic tools and performed data

analysis. The manuscript was written by D.V., M.B., A.B., and U.H.. All authors have given approval to the final version of the manuscript.

Funding Sources

D.V. and M.K. were supported by the international doctoral college “Receptor Dynamics: Emerging Paradigms for Novel Drugs” funded within the framework of the Elite Network of Bavaria (grant number K-BM-2013-247). M.B. was supported by the Deutsche Forschungsgemeinschaft (German Research Foundation – DFG 407626949). A.B. acknowledges funding by the Deutsche Forschungsgemeinschaft (DFG, German Research Foundation) through SFB1423, project number 421152132, subproject C05. This publication was supported by the Open Access Publication Fund of the University of Wuerzburg.

Notes

The authors declare no competing financial interest.

ACKNOWLEDGMENT

Special thanks go to Dr. Timo Littmann for the kind concession of the cells expressing the Split-Luc construct.

ABBREVIATIONS

ACh, acetylcholine; AD, Alzheimer disease; BQCAd, benzyl quinolone carboxylic acid derivative; CCh carbachol; CHO, Chinese hamster ovary; DMEM, Dulbecco’s modified Eagle’s medium; FBS, fetal bovine serum; GPCR, G protein–coupled receptor; [3H]NMS, N-[3H]methylscopolamine; mAChR, muscarinic acetylcholine receptor; PAM, positive allosteric modulator; PLC phospholipase C; RLB radio ligand binding, SARs, structure−activity relationships; 7TMR, seven transmembrane receptor.

Supplemental Materials

Table of Contents

Chemistry

1) Data S1. Syntheses and experimental data of target compounds.

General Procedure for the Synthesis of the Quinolone-Isoxo Derivatives 3-C4, 3-C6, 3-C8, and 3-C10

To a solution of bromoalkyl 4-oxo-quinoline-3-carboxamides **C-C4**, **C-C6**, **C-C8**, and **C-C10** in acetonitrile (5 mL), 2 to 4 equivalents of isoxo-base and a catalytic amount of K_2CO_3 were added. The reaction was heated at 80 °C making use of microwave assistance. After completion of the reaction (4-48 h) controlled by TLC (CH_2Cl_2/MeOH = 85:15, R_f = 0.50 – 0.70), the mixture was cooled to room temperature. The solvent was distilled off. The so obtained solid was crystallized from acetonitrile, filtered and dried *in vacuo*. Compounds **3-C8** and **3-C10** were purified via column alumina chromatography using petroleum CH_2Cl_2/MeOH 9:1 as eluent system.

N-(4-(1-benzyl-6-fluoro-4-oxo-1,4-dihydroquinoline-3-carboxamido)butyl)-4-(isoxazol-3-yloxy)-N,N-dimethylbut-2-yn-1-aminium bromide ***3-C4***

Beige solid; 15% yield; mp 101-104 °C; R_f = 0.55 (MeOH/NH_4NO_2 (0.2 M) = 3:2); ^{1}H NMR ($CDCl_3$): 1.86-1.73 (m, 4H, NH-CH_2-C**H$_2$**-C**H$_2$**), 3.43 (s, 6H, $^+$N(C**H$_3$**)$_2$), 3.55-3.53, (m, 2H, NH-C**H$_2$**), 3.72- 3.66 (m, 2H, C**H$_2$**-N$^+$), 4.87 (s, 2H, ≡C-C**H$_2$**-N$^+$), 4.95 (s, 2H, O-C**H$_2$**-C≡), 5.53 (s, 2H, C**H$_2$**$_{benzyl}$), 6.03 (d, 2H, **H**-4$_{isoxo}$, *J*=1.8) 7.15- 7.14 (m, 2H, C**H**$_{phenyl}$), 7.46 - 7.36 (m, 5H, **H**-7, **H**-8, C**H**$_{phenyl}$), 8.12 (dd, 1H, **H**-5, *J* = 3.0, J_{HF} = 8.7), 8.18 (s, 1H, **H**-5 $_{isoxo}$, *J*=1.8), 8.95 (s, 1H, **H**-2), 10.09 (t, 1H, N**H**, *J* = 5.6). ^{13}C NMR ($CDCl_3$): 19.84, 26.58, 29.69, 37. 45, 50.68, 54.83, 57.18, 58.15, 63.74, 75.89, 86.86, 96.31, 112.01, 112.24, 119.26 (d, J_{CF} = 7.7), 121.50 (d, J_{CF} = 25.4), 123.19, 126.08, 128.83, 129.47, 129.71, 133.85, 135.84, 148.422, 158.70, 160.30, 165.85, 170.39, 176.58. MS (ESI) m/z [M]$^+$ Calcd for $C_{30}H_{32}FN_4O_4^+$: 531,24 Found: 530.7. LS-MS purity 96.58%.

6-(1-benzyl-6-fluoro-4-oxo-1,4-dihydroquinoline-3-carboxamido)-N-(4-(isoxazol-3-yloxy)but-2-yn-1-yl)-N,N-dimethylhexan-1-aminium bromide ***3-C6***

Ochre solid; 28% yield; mp 96-103 °C; R_f = 0.74 (MeOH/NH_4NO_2 (0.2 M) = 3:2); ^{1}H NMR ($CDCl_3$): 1.48-1.42 (m, 4H, NH-CH_2-C**H$_2$**-C**H$_2$**-C**H$_2$**), 1.68-1.64 (m, 2H, NH-CH_2-C**H$_2$**), 1.74-1.76 (m, 2H, NH-CH_2-CH_2-CH_2-C**H$_2$**), 3.48-3.45 (m, 8H, NH-C**H$_2$**, N$^+$(C**H$_3$**)$_2$), 3.66-3.72, (m, 4H, NH-C**H$_2$**, C**H$_2$**-N), 4.90 (s, 2H, ≡C-C**H$_2$**-N$^+$), 4.95 (s, 2H, O-C**H$_2$**-C≡), 5.50 (s, 2H, C**H$_2$**$_{benzyl}$), 6.03 (d, 2H, **H**-4$_{isoxo,}$ *J*=1.8), 7.13- 7.15 (m,

2H, C**H**$_{phenyl}$), 7.35-7.33 (m, 4H, **H**-8, C**H**$_{phenyl}$), 7.42 - 7.44 (m, 1H, **H**-7), 8.13 (dd, 1H, **H**-5, J = 3.0, J_{HF} = 8.8), 8.20 (d, 1H, **H**-5 $_{isoxo,}$ J=1.8), 8.93 (s, 1H, **H**-2), 9.96 (t, 1H, N**H**, J =5.6). ^{13}C NMR: ($CDCl_3$) 22.56, 25.61, 26.26, 29.16, 38.77, 50.63, 54.64, 57.15, 58.09, 64.10, 75.87, 86.79, 96.28, 111.93, 112.16, 119.26 (d, J_{CF} = 7.7), 121.61 (d, J_{CF} = 25.4), 126.06, 128.77, 129.42, 133.91, 135.83, 148.38, 158.63, 160.31, 164.72, 170.37, 176.00. MS (ESI) m/z $[M]^+$ Calcd for $C_{32}H_{35}FN_4O_4^+$: 559,27 Found: 559.5. LS-MS purity 96.86%.

1-((8-(1-benzyl-6-fluoro-4-oxo-1,4-dihydroquinoline-3-carboxamido)octyl)dimethyl-l4-azanyl)-4-(isoxazol-3-yloxy)but-2-yn-1-ylium bromide ***3-C8***

Ochre solid; 30% yield; mp 113-116 °C; R_f = 0.67 (MeOH/NH_4NO_2 (0.2 M) = 3:2); ^{1}H NMR ($CDCl_3$): 1.25-1.55 (m, 8H, NH-CH_2-CH_2-C**H$_2$**-C**H$_2$**-C**H$_2$**-C**H$_2$**), 1.64-1.71 (m, 4H, NH-CH_2-C**H$_2$**, C**H$_2$**-CH_2-N^+), 3.42 (s, 6H,N^+(C**H**$_3$)$_2$), 3.50-3.54 (m, 4H, NH-C**H$_2$**, C**H$_2$**-N^+), 4.84 (s, 2H, $^+$N-C**H$_2$**-C≡), 4.95 (s, 2H, O-C**H$_2$**-C≡), 5.50 (s, 2H, C**H$_2$**$_{benzyl}$), 6.03 (d, 2H, **H**-4$_{isoxo,}$ J=1.8), 7.13- 7.15 (m, 2H, C**H**$_{phenyl}$), 7.33-7.44 (m, 5H, **H**-7, **H**-8, C**H**$_{phenyl}$), 8.13-8.15 (m, 1H, **H**-5), 8.19 (s, 1H, **H**-5$_{isoxo}$), 8.92 (s, 1H, **H**-2), 9.94 (t, 1H, N**H**, J =5.6). ^{13}C NMR: ($CDCl_3$) 22.64, 24.06, 25.85, 26.64, 28.65, 28.67, 29.41, 39.01, 50.76, 53.66, 57.10, 58.11, 64.41, 75.72, 86.99, 96.31, 110.69, 111.77, 119.22 (d, J_{CF} = 8.1), 121.76 (d, J_{CF} = 23.4), 123.19, 126.07, 128.78, 129.43, 129.71, 129.85, 133.94, 148.35, 148.35, 155.69, 160.28, 164.64, 170.38, 176.05. MS (ESI) m/z $[M]^+$ Calcd for $C_{34}H_{39}FN_4O_4^+$: 587,30 Found: 587.6. LS-MS purity 95.04%.

10-(1-Benzyl-6-fluoro-4-oxo-1,4-dihydroquinoline-3-carboxamido)-N,N,N-trimethyldecan-1-aminium bromide ***3-C10***

Ochre solid; 30% yield; mp 108-110 °C; R_f = 0.71 (MeOH/NH_4NO_2 (0.2 M) = 3:2); ^{1}H NMR ($CDCl_3$): 1.22-1.41 (m, 12H, NH-CH_2-CH_2-C**H$_2$**-C**H$_2$**-C**H$_2$**-C**H$_2$**-C**H$_2$**-C**H$_2$**), 1.61-1.68 (m, 4H, NH-CH_2-C**H$_2$**, C**H$_2$**-CH_2-N^+), 3.44 (s, 6H,N^+(C**H**$_3$)$_2$), 3.46-3.58 (m, 4H, NH-C**H$_2$**, C**H$_2$**-N^+), 4.86 (s, 2H, $^+$N-C**H$_2$**-C≡), 4.95 (s, 2H, O-C**H$_2$**-C≡), 5.49 (s, 2H, C**H$_2$**$_{benzyl}$), 6.03 (d, 2H, **H**-4$_{isoxo,}$ J=1.8), 7.13- 7.15 (m, 2H, C**H**$_{phenyl}$), 7.33-7.44 (m, 5H, **H**-7, **H**-8, C**H**$_{phenyl}$), 8.13-8.15 (m, 1H, **H**-5), 8.17 (s, 1H, **H**-5$_{isoxo}$), 8.93 (s, 1H, **H**-2), 9.92 (t, 1H, N**H**, J =5.5). ^{13}C NMR: ($CDCl_3$) 22.76, 25.97,26.97, 28.93, 29.11, 29.54, 39.27, 50.71, 54.76, 57.13, 58.07, 64.40, 75.70, 86.91, 96.28, 111.97, 112.20, 119.17 (d, J_{CF} = 8.0), 121.4 (d, J_{CF} = 25.1), 126.05,

128.75, 129.40, 129.84, 129.92, 133.96, 135.82, 148.82, 158.59, 160.23, 161.06, 164.56, 170.37, 176.0. MS (ESI) m/z $[M]^+$ Calcd for $C_{36}H_{44}FN_4O_4^+$: 615.33. Found:615.15. LC-MC purity 98.17%.

General Procedure for the Synthesis of the Quinolone-Oxotremorine-M Derivatives **4-C4, 4-C6, 4-C8, and 4-C10**

The reaction was performed by combining bromoalkyl 4-oxo-quinoline-3-carboxamides **C-C4**, **C-C6**, **C-C8**, and **C-C10**, 2 to 5 equivalents of oxotremorineM-base and a catalytic amount of K_2CO_3 in acetonitrile (3 mL) using the microwave irradiation (80 °C). The reaction was completed after 4-24h and cooled to room temperature. TLC (CH_2Cl_2/MeOH = 85:15, R_f = 0.20 – 0.35). The solvent was evaporated under reduced pressure. The final compounds were purified by recrystallization in acetonitrile or by alumina chromatography, when crystallization was not feasible (CH_2Cl_2/MeOH 100:0→90:10 as eluent system).

*N-(4-(1-benzyl-6-fluoro-4-oxo-1,4-dihydroquinoline-3-carboxamido)butyl)-N,N-dimethyl-4-(2-oxopyrrolidin-1-yl)but-2-yn-1-aminium bromide 4**-C4***

Beige solid; 35% yield; mp 172-174 °C; R_f = 0.20 (MeOH/CH_2Cl_2 = 95:5); ^{1}H NMR (CD_3OD): 1.71-1.78 (m, 2H, NH-CH_2-C**H**$_2$),1.89-1.92 (m, 2H, NH-CH_2-CH_2-C**H**$_2$), 2.02-2.09 (m, 2H, **H**-4_{oxo}), 2.36 (t, 2H, **H**-3_{oxo}, *J*=8.1), 3.18 (s, 6H, N^+(C**H**$_3$)$_2$), 3.49-3.56 (m, 6H, N^+-C**H**$_2$, **H**-$5_{oxo,}$ NH-C**H**$_2$), 4.24 (s, 2H, **H**-6_{oxo}), 4.35 (s, 2H, **H**-9_{oxo}), 5.73 (s, 2H, C**H**$_{2benzyl}$), 7.24-7.26 (d, 2H, C**H**$_{phenyl}$), 7.32-7.39 (m, 3H, C**H**$_{phenyl}$), 7.54 (ddd, 1H, **H**-8, *J*=3.0, *J*=7.7, *J*=9.4), 7.83 (dd, 1H, **H**-7, *J*=4.3, *J*=9.4), 8.08 (dd, 1H, **H**-5 *J*=3.0, *J*=9.0), 9.03 (s, 1H, **H**-2).^{13}C NMR: (CD_3OD) 19.11, 21.62, 27.98, 31.90, 33.45, 39.49, 48.43, 51.60 55.70, 58.99, 65.45, 72.79, 88.62, 112.47 (d, J_{CF} =23.4), 122.41 (d, J_{CF} =8.2), 123.19 (d, J_{CF} =25.7), 128.14, 129.91, 130.73, 131.25, 136.80, 138.02, 150.54, 163.17, 167.54, 177.91, 206.43. MS (ESI) m/z $[M]^+$ Calcd for $C_{31}H_{36}FN_4O_3^+$: 531.28. Found: 531.10. HPLC purity 98.73%.

*((6-(1-benzyl-6-fluoro-4-oxo-1,4-dihydroquinoline-3-carboxamido)hexyl)(methyl)(4-(2-oxopyrrolidin-1-yl)but-2-yn-1-yl)-l4-azanyl)methylium bromide **4-C6***

Beige solid; 39% yield; mp 181-182 °C; R_f = 0.22 (MeOH/CH_2Cl_2 = 95:5); ^{1}H NMR (CD_3OD): 1.48-1.55 (m, 2H, NH-CH_2-C**H**$_2$),1.69-1.73 (m, 2H, NH-CH_2-CH_2-C**H**$_2$), 1.82-1.86 (m, 2H, NH-CH_2-CH_2-C**H**$_2$), 2.04-

2.08 (m, 2H, **H**-4_{oxo}), 2.36 (t, 2H, **H**-3_{oxo}, *J*=8.1), 3.16 (s, 6H, $N^+(C\mathbf{H_3})_2$), 3.42-3.47 (m, 2H, N^+-$C\mathbf{H_2}$), 3.49 (t, 2H, NH-$C\mathbf{H_2}$, *J*=6.8), 3.53 (t, 2H, **H**-5_{oxo}, *J*=7.1), 4.24 (s, 2H, **H**-6_{oxo}), 4.34 (t, 2H, **H**-9_{oxo}, *J*=1.7), 5.72 (s, 2H, $C\mathbf{H_{2benzyl}}$), 7.24-7.26 (m, 2H, $C\mathbf{H}_{phenyl}$), 7.29-7.39 (m, 3H, $C\mathbf{H}_{phenyl}$), 7.50-7.55 (m, 1H, **H**-8), 7.82 (dd, 1H, **H**-7, *J*=4.2, *J*=9.4), 8.07 (dd, 1H, **H**-5 *J*=3.0, *J*=9.0), 9.02 (s, 1H, **H**-2).^{13}C NMR: (CD_3OD) 18.69, 23.50, 26.87, 27.45, 30.21, 30.74, 31.48, 39.88, 48.32, 51.18, 55.15, 58.61, 65.41, 72.41, 88.10, 112.02 (d, J_{CF} =22.1), 121.97 (d, J_{CF} =8.1), 122.73 (d, J_{CF} =25.3), 127.70, 129.53, 130.30, 130.80, 136.38, 150.06, 162.71, 166.84, 177.46 (d, J_{CF} =17.5), 205.73. MS (ESI) m/z $[M]^+$ Calcd for $C_{33}H_{39}FN_4O_3^+$: 558.30. Found: 559.15. HPLC purity 98.05%.

1-benzyl-N-(8-(dimethyl(4-(2-oxopyrrolidin-1-yl)but-2-yn-1-yl)-l4-azanyl)octyl)-6-fluoro-4-oxo-1,4-dihydroquinoline-3-carboxamide ***4-C8***

Beige solid; 16% yield; mp 174-178 °C; R_f = 0.27 ($MeOH/CH_2Cl_2$ = 95:5); ^{1}H NMR (CD_3OD): 1.29-1.31 (m, 4H, NH-CH_2-CH_2-CH_2-$C\mathbf{H_2}$-$C\mathbf{H_2}$), 1.43-1.46 (m, 4H, NH-CH_2-CH_2-$C\mathbf{H_2}$-CH_2-CH_2-$C\mathbf{H_2}$), 1.67-1.68 (m, 2H, NH-CH_2-$C\mathbf{H_2}$, $C\mathbf{H_2}$-CH_2-N^+), 2.05-2.11 (m, 2H, **H**-4_{oxo}), 2.37 (t, 2H, **H**-3_{oxo}, *J*=8.1), 3.13 (s, 6H,$N^+(C\mathbf{H_3})_2$), 3.38-3.42 (m, 2H, N^+-$C\mathbf{H_2}$), 3.47 (t, 2H, NH-$C\mathbf{H_2}$, *J*=6.7), 3.53 (t, 2H, **H**-5_{oxo}, *J*=7.1), 4.23 (s, 2H, **H**-6_{oxo}), 4.32 (s, 2H, **H**-9_{oxo}), 5.71 (s, 2H, $C\mathbf{H_{2benzyl}}$), 7.25-7.27 (m, 2H, $C\mathbf{H}_{phenyl}$), 7.31-7.38 (m, 3H, $C\mathbf{H}_{phenyl}$), 7.50-7.55 (m, 1H, **H**-8), 7.81 (dd, 1H, **H**-7, *J*=4.1, *J*=9.5), 8.07 (dd, 1H, **H**-5 *J*=2.8, *J*=9.5), 9.01 (s, 1H, **H**-2).^{13}C NMR: (CD_3OD) 18.28, 23.13, 25.57, 26.76, 27.51, 29.60, 30.05, 31.04, 32.57, 39.67, 47.82, 50.67, 54.65, 58.19, 65.06, 71.95, 87.66, 111.61 (d, J_{CF} =23.2), 121.4, 121.53 (d, J_{CF} =7.4), 122.42 (d, J_{CF} =25.8), 127.00, 127.26, 129.10, 129.87, 135.97, 149.65, 162.26, 166.37, 176.46 (d, J_{CF} =115.4), 206.50. MS (ESI) m/z $[M]^+$ Calcd for $C_{35}H_{44}FN_4O_3^+$: 587,34. Found: 587.20. HPLC purity 98.17%.

((10-(1-benzyl-6-fluoro-4-oxo-1,4-dihydroquinoline-3-carboxamido)decyl)(methyl)(4-(2-oxopyrrolidin-1-yl)but-2-yn-1-yl)-l4-azanyl)methylium bromide ***4-C10***

White solid; 27% yield; mp 169-172 °C; R_f = 0.33 ($MeOH/CH_2Cl_2$ = 85:15); ^{1}H NMR (CD_3OD): 1.39-1.49 (m, 12H, NH-CH_2-CH_2-$C\mathbf{H_2}$-$C\mathbf{H_2}$-$C\mathbf{H_2}$-$C\mathbf{H_2}$-$C\mathbf{H_2}$-$C\mathbf{H_2}$), 1.64-1.68 (m, 2H, NH-CH_2-CH_2-CH_2-CH_2-CH_2-CH_2-CH_2-CH_2-$C\mathbf{H_2}$), 1.77-1.79 (m, 2H, NH-CH_2-$C\mathbf{H_2}$), 2.06-2.10 (m, 2H, **H**-4_{oxo}), 2.38 (t, 2H, **H**-3_{oxo}, J=8.1), 3.17 (s, 6H,$N^+(C\mathbf{H_3})_2$), 3.38-3.42 (m, 2H, N^+-$C\mathbf{H_2}$), 3.46 (t, 2H, NH-$C\mathbf{H_2}$, *J*=6.9), 3.55 (t, 2H, **H**-

5_{oxo}, *J*=7.1), 4.24 (s, 2H, **H**-6_{oxo}), 4.33 (s, 2H, **H**-9_{oxo}), 5.72 (s, 2H, C$\mathbf{H_{2benzyl}}$), 7.24-7.26 (m, 2H, C$\mathbf{H}_{phenyl}$), 7.29-7.39 (m, 3H, C$\mathbf{H}_{phenyl}$), 7.53 (ddd, 1H, **H**-8, *J*=3.1. *J*=7.8, *J*=9.4), 7.81 (dd, 1H, **H**-7, *J*=3.0, *J*=9.0), 8.08 (dd, 1H, **H**-5 *J*=3.0, *J*=9.0), 9.02 (s, 1H, **H**-2).^{13}C NMR: (CD_3OD) 18.71, 23.63, 27.29, 28.11, 30.11, 30.32, 30.37, 30.45, 30.55, 34.49, 33.01, 40.18, 50.10, 51.12, 55.13, 58.63, 65.52, 72.39, 88.07, 112.05 (d, J_{CF} =24.4), 121.90, 121.9 (d, J_{CF} =8.1), 122.69 (d, J_{CF} =25.5), 127.67, 129.51, 130.29, 130.77 (d, J_{CF} =7.1), 136.39, 137.57, 150.07, 162.69, 166.77, 177.46, 208.90. MS (ESI) m/z $[M]^+$ Calcd for $C_{37}H_{47}FN_4O_3^+$: 614.36. Found: 615.25. HPLC purity 95.67%.

Pharmacology

2) Data S2. Maximum agonist effect and potency of bitopic compounds in Gα/PLC-β3 split-luciferase complementation assays.

Compound	Split-Luc Assay		
	E_{max}	pEC_{50}	n
1-C4	105.10 ± 2.45	7.40 ± 0.08	**3**
1-C6	71.23 ± 3.27	6.92 ± 0.13	**6**
1-C8	112.00 ± 2.39	8.09 ± 0.08	**3**
1-C10	62.59 ± 4.43	6.01 ± 0.16	**4**
iperoxo	104.60 ± 0.85	8.89 ± 0.04	**4**
2-C4	86.76 ± 1.69	5.79 ± 0.04	**3**
2-C6	57.10 ± 4.46	5.32 ± 0.12	**4**
2-C8	60.08 ± 1.53	6.30 ± 0.06	**3**
2-C10	45.76 ± 2.10	6.47 ± 0.11	**6**
ACh	96.91 ± 1.28	6.88 ± 0.02	**9**
3-C4	34.98 ± 1.25	6.35 ± 0.09	**3**
3-C6	80.36 ± 8.74	6.33 ± 0.27	**3**
3-C8	51.05 ± 1.43	6.74 ± 0.08	**3**
3-C10	54.69 ± 5.56	5.11 ± 0.17	**4**
Isoxo	69.01 ± 3.26	8.25 ± 0.20	**3**
4-C4	88.97 ± 2.16	6.76 ± 0.07	**3**
4-C6	55.86 ± 2.32	6.11 ± 0.11	**4**
4-C8	76.90 ± 1.92	7.31 ± 0.11	**3**
4-C10	50.95 ± 2.03	6.16 ± 0.13	**3**
Oxotremorine-M	71.82 ± 3.56	8.20 ± 0.18	**3**
5-C4	75.44 ± 0.94	6.08 ± 0.04	**3**
5-C6	103.80 ± 4.19	6.03 ± 0.09	**5**
5-C8	98.56 ± 1.56	7.69 ± 0.06	**3**
5-C10	87.51 ± 2.88	6.99 ± 0.10	**5**
CCh	97.78 ± 1.71	6.25 ± 0.04	**5**

TABLE S1. Maximum agonist effect and potency of bitopic compounds derived from concentration-response curves of Gα and PLC-β3 complementation displayed in Figures 1-2 of the main text. Data are expressed as the means ± S.E.M. of 3-6 independent experiments performed in triplicate.

3) Data S3. Radioligand binding experiments: Methods and results

Membrane Preparation

Stably transfected CHO cells overexpressing the human M1 mAChR subtype were grown to a confluence of approx. 80%. Cells were harvested by gently scraping in ice-cold harvesting buffer (20 mM HEPES, 10 mM Na_2EDTA, pH= 7.4). The collected cells were homogenized twice on ice for 25 seconds at level 6 using a polytron homogenizer and the resulting cell fragments were centrifuged using the rotor JA25.50 at 40,000 g for 10 minutes (4 °C). The supernatant was aspirated, and the pellet resuspended in ice-cold storage buffer (20 mM HEPES, 0.1 mM Na_2EDTA, pH= 7.4). This step was repeated twice, and finally the pellets were resuspended in ice-cold assay buffer (10 mM HEPES, 10 mM $MgCl_2$, 100 mM NaCl, pH= 7.4). Aliquots were filled in reaction tubes, frozen quickly in liquid nitrogen, and stored at -80 °C until use. The protein concentration was approximately 2 mg/ml, determined using the Pierce™ BCA Protein Assay Kit according to the manufacturer's instructions.

Radioligand Binding Experiments

Radioligand binding experiments using CHO-hM1 membranes were performed in round bottom 96-well microtiter plates applying 20 µg protein/well. Experiments were conducted at room temperature using [^{3}H]NMS as the radioactive probe (2 nM for [^{3}H]NMS dissociation and 0.2 nM for equilibrium binding experiments). The plate was incubated at room temperature using a microplate shaker (Titramax 101 Platform Shaker, Heidolph) with an incubation time ranging from 1 h for the dissociation to 24 h for the equilibrium experiments. Homologous competition assays were performed as controls to determine the affinity of NMS for M1 receptors (pK_D = 8.88±0.06, n=5).[207] Nonspecific binding was determined in the presence of an excess of atropine (10 µM). Binding reactions were terminated by rapid filtration through glass fiber mats previously soaked with a 1% polyethyleneimine solution in a cell harvester filtration device. After filtration, the filter mats were washed with ice-cold wash water, covered with melt-on scintillator sheets on a heating block, and the radioactivity was counted in a Perkin Elmer MicroBeta 2450 Microplate Counter. The inhibition constants K_i of receptors for the studied compounds were determined in competition experiments in which membranes were incubated in the presence of a constant concentration of 0.2 nM [^{3}H]NMS and increasing concentrations of the competitor. The

incubation lasted 24 h to achieve full equilibrium. Two-point kinetic experiments with measurements of [^{3}H]NMS binding at t = 0 and t = 20 min were performed. By means of two-point dissociation experiments,[208] the dissociation rate constant k_{-1} can be determined by measuring the specific binding just before the start of the dissociation reaction (t = 0, adding a competitive antagonist in excess) and at a predetermined time t during the dissociation process (t = 20 min), as described previously[208].

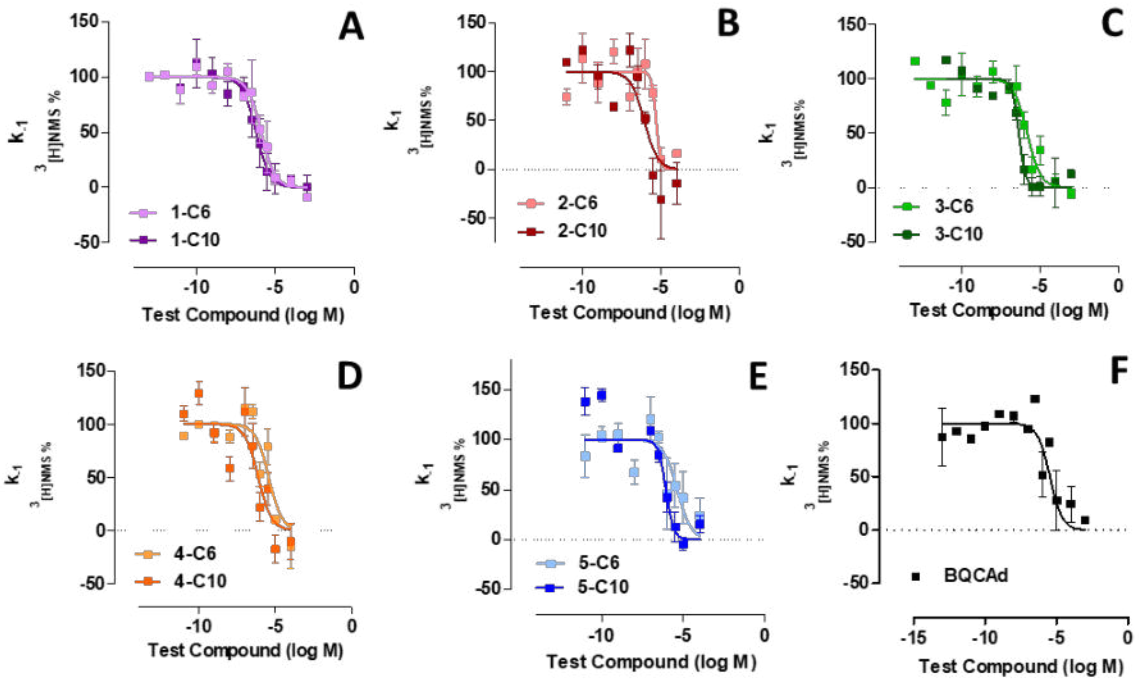

Figure S1. Allosteric effects of the bitopic ligands **1-Cn** (panel **A**), **2-Cn** (panel **B**), **3-Cn** (panel **C**), **4-Cn** (panel **D**), **5-Cn** (panel **E**) and their corresponding allosteric moiety BQCAd (Panel F) as reflected by the inhibition of [^{3}H]NMS dissociation from M1 receptors in CHO-hM1 membranes. The allosteric effect is expressed as the ratio of the rate of [^{3}H]NMS dissociation in the presence of compound relative to the rate of dissociation of [^{3}H]NMS in the absence of test compound expressed in percent k^{-1}. The inflection point represents the concentration that retards the radioligand dissociation by half and is therefore equal to the $IC_{50,diss}$ value. Data represent mean ± S.E.M. from three to four independent two-point kinetic experiments, conducted in quadruplicate.

Table S2. $pIC_{50,diss}$ values of bitopic ligands with a chain of 6 and 10 methylene units at M1R obtained from radioligand dissociation binding experiments.

Compound	Radioligand binding [3H]NMS Dissociation pIC_{50}	Compound	Radioligand binding [^{3}H]NMS Dissociation pIC_{50}
1-C6	5.89 ± 0.09	**1-C10**	6.22±0.08
2-C6	5.23 ± 0.16	**2-C10**	6.07±0.19
3-C6	5.81 ± 0.09	**3-C10**	6.34±0.08
4-C6	5.57 ± 0.09	**4-C10**	6.11±0.09
5-C6	5.43 ± 0.13	**5-C10**	6.12±0.14

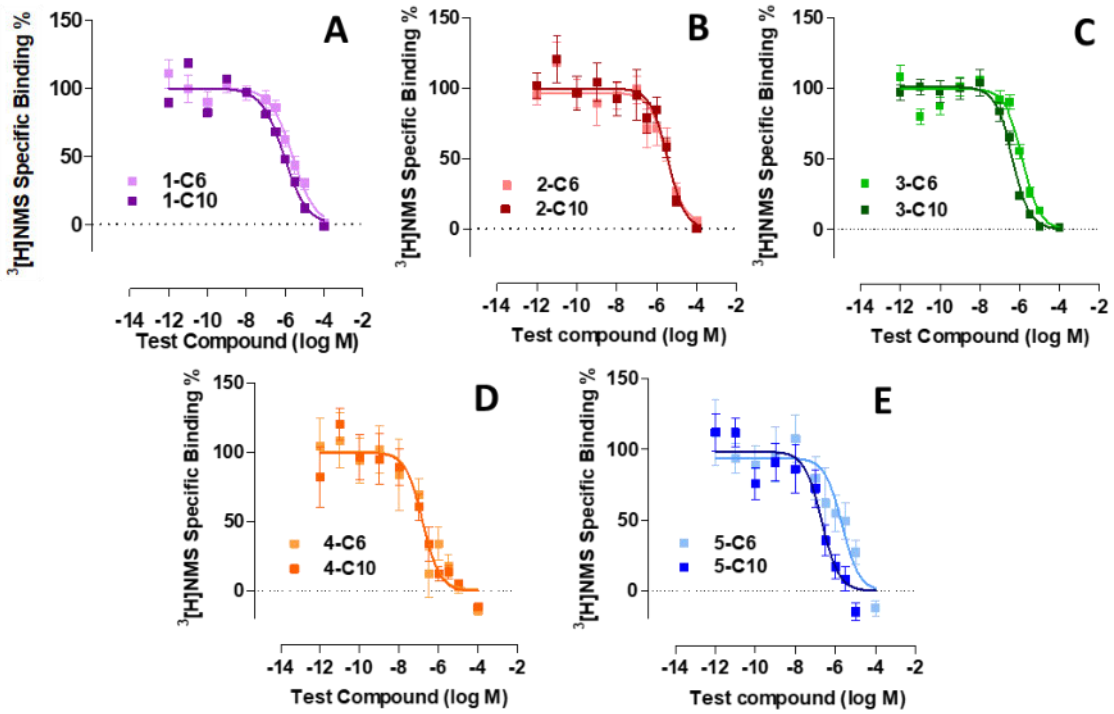

Figure S2. Effect of increasing concentrations of bitopic ligands **1-Cn** (panel **A**), **2-Cn** (panel **B**), **3-Cn** (panel **C**), **4-Cn** (panel **D**), **5-Cn** (panel **E**) on specific equilibrium binding of [^{3}H]NMS in CHO-hM1 membranes. Data represent mean ± S.E.M. from 3–5 independent experiments, conducted in quadruplicate.

Table S3. pIC50 and pKi values for bitopic ligands obtained from radioligand binding experiments.

Compound	Radioligand binding [^{3}H]NMS Equilibrium	Compound	Radioligand binding [^{3}H]NMS Equilibrium
1-C6	pKi 5.93 pIC_{50} 5.52±0.06	**1-C10**	pKi 6.34 pIC_{50} 5.59±0.06
2-C6	pKi 5.86 pIC_{50} 5.46±0.19	**2-C10**	pKi 5.82 pIC_{50} 5.45±0.18
3-C6	pKi 6.32 pIC_{50} 5.90±0.08	**3-C10**	pKi 6.75 pIC_{50} 6.34±0.08
4-C6	pKi 7.22 pIC_{50} 6.79±0.26	**4-C10**	pKi 7.20 pIC_{50} 6.79±0.18
5-C6	pKi 6.13 pIC_{50} 5.68±0.25	**5-C10**	pKi 6.69 pIC_{50} 6.68±0.17

3) Standards agonists and PAMs results in equilibrium and dissociation radioligand binding at M1R and their comparison with values reported in literature.

Table S4. Radioligand binding affinities of standard agonists and [3H]NMS dissociation rates expressed as p$IC_{50,diss}$. The inflection point represents the concentration that retards the radioligand dissociation by half and is therefore equal to the IC50 value. Graphs not shown.

Radioligand binding [^{3}H]NMS			
Compound	**Dissociation p$IC_{50,diss}$**	**Compound**	**Equilibrium**
BQCAd	5.47 ± 0.21 (Lit. 4.26 ± 1.32)[82]	**Iperoxo**	pKi 6.13 pIC_{50} 5.93 ± 0.06 (Lit. 5.67 ± 0.65)[82]
BQCA	5.32 ±0.14	**ACh**	(Lit. 4.32 - 4.76)[82,209]
		Isoxo	pKi 5.90 pIC_{50} 5.49 ± 0.10
		Oxo-M	pKi 6.13 pIC_{50} 5.74 ± 0.33 (Lit. 5.09 ± 0.13)[209]
		CCh	(Lit. 3.17 - 4.46)[209–211]

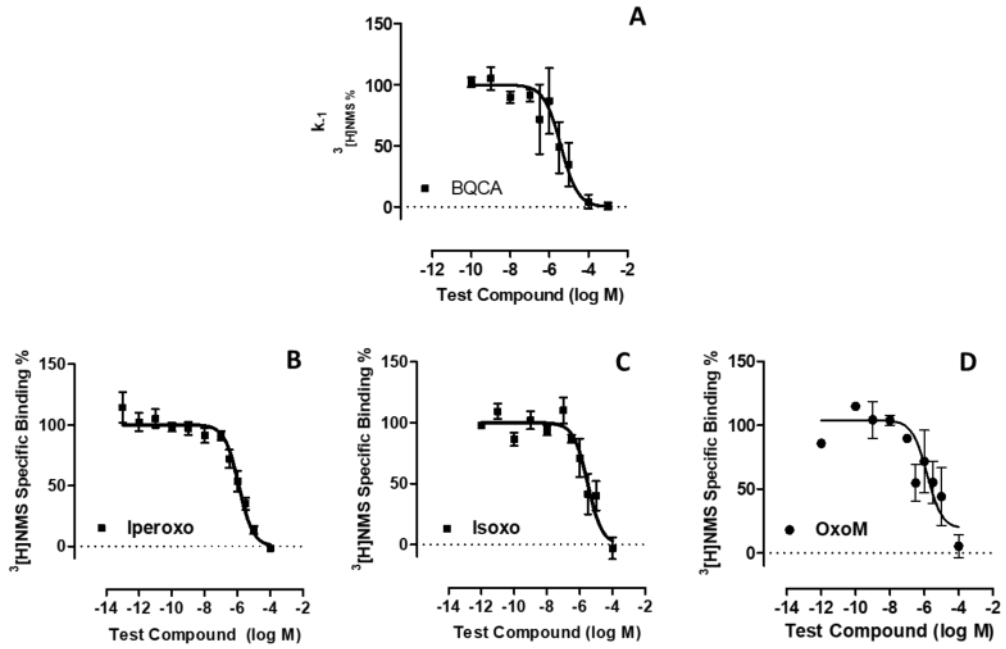

Figure S3.

A. Result for the BQCA allosteric modulator retarding [^{3}H]NMS radioligand dissociation (panel **A**) from M1 receptors in CHO-hM1 membranes. The allosteric effect is expressed as the ratio of the rate of [^{3}H]NMS dissociation in the presence of compound relative to the rate of dissociation of [^{3}H]NMS in the absence of test compound expressed in percent k^{-1}. The inflection point represents the concentration that retards the radioligand dissociation by half and is therefore equal to the $IC_{50,diss}$ value.

B, C, D. Effect of increasing concentrations of agonists (iperoxo (panel **B**), Isoxo (panel **C**), Oxo-M (panel **D**)) on specific equilibrium binding of [^{3}H]NMS in CHO-hM1 membranes. Data represent mean ± S.E.M. from 3–5 independent experiments, conducted in quadruplicate.

4) **Figure S4.** Dose-response evaluation of **n-C4** in G protein-activation assay.

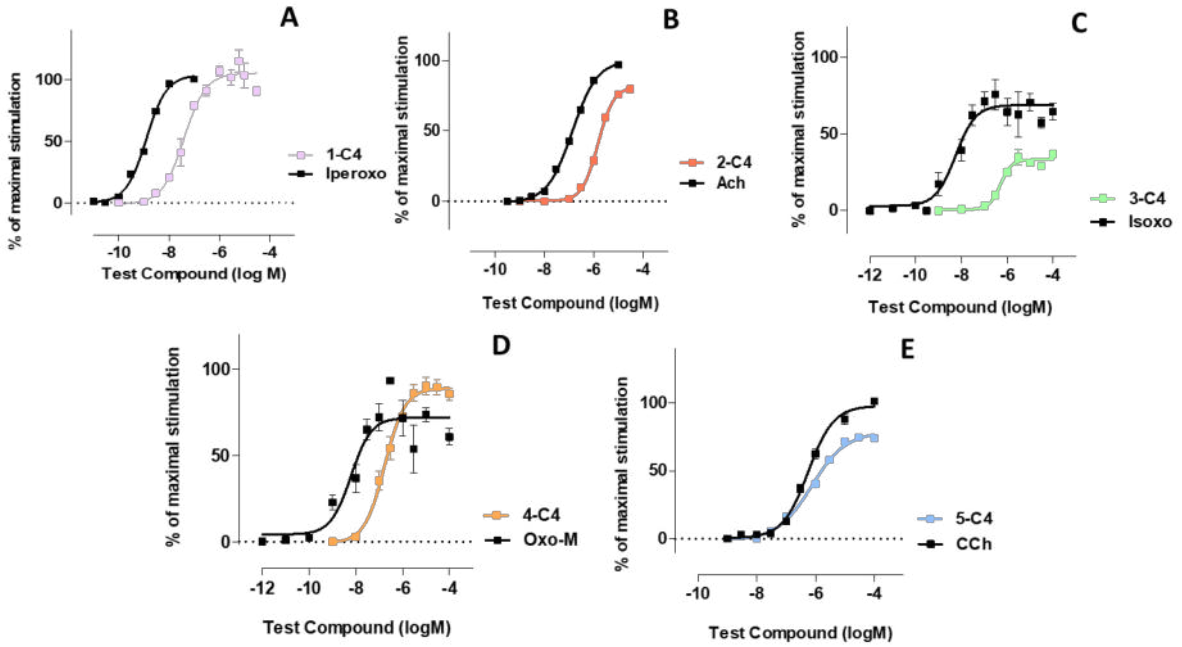

Figure S4. Gα/PLC-β3 split-luciferase interaction assay in HEK293T cells expressing the human muscarinic M1 receptors (hM1). Concentration-response-curves for the reference compound iperoxo (panel **A**), Ach (panel **B**), Isoxo (panel **C**), Oxo-M (panel **D**), Carbachol (CCh) (panel **E**), whose maximum stimulation was defined as 100% and for **n-C4** derivatives. Data represent means ± SEM of 3-6 experiments conducted in triplicate.

Figure S5. Binding mode comparison of dualsteric ligands at the M1 and the M2 receptor

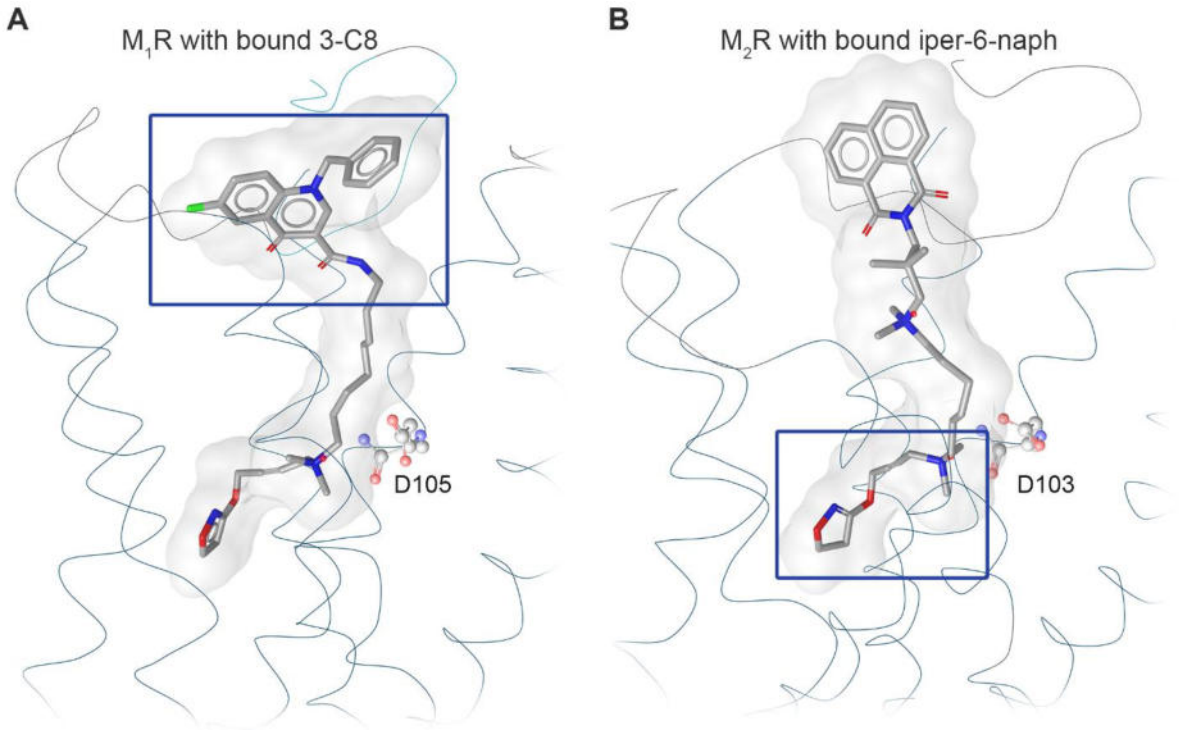

Figure S5. Comparison of proposed binding modes for bitopic (dualsteric) ligands at the M1 (A) and the M2 receptor (B). We suggest that the more specific building blocks (blue frames) control the orientation of the less specific moieties. BQCA and its derivatives have been previously shown to be highly selective for M1 receptors,[106,212] due to subtype specific allosteric vestibules. Although the highly conserved orthosteric binding pocket, iperoxo shows a ten-fold higher affinity to M2 compared to M1 receptors.[213] Due to the flexibility of the linker, the less specific part of the molecule can adopt an optimal position based on steric requirements and interaction possibilities. This allows for more structural variations of the less specific building block. While BQCA derived bitopic ligands haven't been shown to act via M2 receptors, we recently demonstrated that bitopic ligands of the phth- and naph series (e.g. iper-6-phth, or iper-6-naph) can function via M1 receptors.[193] M2 receptor figure was readapted from previous study.[194]

2. Introducing a positively charged pyrrolidine ring in the dualsteric M1 hybrids: Oxotremorine-BQCAd compounds

Introduction

The M1 muscarinic receptor has been identified as an important drug target which may be addressed for the treatment of Alzheimer's disease (AD) and schizophrenia.[143,166] The M1 muscarinic receptor is predominantly expressed in the central nervous system (CNS), especially in the amygdala, hippocampus, cerebral cortex, and striatum[164,165] where it contributes to essential cognitive functions such as memory and learning. Additionally, it is associated with M1 receptors' rescue in neurodegenerative diseases in mouse models.[94,171–173] Although clinically important, potential treatment of neurodegenerative diseases with M1 ligands have proven challenging, mostly due to the severe adverse effects associated with a lack of selectivity of available orthosteric M1 agonists.[201]

Five muscarinic receptors subtypes (M1-M5), associated with very diverse physiological roles, have been cloned.[154,155] The binding site of the endogenous neurotransmitter acetylcholine, synthetic agonists, and antagonists is located deeply inside the transmembrane helical bundle.[156,157] All subtypes of muscarinic receptors share a high sequence identity of their orthosteric binding pocket, making it difficult to discover ligands which are selective for one of the different receptor subtypes.[158] New strategies for more selective ligands have been explored by combining the activation or inhibition properties of orthosteric ligands with the advantages of simultaneously targeting an allosteric site, which is structurally diverse between the different receptor subtypes. These so-called bitopic ligands may prove beneficial due to selective activation of specific receptor subtypes.[25,57,176,177] Previously, we have synthesized bitopic agonists for the M1 receptor which consist of the M1R-selective allosteric moiety BQCAd[106,180,181] and the orthosteric agonist iperoxo.[182,183] Structure-activity-relationship studies suggested that the potency and efficacy of bitopic agonists strongly depend on linker length, geometry between the orthosteric and allosteric moieties, and the substitution pattern of the allosteric moiety.[82,83] Further, partial bitopic agonists for the M1R consisting of orthosteric moieties systematically varied and a portion of the quinolone benzyl carboxylic acid were developed and characterized.[82,83,111] Afterwards

also the non-selective agonist Oxotremorine (**2**) was investigated as an orthosteric fragment in the progressive study of bitopic ligands. The new sets of compounds were tested in a broad spectrum of assays investigating different aspects of receptor activation, signaling cascades, receptor movement, binding affinity, and dissociation rates.

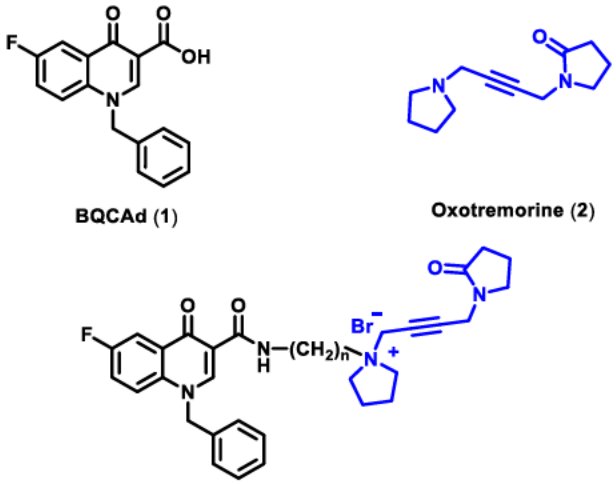

Figure 1: Structures of BQCAd (benzyl quinolone carboxylic acid derivative) (**1**), Oxotremorine (**2**) and of the new hybrid derivatives.

Material and Methods

Materials

Chinese hamster ovary (CHO) cell line stably expressing *h*M1 was obtained from Wyeth Research (Princeton, NJ). 96 well round bottom plates, and white 96 well plates were purchased from Thermo Fisher and from Greiner Bio One, Germany. Dulbecco's modified Eagle's medium (DMEM) and phosphate-buffered saline (PBS) were from Sigma (Schnelldorf, Germany). Leibovitz' L-15 medium (L-15) and Hank's balanced salt solution (HBSS) were from ThermoFisher (Dreieich Germany). Fetal calf serum (FCS), trypsin, and geneticin (G418) were from Merck Biochrom (Berlin, Germany). D-Luciferin was purchased as potassium salt from Pierce (ThermoFisher, Dreieich, Germany) and was dissolved in HBSS at a concentration of 400 mM. Puromycin was obtained from Invivogen (Toulouse, France).

[3H]N-Methylscopolaime]-, 250 µCi (9.25 MBq) was purchased from PerkinElmer (Rodgau, Germany) and Polyethylenimine solution (1%, PEI) from Sigma (Schnelldorf, Germany). For chromatographic applications (HPLC, LC-MS), deionized water produced by means of a Milli-Q® system (Merck, Darmstadt, Germany) was used. HPLC grade and LC-MS grade solvents were from Sigma-Aldrich (Munich, Germany). Unless stated otherwise, all chemicals were purchased from Sigma-Aldrich (Schnelldorf, Germany), VWR (Darmstadt, Germany), and TCI (Eschborn, Germany), and were used without prior purification.

General Medicinal Chemistry Methods

^{1}H (400.132 MHz) and ^{13}C (100.613 MHz) NMR spectra were recorded using a Bruker AV 400 NMR spectrometer (Bruker Biospin, Ettlingen, Germany). As an internal standard, the signals of the deuterated solvents were used (DMSO-d6: 1H 2.5 ppm, 13C 39.52 ppm; CDCl3: 1H 7.26 ppm, 13C 77.16 ppm). Abbreviations for data quoted are s, singlet; d, doublet; t, triplet; q, quartet; m, multiplet; b, broad; dd, doublet of doublets; dt, doublet of triplets; tt, triplet of triplets; and tq, triplet of quartets. Coupling constants (J) are given in Hz. The NMR signals were assigned polarization transfer experiments (DEPT) and two-dimensional experiments, such as ^{1}H-^{1}H correlation (COSY) and ^{1}H-^{13}C-proton-carbon heteronuclear correlation (HMQC, HMBC). TLC analyses were performed on silica gel 60 F254, C18 silica-coated aluminum panels ALUGRAM® RP-18W / UV254 and on pre-coated TLC-plates Alox-25/UV254 (Macherey-Nagel, Düren, Germany); the detection was made using UV light at 254 nm, intrinsic fluorescence at 366 nm or with ethanolic $KMnO_4$, Dragendorff reagent, or phosphomolybdic acid ethanolic solution. For classical purification, column chromatography using silica gel with a grain size of 63-200 µm (Merck, Darmstadt, Germany). Flash chromatography on a puriFlash®430 system (Interchim, Montlucon, France) was performed using prepacked columns (Interchim, Montluçon, France) with silica gel filling (Particle size 30 microns or 50 microns) for normal phase or with C18-silica gel filling (Particle size 15 µm) for the reverse phase. The detection was carried out by means of a UV detector and Evaporative Light Scattering Detector (ELSD). Microwave assisted reactions were carried out using a MLS-rota PREP or synthWAVE instruments (Milestone).

The LC-MS analyses of all the test compounds were performed using a Shimadzu LC-MS-2020 mass spectrometer (Shimadzu Deutschland GmbH, Duisburg, Germany) containing a DGU-20A3R degassing unit, an LC20AB liquid chromatograph and a SPD-20A UV/Vis detector and, an LC / MSD ion trap (Agilent Technologies, Waldbronn, Germany) connected to an Agilent 1100 modular system. A Synergi Fusion-RP (150 mm x 4.6 mm i.d., 4 µm; Phenomenex Ltd., Aschaffenburg, Germany) column and a gradient consisting of solvent A, water with 0.1% formic acid; solvent B, MeOH with 0.1% formic acid. Solvent B was increased from 0% to 90% in 13 min, then decreased from to 5% in 1 min, and 5% for 4 min. The method was run with a flow rate of 1.0 mL/min, UV detection at 254 nm. All compounds were found to have a purity ≥ 95%. Mass spectra were recorded in ESI-positive mode and the data are reported as mass-to-charge ratio (m/z) of the corresponding positively charged molecular ions.

Cell culture

Chinese hamster ovary cells (CHO) stably expressing the hM1 receptor (CHO-hM1 cells) were cultured in Ham's nutrient mixture F-12 (HAM- F12) supplemented with 10 % (v/v) FCS (FCS), 100 U/ml penicillin, 100 µg/ml streptomycin, 0.2 mg/ml G418, and 2 mM L-glutamine at 37 °C in a 5 % CO_2 humidified atmosphere. HEK293T cells stably co-transfected with the human M1 receptor and the $G\alpha_q$-PLC-β3 sensor[192] were kindly provided by Timo Littmann (University of Regensburg). Cells were cultivated in DMEM containing 10% FCS (full medium) at 37 °C in a water-saturated atmosphere containing 5% CO_2 as reported previously.[192] HEK293T cells for BRET assays were cultivated in DMEM high glucose medium containing 10% FCS, 2 mM glutamine, 500 units * ml^{-1} Penicillin and 0,5 mg *ml^{-1} Streptomycin. HEK 293 cells stably expressing the M1-I3N-CFP receptor FRET sensor were maintained in DMEM with 4.5 g L^{-1} 10% (v/v) FCS, 100 U mL^{-1} penicillin, 100 µg mL^{-1} streptomycin sulfate and 2mM L-glutamine, and 200 µg mL^{-1} G-418. The cells were kept at 37 °C in a humidified 7% CO_2 atmosphere.

Membrane Preparation

CHO-hM1 cells were grown adherently to a confluence of approx. 80%. The cells were harvested by gently scraping in ice-cold harvesting buffer (20 mM HEPES, 10 mM Na_2EDTA, pH= 7.4). The collected cells were homogenized on ice twice for 25 seconds at level 6 using a polytron homogenizer and the

resulting cell fragments were centrifuged using the rotor JA25.50 at 40 000 g for 10 minutes (4 °C). The supernatant was aspirated, and the pellet resuspended in ice-cold storage buffer (20 mM HEPES, 0.1 mM Na_2EDTA, pH= 7.4). This step was repeated twice, and finally the pellets were resuspended in ice-cold assay buffer (10 mM HEPES, 10 mM $MgCl_2$, 100 mM NaCl, pH= 7.4). Aliquots were filled in eppendorf tubes, quickly frozen and stored at -80 °C. The protein concentration was of approximately 2 mg/mL, determined using the Pierce™ BCA Protein Assay Kit. The absorbance of the bicinchoninic acid (BCA)/copper complex after the occurrence of the biuret reaction was measured at 562 nm using a UV-Photometer (Synergy™ Neo2 Multi-Mode Microplate, Reader). Values obtained were plotted on a linear calibration curve whereby the protein content was determined.

Radioligand Binding Experiments

Radioligand binding experiments using CHO-hM1 membranes were performed in round bottom 96-well microtiter plates applying 20 µg protein/well. Experiments were conducted at room temperature using [^{3}H]NMS as the radioactive probe (2 nM for [^{3}H]NMS dissociation and 0.2 nM for equilibrium binding experiments). The plate was incubated at room temperature using a microplate shaker (Titramax 101 Platform Shaker, Heidolph) with an incubation time ranging from 1 h for the dissociation to 24 h for the equilibrium experiments. Homologous competition assays were utilized to determine pKd at hM1 for NMS 8.88 and conformed to homologous binding assumptions.[207] Nonspecific binding was determined in the presence of atropine excess. Incubation performed in the assay buffer was terminated by filtration through glass fiber mats, previously coated with a 1% polyethylenimine solution, in a cell harvester filtration device. After filtration, the filter mats were washed with ice-cold wash water, covered with melt-on scintillator sheets on a heating block and the radioactivity was counted in a Perkin Elmer MicroBeta 2450 Microplate Counter. The inhibition constants K_i of receptors for the studied compounds were determined in competition experiments in which membranes were incubated in the presence of a fixed 0.2 nM concentration of [^{3}H]NMS and increasing concentrations of the competitor. The incubation lasted 24 h to achieve full equilibrium. Two-point kinetic experiments with measurements of [^{3}H]NMS binding at t = 0 and t = 20 min were performed. By means of two-point dissociation experiments, the dissociation rate constant k_{-1} was determined by measuring the specific binding just before the start of the

dissociation reaction (t = 0, adding a competitive antagonist in excess) and at a predetermined time t during the dissociation process (t=20 min), as previously described.[208]

FlAsH Labeling

As previously described[214] a FlAsH labeling protocol was applied. Therefore, HEK 293 cells stably expressing the receptor FRET sonsor were grown on poly-D-lysine coated coverslips to near confluency.

Single cell FRET experiments

FRET measurements were performed using a Zeiss Axiovert 200 inverted microscope endued with a PLAN-Neoflar oil immersion 100 objective, a dual emission photometric system, and a Polychrome IV light source (Till Photonica). Experiments were conducted at 25 °C using live HEK293 cells stably expressing the hM1 receptor FRET sensor Single cells were excited at 436 nm (dichroic 460 nm) with a frequency of 10 Hz. Emitted light was recorded using 535/30 nm and 480/40 nm emission filters and a DCLP 505 nm beam splitter for FlAsH and CFP, respectively. FRET was observed as the ratio of FlAsH/CFP, which was corrected offline for bleed-through, direct FlAsH excitation, and photo-bleaching using the 2015 version of the Origin software (OriginLab). To investigate changes in FRET on ligand addition, cells were continuously super fused with buffer complemented with various ligands in saturating concentrations as indicated. Superfusion was done using the ALA-VM8 (ALA Scientific Instruments).

Split-Luciferase Bioluminescence Assay

Cells expressing the developed $G\alpha_q$-PLC-β3 sensor [192] in combination with hM_1R were detached from a 75-cm^2 flask by trypsinization and centrifuged (700 g for 5 min). The pellet was resuspended in assay medium consisting of L-15 with 5% FCS and the density of the suspension was adjusted to $1.25 \cdot 10^6$ cells/mL. Then, 80 µL of this suspension were seeded into each well of a 96 well plate, and the plate was subsequently incubated at 37 °C in a humidified atmosphere (without additional CO_2) overnight. On the next day, 10 µL of a 10 mM D-Luciferin (Pierce) were added to the cells, and the plate was transferred into a pre-warmed microplate luminescence reader (Mithras LB 940 Multimode Microplate Reader, Berthold Technologies, Bad Wildbad, Germany). The cells were allowed to

equilibrate inside the reader for 10 min before the basal luminescence was determined by recording the luminescence for the entire plate ten times with an integration time of 0.5 s per well. In the meantime, serial dilutions of agonists were prepared. The resulting solutions were also pre-warmed to 37 °C and subsequently added to the cells. Thereafter, luminescence was recorded for 15 plate repeats amounting to a time period of 20 min. Negative controls (solvent) and positive controls (reference full agonist, carbachol (hM_1R), eliciting a maximal response (100%) were included for subsequent normalization of the data. In case of the antagonist mode, antagonists were added 15 min prior to the initial thermal equilibration period to ensure an equilibrium between antagonists and receptors, before agonists were added. The pK_b values of antagonists were determined according to the Cheng-Prusoff equation.[215] After acquisition of the data, the peak luminescence intensities obtained after stimulation were used for quantitative analysis using GraphPad Software (San Diego, CA, USA).

β-arrestin2-recruitment Assay

β-arrestin2-recruitment was determined by measuring BRET by using the NanoBRET™ system.[202] BRET was measured between a full length human M1 receptor N-terminally carrying a FLAG-tag and C-terminally carrying a Nano Luciferase. The β-arrestin2 was N-terminally modified with a HALO-tag and labeled with a HALO-618 fluorescent ligand (Promega, Mannheim, Germany). Therefore, $1*10^6$ cells were seeded in a 6 cm dish and after 20 hours transiently transfected with 1 µg receptor, 2 µg β-arrestin and 1 µg human GRK2 with the Effectene® transfection reagent in accordance to the user manual. 20 hours after transfection cells were transferred from 6 well plates to 96 well plates. Cells were counted and 20000 cells per well were ceded into white 96-well plates (Brand GmbH & Co KG, Wertheim, Germany). The next day BRET was measured using the Synergy Neo2 Hybrid Multi-Mode Reader (BioTek Instruments GmbH, Bad Friedrichshall, Germany), and the BRET ratio was corrected against buffer conditions.

Data Treatment

The binding data from individual experiments were analyzed by computer-aided nonlinear regression analysis using Prism 5 (GraphPad Software, San Diego, CA, USA). [^{3}H]NMS dissociation data were analyzed assuming a monoexponential decay as described previously[216]. All sigmoidal concentration-

response curves were obtained by fitting three-parameter (Hill slope constrained to 1) nonlinear regression curves (GraphPad Prism, San Diego, CA, USA). Fluorescence intensities were acquired using Clampex (Axon Instruments). Statistical analysis and curve fitting were performed using Origin (OriginLab). The BRET raw data were analyzed and corrected in Excel (Microsoft Corporation, WA, USA) and plotted in GraphPad Prism 7 (GraphPad Software, San Diego, CA, USA).

Results

Chemistry

The 4-oxo-quinoline skeleton was built up using the Gould-Jacobs synthetic procedure, using diethyl 2-(ethoxymethylene)-malonate for the condensation with 4-fluoroaniline followed by cyclization in diphenyl ether.[184–186] Both synthetic procedures were carried out with microwave assistance to promote conversion and to afford better yields. The quinolone nitrogen was benzylated followed by amidation of the ester function with the aminoalkyl alcohol of the respective spacer length. Finally, the hydroxyl function was replaced by a bromine atom using hydrobromic acid and sulfuric acid.[82]

Oxotremorine was obtained starting from the commercially available 2-pyrrolidinone and propargyl bromide, followed by a Mannich reaction with pyrrolidine and paraformaldehyde in dioxane to afford the tertiary base.[92,188,217]

The final compounds were obtained by reaction of the allosteric moiety connected with the brominated spacer and the corresponding tertiary orthosteric bases as shown in Scheme 1. All the reactions were conducted using microwave assistance to reduce reaction times up to 8-48 h. The final compounds were purified by recrystallization or by chromatography using basic aluminum oxide, when crystallization was not feasible.

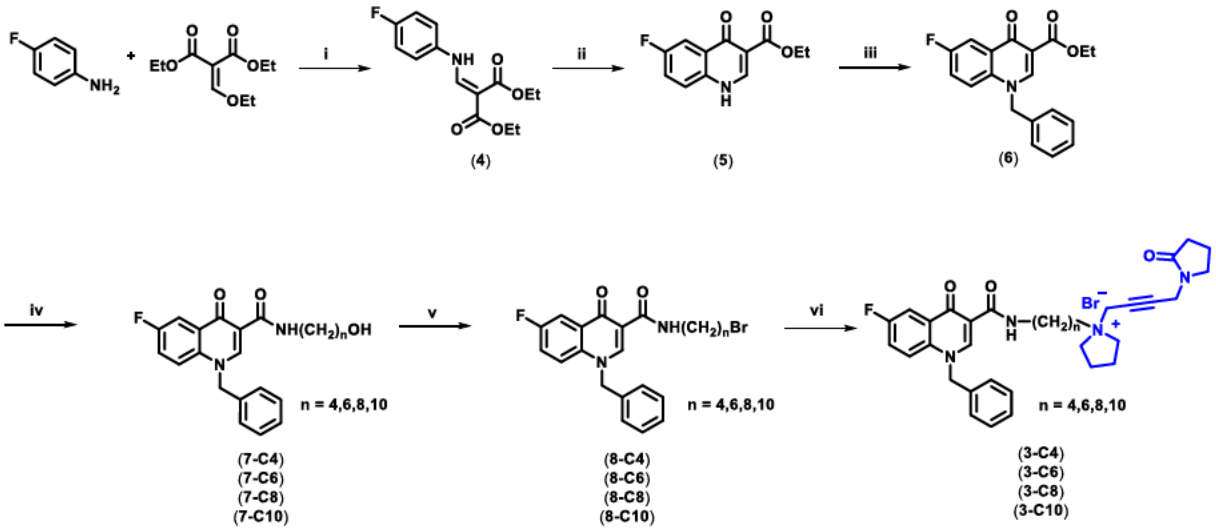

Scheme 1: Synthesis of Quinolone derivatives BQCAd/Oxotremorine Hybrids. Reagents and conditions: (i) toluene, reflux; (ii) diphenyl ether, 210 °C, MW; (iii) benzyl chloride, K_2CO_3, DMF, 80 °C; (iv) $H_2N(CH_2)_nOH$, 150 °C; (v) HBr (48%), H_2SO_4, reflux; (vi) Oxotremorine, KI/K_2CO_3, CH_3CN, 80 °C, MW.

General Procedure for the Synthesis of the Quinolone-Oxotremorine Derivatives 3-C4, 3-C6, 3-C8, and 3-C10

A mixture of a catalytic amount of K_2CO_3, bromoalkyl 4-oxo-quinoline-3-carboxamides **8-C4**, **8-C6**, **8-C8**, and **8-C10** and 2 to 4 equivalents of oxotremorine-base in acetonitrile (5 mL) was heated at 80 °C making use of microwave system. The progress of the reaction was controlled by TLC (CH_2Cl_2/MeOH = 85:15, R_f = 0.25 – 0.45). After 4-16 h, the solvent was distilled in vacuum and the residue was purified via alumina column chromatography using CH_2Cl_2/MeOH 100:0→9:1 as eluent system.

1-(4-(1-benzyl-6-fluoro-4-oxo-1,4-dihydroquinoline-3-carboxamido)butyl)-1-(4-(2-oxopyrrolidin-1-yl)but-2-yn-1-yl)pyrrolidin-1-ium bromide ***3-C4***

Beige solid; 15% yield; mp 158-163 °C; R_f = 0.35 (MeOH/CH_2Cl_2 = 95:5); ^{1}H NMR ($CDCl_3$): 1.75-1.78 (m, 2H, NH-CH2-CH_2),1.85-1.88 (m, 2H, NH-CH2-CH2-CH_2), 2.08 (td, 2H, H-4$_{oxo}$, *J*=7.4, *J*=14.9), 2.21-2.24 (m, 2H, H-5 $_{oxo}$), 2.43-2.36 (m, 4H, H-11 $_{oxo}$), 3.52-3.48 (m, 2H, NH-CH_2), 3.57-3.55 (m, 4H, N^+-CH_2, H-3 $_{oxo}$), 4.16 (s, 2H, ≡C-CH_2), 4.65 (s, 4H,H-10 $_{oxo}$), 5.52 (s, 2H, $CH_{2benzyl}$), 7.15 (d, 2H, CH_{phenyl},

J=6.6), 7.35-7.37 (m, 4H, H-7, CH_{phenyl}), 7.45 (td, 1H, H-8, *J*=4.2, *J*=8.6), 8.13 (ddd, 1H, H-5, *J*=3.1, *J*=4.9, *J*=8.1), 8.91 (s, 1H, H-2), 10.12 (t, 1H, NH, *J*=5.8).^{13}C NMR: ($CDCl_3$) 17.63, 22.30, 26.89, 28.39, 29.68, 30.43, 32.26, 43.54, 46.95, 58.12, 62.38, 77.10,77.20, 112.01, 119.26, 126.06, 126.09, 128.80, 128.83, 129.47, 133.85, 148.47,160.44, 175.05, 205.92. MS (ESI) m/z $[M]^+$ Calcd for $C_{33}H_{38}FN_4O_3^+$: 557.29. Found: 557.15. HPLC purity 94.31%.

1-(6-(1-benzyl-6-fluoro-4-oxo-1,4-dihydroquinoline-3-carboxamido)hexyl)-1-(4-(2-oxopyrrolidin-1-yl)but-2-yn-1-yl)pyrrolidin-1-ium bromide ***3-C6***

White solid; 48% yield; mp 161-164 °C; R_f = 0.46 (CH_2Cl_2/MeOH = 98:02); ^{1}H NMR ($CDCl_3$): 1.49 (br, 4H, NH-CH_2-C**H$_2$**-C**H$_2$**), 1.64-1.67 (m, 2H, NH-CH_2-CH_2-CH_2-C**H$_2$**), 1.79 (br, 2H, NH-CH_2-CH_2-CH_2-CH_2-C**H$_2$**), 2.04-2.08 (m, 2H, **H**-4_{oxo}), 2.21 (br, 2H, **H**-3_{oxo}), 2.36 (t, 4H, **H**-11_{oxo}, *J*=8.1), 3.45-3.48 (m, 4H, **H**-10_{oxo}), 3.52-3.56 (m, 2H, NH-C**H$_2$**), 3.67-3.70 (m, 2H, **H**-5_{oxo}), 4.08 (m, 2H, C**H$_2$**-N^+), 4.16 (s, 2H, **H**-6_{oxo}), 4.67 (s, 2H, **H**-9_{oxo}), 5.50 (s, 2H, C**H$_2$**$_{benzyl}$), 7.13 (d, 2H, C**H**$_{phenyl}$, *J*=6.4), 7.32-7.34 (m, 4H, **H**-8, C**H**$_{phenyl}$), 7.41-7.45 (dd, 1H, **H**-7, *J*=4.1, *J*=9.3), 8.11 (dd, 1H, **H**-5, *J*=2.9, *J*=8.8), 8.92 (s, 1H, **H**-2), 9.94 (t, 1H, N**H**, *J*=5.4).^{13}C NMR: ($CDCl_3$) 16.14, 20.79, 21.93, 24.46, 24.83, 27.71, 28.91, 30.76, 32.23, 37.23, 45.42, 49.51, 56.59, 59.49, 60.95, 70.46, 84.82, 110.15, 110.48 (d, J_{CF} = 22.7), 117.80 (d, J_{CF} = 7.2), 119.99 (d, J_{CF} = 25.2), 124.57, 127.25, 127.91, 128.28, 132.35, 132.47, 134.34, 142.03, 146.91, 157.11, 159.59, 163.21, 173.36, 174.47 (d, J_{CF} = 2.3), 190.03. MS (ESI) m/z $[M]^+$ Calcd for $C_{35}H_{42}FN_4O_3^+$: 585.32. Found: 585.30. HPLC purity 96.38%.

1-(8-(1-benzyl-6-fluoro-4-oxo-1,4-dihydroquinoline-3-carboxamido)octyl)-1-(4-(2-oxopyrrolidin-1-yl)but-2-yn-1-yl)pyrrolidin-1-ium bromide ***3-C8***

White solid; 42% yield; mp 163-165 °C; R_f = 0.25 (CH_2Cl_2/MeOH = 98:02); ^{1}H NMR ($CDCl_3$): 1.24 (br, 4H, NH-CH_2-CH_2-CH_2-C**H$_2$**-C**H$_2$**), 1.39 (br, 2H, NH-CH_2-CH_2-C**H$_2$**-CH_2), 1.62-1.65 (m, 2H, NH-CH_2-CH_2-CH_2-CH_2-CH_2-C**H$_2$**), 1.75 (br, 4H, NH-CH_2-**CH$_2$**-CH_2-CH_2-CH_2-CH_2-C**H$_2$**), 2.05-2.08 (m, 2H, **H**-4_{oxo}), 2.22 (d, 2H, **H**-3_{oxo} J=1.4), 2.37 (t, 4H, **H**-11_{oxo}, J=8.1), 3.45-3.49 (m, 2H, NH-C**H$_2$**), 3.68 (dd, 1H, **H**-5_{oxo}, *J*=6.5, *J*=11.6), 4.08 (m, 2H, C**H$_2$**-N^+), 4.16 (s, 1H, **H**-6_{oxo}), 4.66 (s, 2H, **H**-9_{oxo}), 5.49 (s, 2H, C**H$_2$**$_{benzyl}$), 7.12-7.14 (m, 2H, C**H**$_{phenyl}$), 7.32-7.34 (m, 4H, **H**-8, C**H**$_{phenyl}$), 7.41-7.44 (dd, 1H, **H**-7, *J*=4.2, *J*=9.3), 8.13 (dd, 1H, **H**-5 *J*=3.0, *J*=8.8), 8.92 (s, 1H, **H**-2), 9.92 (t, 1H, N**H**, *J*=5.4). ^{13}C NMR: ($CDCl_3$) 13.92, 17.49,

22.14, 22.49, 23.39, 26.08, 26.57, 28.67, 29.17,29.30, 29.46, 29.51, 29.56, 30.25, 31.74, 32.11, 38.91, 46.79, 50.94, 57.92, 61.00, 62.33, 71.69, 82.91, 86.23, 111.58, 111.86 (d, J_{CF}=22.9), 119.08 (d, J_{CF}=7.7), 121.26 (d, J_{CF}=25.4Hz), 125.90, 128.57, 128.98, 129.23, 133.81, 135.66, 148.21, 158.43, 164.44, 174.72, 175.82. MS (ESI) m/z $[M]^+$ Calcd for $C_{37}H_{46}FN_4O_3^+$: 613.36. Found: 613.20. HPLC purity 98.12%.

1-(10-(1-benzyl-6-fluoro-4-oxo-1,4-dihydroquinoline-3-carboxamido)decyl)-1-(4-(2-oxopyrrolidin-1-yl)but-2-yn-1-yl)-1l4-pyrrolidin-2-ylium bromide ***3-C10***

White solid; 58% yield; mp 130-134 °C; R_f = 0.28 (CH_2Cl_2/MeOH = 95:05); ^{1}H NMR ($CDCl_3$): 1.31-1.36 (m, 10H, NH-CH_2-CH_2-CH_2-C**H$_2$**-C**H$_2$**-C**H$_2$**-C**H$_2$**-C**H$_2$**-CH_2-CH_2), 1.63-1.65 (m, 6H, NH-CH_2-C**H$_2$**-C**H$_2$**-CH_2-CH_2-CH_2-CH_2-CH_2-C**H$_2$**), 1.72-1.74 (m, 2H, **H**-4$_{oxo}$), 2.06-2.09 (m, 2H, **H**-3$_{oxo}$), 2.39 (t, 4H, **H**-11$_{oxo}$, J=8.1Hz), 3.47-3.50 (m, 1H, **H**-5$_{oxo}$, NH-C**H$_2$**), 3.65 (m, 2H, C**H$_2$**-N^+), 4.15 (s, 4H, **H**-10$_{oxo}$), 4.71 (s, 2H, **H**-9$_{oxo}$), 5.48 (s, 2H, C**H$_{2benzyl}$**), 7.13-7.14 (m, 2H, C**H$_{phenyl}$**), 7.33-7.35 (m, 4H, **H**-8, C**H$_{phenyl}$**), 7.40-7.43 (dd, 1H, **H**-7, *J*=4.2, *J*=9.3), 8.15 (dd, 1H, **H**-5 *J*=3.0, *J*=8.8), 8.93 (s, 1H, **H**-2), 9.92 (t, 1H, N**H**, *J*=5.5). ^{13}C NMR: ($CDCl_3$) 18.12, 23.87, 26.85, 27.53, 29.52, 29.73, 29.79, 29.86, 29.96, 30.90, 32.38 39.59, 47.70, 50.04, 58.32, 62.42, 63.19, 72.44, 86.22, 111.46 (d, J_{CF} =24.0), 121.35 (d, J_{CF} =8.0), 122.11 (d, J_{CF} =25.3), 127.09, 128.92, 129.71, 135.80, 136.98, 149.49, 162.11, 166.18, 176.82, 202.83. MS (ESI) m/z $[M]^+$ Calcd for $C_{39}H_{49}FN_4O_3^+$: 641.5. Found: 641.25. HPLC purity 96.07%.

Pharmacology

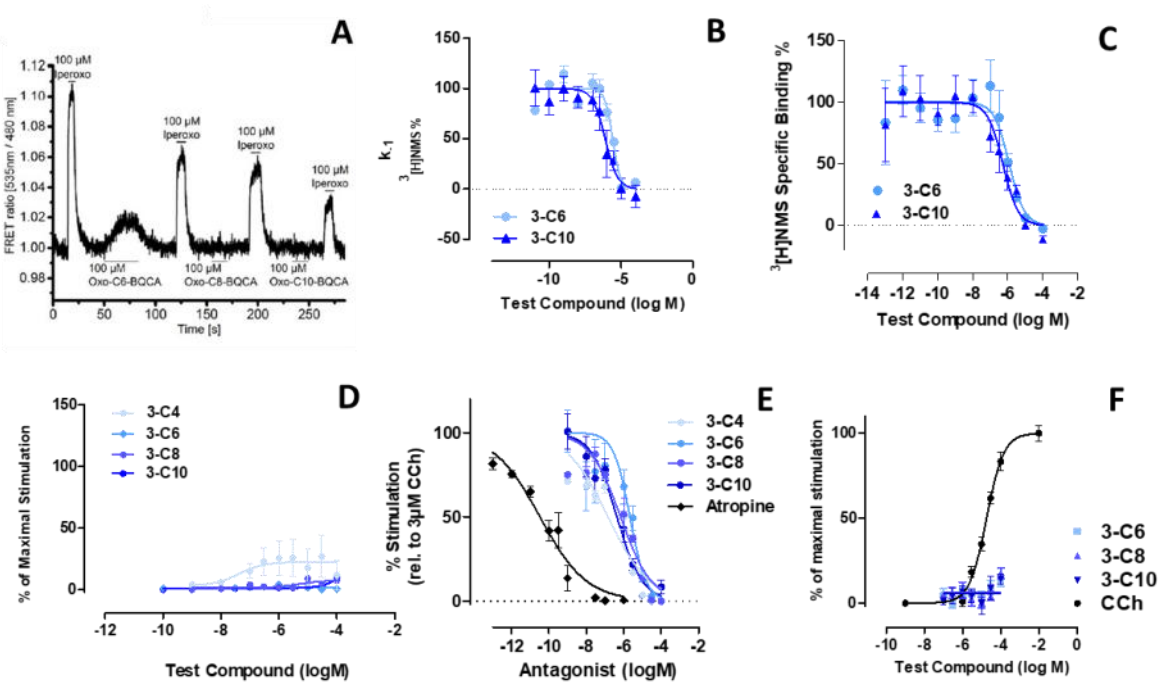

Figure 2. A: Representative single cell recording of a stable HEK293 cell line expressing the M1-IN3-CFP receptor sensor. Iperoxo in a saturating concentration (100 µM) served as reference[83] **B**: Allosteric effects of the hybrids as reflected by the inhibition of [^{3}H]NMS dissociation from M1 receptors in CHO-hM1 membranes. The allosteric effect is expressed as the ratio of the rate of [^{3}H]NMS dissociation in the presence of compound relative to the rate of dissociation of [^{3}H]NMS in the absence of test compound expressed in percent k^{-1}. The inflection point represents the concentration that retards the radioligand dissociation by half and is therefore equal to the $IC_{50,diss}$ value. **C**: Effect of increasing concentrations of bitopic ligands on specific equilibrium binding of [^{3}H]NMS in CHO-hM1 membranes. **D,E**: Characterization of the dualsteric ligands in Gα/PLC-β3 split-luciferase interaction assay at the human muscarinic M1 receptors (hM1). Live HEK293T cells were analyzed regarding their response as agonists (**D**) and antagonist (**E**). Agonist data were normalized to iperoxo as reference, whose maximum stimulation was defined as 100%. **F:** Dose-response-curves obtained with a BRET assay co-expressing the G protein-coupled receptor kinase 2 (GRK2) and β-arrestin labelled with a HALO-618 fluorescent ligand in HEK293T cells. Carbachol (CCh) used as reference was set 100%. Data are expressed as the means ± S.E.M. of 3-6 independent experiments performed at least in triplicate.

For the oxotremorine hybrids, a conformational change detected with the FRET sensor could be observed only for the **3-C6** derivative. This is surprising because the orthoster oxotremorine alone did not induce any conformational change (data not shown). Derivatives of longer or shorter chain length did not induce a FRET receptor response. (Figure 2A). The oxotremorine-based compounds bind to the hM1 muscarinic receptor binding pocket with similar affinities regardless of chain length (Figure 2C,

Table 1). The binding also occurs allosterically, since the **3-Cn** derivatives are able to delay the dissociation kinetics of [^{3}H]NMS (Figure 2B, Table 1). Radioligand binding studies, however, give no clues about the second messenger answer that the ligand will trigger. For this, functional studies are necessary.

TABLE 1. Radioligand binding affinities of the dualsteric hybrids 3-Cn at M1R and their [3H]NMS dissociation rates expressed as pIC50,diss. The inflection point represents the concentration that retards the radioligand dissociation by half and is therefore equal to the IC50 value

Compound	Radioligand binding [^{3}H]NMS	
	Dissociation $pIC_{50,diss}$	Equilibrium
3-C6	5.57 ± 0.09	pKi 6.38 pIC_{50} 5.91±0.20
3-C10	6.11 ± 0.09	pKi 6.69 pIC_{50} 6.31±0.20

The spilt-Luc assay, monitoring the activation via G proteins, reveals that the simple introduction of the oxotremorine skeleton in the bitopic ligand completely blocked the G protein activation (Figure 2D). Replacing the typical quaternary ammonium head of the endogenous orthosteric agonist ACh, with a pyrrolidine ring in the orthosteric moiety, completely inhibits receptor activation. To deepen the understanding of these ligands, the **3-Cn** compounds were investigated with the split assay in the antagonism mode, as described in the “Material and Method” part. As can be seen in Figure 2E, increasing concentrations of compounds **3-Cn** displace the agonist carbachol (used at EC_{80} concentration), producing a typical antagonist dose-response curve and showing how a simple modification of the orthosteric fragment can discriminate between agonism and antagonism. The negative logarithm half maximal inhibitory concentration (−log IC50) values range between 5.6 and 6.3. The data are normalized to the maximum response of the antagonist Atropine (Figure 2E, Table 2).

TABLE 2. Maximum agonist effect and potency of the **3-Cn** dualsteric hybrids derived from concentration-response curves of Gα and PLC-β3 complementation displayed in Figures 1D, E of the main text. Data are expressed as the means ± S.E.M. of 3-6 independent experiments performed in triplicate.

Compound	Split-Luc Assay			
	E_{max}	pEC_{50}	pIC_{50}	n
3-C4	-	-	6.36 ± 0.11	**3**
3-C6	-	-	5.67 ± 0.13	**3**
3-C8	-	-	5.94 ± 0.07	**3**
3-C10	-	-	6.22 ± 0.10	**3**
Atropine	-	-	10.06 ± 0.09	**4**
Oxotremorine	86.37 ± 4.15	7.85 ± 0.15	-	**3**

The **3-Cn** hybrids shown an arrestin recruitment signal only at the highest ligand concentration, not dependent on the spacer linker.

Discussion and conclusion

Really surprisingly, the introduction of the oxotremorine portion in the dualsteric ligands **3-Cn**, elicited no detectable Gα and PLC-β3 interaction in the Split-Luc assay. The assay reveals that the simple insertion of the oxotremorine skeleton in the bitopic ligand fully suppressed the G protein signaling pathway (Figure 2D). Because of the complete absence of G proteins activation response in **3-Cn**, this molecule series was further investigated regarding the antagonism mode of the split-assay. As can be seen from figure 2E and table 2 the pIC50 obtained from the typical antagonist dose-response, this is the first case of antagonism in the whole series of derivatives studied. By comparison of these derivatives with the previously synthesized hybrids[27] a loss in G protein activation is only observed if the quaternary ammonia head is fixed within a heterocycle where the flexibility of the orthosteric fragment is greatly reduced by the presence of the pyrrolidine ring. It is likely that the pyrrolidine ring's sterical encumbrance disturbs the gatekeeper function of the aromatic lid structure which is essential for receptor activation.[218] The introduction of easily rotating methylene substituents by replacement of the pyrrolidine ring – this being the only difference between oxotremorine and oxotremorine-M – reduces the steric interaction and produces bioluminescence derived from the union of the Gα and PLC-β3. Therefore, G protein intracellular activation is attested. The compound with the best antagonist activity

is the shorter chain one **3-C4** with a pIC_{50} value of 6.36 compared to atropine (pIC_{50} of 10.06) used as reference.

3. IP-One accumulation assay

Introduction

The M1 receptor is predominantly coupled to Gq proteins that activate the phospholipase C (PLC) resulting in an increased level of the two second messenger inositol trisphosphate (IP3) and diacylglycerol (DAG). Furthermore, IP3 triggers an intracellular calcium release from the sarcoplasmatic reticulum.[219] Dualsteric ligands can potentially bind in an inactive purely allosteric binding mode or in an active dualsteric binding mode (dynamic ligand binding).[109] Because of a complex landscape of binding possibilities, a dualsteric binding can only be deduced from a set of different experimental approaches rather than from a single assay system. Therefore, experiments elucidating the signaling pathways, β-arrestin recruitment, Gαq and PLC-β3 interaction in combination with radioligand binding assay, and conformational sensitive receptor FRET sensors were carried out in order to reveal how binding, modulation cooperativity, and efficacy can vary with different combinations of orthosteric moieties. Additional experiments to those already published in the Results section 1[27] for compounds **1-Cn** and **2-Cn** were performed using intracellular inositol monophosphate accumulation as the functional readout to complement the downstream signaling investigation. IP1 assays record the inositol monophosphate concentration, a stable downstream metabolite of IP3 induced by activation of a phospholipase C cascade.

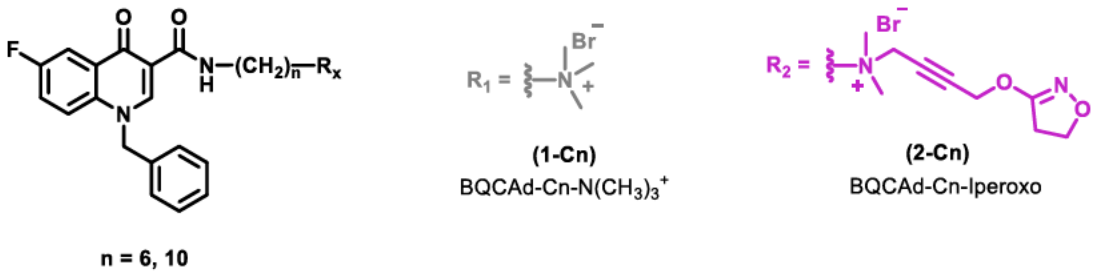

Figure 1: Structures of BQCAd (benzyl quinolone carboxylic acid) bitopic derivatives: TMA-based ligands (**1-Cn**) and Iperoxo derivatives (**2-Cn**).

Material and Methods

Cell culture

CHO cells stably expressing the hM1 receptor (CHO-hM1 cells) were cultured in Ham's nutrient mixture F-12 (HAM- F12) supplemented with 10 % (v/v) FCS (FCS), 100 U/mL penicillin, 100 µg/mL streptomycin, 0.2 mg/mL G418 and 2 mM L-glutamine at 37 °C in a 5 % CO_2 humidified atmosphere.

IP-One Accumulation Assay

The measurement of M1R stimulated activation of the G-protein mediated pathway was performed applying the IP-One HTRF® assay (Cisbio, Codolet, France) according to the manufacturer's protocol. In brief, CHO-hM1 cells were resuspended in assay buffer (HEPES, 10 mM, $CaCl_2$, 1 mM, $MgCl_2$, 0.5 mM, KCl, 4.2 mM, NaCl, 146 mM, glucose 5.5 mM, LiCl, 50 mM, pH 7.4), counted using the Neubauer counting chamber and dispensed in 384-well microplates at a density of $1x10^7$cells/mL. After incubation with th-+e test compounds, dissolved in stimulation buffer at 37 °C, for 30 min the reactions were stopped by the addition of 50 mM Na_2HPO_4/KH_2PO_4 phosphate buffer (pH 7.0), 1 mM KF, and 1.25% Triton X-100 containing HTRFR assay reagents and incubation was continued at room temperature for 60 min. FRET signals were measured after excitation at 320 nm using the Wallac EnVision 2104 Multilabel plate reader. Data analysis was based on the fluorescence ratio emitted by labeled IP1 (665±10 nm) over the light emitted by the europium cryptate-labeled anti-IP1 (615±10 nm). Levels of IP1 were normalized to the amount generated in the presence of 100 µM acetylcholine. All compounds were tested in triplicate in at least three individual experiments.

Result and discussion

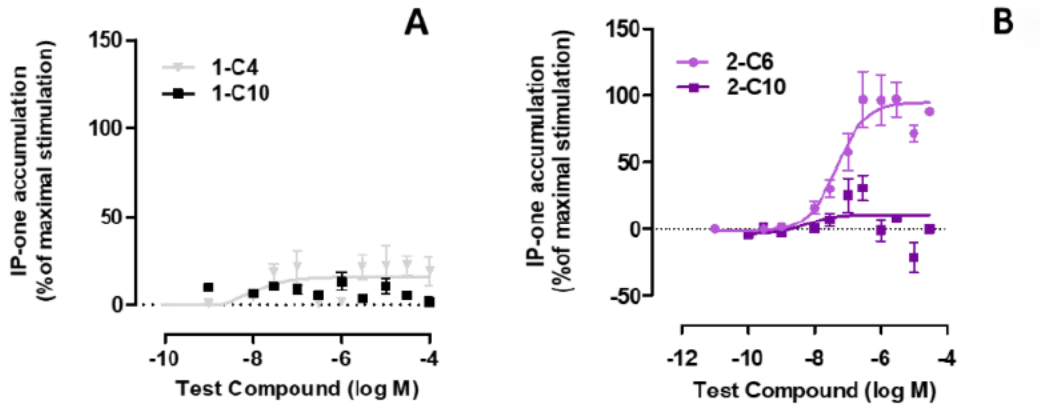

Figure 2. IP1 accumulation results by hybrids **1-C6**, **2C-10**, **2-C6**, **2C-10** in live CHO-hM1 cells. Cells were treated with increasing concentrations of the indicated compounds for 30 min, and the intracellular inositol phosphates concentrations were measured as described under "Materials and Methods". Data points represent the mean ± S.E.M of three to five independent experiments performed in triplicate.

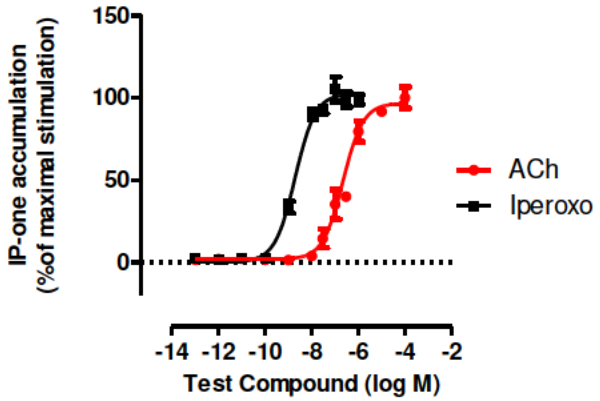

Figure 3. A. Characterization of **Ach** and **Iperoxo** orthosteric agonists on IP1 downstream signaling. Data represent mean ± S.E.M. from three to four independent two-point kinetic experiments, conducted in triplicate.

TABLE 1. Maximum agonist effect and potency of dualsteric hybrids stimulating IP1 accumulation in CHO human M1 membranes. Data are expressed as the means ± S.E.M. of 3-4 independent experiments performed in triplicate.

Compound	IP1 assay		
	E_{max}	pEC_{50}	*n*
1-C6	-	-	**3**
1-C10	-	-	**3**
2-C6	95.06 ± 7.58	7.31 ± 0.24	**3**
2-C10	-	-	**3**
iperoxo	102.50 ± 2.07	8.71 ± 0.07	**4**
ACh	96.73 ± 3.10	6.65 ± 0.09	**3**

The IP-1 accumulation studies reveal that only BQCAd-6-Iperoxo **2-C6** is able to cause a robust stimulation of IP1 accumulation. All the other investigated compounds **2-C10, 1-C6, 1C-10** did not show any appreciable agonist activity at concentrations up to 100 µM (Figure 2). Surprisingly, a completely different pattern of behavior was noted between **2-C6** and **2-C10** both containing the iperoxo moiety. The studied ligands **2-C10, 1-C6, 1C-10**, unable to generate IP1 accumulation, were also characterized by an inverse receptor movement described for the first time by Messerer et al. [83] at the M1 muscarinic receptor. This suggesting a correlation of the inverse FRET signal on the receptor level to G_q activation without IP1 accumulation, thus opening a tight link between the receptor movement and the bias signaling, which must be confirmed and will be further investigated.

4. Synthesis and pharmacological investigation of BQCAd-Xanomeline derivatives at the M1 receptor

Introduction

Alzheimer's disease (AD) is a progressive neurological disease that is characterized by cognitive dysfunction and neuropathology of the brain. The characteristic features include decrease in Acetylcholine (ACh) levels, formation of amyloid-containing plaques and neurofibrillary tangles in the nervous tissue of brain.[136] M1 muscarinic receptors were found in higher concentrations in the cortex and hippocampus in patients affected from the neurodegenerative disease. Muscarinic acetylcholine receptors (mAChRs) are members of the G protein-coupled receptor superfamily (GPCRs) and are responsible for the neurotransmission of ACh response in both the peripheral and central nervous systems (CNS).[93] Postsynaptic M1 receptors preservation was observed in AD brain tissue, therefore enhancement of ACh at these receptors was hypothesized as advantageous in the treatment of Alzheimer's disease.[220] The five muscarinic receptor subtypes (M1-M5) bind their physiological transmitter in the highly conserved orthosteric site within the transmembrane domains. Adverse effects, due to indiscriminate activation of all muscarinic receptor subtypes are common.[212] Despite intense investigation, development of agents that selectively activate this receptor via the orthosteric site has been blocked by the high sequence homology of the binding site between the five muscarinic receptor subtypes and the large distribution of this receptor family in both the CNS and the periphery.[29] Orthosteric muscarinic activators have no binding selectivity and poor signaling specificity. However, all subtypes possess at least one less conserved allosteric binding site which is located in the extracellular region of the receptor on top of the ACh (i.e. orthosteric) binding site.[57] To gain subtype-selective receptor activation, we synthesized hybrid molecules fusing[81] the potent Xanomeline orthosteric activator with the M1 highly selective positive allosteric fragment. Compared to the conventional orthosteric and allosteric ligands, a bitopic ligand may select a unique receptor conformation, which can selective activate some signaling pathways at the expense of others (biased signaling).[221] A muscarinic positive allosteric modulator/allosteric agonist moiety, i.e. benzyl quinolone carboxylic acid derivative (BQCAd) was included in the new hybrids, being exquisitely M1-selective over other muscarinic

subtypes.[212,222,223] Site-directed mutagenesis experiments indicate that the BQCA scaffold transmits the positive cooperativity with the orthosteric agonist through binding at an allosteric site involving residues Tyr-85 in transmembrane domain 2 (TM2), Tyr-179 and Phe-182 in the second extracellular loop (ECL2) and Glu-397 and Trp-400 in transmembrane domain 7 (TM7).[106,198,224] Accordingly, the BQCA binding pocket partially overlaps with the previously described "common" allosteric site in the extracellular vestibule of the M1 mAChR, suggesting that its high subtype selectivity derives from either additional contacts outside this region or through a subtype-specific cooperativity mechanism.[198] In summary, the BQCA allosteric potentiation mechanism can be exploited in the context of cognitive diseases and represents a promising strategy for M1 muscarinic subtype selectivity.[106] Xanomeline was selected as orthosteric fragment incorporated in the new hybrids because of its higher affinity, potency and efficacies for M1/M4 muscarinic receptors, compared to other muscarinic subtypes.[136] Xanomeline is recognized for its efficacy in patients with moderate AD leading to a significant improvement in the cognitive function of patients.[136,225] Xanomeline also dramatically decreased some of the behavioral symptoms associated with dementia such as vocal outbursts, suspiciousness, delusions, agitation and hallucinations.[136] Some years ago, it underwent phase III clinical trial, but in the 6-month double-blind, placebo-controlled, parallel group efficacy study, roughly 59% of patients discontinued treatment after receiving 75 mg xanomeline orally three times daily because of adverse events, predominantly gastrointestinal.[138] Its undesirable activity for the dopaminergic and serotonin (5-HT) receptors[137,138] together with the dose-limited cholinomimetic side effects[167,225] related to the lack of selectivity of its metabolites towards the M1 receptor stopped the compound in clinical studies progression. Nevertheless, the strength of the preclinical data and of the early clinical data of Xanomeline suggests that future efforts to develop subtype selective muscarinic receptor agonists to treat neurodegenerative diseases may hold promise.[138] Bipharmacophoric ligands consisting of the agonist iperoxo and the fluoro-BQCA-derived moiety (**1**) linked via a hexamethylene chain were found to act as partial human muscarinic M1 (*h*M1) receptor agonists.[82,132] Since the carboxylic group is a suitable contact point for improving allosteric modulation[29,74] it was chosen as attachment point to connect the Xanomeline (**2**) moiety with the BQCAd fragment through an alkylene linker of different lengths (Figure 1, Compounds **3-C4**, **3-C6**, **3-C8**, **3C-**

10). All compounds were synthesized and evaluated for the ability to bind and activate the M1 receptor, aiming for a better understanding of the binding pose of Xanomeline itself.

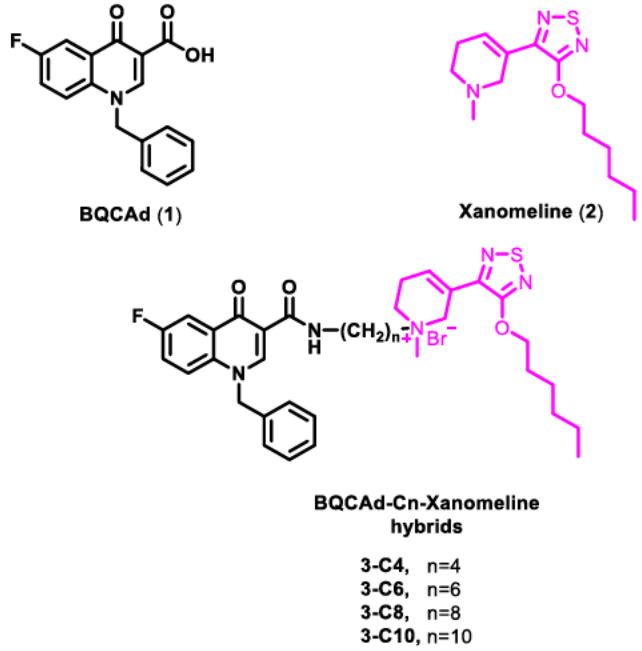

Figure 1: Structures of Xanomeline, BQCAd (benzyl quinolone carboxylic acid derivative) and of the new hybrid derivatives.

Material and Methods

Materials

Chinese hamster ovary (CHO) cell line stably expressing *h*M1 was obtained from Wyeth Research (Princeton, NJ). 384-well microplates, 96-well round bottom plates and white 96-well plates were purchased from Thermo Fisher and Greiner Bio One, Germany. Dulbecco's modified Eagle's medium (DMEM) and phosphate-buffered saline (PBS) were from Sigma-Aldrich (Germany). Leibovitz' L-15 medium (L-15) and Hank's balanced salt solution (HBSS) were from Gibco (Germany). Fetal calf serum (FCS), trypsin and geneticin (G418) were from Merck Biochrom (Germany). D-Luciferin was purchased as potassium salt from Pierce (Germany) and was dissolved in HBSS at a concentration of 400 mM. Puromycin was obtained from Invivogen (France). Scopolamine Methyl Chloride, [N-methyl-3H]-, 250 µCi (9.25MBq) was purchased from PerkinElmer (Rodgau, Germany) and Polyethylenimine solution (1%, PEI) from Sigma. For

chromatographic applications (HPLC, LC-MS) deionized water produced by means of a Milli-Q® system (Merck, Darmstadt, Germany) was used. HPLC grade and LC-MS grade solvents were from Sigma-Aldrich (Munich, Germany). All chemicals were purchased from Sigma-Aldrich (Schnelldorf, Germany), VWR (Darmstadt, Germany) and TCI (Eschborn, Germany) and were used without prior purification.

General Medicinal Chemistry Methods

^{1}H (400.132 MHz) and ^{13}C (100.613 MHz) NMR spectra were recorded using a Bruker AV 400 NMR spectrometer (Bruker Biospin, Ettlingen, Germany). As an internal standard, the signals of the deuterated solvents were used (DMSO-d6: 1H 2.5 ppm, 13C 39.52 ppm; CDCl3: 1H 7.26 ppm, 13C 77.16 ppm). Abbreviations for data quoted are s, singlet; d, doublet; t, triplet; q, quartet; m, multiplet; b, broad; dd, doublet of doublets; dt, doublet of triplets; tt, triplet of triplets; and tq, triplet of quartets. Coupling constants (J) are given in Hertz. The specific NMR assignments were determined by using typical techniques including polarization transfer experiments (DEPT) and two-dimensional experiments, such as ^{1}H-^{1}H correlation (COSY) and ^{1}H-^{13}C-proton-carbon heteronuclear correlation (HMQC, HMBC). TLC analyses were performed on commercial precoated plates, silica gel 60 F254, C18 silica-coated aluminum panels ALUGRAM® RP-18W / UV254 and on pre-coated TLC-plates Alox-25/UV254 (Macherey-Nagel); the detection was made using UV light at 254 nm, intrinsic fluorescence at 366 nm or with ethanolic $KMnO_4$, Dragendorff reagent or phosphomolybdic acid ethanolic solution. For classical purification, gravity column chromatography was carried out. Silica gel with a grain size of 63-200 µm (Merck, Darmstadt, Germany) was used as stationary phase. Flash chromatography on a puriFlash®430 system (Interchim, Montlucon, France) was performed using prepacked columns (Interchim, Montluçon, France) with silica gel filling (Particle size 30 microns or 50 microns) for normal phase or with C18-silica gel filling (Particle size 15 µm) for the reverse phase. The detection was carried out by means of a UV detector and Evaporative Light Scattering Detector (ELSD). Microwave assisted reactions were carried out by use of MLS-rota PREP or synthWAVE instruments (Milestone).

The LC-MS analyses of all the test compounds were performed using either a Shimadzu LC-MS-2020 mass spectrometer (Shimadzu Deutschland GmbH, Duisburg, Germany) containing a DGU-20A3R

degassing unit, a LC20AB liquid chromatograph and a SPD-20A UV/Vis detector or a LC / MSD ion trap (Agilent Technologies, Waldbronn, Germany) connected to an Agilent 1100 modular system. A Synergi Fusion-RP (150 mm x 4.6 mm i.d., 4 µm; Phenomenex Ltd., Aschaffenburg, Germany) column and a gradient of MeOH/water, as a mobile phase, were used. Parameters of the HPLC method: solvent A, water with 0.1% formic acid; solvent B, MeOH with 0.1% formic acid. Solvent B was increased from 0% to 90% in 13 min, then decreased from 90% for 5 min, from 90% to 5% in 1 min, and then 5% for 4 min. The method was performed with a flow rate of 1.0 mL/min. UV detection was measured at 254 nm. All compounds were found to have a purity ≥ 95%. Mass spectra were recorded in ESI-positive mode and the data are reported as mass-to-charge ratio (m/z) of the corresponding positively charged molecular ions.

Cell culture

CHO cells stably expressing the hM1 receptor (CHO-hM1 cells) were cultured in Ham's nutrient mixture F-12 (HAM- F12) supplemented with 10 % (v/v) FCS (FCS), 100 U/mL penicillin, 100 µg/mL streptomycin, 0.2 mg/mL G418 and 2 mM L-glutamine at 37 °C in a 5 % CO_2 humidified atmosphere. The human embryonic kidney (HEK293T) cells stably co-transfected with the human M1 receptor and the $G\alpha_q$-PLC-β3 sensor were kindly provided by Timo Littmann (University of Regensburg). Cells were cultivated in DMEM containing 10% FCS (full medium) at 37 °C in a water-saturated atmosphere containing 5% CO_2 as previously reported.[192]

Membrane Preparation

CHO-hM1 cells were grown adherently to a confluence of approx. 80%. The cells were harvested by gently scraping in ice-cold harvesting buffer (20 mM HEPES, 10 mM Na_2EDTA, pH= 7.4). The collected cells were homogenized on ice twice for 25 seconds at level 6 using a polytron homogenizer and the resulting cell fragments were centrifuged using the rotor JA25.50 at 40 000 g for 10 minutes (4 °C). The supernatant was aspirated, and the pellet resuspended in ice-cold storage buffer (20 mM HEPES, 0.1 mM Na_2EDTA, pH= 7.4). This step was repeated twice, and finally the pellets were resuspended in ice-cold assay buffer (10 mM HEPES, 10 mM $MgCl_2$, 100 mM NaCl, pH= 7.4). Aliquots were filled in eppendorf tubes, quickly frozen and stored at -80 °C. The protein concentration was of approximately 2

mg/mL, determined using the Pierce™ BCA Protein Assay Kit. The absorbance of the bicinchoninic acid (BCA)/copper complex after the occurrence of the biuret reaction was measured at 562 nm using a UV-Photometer (Synergy™ Neo2 Multi-Mode Microplate, Reader). Values obtained were plotted on a linear calibration curve whereby the protein content was determined.

Radioligand Binding Experiments

Radioligand binding experiments using CHO-hM1 membranes were performed in round bottom 96-well microtiter plates applying 20 µg protein/well. Experiments were conducted at room temperature using [^{3}H]NMS as the radioactive probe (2 nM for [^{3}H]NMS dissociation and 0.2 nM for equilibrium binding experiments). The plate was incubated at room temperature using a microplate shaker (Titramax 101 Platform Shaker, Heidolph) with an incubation time ranging from 1 h for the dissociation to 24 h for the equilibrium experiments. Homologous competition assays were utilized to determine pKd at hM1 for NMS 8.88 and conformed to homologous binding assumptions [207]. Nonspecific binding was determined in the presence of atropine excess. Incubation performed in the assay buffer was terminated by filtration through glass fiber mats, previously coated with a 1% polyethylenimine solution, in a cell harvester filtration device. After filtration, the filter mats were washed with ice-cold wash water, covered with melt-on scintillator sheets on a heating block and the radioactivity was counted in a Perkin Elmer MicroBeta 2450 Microplate Counter. The inhibition constants Ki of receptors for the studied compounds were determined in competition experiments in which membranes were incubated in the presence of a fixed 0.2 nM concentration of [^{3}H]NMS and increasing concentrations of the competitor. The incubation lasted 24 h to achieve full equilibrium. Two-point kinetic experiments with measurements of [^{3}H]NMS binding at t = 0 and t = 20 min were performed. By means of two-point dissociation experiments, the dissociation rate constant k_{-1} was determined by measuring the specific binding just before the start of the dissociation reaction (t = 0, adding a competitive antagonist in excess) and at a predetermined time t during the dissociation process (t=20 min), as previously described.[208]

Split-Luciferase Bioluminescence Assay

Cells expressing the developed $G\alpha_q$-PLC-β3 sensor in combination with hM_1R, were detached from a 75-cm^2 flask by trypsinization and centrifuged (700 g for 5 min). The pellet was resuspended in assay

medium consisting of L-15 with 5% FCS and the density of the suspension was adjusted to $1.25 \cdot 10^6$ cells/mL. Then, 80 µL of this suspension were seeded into each well of a 96-well plate, and the plate was incubated at 37 °C in a humidified atmosphere (without additional CO_2) overnight. On the next day, 10 µL of 10 mM D-Luciferin (Pierce) were added to the cells, and the plate was transferred into a pre-warmed microplate luminescence reader (Mithras LB 940 Multimode Microplate Reader, Berthold Technologies, Bad Wildbad, Germany). The cells were allowed to equilibrate inside the reader for 10 min, before the basal luminescence was determined by recording the luminescence for the entire plate ten times with an integration time of 0.5 s per well. In the meantime, serial dilutions of agonists were prepared. The resulting solutions were also pre-warmed to 37 °C and subsequently added to the cells. Thereafter, luminescence was recorded for 15 plate repeats amounting to a time period of 20 min. Negative controls (solvent) and positive controls (reference full agonist, carbachol (hM_1R), eliciting a maximal response (100%) were included for subsequent normalization of the data. After acquisition of the data, the peak luminescence intensities obtained after stimulation were used for quantitative analysis using GraphPad Software, San Diego, CA.

IP-One Accumulation Assay

The measurement of M1R stimulated activation of the G-protein mediated pathway was performed applying the IP-One HTRF® assay (Cisbio, Codolet, France) according to the manufacturer's protocol. In brief, CHO-hM1 cells were resuspended in assay buffer (HEPES, 10 mM, $CaCl_2$, 1 mM, $MgCl_2$, 0.5 mM, KCl, 4.2 mM, NaCl, 146 mM, glucose 5.5 mM, LiCl, 50 mM, pH 7.4), counted using the Neubauer counting chamber and dispensed in 384-well microplates at a density of $1x10^7$cells/mL. After incubation with the test compounds, dissolved in stimulation buffer at 37 °C, for 30 min the reactions were stopped by the addition of 50 mM Na_2HPO_4/KH_2PO_4 phosphate buffer (pH 7.0), 1 mM KF, and 1.25% Triton X-100 containing HTRFR assay reagents and incubation was continued at room temperature for 60 min. FRET signals were measured after excitation at 320 nm using the Wallac EnVision 2104 Multilabel plate reader. Data analysis was based on the fluorescence ratio emitted by labeled IP1 (665±10 nm) over the light emitted by the europium cryptate-labeled anti-IP1 (615±10 nm). Levels of IP1 were normalized to the amount generated in the presence of 100 µM acetylcholine. All compounds were tested in triplicate in at least three individual experiments.

Data Treatment

The binding data from individual experiments were analyzed by computer-aided nonlinear regression analysis using Prism 5. (GraphPad Software, San Diego, CA). [^{3}H]NMS dissociation data were analyzed assuming a monoexponential decay as described previously[216]. All sigmoidal concentration-response curves were obtained by fitting three-parameter (Hill slope constrained to 1) nonlinear regression curves (GraphPad Prism, San Diego, CA).

Results and discussion

Chemistry

The orthosteric M1 fragment Xanomeline, was prepared following the synthetic sequence of Strecker according to a known procedure.[226] As already reported, the fluoro-4-oxo-quinolone skeleton of **5** was synthesized using the Gould-Jacobs procedure, starting with the condensation of 4-fluoroaniline with diethyl 2-(ethoxymethylene)-malonate and subsequent cyclization in boiling diphenyl ether.[184,227,228] Derivative (**6**) was then subjected to conversion of the ester function with the aminoalcohols of the corresponding spacer length (C4, C6, C8, C10). Substitution of the alcohol function with a bromine atom using HBr/H_2SO_4 and subsequent reaction with the Xanomeline fragment in acetonitrile at 80 °C led to the monoquaternary ammonium salt hybrids **3-C4**, **3-C6**, **3-C8**, and **3-C10** in 25-74% yield. The schematic representation and the synthetic steps involved in the preparation of the BQCAd-Xanomeline hybrids and their intermediates are shown in Scheme 1. More detailed syntheses and spectral data of target compounds are reported below.

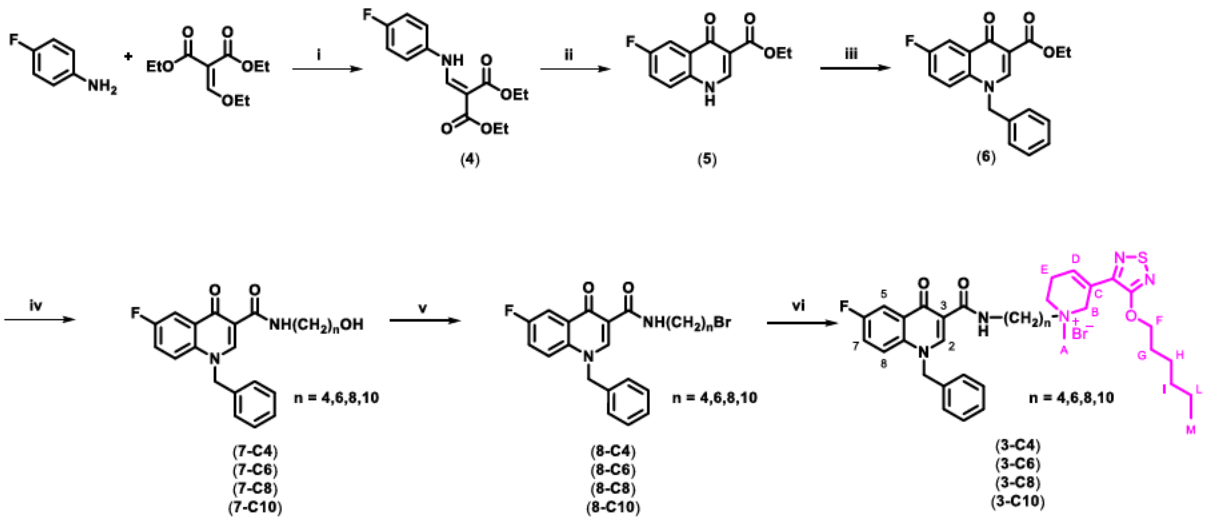

Scheme 1: Synthesis of Quinolone derivatives BQCAd/Xanomeline Hybrids. Reagents and conditions: (i) toluene, reflux; (ii) diphenyl ether, 210 °C, MW; (iii) benzyl chloride, K_2CO_3, DMF, 80 °C; (iv) $H_2N(CH_2)_nOH$, 150 °C; (v) HBr (48%), H_2SO_4, reflux; (vi) xanomeline, KI/K_2CO_3, CH_3CN, 80 °C, MW.

General Procedure for the Synthesis of the Quinolone Derivatives **3-C4**, **3-C6**, **3-C8**, and **3-10**

To a solution of bromoalkyl 4-oxo-quinoline-3-carboxamides **8-C4**, **8-C6**, **8-C8**, and **8-C10** (0.11 mmol) in acetonitrile (5 mL), a catalytic amount of K_2CO_3/KI and xanomeline (0.11 mmol) were added. The reaction was heated at 80 °C making use of microwave system After completion of the reaction (8-24 h) controlled by TLC (CH_2Cl_2/MeOH = 90:10, R_f = 0.16 – 0.22), the mixture was cooled to room temperature. The solvent was distilled off. The so obtained solid was purified through silica column chromatography, using CH_2Cl_2/MeOH as gradient mobile phase (from 99:1 → 9:1). The isolated fraction was dried *in vacuo* to give the desired product.

4-(1-benzyl-6-fluoro-4-oxo-1,4-dihydroquinoline-3-carboxamido)-1-(5-(4-(hexyloxy)-1,2,5-thiadiazol-3-yl)-1-methyl-3,6-dihydro-1l4-pyridin-1(2H)-yl)butan-1-ylium bromide ***3-C4***

Yellow oil; 48% yield; R_f = 0.22 (CH_2Cl_2/MeOH = 9:1); ^{1}H NMR ($CDCl_3$): 0.87-0.90 (m, 5H, Alkyl $\mathbf{H_M}$, $\mathbf{H_L}$), 1.25-1.36 (m, 6H, Alkyl, $\mathbf{H_I}$, $\mathbf{H_H}$, NH-CH_2-C$\mathbf{H_2}$), 1.67-1.63 (m, 6H, Alkyl, N^+-CH_2-C$\mathbf{H_2}$, $\mathbf{H_G}$, $\mathbf{H_C}$), 1.78-1.84 (m, 2H, NH-C$\mathbf{H_2}$), 1.96-2.02 (m, 2H, N^+-C$\mathbf{H_2}$), 3.44-3.48 (m, 7H, $\mathbf{H_E}$, $\mathbf{H_B}$, $\mathbf{H_A}$), 4.46 (t, 2H, J=6.7, $\mathbf{H_F}$), 5.49 (s, 2H, C$\mathbf{H_{2benzyl}}$), 7.12-7.14 (m, 2H, H_7, C$\mathbf{H_{phenyl}}$), 7.21-7.24 (m, 1H, $\mathbf{H_D}$), 7.32-7.37 (m, 5H, C$\mathbf{H_{phenyl}}$), 7.44 (dd, 1H, J=4.2, J=9.3, $\mathbf{H_8}$), 8.13 (dd, 1H, J=3.0, J=8.8, $\mathbf{H_5}$), 8.87 (s, 1H, $\mathbf{H_2}$), 10.08 (t, 1H, J=6.2,

N**H**). ^{13}C NMR ($CDCl_3$): 14.28, 18.21, 21.52, 22.81, 25.91, 29.06, 30.00, 31.66, 35.91, 41.03, 42.16, 55.4, 58.88, 62.87, 63.92, 73.47, 111.62, 112.39, 117.66, 122.21, 122.28, 125.98, 129.79, 130.64, 136.18, 137.08,139.58, 148.75,148.02, 159.11, 161.51, 176.51, 195.24. MS (ESI) m/z $[M]^+$ Calcd for $C_{35}H_{43}FN_5O_3S^+$: 632.31. Found: 632.20. HPLC purity 95.40 %.

1-(6-(1-benzyl-6-fluoro-4-oxo-1,4-dihydroquinoline-3-carboxamido)hexyl)-5-(4-(hexyloxy)-1,2,5-thiadiazol-3-yl)-1-methyl-1,2,3,6-tetrahydropyridin-1-ium bromide ***3-C6***

Yellow oil; 63% yield; R_f = 0.19 (CH_2Cl_2/MeOH = 9:1); ^{1}H NMR ($CDCl_3$): 0.88-0.92 (m, 5H, Alkyl **H**$_M$, **H**$_L$), 1.25-1.37 (m, 8H, **H**$_I$, **H**$_H$, NH-CH_2-C**H$_2$**, NH-CH_2-CH_2-C**H$_2$**), 1.40-1.49 (m, 6H, N^+-CH_2-CH_2-C**H$_2$**, **H**$_G$, **H**$_C$), 1.64 -1.67 (m, 4H, NH-C**H$_2$**, N^+-CH_2-C**H$_2$**), 1.84 -1.86 (m, 3H, **H**$_A$), 3.45-3.47 (m, 4H, **H**$_E$, **H**$_B$), 4.45 (t, 2H, J=6.5, **H**$_F$), 5.47 (s, 2H, C**H$_{2benzyl}$**), 6.97-7.03 (m, 1H, H_7, C**H$_{phenyl}$**), 7.11-7.14 (m, 1H, **H**$_D$), 7.30-7.37 (m, 5H, C**H$_{phenyl}$**), 7.41 (dd, 1H, J= 4.2, J=9.3, **H**$_8$), 8.16 (dd, 1H, J= 2.9, J=8.8, **H**$_5$), 8.91 (s, 1H, **H**$_2$), 9.91 (t, 1H, J=5.5, N**H**). ^{13}C NMR ($CDCl_3$): 14.56, 14.59, 23.10, 23.11, 23.15, 23.19, 26.37, 29.33, 29.49, 29.51, 30.27, 31.94, 31.96, 32.05, 39.91, 58.65, 112.47, 112.68, 112.91, 119.63, 119.71, 126.00, 129.35, 130.01, 130.49, 134.57, 136.40, 148.98, 153.09, 153.09, 153.96, 154.61, 159.49, 165.14, 176.58. MS (ESI) m/z $[M]^+$ Calcd for $C_{37}H_{48}FN_5O_3S^+$: 660.34. Found: 660.25. HPLC purity 96.77%.

1-(8-(1-benzyl-6-fluoro-4-oxo-1,4-dihydroquinoline-3-carboxamido)octyl)-5-(4-(hexyloxy)-1,2,5-thiadiazol-3-yl)-1-methyl-1,2,3,6-tetrahydropyridin-1-ium bromide ***3-C8***

Transparent oil; 74% yield; R_f = 0.18 (CH_2Cl_2/MeOH = 9:1); ^{1}H NMR ($CDCl_3$): 0.89-0.92 (m, 3H, **H**$_M$), 1.25-1.44 (m, 12H, **H**$_I$, **H**$_H$, **H**$_L$, NH-CH_2-C**H$_2$**, Alkyl), 1.58-1.65 (m, 4H, **H**$_G$, Alkyl), 1.83 -1.86 (m, 2H, Alkyl), 2.75-2.77 (m, 4H, Alkyl, **H**c), 2.88-2.94 (m, 2H, Alkyl), 3.43-3.48 (m, 5H, **H**$_A$, Alkyl), 3.57-3.65 (m, 2H, **H**$_E$), 3.75-3.80 (m, 2H, **H**$_B$), 4.47 (t, 2H, J=6.8, **H**$_F$), 5.49 (s, 2H, C**H$_{2benzyl}$**), 7.13-7.15 (m, 2H, **H**$_7$, **H**$_D$), 7.32-7.35 (m, 5H, C**H$_{phenyl}$**), 7.42 (dd, 1H, J= 4.2, J=9.3, **H**$_8$), 8.14 (dd, 1H, J= 3.0, J=8.8, **H**$_5$), 8.92 (s, 1H, **H**$_2$), 9.92 (t, 1H, J=5.5, N**H**).

^{13}C NMR ($CDCl_3$): 14.14, 2.10, 22.40, 22.42, 22.66, 25.76, 26.19, 26.81, 28.82, 28.93, 29.56, 31.17, 39.18, 48.82,57.17, 58.30, 64.48, 71.86, 77.36, 111.01, 112.13, 119.33, 119.40, 121.45, 122.99, 125.95,

126.22, 128.93, 129.58, 134.13, 135.98, 143.53, 148.55, 153.32, 162.80, 164.77, 170.43, 176.15. MS (ESI) m/z $[M]^+$ Calcd for $C_{39}H_{51}FN_5O_3S^+$: 688.37. Found: 688.25. HPLC purity 96.92%.

1-*(10-(1-benzyl-6-fluoro-4-oxo-1,4-dihydroquinoline-3-carboxamido)decyl)-5-(4-(hexyloxy)-1,2,5-thiadiazol-3-yl)-1-methyl-1,2,3,6-tetrahydropyridin-1-ium bromide* ***3-C10***

Transparent oil; 25% yield; R_f = 0.16 (CH_2Cl_2/MeOH = 9:1); ^{1}H NMR ($CDCl_3$): 0.84 (t, 3H, Alkyl, **H**$_M$), 1.23-1.38 (m, 16H, **H**$_I$, **H**$_H$, **H**$_L$, Alkyl), 1.56-1.58 (m, 4H, Alkyl), 1.76 -1.80 (m, 4H, Alkyl, **H**$_G$), 2.66-2.87 (m, 2H, **H**c), 2.88-2.89 (m, 2H, Alkyl), 3.38-3.57 (m, 5H, **H**$_A$, Alkyl), 3.75-3.70 (m, 2H, **H**$_E$), 3.80-3.82 (m, 2H, **H**$_B$), 4.40 (t, 2H,J=6.7, **H**$_F$), 5.42 (s, 2H, C**H**$_{2benzyl}$), 7.06-7.08 (m, 2H, **H**$_7$, **H**$_D$), 7.26-7.28 (m, 5H, C**H**$_{phenyl}$), 7.36 (dd, 1H, J= 4.2, J=9.3, **H**$_8$), 8.08 (dd, 1H, J= 3.0, J=8.8, **H**$_5$), 8.86 (s, 1H, **H**$_2$), 9.84 (t, 1H, J=5.5, N**H**).

^{13}C NMR ($CDCl_3$): 13.99, 21.92. 22.51, 25.61, 26.19, 26.99, 28.77, 29.08, 29.13, 29.15, 29.19, 29.57, 31.37, 39.29, 48.68, 56.91, 58.11, 64.16, 71.69, 76.71, 111.85, 112.11, 119.23, 121.40, 122.86, 125.82, 126.07, 128.76, 129.42, 129.87, 129.94, 133.99, 135.82, 135.54, 140.02, 143.43, 148.37, 162.64, 164.57, 170.50, 176.01. MS (ESI) m/z $[M]^+$ Calcd for $C_{41}H_{55}FN_5O_3S^+$:716.40. Found: 716.20. HPLC purity 97.11%.

Pharmacology

The bitopic compounds **3-Cn**, were evaluated through radioligand binding assay in dissociation and equilibrium studies to assess the affinity of ligands to both the allosteric and the orthosteric binding site, respectively. The signaling pathway following receptor activation was evaluated in IP1 accumulation assay. Additionally, making use of the new Split luciferase complementation assay[192] the degree of G_a and PLC-b3 interaction was measured. After study of the receptor binding of the new molecules, $G_{\alpha q}$ activation was investigated by measuring the degree of approach of the $G_{\alpha q}$ protein and the effector protein phospholipase involved in the signaling cascade of the M1 muscarinic receptor. The engineered cells were kindly provided by Timo Littmann. In this assay the two luciferase fragments were

incorporated into the effector proteins rather than to the receptor, leaving the latter genetically unmodified.

The IP1 assay developed by CisBio Bioassays[229,230] was conducted to evaluate receptor responses through the phospholipase C pathway. As described above, binding of an agonist to $G_{q/11}$-proteins causes activation of phospholipase C. Subsequently PIP2 is hydrolysed, releasing DAG and IP3. By measuring the IP3 concentration, a ligand-mediated G_q-coupled receptor response can be quantified. Due to IP3 instability its measurement is not possible directly. However, IP3 hydrolyses rapidly to inositol biphosphate (IP2) and inositol monophosphate (IP1), which accumulates in the cell. IP1 is stabilized through LiCl addition in the well plate. The concentration of IP1 can be determined as a surrogate for IP3 concentration.

Radioligand binding assay: Equilibrium and Dissociation binding data

The novel heterobivalent hybrids **3-Cn** were pharmacologically evaluated in radioligand binding assays at human M1 mAChR expressed in CHO cell lines by competition assays using [^{3}H]NMS as a radioligand, following a previously described protocol.[135]

The allosteric component of the bitopic compounds was also investigated. The experiments were conducted following the two-kinetics experiment protocol.[208]

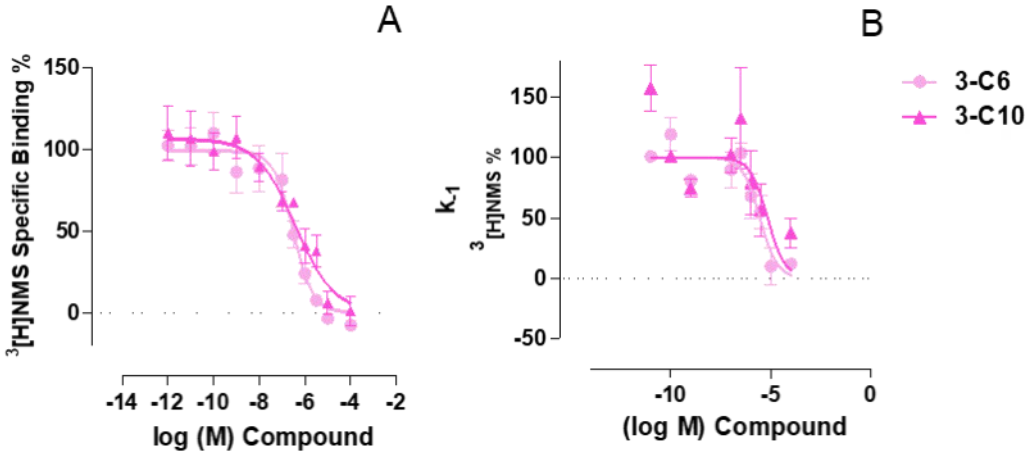

Figure 2. A. Effect of increasing concentrations of the hybrid compounds (**3-Cn**) on specific percent equilibrium binding of [^{3}H]NMS in CHO-hM1 membranes. **B.** Allosteric effects of the hybrids (**3-Cn**) as

reflected by the inhibition of [^{3}H]NMS dissociation from M1 receptors in CHO hM1 membranes. The allosteric effect is expressed as the ratio of the rate of [^{3}H]NMS dissociation in the presence of compound relative to the rate of dissociation of [3H]NMS in the absence of test compound expressed in percent k^{-1}. Data represent mean ± S.E.M. from three to four independent two-point kinetic experiments, conducted in quadruplicate.

The affinity values, expressed as pKi, and the dissociation half maximal inhibitory concentration pIC_{50} of compounds **3-Cn** are reported in Table 1. The pKi values of 6.48 and 6.33 show excellent affinity of the BQCAd/Xano compounds to the orthosteric site of the M1 muscarinic receptor, overcoming the affinity of Iperoxo itself. The compounds are even able to delay the dissociation of [^{3}H]NMS from the hM1 receptor with pIC_{50} values (pIC_{50}: 5.55 and 5.54) absolutely comparable to the BQCAd allosteric modulator itself (pIC_{50}: 5.47).

Table 1. Affinity Constants, expressed as pKi of Compounds **3-Cn** and reference compound Iperoxo for cloned hM1 mAChRs, expressed in CHO Cells.

Compound	Radioligand Binding Assay Equilibrium		Radioligand Binding Assay Dissociation
	pIC_{50}	pKi	pIC_{50}
Iperoxo	5,93 ± 0,06	6,13	n.d.
BQCAd	n.d.	n.d.	5,47±0,20
BQCA-4-Xano	n.d.	n.d.	n.d.
BQCA-6-Xano	6,48±0,14	6,90	5,55 ± 0,30
BQCA-8-Xano	n.d.	n.d.	n.d.
BQCA-10-Xano	6,33±0,25	6,74	5,54±0,30

Both binding experiments of the new investigated molecules suggest a bitopic binding mode with the M1 muscarinic receptor. The dissociation experiments propose that the hybrids stick to the allosteric binding topography, slowing down the dissociation of the radioligand.

BQCAd probably binds to the allosteric core region which is located next to the entrance to the orthosteric binding cavity[231], thereby favoring Xanomeline's access to the orthosteric site, as shown by the equilibrium binding experiments. The bitopic binding pose, in which both orthosteric and allosteric sites are concomitantly engaged in one receptor by one molecule can therefore be assumed. The alternative possibility, the purely allosteric binding pose cannot be completely excluded. More probably

the ligand adopts the two poses simultaneously in the dynamic ligand binding phenomenon, as already described for other dualsteric ligands.[109]

M1 functional activity through Split-Assay and IP1 accumulation assay

In order to check how the interaction properties of the hybrids with muscarinic receptors, determined in RLB assay, would translate into functional effects, we tested the compounds *in vitro* using CHO cell line stably expressing *h*M1 for the IP1 experiment and HEK293T cells stably co-transfected with the human M1 receptor and the $G\alpha_q$-PLC-β3 sensor for the Split-Luc assay.

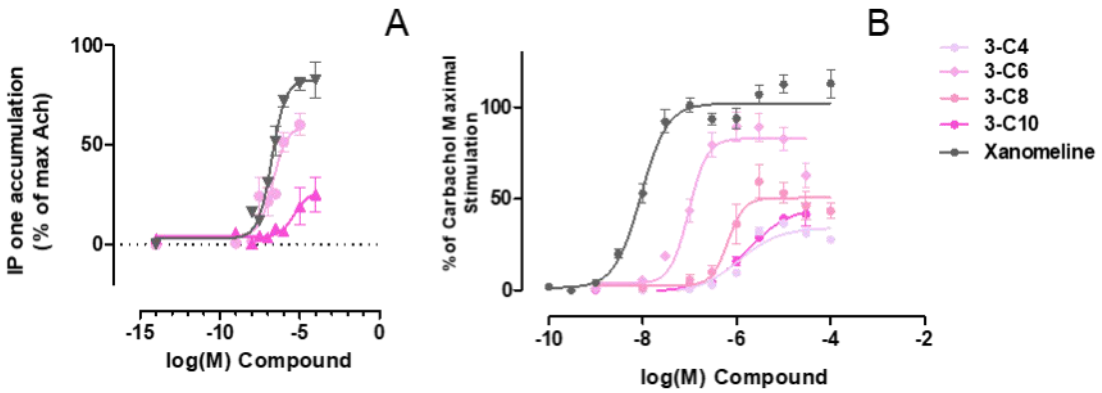

Figure 3. A. Characterization of the dualsteric BQCAd/Xanomeline hybrids compound on downstream signaling. **B.** Dose response curve of Split-Luc assay. Data represent mean ± S.E.M. from three to four independent two-point kinetic experiments, conducted in triplicate.

Figure 3A shows the dose-response curves of the dualsteric BQCAd-Xanomeline compounds **3-Cn** and Xanomeline (**2**) as reference compounds in comparison to ACh as the positive control, with its maximum response set to 100%. The reference compounds **3-C6, 3-C10** shown show partial receptor response depending on their chain lengths. The longer chain compound shows a maximum activation of 29%, while the derivative with 6 methylene units of 59% (Table 2). This finding is in line with the previously published results for similar dualsteric compounds[82], strengthening the hybrid approach to generate partial M1 receptor agonists.

From the study of the phospholipase C pathway via Split-Luc assay (Figure 3B) it emerges that all the synthesized compounds act as partial agonists, with a maximum activation of 85% for the

derivative of 6 methylene units spacer. The derivatives of 4 and 10 carbon atoms linker produce the lowest G_a protein activation (E_{max}: 34% and 45% for **3-C4** and **3-C10**, respectively). The compound with higher potency is again the compound **3-C6** with 6 methylene units, which is therefore confirmed to be the best derivative of the entire series.

TABLE 2. Pharmacological parameters characterizing the effects of the indicated compounds on IP1-accumulation, Split-Luc assay and Radioligand binding assay. pEC50, concentration of the indicated compounds inducing a half-maximal response, % Emax, maximum effect as a percentage of ACh (100 µM) in the IP1 assay and of CCh (100 µM) and *n* number of repetitions. n.d.: not determined.

Compound	IP1 Assay pEC50		Split-Luc Assay pEC50	
	pEC50	Emax	pEC50	Emax
Ach	6.66 ± 0.09	96.73 ± 3.10	6.88 ± 0.02	96.91 ± 1.28
Iperoxo	8.71 ± 0.07	102.50 ± 2.07	8.89 ± 0.04	104.60 ± 0.85
Xanomeline	6.65 ± 0.14	83.39 ± 3.34	8.00 ± 0.07	100.7 ± 2.16
BQCA-4-Xano	n.d.	n.d.	5.95 ± 0.10	34.18 ± 1.47
BQCA-6-Xano	6,67±0,24	59.27 ± 7.52	7,18 ± 0,13	85.35 ± 3.50
BQCA-8-Xano	n.d.	n.d.	6.31 ± 0.19	52.27 ± 3.71
BQCA-10-Xano	5,34±0,47	26.11 ± 5.11	5,75 ± 0,11	45.13 ± 2.47

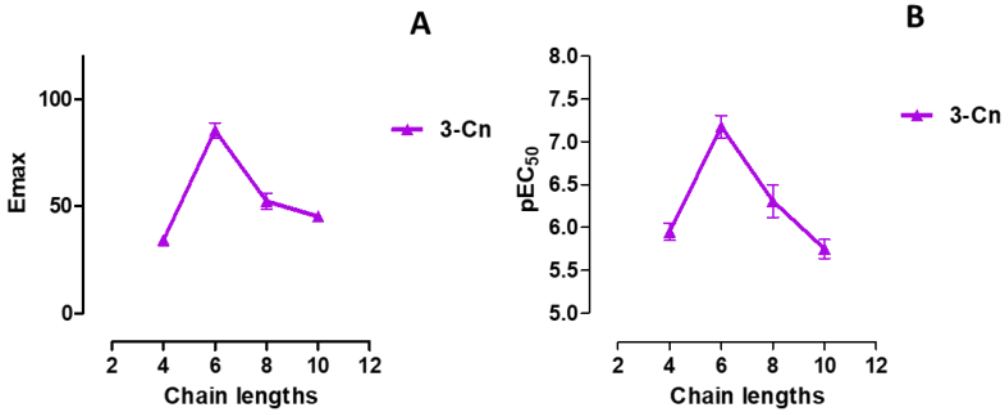

Figure 3. Efficacy (A) and potency (B) dependence on the chain lengths in the split assay.

Plotting the efficacy and potency of the new series of compounds in function of the linker elongation, the 6-carbon chain compound **3-C6** is highlighted as the molecule with the optimal spacer length between the two allosteric and orthosteric portions. The bell-shape curves indicate an increase in

potency and efficacy with the lengthening of linker chain, until reaching a maximum, followed by a gradual decrease.

Comparison with other Xanomeline Hybrids

In contrast to similar hybrids containing tacrine and xanomeline **4-Cn** previously synthesized by Fang et al.[135] (Figure 4) the new compounds show functional activity, completely absent in the formerly investigated hybrids. However, for both series of compound similar affinity at the M1 receptor was measured. Instead of a simultaneous allosteric/orthosteric binding, Fang's compounds prefer a purely allosteric binding mode. It should be noted that the connection point chosen between the two allosteric and orthosteric units is different. While in the antecedent Tac/Xano hybrids, the xanomeline's O-hexyl chain was used as connecting linker to tacrine, in the new **3-Cn** hybrids the 1-methyl-1,2,3,6-tetrahydropyridine nitrogen is bound to the spacer generating a quaternary ammonic head.

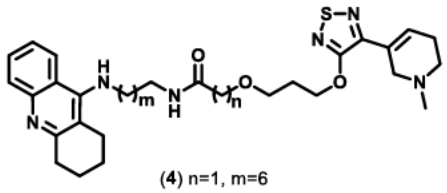

Figure 4. Xanomeline/ Tacrine hybrids from Fang at al.[135]

Again the xanomeline hexyl chain was used by Bonifazi et al.[12] to connect xanomeline with the allosteric modulator 77-LH-28-1 (**5**). In this case, in addition to affinity for the M1 receptor, the hybrids **6-Cn** show also weak agonistic or an antagonistic activity in function of the length of the spacer chain.

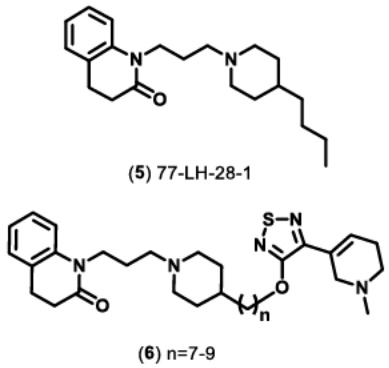

Figure 5. Xanomeline/77-LH-28-1 bitopic compounds from Bonifazi et al.[12]

By comparison of the newly synthesized Xanomeline-bitopic compounds with the hybrids (presented in Results part 3: IP1 accumulation assay) containing the BQCAd fragment and different orthosteric moieties, they represent the only case in which even with a linker of 10 carbon atoms IP-1 accumulation can be observed. This could be due to the atypical binding pose of xanomeline[141,142,232] at the M1 muscarinic orthosteric binding site, which could guide even the bitopic ligand, in a unique hM1 binding mode among all the series of investigated compounds. *X*anomeline induces a specific mode of M1 receptor activation by interacting with a site that does not fully overlap with the acetylcholine orthosteric site. The molecular mode of xanomeline binding to the M1 receptor is complex: besides an orthosteric interaction there is a wash-resistant component (persistent binding) that seems to result not only from hydrophobic interactions but also from ionic interactions with a secondary M1 receptor binding site, excluding the first hypothesis of a simple hydrophobic interaction of xanomeline's O-hexyl chain with the membrane.[135,141,233] Figure 6 shows the docking poses at the M1 muscarinic acetylcholine receptor of the atypical M_1-preferring agonists (xanomeline) and the classical non-selective orthosteric agonists (carbachol).[142]

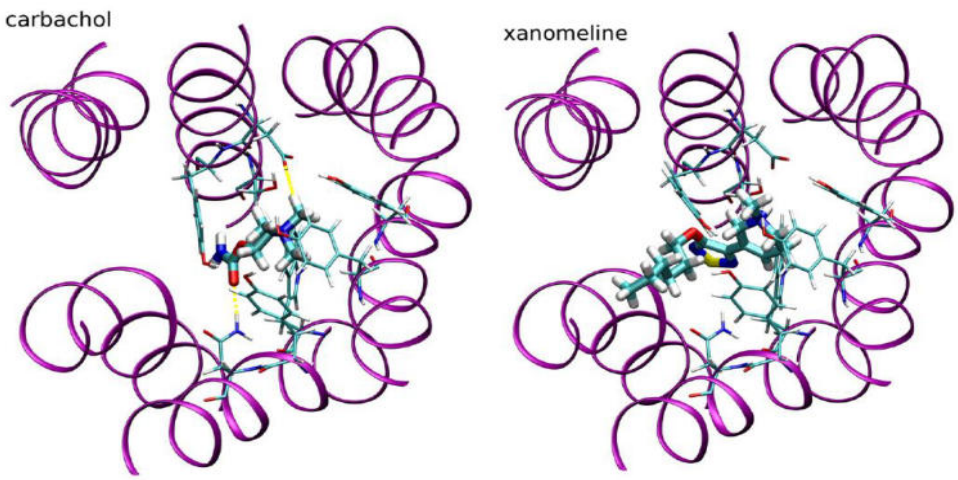

Figure 6. Top docking poses of carbachol (left) and xanomeline (right) shown from the extracellular view. Orientation, TM III up and TM VI down. Helices TM II to TM VII are shown in purple. Ligands and displayed amino acids (D105, Y106, S109, W378, Y381, N382 and Y404) are colored according elements: cyan – carbon, white – hydrogen, blue – nitrogen, red – oxygen, yellow – sulfur. Yellow dashed lines denote ligand-receptor hydrogen bonds. Modified from Randáková et al.[142]

Several lines of evidence suggest that the atypical agonist may induce different receptor conformations and possibly utilize different activation mechanisms at the molecular level. This combined with the design of bitopic derivatives could result in exceptionally interestingly compounds having significant implications in terms of understanding alternate modes of mAChR activation, key regions in obtaining subtype-selectivity and the therapeutic use of xanomeline derivatives.

Conclusion

A series of BQCAd-Xanomeline (**3-Cn**) hybrids was designed by conjugating an M1/M4 active agonist (Xanomeline) with a benzyl quinolone carboxylic acid derivative moiety (BQCAd) through an alkyl chain with adequate length capable of assuring a dual-binding mode of M1 activation. Thus, the initial hypothesis to obtain dualsteric compounds acting directly at the M1 receptor proved correct, demonstrating the hybrids' binding mode and their functional activity at the M1 receptor.

Understanding the mechanism(s) of interaction of xanomeline with the M1 mAChR is fundamental for the potential therapeutic use of this agent and its derivatives in the treatment of AD.[232] In particular,

further studies in terms of selectivity on the M1 receptor subtype are expected to be pursued. Additionally, computational modeling could be important for exploring the mechanism of the hybrid's interaction with the M1 receptor in order to improve the understanding of the allosteric and orthosteric key regions and give an important contribution in the field of AD research.

5. Tacrine-Xanomeline and Tacrine-Iperoxo hybrid ligands: Synthesis and biological evaluation at acetylcholinesterase and M1 muscarinic acetylcholine receptors

Marco Maspero[a,1], Daniela Volpato[b,1], Davide Cirillo[a], Natalia Yuan Chen[b], Regina Messerer[b], Christoph Sotriffer[b], Marco De Amici[a], Ulrike Holzgrabe[b,*], Clelia Dallanoce [a,*]

[a] Department of Pharmaceutical Sciences, Medicinal Chemistry Section "Pietro Pratesi", University of Milan, Via L. Mangiagalli 25, 20133 Milan, Italy

[b] Pharmaceutical and Medicinal Chemistry, Institute of Pharmacy and Food Chemistry, University of Würzburg, Am Hubland, 97074 Würzburg, Germany

* Corresponding authors:

E-mail addresses: clelia.dallanoce@unimi.it (C. Dallanoce), ulrike.holzgrabe@uni-wuerzburg.de (U. Holzgrabe)

[1] These authors contributed equally to this work.

Reprinted/adapted with permission from Maspero, M.; Volpato, D.; Cirillo, D.; Yuan Chen, N.; Messerer, R.; Sotriffer, C.; Amici, M. de; Holzgrabe, U.; Dallanoce, C. Tacrine-xanomeline and tacrine-iperoxo hybrid ligands: Synthesis and biological evaluation at acetylcholinesterase and M1 muscarinic acetylcholine receptors. Bioorganic chemistry 2020, 96, 103633.

Abbreviations:

ACh, acetylcholine; AChE, acetylcholinesterase; AChEIs, acetylcholinesterase inhibitors; AD, Alzheimer's disease; ASP, Astex statistical potentials; ATC, acetylthiocholine iodide; BChE, butyrylcholinesterase; CAS, catalytic active site; CCh, carbachol; CHO, Chinese hamster ovary; CSD, Cambridge structural database; DAG, 1,2-diacylglycerol; DMEM, Dulbecco's modified Eagle's medium; DSX, DrugScoreX; DTNB, 5,5'-dithiobis-(2-nitrobenzoic acid); ELSD, evaporative light scattering detector; ESI, electrospray ionization; FCS, fetal calf serum; FRET, fluorescence resonance energy transfer; GDP, guanosine 5'-diphosphate; GTP, guanosine 5'-triphosphate; HAM- F12, Ham's nutrient mixture F-12; HBSS, Hank's balanced salt solution; HEPES, 4-(2-hydroxyethyl)-1-piperazineethanesulfonic acid; HepG2, human hepatocellular carcinoma; hM_1R, human M_1 receptor; HTRF, time-resolved fluorescence resonance energy transfer; IP1, inositol 1-phosphate; IP_3, inositol 1,4,5-trisphosphate; L-15, Leibovitz's L-15 medium; LC-MS, liquid chromatography mass spectrometry; mAChRs, muscarinic acetylcholine receptors; MOE, molecular operating environment; PAS, peripheral anionic site; PBS, phosphate-buffered saline; PIP_2, phosphatidylinositol 4,5-bisphosphate; PLC, phospholipase C; PLCβ, phospholipase Cβ; RMSD, root-mean-square deviation; R_f, retention factor; CNS, central nervous system; TcAChE, *Torpedo californica* acetylcholinesterase.

Keywords:

Multitarget compounds, Bitopic ligands, Allosteric modulation, M_1 muscarinic acetylcholine receptor, Ellman's assay, Inositol monophosphate, Phospholipase C , Iperoxo, Tacrine, Xanomeline

Abstract: We synthesized a set of new hybrid derivatives (**7-C8**, **7-C10**, **7C12** and **8-C8**, **8-C10**, **8-C12**), in which a polymethylene spacer chain of variable length connected the pharmacophoric moiety of xanomeline, an M_1/M_4-preferring orthosteric muscarinic agonist, with that of tacrine, a well-known acetylcholinesterase (AChE) inhibitor able to allosterically modulate muscarinic acetylcholine receptors (mAChRs). When tested *in vitro* in a colorimetric assay for their ability to inhibit AChE, the new compounds showed higher or similar potency compared to that of tacrine. Docking analyses were performed on the most potent inhibitors in the series (**8-C8**, **8-C10**, **8-C12**) to rationalize their experimental inhibitory power against AChE. Next, we evaluated the signaling cascade at M_1 mAChRs by exploring the interaction of $G\alpha_q$-PLC-β3 proteins through split luciferase assays and the *myo*-Inositol 1 phosphate (IP1) accumulation in cells. The results were compared with those obtained on the known derivatives **6-C7** and **6-C10**, two quite potent AChE inhibitors in which tacrine is linked to iperoxo, an exceptionally potent muscarinic orthosteric activator. Interestingly, we found that **6-C7** and **6-C10** behaved as partial agonists of the M_1 mAChR, at variance with hybrids **7-Cn** and **8-Cn** containing xanomeline as the orthosteric molecular fragment, which were all unable to activate the receptor subtype response.

1. Introduction

The decrease in acetylcholine (ACh) levels as well as the dysfunction and decline of cholinergic neurons, which were the basis to formulate the "cholinergic hypothesis" of Alzheimer's disease (AD), are typical hallmarks associated with the neurodegenerative impairment of this pathology[1-3]. To improve the cholinergic neurotransmission, different approaches have been explored, including the enhancement of ACh synthesis, the augmentation of its presynaptic release, the stimulation of cholinergic postsynaptic muscarinic and nicotinic receptors, and the reduction of ACh synaptic degradation by means of cholinesterase inhibitors. Unfortunately, no resolution therapy for AD is currently available, and drugs on the market that inhibit acetylcholinesterase (AChEIs) are simply able to alleviate the disease symptoms and/or delay its progression.

Tacrine **1** (Fig. 1), the first AChEI approved by FDA for the AD therapy, was withdrawn from the market due to its dose-dependent hepatotoxicity[4]. Nevertheless, it still represents an interesting scaffold to be studied, since it positively modulates the affinity and functional response of ligands binding the orthosteric ACh site[5], showing some selectivity for the M_1 and M_2 mAChR subtypes[6]. Therefore, the

molecular skeleton of tacrine has been used to develop a variety of hybrid molecules[3,7-11] with the purpose of combining the relevant AChE inhibition of the parental compound with other favorable pharmacological properties[12,13]. In addition, due to the ability of tacrine to occupy both the catalytic active site (CAS) and the peripheral anionic site (PAS) of the enzyme, bistacrine dimers like **2** (Fig. 1) showed a 1000-fold higher AChE inhibitory potency than tacrine itself[14].

As far as complementary or alternative approaches to the therapy of AD are considered, the current data do not support the application of orthosteric muscarinic agonists. In this respect, the most studied mAChR has been the M_1 subtype, which is widely expressed in the central nervous system and is involved in many physiological and pathological brain functions as well as motor control and regulation of body temperature[15,16]. However, the orthosteric binding site of the M_1 receptor has high homology with the other mAChR subtypes, which results in pronounced side effects of the "selective" M_1 agonists developed so far[5]. On the other hand, the less conserved allosteric binding site of the M_1 receptor could be selectively targeted by allosteric M_1-selective enhancers, albeit to date compounds with this profile show comparatively weak potencies[17]. Among the investigated M_1 activators, xanomeline **3** (Fig. 1) is a M_1/M_4-preferring orthosteric agonist with promising antidementive properties *in vivo*, but its dose-limiting side effects precluded any clinical development[5,18]. Additionally, xanomeline has a peculiar mode of mAChR activation, being different from that of conventional agonists such as carbachol and endogenous ACh[19]. It was also reported to have a wash-persistent binding to the M_1 subtype, which may arise not only from hydrophobic interactions between the xanomeline's *O*-hexyl-containing chain and the receptor protein, but also from the ligand recognition of a secondary binding site on the receptor[20,21].

In this paper, we designed a new set of hybrid ligands containing the pharmacophoric moieties of tacrine and xanomeline, by exploiting our experience in the study of dualsteric (i.e. simultaneous orthosteric/allosteric) ligands[22-26] of mAChRs and hybrid derivatives active at the M_1 mAChR subtype as alleged antidementive agents[3,5,27,28] as well as with the purpose of developing new strategies for therapeutic intervention on AD. We aimed at multifunctional molecules combining synergistic effects. First, the direct activation of the M_1 receptor subtype at the orthosteric site by xanomeline, then AChE inhibition by the tacrine molecular portion coupled with a positive allosteric cooperativity between the two moieties at the examined receptor subtype. Hybrid compounds containing the same

pharmacophoric fragments connected by various chemical spacers (amines **4** and amides **5**, Fig. 1)[5] showed a relevant AChE inhibition and a purely allosteric binding at the inactive M_1 mAChR, which precluded any activation of the receptor response.

Thus, we explored if a different molecular connection between the two pharmacophoric moieties could promote the expected pharmacological profile of the resulting hybrids, in particular their behavior as M_1 mAChR activators. To such an end, in the designed compounds the primary amine group of tacrine was linked to the nitrogen atom of the tetrahydropyridine nucleus of xanomeline by means of alkyl chains of different length (Fig. 1). In this respect, we used as model compounds our prominent hybrid derivatives **6-C7**, **6-C10** (Fig.1)[3], in which tacrine was combined with the orthosteric muscarinic agonist iperoxo[29,30]. The new, putative bipharmacophoric ligands were prepared as tertiary amines **7-Cn** (**7-C8**, **7C-10**, **7-C12**) and their corresponding quaternary tetrahydropyridinium salts **8-Cn** (**8-C8**, **8-C10** and **8-C12**). All synthesized compounds were evaluated *in vitro* for their ability to inhibit AChE and activate M_1 receptors. To further investigate ligand-enzyme interactions, molecular modeling studies were also performed on the most potent inhibitors. For comparison, also hybrids **6-C7**, **6-C10** were evaluated for M_1 receptor activation, revealing a promising biological profile.

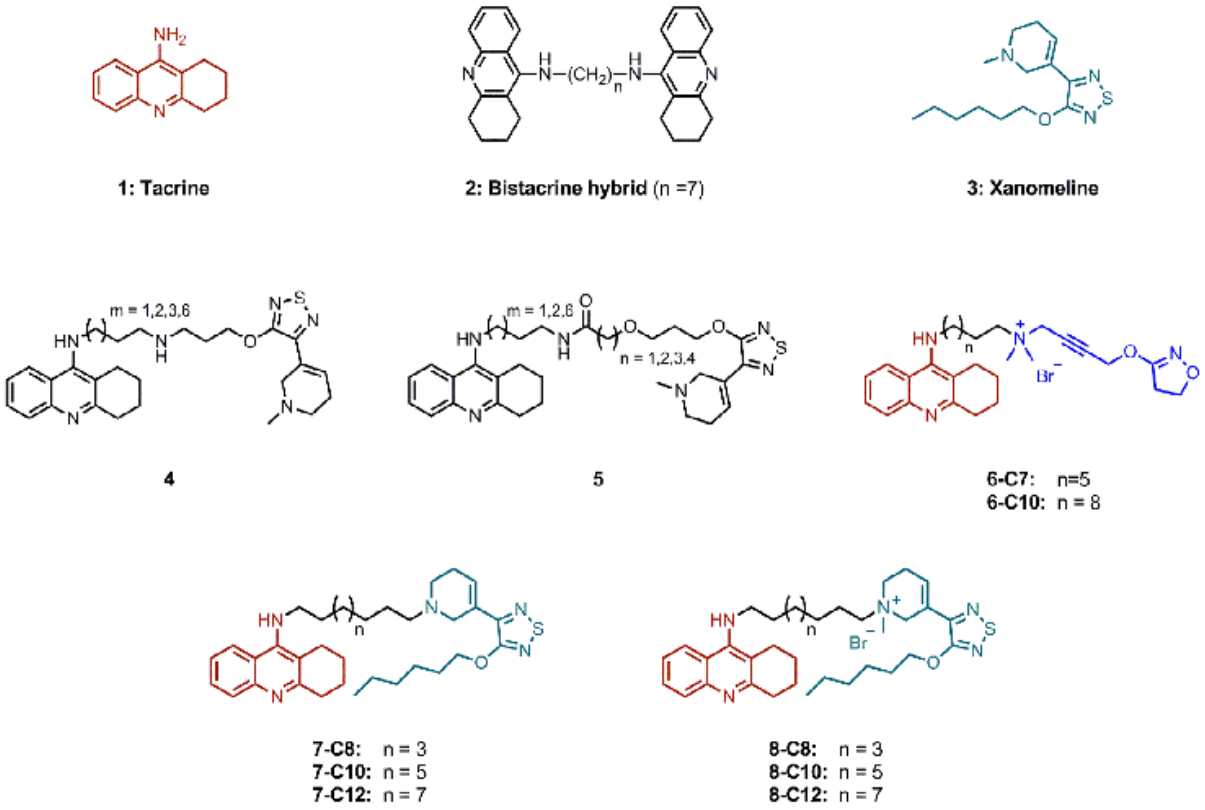

Fig. 1. Structures of reference compounds and of the known (**6-C7** and **6-C10**) and new (**7-C8**, **7-C10**, **7C12**, **8-C8**, **8-C10**, **8-C12**) tacrine-containing hybrid derivatives investigated in this study.

2. Results and discussion

2.1. Chemistry

Tacrine **1** was synthesized following the literature procedure reported in Scheme 1[31], which exploits the reaction of cyclohexanone with 2-aminobenzonitrile in the absence of solvent under zinc chloride catalysis. To import an alkyl linker chain at the amine function, **1** was reacted, in the presence of potassium hydroxide, with a large excess of commercially available dibromide derivatives of the respective spacer length, thus providing intermediate bromides **9a**, **9b**[32] and **9c**.

The orthosteric pharmacophoric moiety xanomeline was prepared following a Strecker-like known procedure[33], as reported in Scheme 1.

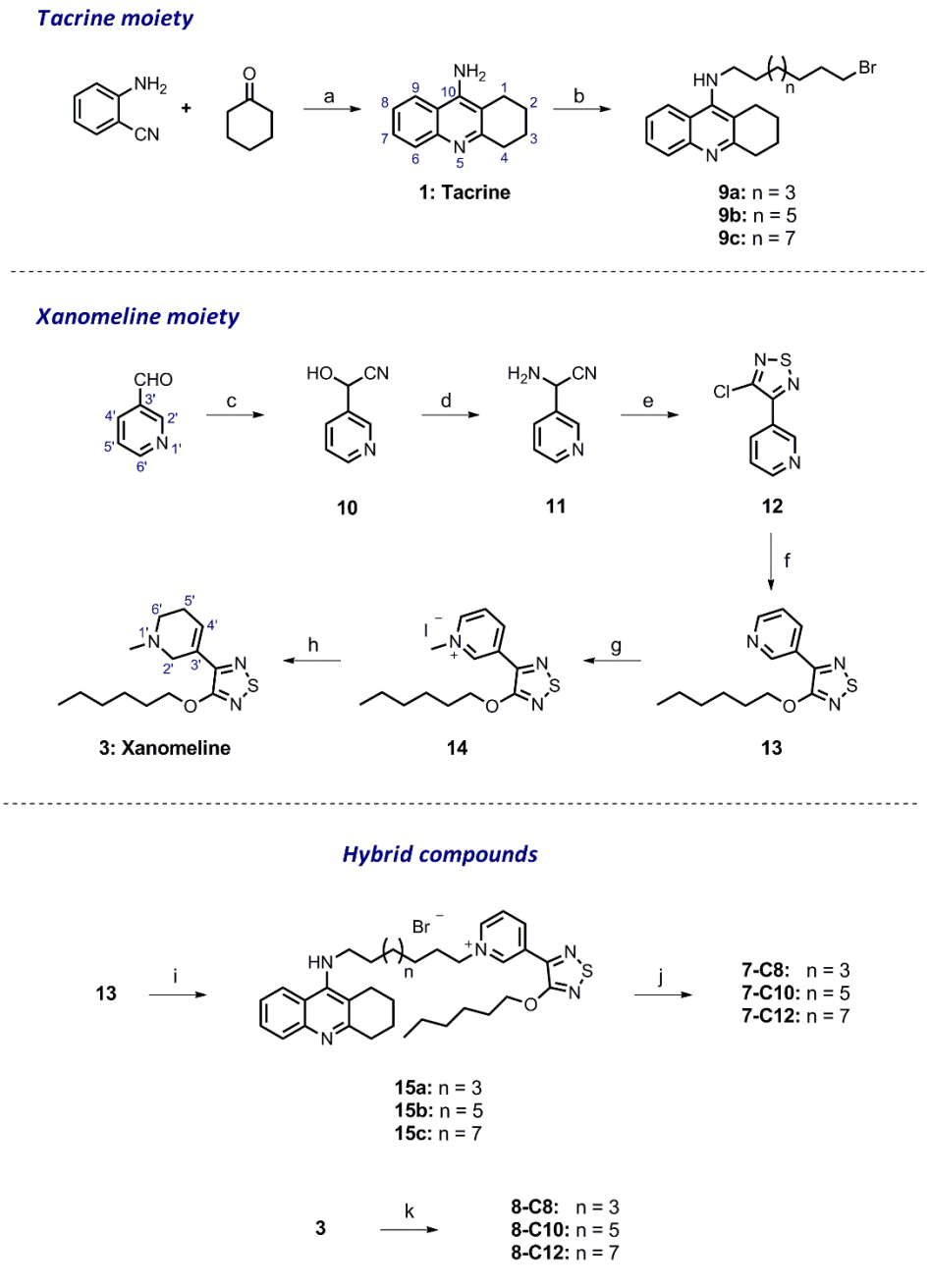

Scheme 1. Synthesis of target compounds. Reagents and conditions: (a) $ZnCl_2$, 120°C, 16 h; (b) $Br(CH_2)_nBr$ (n = 8 or 10 or 12), KOH, CH_3CN, 40°C, 72 h; (c) TMSCN, AcOH, r.t., 23 h; (d) NH_3/NH_4Cl, r.t., 22 h; (e) S_2Cl_2, DMF, 0 °C, 30 min; (f) 1-hexanol, NaH, THF, reflux, 3 h; (g) CH_3I, acetone, r.t., 22h; (h) $NaBH_4$, MeOH, r.t., 24 h; (i) **9a** (or **9b** or **9c**), DMF, 100 °C, 36 h; (j) $NaBH_4$, MeOH, r.t., 5 h. (k) **9a** (or **9b** or **9c**), CH_3CN, MW, 80 °C, 19 atm, 500 W, 10 h.

Briefly, the cyanohydrin **10** was obtained by treating commercially available 3-pyridinecarboxaldehyde with trimethylsilyl cyanide in the presence of acetic acid. Intermediate **10** was then converted into the corresponding aminonitrile derivative **11** by treatment with ammonium chloride in ammonium hydroxide.

This intermediate was cyclized by reaction with disulfur dichloride in *N*,*N*-dimethylformamide to give thiadiazole **12**, which, after nucleophilic substitution with 1-hexanol in the presence of sodium hydride, produced the functionalized thiadiazole **13**. The latter was reacted with methyl iodide in acetone to afford the corresponding quaternary ammonium salt **14**, which underwent reduction with sodium borohydride in methanol to the related tetrahydropyridinium moiety characterizing xanomeline **3**. Synthesis of the pyridine quaternary ammonium salts **15a-c** (Scheme 1) was performed by condensation of thiadiazole **13** with the respective tacrine-containing bromides **9a-c**; subsequent reduction of the pyridinium ring of intermediates **15a-c** with sodium borohydride afforded the desired hybrid compounds **7-Cn** (**7-C8**, **7C-10** and **7-C12**). Similarly, reaction of xanomeline **3** with bromides **9a-c** under microwave irradiation provided the permanently charged methylated analogs **8-Cn** (**8-C8**, **8C-10** and **8-C12**).

2.2. Biological activity and molecular modeling investigations

2.2.1. Acetylcholinesterase inhibitory activity

The two groups of tacrine-xanomeline analogs **7-Cn** and **8-Cn** were tested for AChE inhibition by using the Ellman's test[34], and the resulting pIC_{50} values were compared with those available for hybrids **6-Cn** (Table 1). We used the AChE from electric eel which, in our hands, gave quite comparable results to those obtained on related hybrids with the recombinant hAChE expressed in HEK 293 cells[3,27]. Both sets of compounds **7-Cn** and **8-Cn** were able to inhibit AChE; the tertiary amines **7-Cn** exhibited anticholinesterase activity (pIC_{50} between 6.95 and 7.83) comparable to that of the model compound tacrine (pIC_{50} = 7.73). Conversely, the quaternary tetrahydropiridinium derivatives **8-Cn** were more active (pIC_{50} values between 8.12 and 9.55) than tacrine, with inhibitory potencies in the range of those shown by the tacrine-iperoxo hybrids **6-C7** (pIC_{50} = 8.76) and **6-C10** (pIC_{50} = 9.81).

Table 1. Cholinesterase activity of Tacrine and related hybrid compounds determined through the Ellman's test.

Entry	AChE[a] pIC_{50}[b] [M]
Tacrine	7.73 ± 0.04
7-C8	7.60 ± 0.12
7-C10	7.83 ± 0.06
7-C12	6.95 ± 0.13
8-C8	9.55 ± 0.12
8-C10	9.08 ± 0.06
8-C12	8.12 ± 0.08
6-C7	8.76[27]
6-C12	9.81[27]

[a]Experiments were performed in triplicate at AChE from electric eel (E.C. 3.1.1.7). [b]pIC_{50} values are the negative logarithm of the concentration causing half-maximal inhibition of cholinesterase activity. Data are expressed as the mean ± S.E.M.

As far as the length of the spacer is taken into account, eight methylene units were optimal to impart the highest AChE inhibitory activity to the positively charged compounds (**8-C8**: pIC_{50} = 9.55). For both series of tacrine-xanomeline derivatives, the longest chain compounds, with twelve methylene units, were those with the lowest inhibitory potency (pIC_{50} = 6.95 for **7-C12** and pIC_{50} = 8.12 for **8-C12**). On the other hand, comparison of the data evidenced in both **7-Cn** and **6-Cn** sets an inhibition peak with a spacer of ten methylene units (pIC_{50} = 7.83 for **7-C10** and pIC_{50} = 9.81 for **6-C10**), thus emphasizing a good tolerability of the linker length in the enzyme gorge between CAS and PAS.

2.2.2. Functional activity at M_1 mAChRs

We studied the functional activity of all the compounds at the M_1 mAChR. Hence, we chose to investigate M_1AChR-mediated PLC response (see Split Luciferase Bioluminescence Assay) and inositol phosphate accumulation (see IP1 Accumulation Assay). Binding of ACh to mAChRs causes a conformational change in the receptor that promotes its association with an intracellular G protein determining its

activation through the conversion of GTP to GDP on the G protein α subunit. The activated G protein dissociates from the receptor, acting as an enzyme to catalyze downstream intracellular events. The functional activity is mediated mainly by the physiologically relevant Gq-signaling pathway. Proteins of the $G\alpha_q$ family trigger the effector proteins phospholipases Cβ1-3 (PLCβ), leading to the hydrolysis of phosphatidylinositol 4,5-bisphosphate (PIP_2) to 1,2-diacylglycerol (DAG) and inositol-1,4,5-trisphosphate (IP_3). IP_3 mediates the release of Ca^{2+} from intracellular compartments, notably from the endoplasmic reticulum.

2.2.3. Split Luciferase bioluminescence assay

Littmann et al.[35] developed a split luciferase complementation assay to study the interaction of M1 mAChR G protein with Phospholipase C, by expression of the newly Gαq-PLC-β3 sensor in combination with hM1R. With this assay, we assessed the early activation stage of interaction between the Gαq and phospholipase C-β3 for the new hybrids. Gα and PLC-β3 were fused on a DNA level with the split luciferase, in order to measure their interaction in terms of bioluminescence. The assay revealed the absence of receptor activation for the tacrine-xanomeline hybrids **7-Cn** and **8-Cn**. Regardless of the presence/absence of a quaternary ammonium head or the length of the spacer chain, these compounds did not show agonism at the M1 mAChR since no activation of the phospholipase C was observed (Fig. 2A and 2B). Therefore, we may assume that these hybrids are unable to adopt a dualsteric binding mode, which triggers the activating functional response at the studied receptor. These findings are in line with those of Fang et al.[5], since also those tacrine-xanomeline hybrids (compounds **4** and **5**, Fig. 1) were found to prefer a purely allosteric binding mode[26,36], which generates an inactive ligand-receptor complex at the M1 subtype. On the contrary, the tacrine-iperoxo hybrids **6-C7** and **6-C10**, which already showed affinity for the M1 mAChR in radioligand binding studies[27], activated the heterodimeric G protein (Fig. 2C), with pEC50 values of 8.24 and 8.06, respectively (Table 2). These iperoxo-containing hybrids are indeed the most potent AChE inhibitors in the series with the additional ability to bind M1 as well as M2 mAChR subtypes.

Table 2. Maximal agonist effect and potency of hybrid compounds stimulating Gα and PLC-β3 interaction in CHO human M_1 cells.

	Split-Luc assay		
Entry	E_{max}[a]	pEC_{50}[b]	n
6-C7	85.57 ± 1.50	8.24 ± 0.05	4
6-C10	78.14 ± 1.45	8.06 ± 0.05	4
7-C8	n.a.[c]	n.a.	3
7-C10	n.a.	n.a.	3
7-C12	n.a.	n.a.	3.
8-C8	n.a.	n.a.	3
8-C10	n.a.	n.a.	3
8-C12	n.a.	n.a.	3
Xanomeline	100.70 ± 2.16	8.00 ± 0.07	3
Iperoxo	104.60 ± 0.85	8.89 ± 0.04	4
CCh	97.78 ± 1.71	6.25 ± 0.04	5
ACh	96.91 ± 1.28	6.88 ± 0.02	9
		pIC_{50}	
Atropine	-	10.06 ± 0.09	4

[a]E_{max} is the maximal effect expressed as percentage. [b]pEC_{50} is the concentration of the indicated compound inducing a half-maximal $G\alpha_q$-PLC activation. Data are normalized to the maximum response of the agonist carbachol. Data are expressed as the mean ± S.E.M. of three to nine independent experiments performed in triplicate. [c] n.a.: not applicable.

In terms of functional behavior, at the M_1 receptor derivatives **6-C7** and **6-C10** showed potency values comparable to those of iperoxo and xanomeline and even higher than those of carbachol and the endogenous agonist ACh. The measured efficacy values normalized to the carbachol (CCh) reference (E_{max} = 85.57% for **6-C7** and E_{max} = 78.14% for **6-C10**) were instead lower than those of reference agonists (Fig. 2D and Table 2), thus engendering hybrid derivatives with a partial agonist profile. According to a model illustrated for bipharmacophoric partial agonists of M_2 mAChRs[36], **6-C7** and **6-C10** behave as "dynamic ligands", i.e. compounds that may bind to a receptor population in two distinct

orientations, the dualsteric binding pose, inducing activation, and the purely allosteric binding pose that precludes receptor activation.

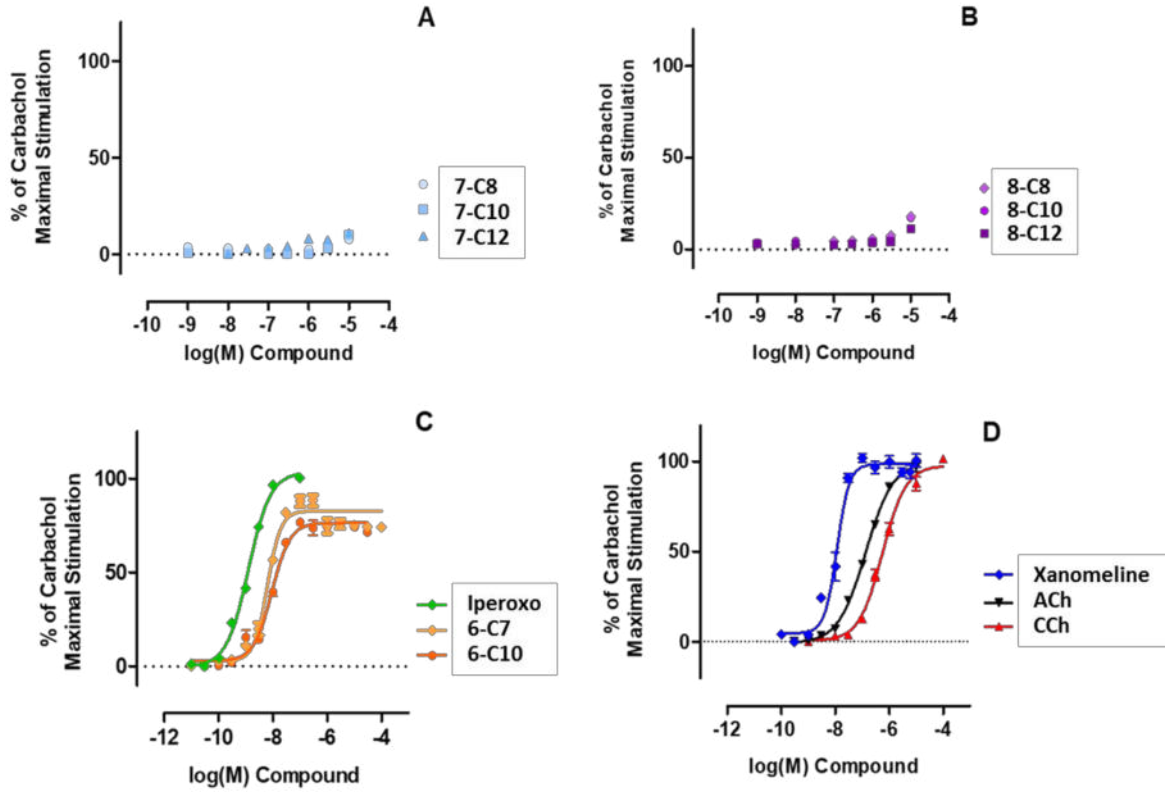

Fig. 2. Dose response curves obtained with the split luciferase assay.

Compounds **7-Cn** and **8-Cn** did not stabilize a G protein active conformation of the M_1 receptor and did not induce receptor stimulation when studied in the agonist mode (Fig. 2A and 2B); therefore, we evaluated their putative antagonist profile, by assessing the ability to counteract the effect of CCh at a concentration corresponding to EC_{80} (3 μM). As illustrated in Fig. 3A and 3B, none of the six structural analogs was able to compete with the agonist to reduce the degree of $G\alpha_q$-PLC activation. Conversely, as expected, the orthosteric antagonist atropine (blue curve) potently competed with CCh, with a pIC_{50} value of 10.06 ± 0.09.

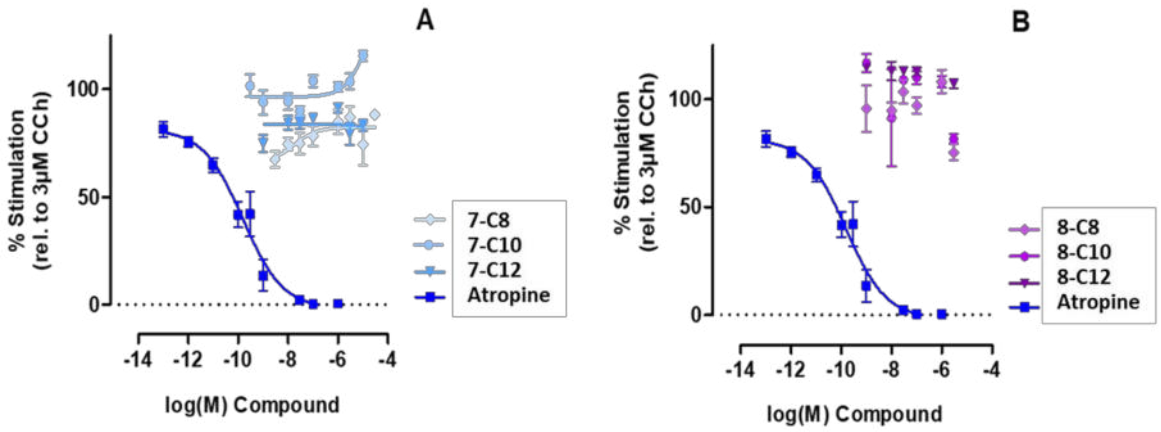

Fig. 3. Dose response curve of Split-Luc assay. Compounds **7-Cn** and **8-Cn** were measured in the antagonist mode. Data represent the mean ± S.E.M. of at least three independent experiments performed in triplicate.

Of note, compounds **7-Cn** and **8-Cn** did not cause cell death, since, despite their application up to 10 µM concentrations, hM_1 cells maintained the maximal response to G protein activation by 3 µM CCh. Therefore, in this cell line, these bipharmacophoric derivatives functionalized on the primary amine of tacrine with chains of different lengths linking orthosteric moieties (xanomeline as well as iperoxo), showed a marked reduction of toxicity with respect to tacrine. This behavior parallels the results we previously reported[3], since the toxicity of the **6-C10** bifunctional compound was also tested in HepG2 cells and found to be very low (IC_{50}: 32.2 ± 0.41 µM), making it an interesting outcome in view of developing putative drug candidates.

2.2.4. IP1 accumulation assay

The measurement of M_1R-stimulated activation of the G protein-mediated pathway was performed applying the IP-One HTRF® assay (Cisbio, Codolet, France), which quantifies the accumulation of inositol phosphate, the degradation product of the second messenger inositol triphosphate (IP3), through FRET-based experiments. The results obtained with the reference compounds and the hybrids **7-Cn** and **8-Cn** in the HTRF-IP1 assay are reported in Fig. 4. Xanomeline and ACh showed their ability to activate the downstream signaling response at the M_1 receptor, with pIC_{50} values of 6.65 and 6.66,

respectively (Fig. 4 and 5A), an outcome matching the second messenger assays reported in the literature[19,37-39]. By contrast, the allosteric fragment tacrine alone is unable to generate IP1 accumulation (Fig. 4).

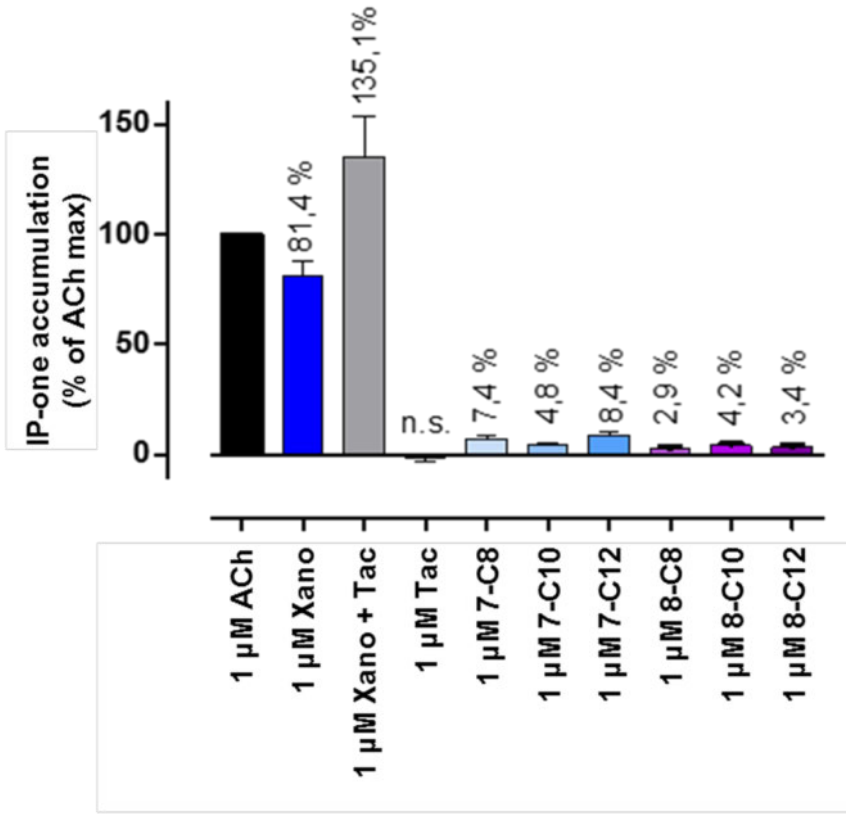

Fig. 4. Absence of IP1-accumulation by xanomeline (Xano)-tacrine (Tac) hybrids in live CHO-hM1 cells. Graph bars represent the mean ± S.E.M of three independent experiments performed in triplicate. Data not significantly different with ANOVA Tukey's Multiple Comparison Test ($P < 0.05$). n.s.: not significantly different from zero (one sample t test) ($P < 0.05$).

The application of a 1 µM tacrine and xanomeline combination resulted in a receptor activation response higher than that measured for xanomeline alone, which is indicative of the positive modulatory effect of tacrine at M_1 mAChRs. Conversely, the covalently bound tacrine-xanomeline molecular fragments were devoid of agonist activity in both sets of target hybrids **7-Cn** and **8-Cn** (Fig. 4), due to the lack of ligand-receptor interaction at the orthosteric recognition site and the consequent inability to cause receptor activation. We extended the IP1 accumulation assay also to the tacrine-iperoxo hybrids **6-C7** and **6-C10**

and obtained a very similar qualitative readout, in accordance with preliminary functional data[27]. After incubation with test compounds for 30 min at 37 °C, addition of detection reagents revealed the partial agonist profile of both dualsteric hybrids, with pIC_{50} values of 7.05 and 6.90 for **6-C7** and **6-C10**, respectively (Table 3, Fig. 5B). Thus, in this second messenger IP1 assay, the partial agonism characterizing the two ligands (E_{max} = 59.0 for **6-C7** and E_{max} = 43.9 for **6-C10**, Table 3) became more evident than in the previous bioluminescence test.

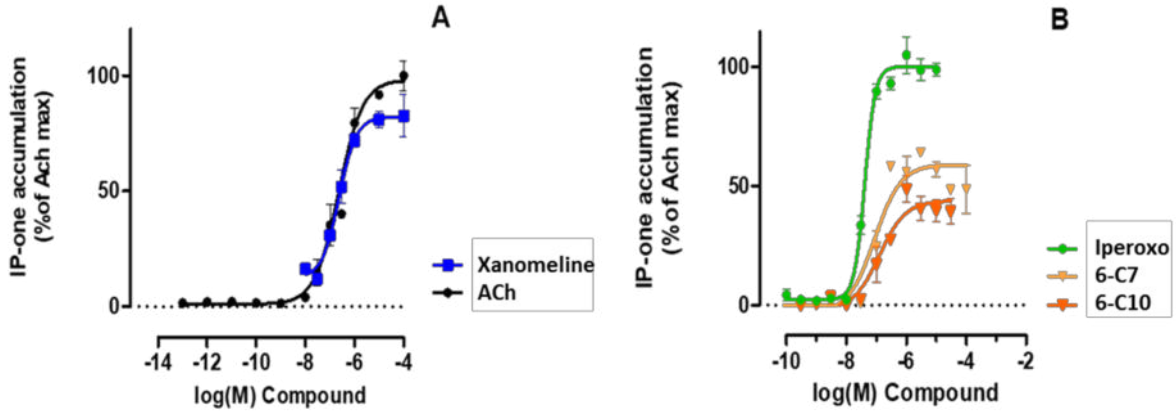

Fig. 5. Partial agonism for IP1 accumulation by hybrids **6-C7** and **6-C10** in live CHO-hM1 cells. Cells were treated with increasing concentrations of the indicated compounds for 30 min, and the resulting increase in intracellular inositol phosphates was measured as described in Materials and Methods. Curves drawn through the data points represent the best fit to the operational model of agonism. Data points are the mean ± S.E.M of three to five independent experiments performed in triplicate.

Table 3. Pharmacological parameters characterizing the effects of the indicated compounds on IP1-accumulation in live CHO-hM1 cells.

	IP1 assay		
Entry	E_{max}[a]	pEC_{50}[b]	n
6-C7	59.00 ± 2.34	7.05 ± 0.11	4
6-C10	43.91 ± 2.80	6.90 ± 0.17	4
Iperoxo	102.50 ± 2.07	8.71 ± 0.07	4
Xanomeline	83.39 ± 3.34	6.65 ± 0.14[c]	3
ACh	96.73 ± 3.10	6.66 ± 0.09[d]	3

[a]E_{max} is the maximal effect expressed as percentage of ACh (100 µM) effect. [b]pEC_{50} is the concentration of the indicated compound inducing a half-maximal IP1 activation. Data are the mean ± S.E.M. of three or four independent experiments performed in triplicate. [c]Literature values: 6.08[40], 6.96[39]. [d]Literature values: 5.79[39], 7.24 [37], 7.25[41], 7.41[40].

2.2.5. Docking of Tacrine-Xanomeline hybrid compounds to AChE

Computational docking studies were carried out to determine putative binding modes of the tacrine-xanomeline hybrid series **7-Cn** and **8-Cn**. Building on crystal structures of bis-tacrine derivatives[42] and previous docking calculations for other tacrine hybrids[3], a conserved binding mode of the tacrine moiety was assumed and a scaffold match constraint was applied to ensure its proper placement in the CAS, thereby reducing the search space and improving the convergence of the docking runs. For all hybrids, the constraint was readily satisfied in all docking calculations, leading to unstrained and well-scored binding poses in which the tacrine moiety adopts the standard orientation in the CAS (i.e., sandwiched between Trp84 and Phe330 and further stabilized by hydrogen bonding to His440, as known from crystal structures) and the linker protrudes into the AChE binding gorge.

The best representative poses of the methylammonium hybrids **8-Cn** show that the xanomeline moiety can be favorably placed in the PAS, yet with differences depending on the linker length (Fig. 6). For **8-C8**, the 1,2,5-thiadiazole ring is sandwiched between Tyr70 and Trp279 at ring-center distances of 4.0 and 3.7 Å, respectively (Fig. 6A). The tetrahydropyridine moiety remains in close contact (< 4 Å) with the indole ring of Trp279, whereas the hexyl chain spans the cavity between Tyr70 and Ile275. In the case of **8-C10**, the thiadiazole is also stacked between Tyr70 and Trp279 (with distances of 3.7 and 3.6 Å, respectively) (Fig. 6A). This, however, occurs in a slightly tilted orientation in which the thiadiazole ring is inverted with respect to **8-C8**, leading to a different orientation of the hexyl chain (directed back

towards the gorge). This is a consequence of the extended linker and results in less favorable scores in comparison to **8-C8**. For **8-C12**, a similar binding mode as for **8-C10** can be identified among the docking results; however, this is found less frequently and scored much poorer by DSX than the binding pose shown in Fig. 6C. In the latter, the linker adopts a relaxed, extended conformation and the xanomeline moiety is no longer sandwiched in the PAS but interacts through weak polar contacts with Tyr70. Nevertheless, the scores do not reach the values obtained by **8-C8**. As a consequence, the absolute values of both the DSX- and ASP-per-atom-scores of the **8-Cn** hybrids decrease in the order **8-C8** > **8-C10** > **8-C12**, in line with the ranking based on the experimental pIC_{50} values.

The binding modes obtained for the **7-Cn** derivatives are very similar to those of the corresponding analogues **8-Cn** and are hence not discussed in detail here. The difference in inhibition potency between the **7-Cn** and **8-Cn** analogs can be rationalized on the basis of a higher desolvation cost for the tertiary nitrogen (in **7-Cn**) compared to the quaternary ammonium (in **8-Cn**), in analogy to other examples discussing the effect of amine methylation on binding affinity[43].

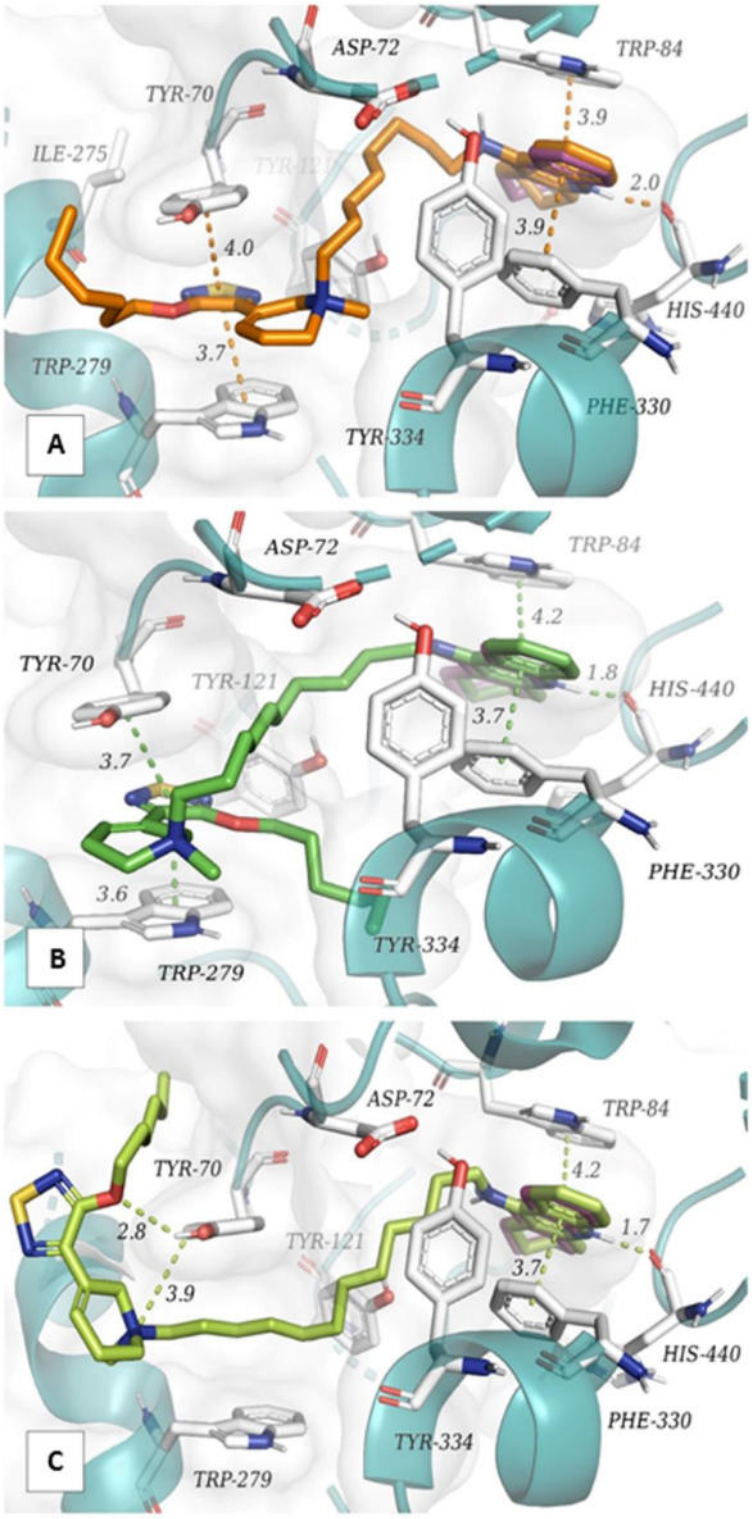

Fig. 6. Representative docking solutions for the methylammonium xanomeline-tacrine hybrids **8-C8** (A), **8-C10** (B) and **8-C12** (C). The binding poses illustrate the placement of the tacrine moiety in the CAS (with the tacrine scaffold match constraint depicted with magenta sticks), the linker chain in the gorge and the xanomeline part in or near the PAS. Most relevant contacts are highlighted and labeled with the corresponding distance (measured in Å).

3. Conclusions

In this study, we aimed at combining the multitarget with the bitopic ligand approaches through the synthesis of new hybrid ligands targeting both AChE and the M_1 mAChR subtype. The newly designed tacrine-xanomeline hybrids inhibited AChE with potency values higher than (**8-Cn**) or comparable to (**7-Cn**) that measured for the model compound tacrine. We found that the extent of anticholinesterase activity is affected by both, the permanently charged ammonium head and the length of the polymethylene spacer, derivative **8-C8** being the most potent inhibitor in the set of studied compounds. Docking calculations suggested a binding mode in which the tacrine moiety is placed in the catalytic active site, whereas the xanomeline moiety occupies the peripheral recognition pocket. This occurs most favorably with the C8 linker and least favorably with the C12 linker, in line with the observed activity profile.

In addition to their AChE inhibitory activity, the novel derivatives were assayed for M_1 mAChR agonism, the additional property we were searching for in their biological profile. However, hybrids **7-Cn** and **8-Cn** were unable to activate the M_1 receptor subtype, indicating that the response-activating dualsteric binding mode does not occur in this instance. We performed a parallel analysis on the two selected tacrine-iperoxo hybrids **6-C7** and **6-C10**, previously characterized by us for their relevant subnanomolar IC_{50} values towards cholinesterases and their ability to bind M_1 and M_2 mAChRs. In this instance, the presence of the superagonist iperoxo as the orthosteric molecular fragment dictated G protein activation and IP1 accumulation, characterizing these two hybrid compounds as partial agonists at the M_1 receptor subtype. On the other hand, the xanomeline moiety, probably due to its hairpin structure, is not able to gain access to the orthosteric site, thus preventing activation of the M_1 receptor by hybrids **7-Cn** and **8-Cn**. Overall, comparable results were reported for the related hybrids **4** and **5**, bearing the same pharmacophoric elements (tacrine and xanomeline) with a different structural connection as well as different linker moieties.

Consistent with our data on M_2 mAChRs, the dualsteric binding mode of iperoxo-containing hybrid ligands also at the M_1 receptor is a useful starting point in view of further investigations. Moreover, **6-C7** and **6-C10**, despite their permanently charged nitrogen, showed an overall lipophilicity (log*P* equal to 2.05 and 3.28, respectively)[131], which is an indication of their propensity to act at the CNS. Taken

together, these preliminary results suggest that a dual mechanism of action, i.e., combining AChE inhibition with activation of M_1 receptors in a single molecular entity, may represent a promising approach for a putative therapeutic intervention on a multifactorial pathology like Alzheimer's disease.

4. Materials and methods

4.1. Chemistry

All chemicals were purchased from Sigma-Aldrich Srl (Milan, Italy and Schnelldorf, Germany), VWR (Darmstadt, Germany) and TCI (Eschborn, Germany) and were used without further purification. For chromatographic applications (HPLC, LC-MS), deionized water produced by means of a Milli-Q® system (Merck, Darmstadt, Germany) was used. HPLC grade and LC-MS grade solvents were from Sigma-Aldrich (Munich, Germany). The synthesis of some intermediates required inert atmosphere of argon or nitrogen and anhydrous conditions. The reactions was monitored by thin-layer chromatography (TLC) on commercial aluminum plates precoated with silica gel 60 (F-254, Merck) or with aluminum oxide (F-254, Fluka). Visualization was performed with UV light at 254 nm. Spots were further evidenced by spraying with a dilute alkaline potassium permanganate solution or an ethanol solution of phosphomolybdic acid and, for tertiary amines, with the Dragendorff reagent. The synthesized compounds were purified on glass chromatography columns packed with silica gel (230–400 mesh particle size, pore size 60 Å, Merck) or by flash chromatography on a puriFlash®430 system (Interchim, Montlucon, France) employing prepacked columns (Interchim, Montluçon, France) with silica gel filling (particle size 30 μm or 50 μm) for normal-phase purifications; eluents have been specified from time to time. The detection was carried out by means of an UV detector and an Evaporative Light Scattering Detector (ELSD). Microwave assisted reactions were accomplished by means of a synthWAVE instrument (Milestone, Leutkirch, Germany). ^{1}H NMR and ^{13}C NMR spectra have been registered with a Bruker Avance 400 instrument (400 MHz and 100 MHz, respectively) or a Varian Mercury 300 instrument (300 MHz and 75 MHz, respectively). Chemical shifts (δ) are expressed in parts-per-million (ppm) and coupling constants (J) in hertz (Hz). Abbreviations used for peak multiplicities are given as follows: s (singlet), bs (broad singlet), d (doublet), dd (doublet of doublets), ddd (doublet of doublet of doublets), dddd (doublet of doublet of doublet of doublets), t (triplet), q (quartet), quint (quintet), m

(multiplet). Melting points have been determined with a Büchi Mod. B 540 apparatus and are uncorrected. The HPLC and mass analyses were performed on a Shimadzu LCMS-2020 system equipped with a DGU-20A3R degassing unit, a LC20AB liquid chromatograph and a SPD-20A UV/Vis detector. A Synergi 4U fusion -RP (150 × 4.6 mm) column was used as stationary phase. A gradient mobile phase consisting of 0.1% formic acid in water (solvent A) and 0.1% formic acid in MeOH (solvent B) was used. The time program elution was as follows: solvent A from 0% to 90% in 13 min, then 90% for 5 min, from 90% to 5% in 1 min, then 5% for 4 min. The flow rate was 1.0 mL/min and UV detection was measured at 254 nm. All final compounds were found to have a ≥ 95% purity. Mass spectra were recorded in ESI-positive mode and the data are reported as mass-to-charge ratio (m/z) of the corresponding positively charged molecular ions. The tacrine-iperoxo hybrid derivatives **6-C7** and **6-C10** were prepared according to known procedures[131].

4.2. Preparation of Tacrine moiety: Synthesis of 1,2,3,4-tetrahydroacridin-9-amine (**1**)

Zinc chloride (3.47 g, 25.4 mmol) was added to a mixture of 2-aminobenzonitrile (3 g, 25.4 mmol) and cyclohexanone (30.5 mL, 294.6 mmol). The reaction was kept at 120°C for 16 h, then cooled to room temperature and the solvent was evaporated under reduced pressure. To the residue, 50 mL of AcOEt were added and the resulting solid was collected after filtration. To the solid, 65 mL of a 10% solution of NaOH in water was poured and kept under stirring overnight. After filtration, the cake was washed with H_2O (3 × 20 mL), and then kept under stirring overnight with 30 mL of MeOH. The solid was filtered and the solvent was evaporated under reduced pressure to give tacrine **1** as a yellow solid (4,95 g, 98%): R_f = 0.47 ($CHCl_3$/MeOH/NH_3 7:3:0,1). mp = 178–181 °C. ^{1}H NMR (400 MHz, $CDCl_3$): δ 7.89 (dd, J = 8.5, 0.6 Hz, 1H; H9), 7.68 (dd, J = 8.4, 0.8 Hz, 1H; H6), 7.55 (ddd, J = 8.4, 6.8, 1.3 Hz, 1H; H7), 7.35 (ddd, J = 8.2, 6.8, 1.2 Hz, 1H; H8), 4.65 (s, J = 42.8 Hz, 2H; NH_2), 3.01 (t, J = 9.9 Hz, 2H; H4), 2.60 (t, J = 6.2 Hz, 2H; H1), 1.99-1.84 (m, 4H; 2×H2, 2×H3). ^{13}C NMR (101 MHz, CD_3OD): δ 158.45, 150.72, 146.73, 129.84, 127.25, 124.51, 122.32, 118.20, 110.50, 33.86, 24.53, 23.76, 23.71.

4.3. General procedure for the synthesis of intermediates **9a-c**

To a solution of tacrine (**1**) (1 equiv) in CH_3CN (0.1 M) was added KOH (2 equiv) and the reaction was kept under stirring for 2 h. Then, a solution of the appropriate dibromoalkane (10 equiv) in CH_3CN (4 M) was added. The reaction was kept for 3 days at 40 °C, then the mixture was purified through silica gel column chromatography, using DCM/MeOH 99:1 → 9:1 as eluent, thus providing intermediates **9a-c** as pure compounds.

4.3.1. N-(8-Bromooctyl)-1,2,3,4-tetrahydroacridin-9-amine (**9a**)

The title compound was prepared by reacting **1** (400 mg, 2.02 mmol), KOH (135 mg, 2.42 mmol) and 1,8-dibromooctane (5.48 g, 20.18 mmol) in CH_3CN (25 mL). After standard workup, **9a** was obtained as a yellow oil (250 mg, 32%): R_f = 0.50 (DCM/MeOH 9:1). ^{1}H NMR (400 MHz, $CDCl_3$): δ 8.68 (d, J = 8.5, 1H; H9), 8.18 (d, J = 8.6 Hz, 1H; H6), 7.73 (m, 1H; H7), 7.47 (t, J = 7.85 Hz, 1H; H8), 5.51 (s, 1H; NH), 3.94 (dd, J = 12.3, 6.8 Hz, 2H; CH_2−Br), 3.40 (m, 4H; HN−CH_2, H4), 2.58 (t, J = 5.9, 2H; H1), 1.92–1.83 (m, 8H; 2×H2, 2×H3, CH_2−CH_2−Br, HN−CH_2−CH_2), 1.48–1.38 (m, 8H; HN−$(CH_2)_2$−CH_2−CH_2−CH_2−CH_2−$(CH_2)_2$−Br). ^{13}C NMR (101 MHz, $CDCl_3$): δ 155.41, 151.19, 139.29, 131.91, 124.89, 124.61, 120.76, 116.06, 111.41, 48.26, 34.06, 32.60, 3.91, 28.97, 28.81, 28.52, 27.91, 26.56, 24.25, 22.00, 20.82.

4.3.2. N-(10-Bromodecyl)-1,2,3,4-tetrahydroacridin-9-amine (**9b**)

The title compound was prepared by reacting **1** (450 mg, 2.27 mmol), KOH (255 mg, 4.54 mmol) and 1,10-dibromodecane (6.81 g, 22.70 mmol) in CH_3CN (25 mL). After standard workup, **9b** was obtained as a yellow oil (308 mg , 35%): R_f = 0,51 (DCM/MeOH 9:1). ^{1}H NMR (400 MHz, $CDCl_3$): δ 7.94 (t, J = 8.1 Hz, 2H; H9, H6), 7.50 (t, J = 7.6 Hz, 1H; H7), 7.30 (t, J = 7.6, 1H; H8), 4.28 (s, 1H; NH), 3.49 (t, J = 7,1 Hz, 2H; CH_2−Br), 3.34 (td, J = 6.8, 1.5 Hz, 2H; HN−CH_2), 3.04 (s, 2H; H4), 2.65 (s, 2H; H1), 1.92–1.83 (m, 4H; 2×H2, 2×H3), 1.83–1.74 (m, 2H; CH_2−CH_2−Br), 1.68–1.58 (m, 2H; HN−CH_2−CH_2), 1.44–1.13 (m, 12H; HN−$(CH_2)_2$−CH_2−CH_2−CH_2−CH_2−CH_2−CH_2−$(CH_2)_2$−Br). ^{13}C NMR (101 MHz, $CDCl_3$). δ 155.11, 151.13, 139.41, 131.51, 124.58, 124.47, 120.72, 116.06, 111.49, 48.06, 33.94, 32.52, 30.75, 29.11, 29.05, 28.94, 28.84, 28.43, 27.85, 26.49, 24.21, 21.88, 20.74.

4.3.3. N-(10-Bromododecyl)-1,2,3,4-tetrahydroacridin-9-amine (**9c**)

The title compound was prepared by reacting **1** (250 mg, 1.26 mmol), KOH (141 mg, 2.52 mmol) and 1,12-dibromododecane (3.31 g, 10.09 mmol) in CH_3CN (15 mL). After standard workup, **9c** was obtained as a yellow oil (250 mg , 51%): R_f = 0,56 (DCM/MeOH 9:1). ^{1}H NMR (400 MHz, $CDCl_3$): δ 8.32 (d, J = 8.3, 1H; H9), 8.22 (d, J = 8.7, 1H; H6), 7.54 (t, J = 7.6, 1H; H7), 7.33 (t, J = 7.7, 1H; H8), 3.87 (t, J = 7.1 Hz, 2H; CH_2−Br), 3.29 (t, J = 6.8 Hz, 2H; HN−CH_2), 3.19–3.06 (m, 2H; H4), 2.73–2.58 (m, 2H; H1), 1.88–1.59 (m, 8H; 2×H2, 2×H3, CH_2−CH_2−Br, HN−CH_2−CH_2), 1.39–0.96 (m, 16H; HN−$(CH_2)_2$−CH_2−CH_2−CH_2−CH_2−CH_2−CH_2−CH_2−CH_2−$(CH_2)_2$−Br). ^{13}C NMR (101 MHz, $CDCl_3$): δ 155.74, 150.46, 138.55, 132.03, 124.82, 124.74, 120.01, 115.68, 111.05, 103.13, 48.06, 45.11, 34.04, 32.68, 30.81, 29.35, 29.27, 29.11, 28.60, 28.31, 28.01, 26.62, 24.24, 21.88, 20.62.

4.4. Preparation of Xanomeline moiety: Synthesis of 2-hydroxy-2-(pyridin-3-yl)acetonitrile (**10**)

A water solution of 3-pyridinecarboxaldheyde (3.00 g, 28.01 mmol) and acetic acid (28.01 mmol, 1.68 g) were added to a water solution of TMSCN (3.71 g, 37.21 mmol) at 0°C. The reaction proceeded at room temperature for 23 h and then was extracted with AcOEt (3 × 20 mL). The pooled organic phases were dried over anhydrous Na_2SO_4 and the solvent was evaporated under reduced pressure, giving the desired product **10** as a yellow-orange oil (3,36 g, 78%): R_f = 0.44 (AcOEt). ^{1}H NMR (300 MHz, $CDCl_3$): δ 8.62 (d, J = 2.0 Hz, 1H; H2′), 8.53 (d, J = 4.7 Hz, 1H; H6′), 7.96 (dt, J = 7.9, 1.6 Hz, 1H; H4′), 7.42 (dd, J = 7.9, 5.0 Hz, 1H; H5′), 5.65 (s, 1H; CH−CN). ^{13}C NMR (75 MHz, $CDCl_3$): δ 149.70, 147.10, 135.58, 133.08, 124.50, 118.81, 61.05.

4.4.1. 2-Amino-2-(pyridin-3-yl)acetonitrile (**11**)

To a water solution of NH_4Cl (7.93 g, 148.17 mmol), 4 mL of NH_3 (33% in water) and then a water solution of **10** (2.65 g, 19.76 mmol) were added dropwise. The reaction was kept at room temperature for 22 h. The aqueous phase was extracted four times with 10 mL of DCM, and four times with 10 mL of a mixture of DCM/*i*PrOH (7:3). The pooled organic phases were dried over anhydrous Na_2SO_4 and concentrated under reduced pressure, giving the desired product **11** as an orange oil (1.160 g, 44%): R_f = 0.52 (DCM/MeOH 9:1). ^{1}H NMR (300 MHz, $CDCl_3$): δ 8.80 (d, J = 2.3 Hz, 1H; H2′), 8.64 (dd, J = 4.8,

1.4 Hz, 1H; H6′), 7.89 (dt, *J* = 8.0, 1.7 Hz, 1H; H4′), 7.36 (dd, *J* = 8.0, 4.8 Hz, 1H; H5′), 4.97 (s, 1H; CH−CN), 2.00 (s, 2H; NH_2). ^{13}C NMR (75 MHz, $CDCl_3$): *δ* 150.28, 148.24, 134.37, 132.09, 123.70, 120.02, 45.20.

4.4.2. 3-Chloro-4-(pyridin-3-yl)-1,2,5-thiadiazole (**12**)

A solution of **11** (1.15 g, 8.64 mmol) in 5 mL of DMF and S_2Cl_2 (1.38 mL, 17.27 mmol) was added dropwise to 10mL of DMF at 0°C. After 30 min, 20 mL of water were poured and the suspension was filtered. The filtrate was basified with 9M NaOH (10 mL), and the aqueous phase was extracted with DCM (3 × 20 mL). The pooled organic phases were dried over anhydrous Na_2SO4, concentrated under reduced pressure, affording the desired product **12** as a brown solid (1.35 g, 79%): R_f = 0.30 (cyclohexane/AcOEt 3:2). mp = 51–53 °C. ^1H NMR (300 MHz, $CDCl_3$): *δ* 9.14 (d, *J* = 2.1 Hz, 1H; H2′), 8.66 (dd, *J* = 4.8, 1.5 Hz, 1H; H6′), 8.21 (dt, *J* = 8.1, 1.7 Hz, 1H; H4′), 7.38 (dd, *J* = 7.9, 4.8 Hz, 1H; H5′). ^{13}C NMR (75 MHz, $CDCl_3$): *δ* 155.09, 150.83, 149.21, 143.44, 135.68, 126.82, 123.31.

4.4.3. 3-(Hexyloxy)-4-(pyridin-3-yl)-1,2,5-thiadiazole (**13**)

A suspension of 60% NaH (1,48 g, 61.47 mmol) in anhydrous THF (3mL) was added dropwise to a solution of 1-hexanol (2.09 g, 20.49 mmol) in anhydrous THF (6mL) at 0 °C. The suspension was kept under stirring at room temperature for 2 h. A solution of **12** (1.35 g, 6.83 mmol) in anhydrous THF (5mL) was added dropwise to the suspension. The reaction was kept under reflux for 3h and then quenched with 10 mL of a saturated aqueous solution of $NaHCO_3$. The aqueous phase was extracted with DCM (3 × 10 mL), the pooled organic phases were dried over anhydrous Na_2SO_4 and then concentrated under reduced pressure. The crude was purified through silica gel column chromatography, using as eluent cyclohexane/AcOEt 9:1. The desired product **13** was obtained as a white solid (1.53 g, 85%): R_f = 0.41 (cyclohexane/AcOEt 4:1). mp = 49–51 °C. ^1H NMR (300 MHz, $CDCl_3$): *δ* 9.41 (dd, *J* = 2.2, 0.7 Hz, 1H; H2′), 8.66 (dd, *J* = 4.8, 1.6 Hz, 1H; H6′), 8.46 (dt, *J* = 8.1, 1.9 Hz, 1H; H4′), 7.42 (ddd, *J* = 8.1, 4.9, 0.7 Hz, 1H; H5′), 4.53 (t, *J* = 6.7 Hz, 2H; CH_2−O), 1.89 (quint, *J* = 6.9 Hz, 2H; C*H*$_2$−CH_2−O), 1.67–0.89 (m, 6H; CH_3−C*H*$_2$−C*H*$_2$−C*H*$_2$−$(CH_2)_2$−O), 0.91 (t, *J* = 5.6 Hz, 3H; C*H*$_3$−$(CH_2)_5$−O). ^{13}C NMR (75 MHz, $CDCl_3$): *δ* 162.85, 150.12, 148.65, 144.95, 134.66, 127.67, 123.37, 71.45, 31.44, 28.88, 25.69, 22.54, 14.00.

4.4.4. 1-Methyl-3-(4-(pentyloxy)-1,2,5-thiadiazol-3-yl)pyridin-1-ium iodide (**14**)

Iodomethane (1.08 g, 7.59 mmol) was added dropwise to a solution of **13** (500 mg, 1.90 mmol) in 4 mL of acetone. The reaction proceeded for 26 h at room temperature, then the solution was concentrated under reduced pressure, and washed with Et_2O (10 mL). The desired product **14** was obtained as a yellow oil (733 mg, 95%): R_f = 0.30 (DCM/MeOH 4:1). ^{1}H NMR (300 MHz, $CDCl_3$): δ 9.60 (d, J = 5.4 Hz, 1H; H2′), 9.45 (s, 1H; H6′), 9.11 (d, J = 8.2 Hz, 1H; H4′), 8.28 (dd, J = 8.3, 5.4 Hz, 1H; H5′), 4.79 (s, 3H; CH_3−N^+), 4.57 (t, J = 6.9 Hz, 2H; CH_2−O), 1.91 (quint, J = 6.9 Hz, 2H; CH_2−CH_2−O), 1.59–1.13 (m, 6H; CH_3−CH_2−CH_2−CH_2−$(CH_2)_2$−O), 0.88 (t, J = 6.3 Hz, 3H; CH_3−$(CH_2)_5$−O). ^{13}C NMR (75 MHz, $CDCl_3$): δ 163.13, 145.73, 142.86, 141.88, 139.45, 131.47, 128.65, 72.49, 50.67, 31.34, 28.72, 25.54, 22.52, 13.99.

4.4.5. 3-(Hexyloxy)-4-(1-methyl-1,2,5,6-tetrahydropyridin-3-yl)-1,2,5-thiadiazole (**3**)

A solution of $NaBH_4$ (273 mg, 7.20 mmol) in 3 mL of MeOH was added dropwise to a solution of **14** (730 mg, 1.80 mmol) in 5 mL of MeOH. The reaction was kept under stirring at room temperature for 2.5 days. After quenching with 10 mL of water, the aqueous phase was extracted with DCM (3 × 10 mL). The pooled organic phases were dried over anhydrous Na_2SO_4 and then concentrated under reduced pressure. The crude was purified through silica gel column chromatography, using as eluent DCM/MeOH 95:5. Xanomeline **3** was obtained as a yellow-orange oil (383 mg, 75%): R_f = 0.30 (DCM/MeOH 95:5). ^{1}H NMR (300 MHz, $CDCl_3$): δ 7.16–6.96 (m, 1H; H4′), 4.44 (t, J = 6.6 Hz, 2H; CH_2−O), 3.51 (d, J = 2.0 Hz, 2H; H2′), 2.63 (t, J = 5.7 Hz, 2H; H6′), 2.50 (s, 5H; CH_3−N, 2×H5′), 1.83 (quint, J = 6.9 Hz, 2H; CH_2−CH_2−O), 1.58–1.12 (m, 6H; CH_3−CH_2−CH_2−CH_2−$(CH_2)_2$−O), 0.90 (t, J = 6.6 Hz, 3H; CH_3−$(CH_2)_5$−O). ^{13}C NMR (75 MHz, $CDCl_3$): δ 162.49, 146.55, 128.86, 128.18, 70.93, 54.74, 51.08, 45.68, 31.34, 28.76, 26.28, 25.60, 22.48, 13.94.

4.5. Preparation of Tacrine-Xanomeline hybrid compounds: General procedure for the synthesis of intermediates **15a-c**

A solution of compound **13** (1 equiv) in DMF (0.1 M) was added to a solution of functionalized tacrine-incorporating bromide (**9a-c**) (1 equiv) in DMF (0.1 M). The mixture was stirred in a sealed reaction tube for 36 h at 100 °C. The crude reaction mixture was passed through a silica plug, eluting with DCM/MeOH 100:0 → 4:1. The isolated desired compound was used without any further purification.

4.5.1. 3-(4-(Hexyloxy)-1,2,5-thiadiazol-3-yl)-1-(8-((1,2,3,4-tetrahydroacridin-9-yl)amino)octyl)pyridin-1-ium bromide (**15a**)

The title compound was prepared by reacting **13** (300 mg, 1,14 mmol) and **9a** (443 mg, 1.14 mmol) in DMF (20 mL). After standard workup, **15a** was obtained as a yellow oil (159 mg , 21%): R_f = 0.20 (DCM/MeOH 9:1). ^{1}H NMR (400 MHz, CD_3OD): δ 9.61 (s, 1H; H2′), 9.23 (dt, J = 8.3, 1.3 Hz, 1H; H4′), 9.10 (d, J = 6.1 Hz, 1H; H6′), 8.39 (d, J = 8.6 Hz, 1H; H5′), 8.26 (dd, J = 8.2, 6.1 Hz, 1H; H9), 7.84 (ddd, J = 6.8, 3.1, 1.5 Hz, 1H; H6), 7.79 (dd, J = 8.5, 1.2 Hz, 1H; H7), 7.58 (ddd, J = 7.1, 3.3, 1.5 Hz, 1H; H8), 4.77 (t, J = 7.6 Hz, 2H; CH_2−N^+), 4.62 (t, J = 6.7 Hz, 2H; CH_2−O), 3.95 (t, J = 7.4 Hz, 2H; HN−CH_2), 3.03 (t, J = 5.6 Hz, 2H; H4), 2.71 (t, J = 5.4 Hz, 2H; H1), 2.09 (quint, J = 7.2 Hz, 2H; CH_2−CH_2−O), 2.00–1.91 (m, 6H; CH_2−CH_2−N^+, 2×H2, 2×H3), 1.89–1.78 (m, 2H; HN−CH_2−CH_2), 1.54–1.28 (m, 14H; HN−$(CH_2)_2$−CH_2−CH_2−CH_2−CH_2−$(CH_2)_2$−N^+, CH_3−CH_2−CH_2−CH_2−$(CH_2)_2$−O), 0.91 (t, J = 7.1 Hz, 3H; CH_3−$(CH_2)_5$−O). ^{13}C NMR (101 MHz, CD_3OD): δ 164.47, 157.91, 151.70, 145.57, 144.21, 143.81, 141.87, 139.77, 134.04, 133.22, 129.67, 126.46, 126.31, 120.15, 117.03, 112.82, 73.32, 63.60, 49.10, 32.64, 32.45, 31.52, 30.08, 30.00, 29.85, 29.30, 27.63, 27.12, 26.74, 24.93, 23.62, 22.98, 21.83, 14.38.

4.5.2. 3-(4-(Hexyloxy)-1,2,5-thiadiazol-3-yl)-1-(10-((1,2,3,4-tetrahydroacridin-9-yl)amino)decyl)pyridin-1-ium bromide (**15b**)

The title compound was prepared by reacting **13** (250 mg, 0.949 mmol) and **9b** (396 mg, 0.949 mmol) in DMF (20 mL). After standard workup, **15b** was obtained as a yellow oil (148 mg, 23%): R_f = 0.24 (DCM/MeOH 9:1). ^{1}H NMR (400 MHz, $CDCl_3$): δ 10.36 (d, J = 6.0 Hz, 1H; H2′), 9.38 (s, 1H; H4′), 9.07 (dd, J = 9.7, 1.3 Hz, 1H; H6′), 8.25 (dd, J = 8.2, 6.1 Hz, 1H; H5′), 7.94 (dd, J = 23.1, 8.3 Hz, 2H; H9, H6),

7.51 (ddd, J = 8.3, 6.8, 1.3 Hz, 1H; H7), 7.31 (ddd, J = 8.2, 6.8, 1.2 Hz, 1H; H8), 5.14 (t, J = 7.5 Hz, 2H; CH_2−N^+), 4.57 (t, J = 6.8 Hz, 2H; CH_2−O), 3.55–3.42 (m, 2H; HN−CH_2), 3.05 (s, 2H; H4), 2.70 (s, 2H; H1), 2.06 (dd, J = 14.6, 7.5 Hz, 2H; CH_2−CH_2−O), 1.95–1.84 (m, 6H CH_2−CH_2−N^+, 2×H2, 2×H3), 1.63 (dd, J = 14.0, 7.1 Hz, 2H; HN−CH_2−CH_2), 1.51–1.09 (m, 18H; HN−$(CH_2)_2$−CH_2−CH_2−CH_2−CH_2−CH_2−CH_2−$(CH_2)_2$−N^+, CH_3−CH_2−CH_2−CH_2−$(CH_2)_2$−O), 0.89 (t, J = 7.1 Hz, 3H; CH_3−$(CH_2)_5$−O) ^{13}C NMR (101 MHz, CD_3OD): δ 164.46, 157.91, 151.75, 145.57, 144.16, 143.84, 141.85, 139.82, 134.00, 133.23, 129.68, 126.41, 126.26, 120.22, 117.05, 112.81, 73.32, 63.63, 49.13, 32.64, 32.48, 31.55, 30.50, 30.41, 30.29, 30.13, 29.86, 29.28, 27.72, 27.20, 26.75, 24.88, 23.62, 22.98, 21.84, 14.39.

4.5.3. 3-(4-(Hexyloxy)-1,2,5-thiadiazol-3-yl)-1-(12-((1,2,3,4-tetrahydroacridin-9-yl)amino)dodecyl)pyridin-1-ium bromide (**15c**)

The title compound was prepared by reacting **13** (100 mg, 0.380 mmol) and **9c** (200 mg, 0.449 mmol) in DMF (10 mL). After standard workup, **15c** was obtained as a yellow oil (60 mg , 22%): R_f = 0.26 (DCM/MeOH 9:1). ^{1}H NMR (400 MHz, CD_3OD): δ 9.61 (s, 1H; H2′), 9.24 (dt, J = 8.3, 1.3, 1.2 Hz, 1H; H4′), 9.07 (d, J = 6.1 Hz, 1H; H6′), 8.39 (d, J = 8.3 Hz, 1H; H5′), 8.25 (dd, J = 8.1, 6.2 Hz, 1H; H9), 7.85 (ddd, J = 8.1, 6.9, 1.1 Hz, 1H; H6), 7.77 (dd, J = 8.5, 0.9 Hz, 1H; H7), 7.58 (ddd, J = 8.4, 6.9, 1.3 Hz, 1H; H8), 4.75 (t, J = 7.6 Hz, 2H; CH_2−N^+), 4.63 (t, J = 6.7 Hz, 2H; CH_2−O), 3.95 (t, J = 7.4 Hz, 2H; HN−CH_2), 3.02 (t, J = 5.6 Hz, 2H; H4), 2.71 (t, J = 5.4 Hz, 2H; H1), 2.09 (quint, J = 7.9 Hz, 2H; CH_2−CH_2−O), 2.01–1.92 (m, 6H; CH_2−CH_2−N^+, 2×H2, 2×H3), 1.83 (quint, J = 7.7 Hz, 2H; HN−CH_2−CH_2), 1.57–1.25 (m, 22H; HN−$(CH_2)_2$−CH_2−CH_2−CH_2−CH_2−CH_2−CH_2−CH_2−CH_2−$(CH_2)_2$−N^+, CH_3−CH_2−CH_2−CH_2−$(CH_2)_2$−O), 0.93 (t, J = 7.1 Hz, 3H; CH_3−$(CH_2)_5$−O). ^{13}C NMR (101 MHz, CD_3OD): δ 178.08, 164.50, 158.04, 151.69, 145.55, 144.15, 143.90, 141.86, 139.80, 134.12, 133.30, 129.67, 126.52, 126.31, 120.11, 117.07, 112.86, 73.35, 63.67, 49.07, 32.68, 32.50, 31.56, 30.64, 30.54, 30.35, 30.19, 29.90, 29.31, 27.75, 27.24, 26.79, 24.89, 23.65, 22.99, 22.95, 21.86, 14.38.

4.6. General procedure for the synthesis of target compounds **7-Cn**

To a solution of intermediate pyridinium salt (**15**) (1 equiv) in MeOH (0.03 M), a solution of $NaBH_4$ (5 - 8 equiv) in MeOH (0.5 M) was added dropwise at 0°C, and the reaction was stirred for 5 h at room temperature. After quenching with a saturated solution of $NaHCO_3$, the aqueous phase was extracted with DCM. The pooled organic phases were dried over anhydrous Na_2SO_4 and concentrated under reduced pressure. The crude reaction mixtures were submitted to silica gel column chromatography (eluent: DCM/MeOH 95:5), providing the pure target derivatives **7-C8**, **7-C10** and **7-C12**.

4.6.1. N-(8-(5-(4-(Hexyloxy)-1,2,5-thiadiazol-3-yl)-3,6-dihydropyridin-1(2H)-yl)octyl)-1,2,3,4-tetrahydroacridin-9-amine (**7-C8**)

The title compound was prepared by reacting **15a** (100 mg, 0.153 mmol), and $NaBH_4$ (35 mg, 0.919 mmol) in 7 mL of MeOH. After standard workup, **7-C8** was obtained as a brown oil (21 mg, 24%): R_f = 0.31 (DCM/MeOH 95:5). ^{1}H NMR (400 MHz, CD_3OD): δ 8.38 (d, J = 8.7 Hz, 1H; H9), 7.81 (dt, J = 18.7, 7.9 Hz, 2H; H6, H7), 7.57 (dd, J = 11.2, 4.3 Hz, 1H; H8), 7.14 (s, 1H; H4′), 4.47 (t, J = 6.5 Hz, 2H; CH_2−O), 3.94 (t, J = 7.3 Hz, 2H; HN−CH_2), 3.65 (s, 2H; H2′), 3.02 (d, J = 5.7 Hz, 2H; H4), 2.83 (t, J = 5.8 Hz, 2H; H1), 2.68 (dd, J = 9.6, 6.4 Hz, 4H; 2×H6′, CH_2−N), 2.51 (d, J = 3.7 Hz, 2H; H5′), 2.03–1.91 (m, 4H; 2×H2, 2×H3), 1.84 (dt, J = 13.2, 6.5 Hz, 4H; CH_2−CH_2−O, HN−CH_2−CH_2), 1.65 (s, 2H; CH_2−CH_2−CH_2−O), 1.50–1.30 (m, 14H; HN−$(CH_2)_2$−CH_2−CH_2−CH_2−CH_2−CH_2−N, CH_3−CH_2−CH_2−$(CH_2)_3$−O), 0.92 (t, J = 7.0 Hz, 3H; CH_3−$(CH_2)_5$−O). ^{13}C NMR (101 MHz, CD_3OD): δ 163.81, 155.88, 154.84, 147.84, 143.32, 132.15, 129.90, 129.85, 127.30, 125.57, 123.55, 118.89, 114.49, 72.19, 59.46, 54.06, 50.35, 49.39, 32.56, 31.82, 31.44, 30.76, 30.42, 30.19, 29.89, 28.50, 27.71, 27.51, 26.82, 25.44, 23.61, 23.48, 22.67, 14.35. MS (ESI) m/z $[M+H]^+$ calcd for $C_{34}H_{50}BrN_5OS^+$: 575.37, found: 576.25. HPLC analysis: retention time = 8.275 min, purity 96.91%.

4.6.2. N-(10-(5-(4-(Hexyloxy)-1,2,5-thiadiazol-3-yl)-3,6-dihydropyridin-1(2H)-yl)decyl)-1,2,3,4-tetrahydroacridin-9-amine (**7-C10**)

The title compound was prepared by reacting **15b** (140 mg, 0.206 mmol), and $NaBH_4$ (474 mg, 1.066 mmol) in 9 mL of MeOH. After standard workup, **7-C10** was obtained as a brown oil (20 mg, 16%): R_f = 0.41 (DCM/MeOH 95:5). ^{1}H NMR (400 MHz, CD_3OD): δ 8.09 (d, J = 8.6 Hz, 1H; H9), 7.66 (d, J = 8.4 Hz, 1H; H6), 7.55 (t, J = 7.6 Hz, 1H; H7), 7.33 (t, J = 7.7 Hz, 1H; H8), 6.99 (t, J = 3.8 Hz, 1H; H4′), 4.36 (t, J = 6.4 Hz, 2H; CH_2−O), 3.57 (t, J = 7.1 Hz, 2H; HN−CH_2), 3.38 (s, 2H; H2′), 2.89 (s, 2H; H4), 2.63 (s, 2H; H1), 2.55 (t, J = 5.7 Hz, 2H; H6′), 2.45–2.37 (m, 2H; CH_2−N), 2.37–2.30 (m, 2H; H5′), 1.87–1.80 (m, 4H; 2×H2, 2×H3), 1.73 (quint, J = 7.0 Hz, 2H; HN−CH_2−CH_2), 1.60 (d, J = 7.2 Hz, 2H; CH_2−CH_2−O), 1.54–1.44 (m, 2H; CH_2−CH_2−CH_2−O), 1.43–1.12 (m, 18H; HN−$(CH_2)_2$−CH_2−CH_2−CH_2−CH_2−CH_2−CH_2−CH_2−CH_2−N, CH_3−CH_2−CH_2−$(CH_2)_3$−O), 0.82 (t, J = 7.0 Hz, 3H; CH_3−$(CH_2)_5$−O). ^{13}C NMR (101 MHz, CD_3OD): δ 163.86, 156.60, 154.94, 147.93, 139.81, 133.93, 131.23, 130.00, 129.88, 125.24, 125.14, 119.91, 115.45, 72.20, 59.55, 54.09, 50.39, 49.56, 32.57, 32.01, 30.79, 30.75, 30.52, 30.45, 30.44, 30.25, 29.91, 28.63, 27.78, 27.58, 26.83, 25.72, 23.75, 23.61, 23.10, 14.32. MS (ESI) *m/z* $[M+H]^+$ calcd for $C_{36}H_{54}BrN_5OS^+$: 603.40, found: 604.25. HPLC analysis: retention time = 8.3 min, purity 96.7%.

4.6.3. N-(12-(5-(4-(Hexyloxy)-1,2,5-thiadiazol-3-yl)-3,6-dihydropyridin-1(2H)-yl)dodecyl)-1,2,3,4-tetrahydroacridin-9-amine (**7-C12**)

The title compound was prepared by reacting **15c** (200 mg, 0.282 mmol), and $NaBH_4$ (86 mg, 2.26 mmol) in 12 mL of MeOH. After standard workup, **7-C12** was obtained as a brown oil (84 mg, 47%): R_f = 0.46 (DCM/MeOH 95:5). ^{1}H NMR (400 MHz, CD_3OD): δ 8.35 (d, J = 8.7 Hz, 1H; H9), 7.86–7.73 (m, 2H; H6, H7), 7.55 (ddd, J = 8.5, 6.6, 1.6 Hz, 1H; H8), 7.11 (dd, J = 3.7, 2.0 Hz, 1H; H4′), 4.46 (t, J = 6.5 Hz, 2H; CH_2−O), 3.90 (t, J = 7.2 Hz, 2H; HN−CH_2), 3.66–3.53 (m, 2H; H2′), 3.01 (s, 2H; H4), 2.78–2.65 (m, 4H; 2×H1, 2×H6′), 2.65–2.55 (m, 2H; CH_2−N), 2.48 (s, 2H; H5′), 1.96 (s, 4H; H2), 1.90–1.71 (m, 4H; 2×H3, HN−CH_2−CH_2), 1.69–156 (m, 2H; CH_2−CH_2−O), 1.56–1.14 (m, 24H; HN−$(CH_2)_2$−CH_2−CH_2−CH_2−CH_2−CH_2−CH_2−CH_2−CH_2−CH_2−N, CH_3−CH_2−CH_2−CH_2−$(CH_2)_2$−O), 0.92 (t, J = 7.0 Hz, 3H; CH_3−$(CH_2)_5$−O). ^{13}C NMR (101 MHz, CD_3OD): δ 163.84, 157.47, 152.49, 147.66,

133.59, 129.75, 129.50, 127.33, 126.27, 126.11, 121.02, 117.55, 113.28, 72.24, 59.38, 53.83, 50.28, 49.24, 32.57, 31.59, 30.63, 30.60, 30.56, 30.53, 30.25, 29.90, 29.88, 28.57, 27.70, 27.36, 27.24, 26.82, 26.51, 25.01, 23.61, 23.13, 22.08, 14.34. MS (ESI) *m/z* $[M+H]^+$ calcd for $C_{38}H_{58}BrN_5OS^+$: 631.43, found: 632.35. HPLC analysis: retention time = 8.9 min, purity 95.7%.

4.7. General procedure for the synthesis of target compounds **8-Cn**

The reaction was conducted under Argon atmosphere. To a solution of Xanomeline **3** (1 equiv) in dry CH_3CN (0.1 M) a solution of functionalized tacrine bromide (**9**) (1 equiv) in dry CH_3CN (0.1 M) was added. The mixture was reacted for 10 h at 80 °C in a microwave apparatus (pressure: 19 atm, power of 500 W). The crude reaction mixtures were submitted to silica gel column chromatography (eluent: DCM/MeOH 99:1 → 9:1), providing the pure target derivatives **8-C8**, **8-C10** and **8-C12**.

4.7.1. 5-(4-(Hexyloxy)-1,2,5-thiadiazol-3-yl)-1-methyl-1-(8-((1,2,3,4-tetrahydroacridin-9-yl)amino)octyl)-1,2,3,6-tetrahydropyridin-1-ium bromide (**8-C8**)

The title compound was prepared by reacting **3** (150 mg, 0.533 mmol) and **9a** (228 mg, 0.586 mmol) in CH_3CN (10 mL). After standard workup, **8-C8** was obtained as a beige solid (90 mg , 25%): R_f = 0.36 (DCM/MeOH 9:1). mp = 96–98 °C. ^{1}H NMR (400 MHz, CD_3OD): δ 8.43 (d, J = 8.7 Hz, 1H; H9), 7.87 (ddd, J = 8.5, 7.0, 1.1 Hz, 1H; H6), 7.81 (dd, J = 8.5, 1.2 Hz, 1H; H7), 7.61 (ddd, J = 8.4, 6.8, 1.4 Hz, 1H; H8), 7.32 (dd, J = 4.8, 3.3 Hz, 1H; H4′), 4.56–4.48 (m, 4H; CH_2−O, 2×H2′), 3.99 (d, J = 7.3 Hz, 2H; HN−CH_2), 3.72–3.62 (m, 2H; CH_2−N^+), 3.52 (t, J = 8.3 Hz, 2H; H6′), 3.21 (s, 3H; CH_3−N^+), 3.05 (t, J = 5.6 Hz, 2H; H4), 2.83 (s, 2H; H1), 2.74 (t, J = 5.4 Hz, 2H; H5′), 2.05–1.80 (m, 10H; 2×H2, 2×H3, C$H_2$$CH_2O, CH_2$$CH_2$$N^+$, NH$CH_2CH_2$), 1.56–1.33 (m, 14H; HN−$(CH_2)_2$−CH_2−CH_2−CH_2−CH_2−$(CH_2)_2$−N^+, CH_3−CH_2−CH_2−CH_2−$(CH_2)_2$−O), 0.95 (t, J = 7.1 Hz, 3H; CH_3−$(CH_2)_5$−O). ^{13}C NMR (101 MHz, CD_3OD): δ 163.94, 157.91, 151.69, 145.53, 139.82, 134.03, 127.67, 126.50, 126.29, 124.34, 120.17, 117.07, 112.87, 72.63, 65.60, 60.25, 57.26, 49,14, 48.37, 32.58, 31.53, 30.57, 30.28, 29.86, 29.38, 27.70, 27.42, 26.75, 24.97, 23.59, 23.12, 23.00, 22.60, 21.87, 14.37. MS (ESI) *m/z* $[M+H]^+$ calcd for $C_{35}H_{53}BrN_5OS^+$: 590,39, found: 590.25. HPLC analysis: retention time = 8.2 min, purity 97.8%.

4.7.2. 5-(4-(Hexyloxy)-1,2,5-thiadiazol-3-yl)-1-methyl-1-(10-((1,2,3,4-tetrahydroacridin-9-yl)amino)decyl)-1,2,3,6-tetrahydropyridin-1-ium bromide (**8-C10**)

The title compound was prepared by reacting **3** (140 mg, 0.497 mmol) and **9b** (270 mg, 0.647 mmol) in CH_3CN (10 mL). After standard workup, **8-C10** was obtained as a yellow oil (135 mg, 39%): R_f = 0.42 (DCM/MeOH 9:1). ^{1}H NMR (400 MHz, CD_3OD): δ 8.40 (d, J = 8.7 Hz, 1H; H9), 7.85 (ddd, J = 8.4, 7.0, 1.1 Hz, 1H; H6), 7.79 (d, J = 7.6 Hz, 1H; H7), 7.59 (ddd, J = 8.4, 6.8, 1.3 Hz, 1H; H8), 7.30 (t, J = 4.0 Hz, 1H; H4′), 4.53–4.48 (m, 4H; CH_2−O, 2×H2′), 3.96 (t, J = 7.3 Hz, 2H; HN−CH_2), 3.71–3.61 (m, 2H; CH_2−N^+), 3.49 (t, J = 8.0 Hz, 2H; H6′), 3.19 (s, 3H; CH_3−N^+), 3.03 (t, J = 5.5 Hz, 2H; H4), 2.81 (s, 2H; H1), 2.72 (t, J = 5.3 Hz, 2H; H5′), 2.01–1.80 (m, 10H; 2×H2, 2×H3, C$H_2$$CH_2O, CH_2$$CH_2$$N^+$, NHC$H_2CH_2$), 1.53–1.28 (m, 18H HN−$(CH_2)_2$−C$H_2$−C$H_2$−C$H_2$−C$H_2$−C$H_2$−C$H_2$−$(CH_2)_2$−$N^+$, CH_3−CH_2−CH_2−CH_2−$(CH_2)_2$−O), 0.93 (t, J = 7.1 Hz, 3H; CH_3−$(CH_2)_5$−O). ^{13}C NMR (101 MHz, CD_3OD): δ 163.97, 158.00, 151.67, 145.54, 139.79, 134.09, 127.67, 126.54, 126.33, 124.36, 120.10, 117.07, 112.86, 72.65, 65.63, 60.27, 57.28, 49.28, 49.14, 32.58, 31.54, 30.44, 30.39, 30.26, 30.15, 29.86, 29.34, 27.71, 27.41, 26.75, 24.95, 23.59, 23.12, 22.99, 22.59, 21.86, 14.34. MS (ESI) *m/z* $[M+H]^+$ calcd for $C_{37}H_{57}BrN_5OS^+$: 618.42, found: 618.30. HPLC analysis: retention time = 8.6 min, purity 97.3%.

4.7.3. 5-(4-(Hexyloxy)-1,2,5-thiadiazol-3-yl)-1-methyl-1-(12-((1,2,3,4-tetrahydroacridin-9-yl)amino)dodecyl)-1,2,3,6-tetrahydropyridin-1-ium bromide (**8-C12**)

The title compound was prepared by reacting **3** (150 mg, 0.533 mmol) and **9c** (237 mg, 0.533 mmol) in CH_3CN (10 mL). After standard workup, **8-C12** was obtained as a beige solid (115 mg , 30%): R_f = 0.54 (DCM/MeOH 9:1). mp = 93–96 °C. ^{1}H NMR (400 MHz, CD_3OD): δ 8.40 (d, J = 8.7 Hz, 1H; H9), 7.88–7.78 (m, 2H; H6, H7), 7.58 (ddd, J = 8.4, 6.6, 1.5 Hz, 1H; H8), 7.29 (t, J = 3.9 Hz, 1H; H4′), 4.56–4.45 (m, 4H; CH_2−O, 2×H2′), 3.95 (t, J = 7.3 Hz, 2H; HN−CH_2), 3.74–3.59 (m, 2H; CH_2−N^+), 3.51 (t, J = 7.8 Hz, 2H; H6′), 3.20 (s, 3H; CH_3−N^+), 3.03 (t, J = 5.6 Hz, 2H; H4), 2.82 (s, 2H; H1), 2.71 (t, J = 5.4 Hz, 2H; H5′), 2.04–1.78 (m, 10H; 2×H2, 2×H3, C$H_2$$CH_2O, CH_2$$CH_2$$N^+$, NHC$H_2CH_2$), 1.54–1.22 (m, 22H HN−$(CH_2)_2$−C$H_2$−C$H_2$−C$H_2$−C$H_2$−C$H_2$−C$H_2$−C$H_2$−C$H_2$−$(CH_2)_2$−$N^+$, CH_3−CH_2−CH_2−CH_2−$(CH_2)_2$−O), 0.92 (t, J = 7.0 Hz, 3H; CH_3−$(CH_2)_5$−O). ^{13}C NMR (101 MHz, CD_3OD): δ 163.94, 157.90, 151.69, 145.54, 139.80, 134.03, 127.69, 126.50, 126.30, 124.34, 120.16, 117.06, 112.86, 72.63, 65.61, 60.25, 57.27,

49,27, 49.13, 32.57, 31.52, 30.55, 30.48, 30.26, 30.18, 29.85, 29.38, 27.68, 27.41, 26.74, 24.98, 23.57, 23.12, 22.99, 22.60, 21.86, 14.35. MS (ESI) *m/z* $[M+H]^+$ calcd for $C_{40}H_{62}BrN_5OS^+$: 646.45, found: 646.30. HPLC analysis: retention time = 8.9 min, purity 96.8%.

4.8. Biology

The Chinese hamster ovary (CHO) cell line stably expressing hM_1 receptor was obtained from Wyeth Research (Princeton, NJ). 384-well microplates and white 96-well plates were purchased from Thermo Fisher and Greiner Bio One, Germany, respectively. Dulbecco's modified Eagle's medium (DMEM) and phosphate-buffered saline (PBS) were from Sigma (Germany). Leibovitz's L-15 medium (L-15) and Hank's balanced salt solution (HBSS) were from Gibco (Germany). Fetal calf serum (FCS), trypsin and geneticin (G418) were from Merck Biochrom (Germany). D-Luciferin was purchased as potassium salt from Pierce (Germany) and was dissolved in HBSS at a 400 mM concentration. Puromycin was obtained from Invivogen (France).

4.8.1. Inhibition of Acetylcholinesterase

AChE (E.C. 3.1.1.7, from electric eel) was purchased from Sigma Aldrich (Steinheim, Germany). 5,5'-Dithiobis-(2-nitrobenzoic acid) (DTNB or Ellman's reagent) and acetylthiocholine iodide (ATC) were obtained from Fluka (Buchs, Switzerland). For buffer preparation, 2.40 g of potassium dihydrogen phosphate were dissolved in 500 mL of water and adjusted to pH 8.0 with a NaOH solution (0.1 M). Enzyme solutions were prepared with buffer to give 2.5 units per mL and stabilized with 2 mg bovine serum albumin (SERVA, Heidelberg, Germany) per mL of enzyme solution. 396 mg of DTNB were dissolved in 100 mL of buffer to give a 10 mM solution (0.3 mM in assay). The stock solutions of the test compounds were prepared either in pure buffer or, if insoluble, in pure ethanol with a concentration of 33.3 mM (1 mM in assay) and diluted stepwise with ethanol to a concentration of 33.3 nM (1 nM in assay). The highest concentration of the test compounds applied in the assay was 10^{-3} M (the amount of EtOH in the stock solution did not influence the enzyme activity in the assay). The assay was performed at 25 °C according to a previously described protocol[3] . Spectrophotometric measurements were performed on a Shimadzu UVmini-1240 spectrophotometer (Duisburg, Germany) at 412 nm.

4.8.2. Cell cultures

Chinese hamster ovary (CHO) cells stably expressing the hM_1 receptor (CHO-hM_1 cells) were cultured in Ham's nutrient mixture F-12 (HAM- F12) supplemented with 10 % (v/v) FCS, 100 U/mL penicillin, 100 µg/mL streptomycin, 0.2 mg/mL G418 and 2 mM L-glutamine at 37°C in a 5 % CO_2 humidified atmosphere. The HEK293T cells stably co-transfected with the human M_1 receptor and the $G\alpha_q$-PLC-β3 sensor were kindly provided by Timo Littmann (University of Regensburg). Cells were cultivated in DMEM containing 10% FCS (full medium) at 37 °C in a water-saturated atmosphere containing 5% CO_2 as previously reported[35].

4.8.3. Split Luciferase bioluminescence assay

In brief, cells were detached from a 75-cm^2 flask by trypsinization and centrifuged (700 × *g* for 5 min). The pellet was resuspended in the assay medium consisting of L-15 with 5% FCS and the density of the suspension was adjusted to $1.25 \cdot 10^6$ cells/mL. Then, 80 µL of this suspension were seeded into each well of a 96-well plate, and the plate was incubated at 37 °C in a humidified atmosphere (without additional CO_2) overnight. On the next day, 10 µL of 10 mM D-Luciferin were added to the cells, and the plate was transferred into a pre-warmed microplate luminescence reader (Mithras LB 940 Multimode Microplate Reader, Berthold Technologies). The cells were allowed to equilibrate inside the reader for 10 min before the basal luminescence was determined by recording the luminescence for the entire plate ten times with an integration time of 0.5 s per well. In the meantime, serial dilutions of agonists were prepared. The resulting solutions were also pre-warmed to 37 °C and subsequently added to the cells. Thereafter, luminescence was recorded for 15 plate repeats amounting to a time period of 20 min. Negative controls (solvent) and positive controls (reference full agonist, carbachol (hM_1R), eliciting a maximal 100 % response) were included for subsequent normalization of the data. When the antagonist mode was evaluated, antagonists were added 15 min prior to the initial thermal equilibration period, to ensure their equilibrium with the receptors before adding the agonists. The pK_b values of antagonists were determined according to the Cheng-Prusoff equation[44]. After data acquisition, the peak luminescence intensities obtained after stimulation were used for quantitative analysis using the Graph

Pad Software, San Diego, CA. The hM_1R construct was kindly provided by Timo Littmann (University of Regensburg).

4.8.4. IP-One accumulation assay

In brief, CHO-hM_1 cells were grown to a confluence of about 80%, were detached from the culture dish, resuspended in assay buffer (HEPES, 10 mM, $CaCl_2$, 1 mM, $MgCl_2$, 0.5 mM, KCl, 4.2 mM, NaCl, 146 mM, glucose, 5.5 mM, LiCl, 50 mM, pH 7.4), counted using the Neubauer counting chamber and dispensed in 384-well microplates at a density of 1×10^7cells/mL. After incubation with the test compounds dissolved in stimulation buffer at 37 °C for 30 min, the detection reagents were added (IP1-d2 conjugate and Anti-IP1cryptate TB conjugate, each dissolved in lysis buffer), and incubation was maintained at room temperature for 60 min. Time-resolved fluorescence resonance energy transfer (HTRF) was determined after excitation at 320 nm using the Wallac EnVision 2104 Multilabel plate reader. Data analysis was based on the fluorescence ratio emitted by labeled IP1 (665 ± 10 nm) over the light emitted by the europium cryptate-labeled anti-IP1 (615 ± 10 nm). Levels of IP1 were normalized to the amount generated in the presence of 100 µM ACh. All compounds were tested in triplicate in at least three individual experiments.

4.8.5. Data processing

Data are shown as means ± S.E.M. for n independent experiments. Statistical analysis and curve fitting were performed using Prism 5.01 (GraphPad Software, San Diego, CA). In the Ellman's assay, the percentage of enzyme activity was plotted against the logarithm of the compound concentrations from which the IC_{50} values were calculated. Data of the IP1 accumulation assay were processed by plotting the ratios (emission at 665 nm/emission at 615 nm) of the HTRF measurements against log (concentration of compounds) and analyzed by a four-parameter logistic equation (log(agonist) vs. response - variable slope) (GraphPad Software, San Diego, CA), followed by normalization using CCh as reference compound.

4.9. Computational analysis

The docking studies followed a previously developed protocol for tacrine-based bivalent compounds[45], with slight adaptation of search parameters to improve convergence in the present case. The protein structure was prepared from the high-resolution crystal structure of *Torpedo californica* AChE (TcAChE) complexed with a bis-tacrine compound (PDB 2CKM)[46]. The continuously resolved polypeptide chain from Ser4 to Pro485 of this PDB structure was used for docking after removing two *N*-acetyl-glucosamine residues and all water molecules and adding missing side chain atoms. Protein and ligand preparations were carried out with the Molecular Operating Environment (MOE) 2018.01[47]. Protonation states were set according to the expected ionization at pH 8 (corresponding to Ellman assay conditions), which resulted in a protonated tacrine moiety. The ligand structures were built in MOE (using the S-configuration for the methylated **8-Cn** hybrids) and energy minimized with the MMFF94x force field to an rms-gradient of 0.001 kcal/(mol·Å).

Docking calculations were carried out with GOLD v5.2.2[48,49], using the Astex Statistical Potentials (ASP) as scoring function. Each ligand was subjected to 50 independent runs, with the number of operations set to 4.000.000 per run. Due to the large conformational flexibility of the compounds, the search parameters of the genetic algorithm were adjusted with respect to population size (500), crossover frequency (90) and migration frequency (20). Following the previous approach of Chen et al.[45] and Messerer et al.[3], a scaffold match constraint was applied to place the tacrine moiety in the catalytic active site as observed in the crystal structures. Unconstrained docking supported the feasibility of the placement of the tacrine moiety (results not shown). The 50 docking poses obtained from GOLD were clustered with respect to binding-mode similarity, using a root-mean-square-deviation (RMSD) of 2 Å as cutoff, and re-scored with DrugScoreX (DSX) based on CSD potentials[50]. The before discussed representative docking solutions were obtained from the best-ranked cluster containing at least 10 poses by selecting the pose with the best consensus score from DSX and ASP. The PyMOL Molecular Graphics System v2.2.3 was used for visual analysis and figure preparation[51].

Acknowledgments

Special thanks are due to Timo Littmann for the generous gift of the cells expressing the Split-Luc construct. D.V. received financial support by the international doctoral college “Receptor Dynamics: Emerging Paradigms for Novel Drugs” funded within the framework of the Elite Network of Bavaria (ENB). (Grant number K-BM-2013-247). N.Y.C. was supported by a fellowship of the Bavarian Ministry for Science and Arts. The PhD position of M.M. is financed by the University of Milan.

Declaration of Competing Interest

The authors declared that they have no conflicts of interest.

Supplementary data to this article can be found online.

Compound 1

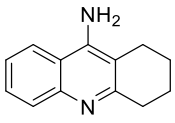

^{1}H NMR spectrum

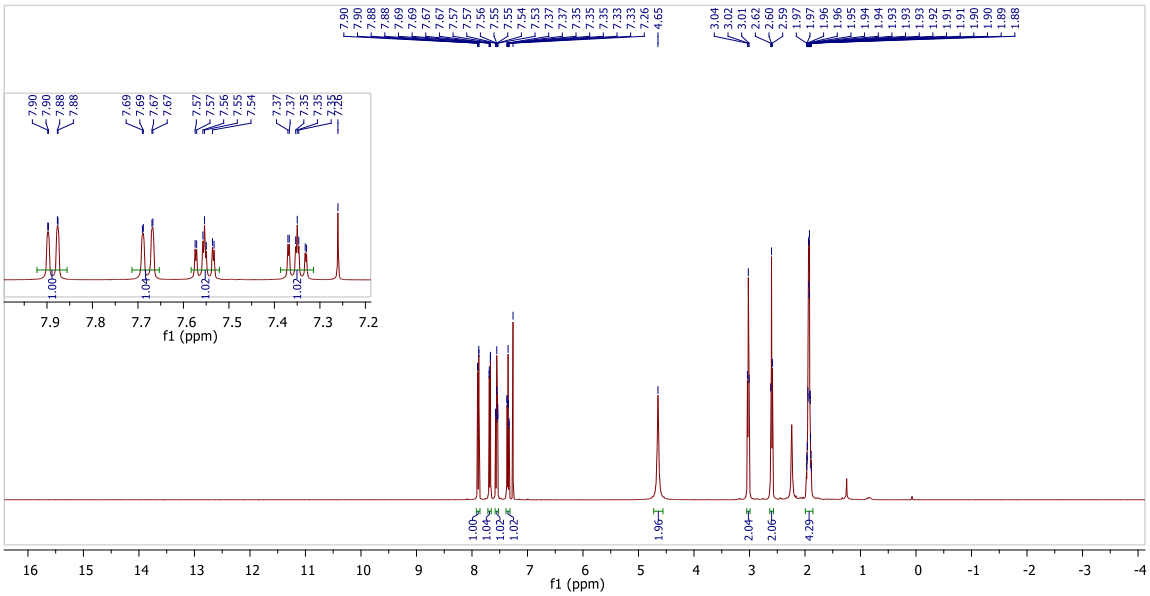

^{13}C NMR spectrum

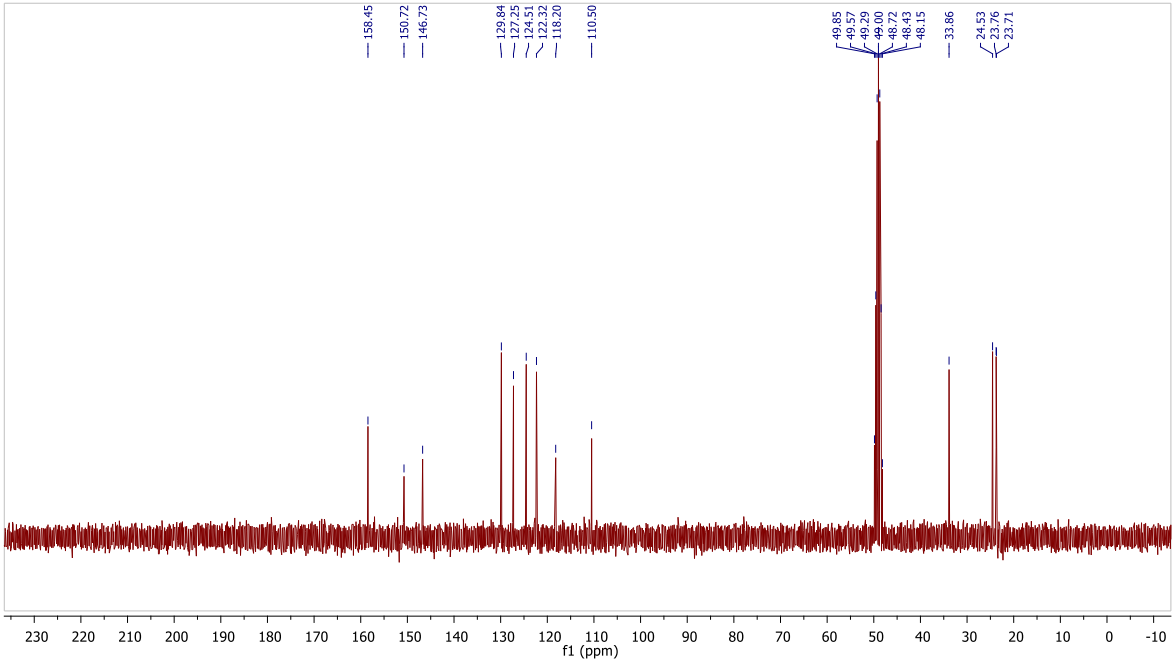

Compound 9a

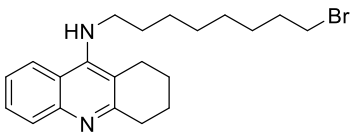

^{1}**H NMR** spectrum

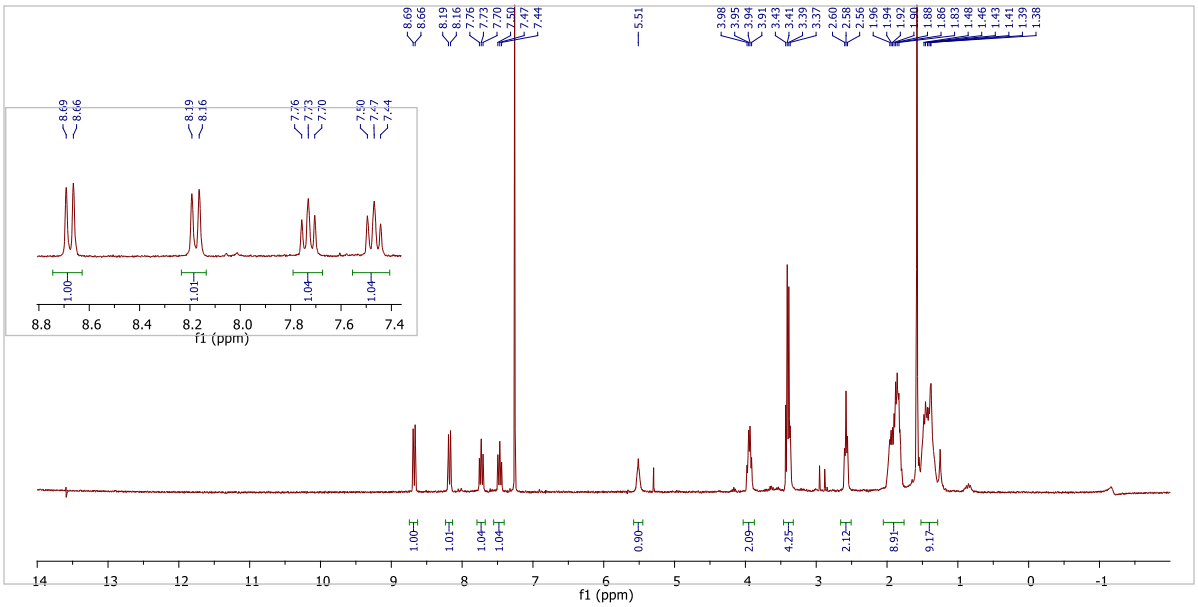

^{13}**C NMR** spectrum

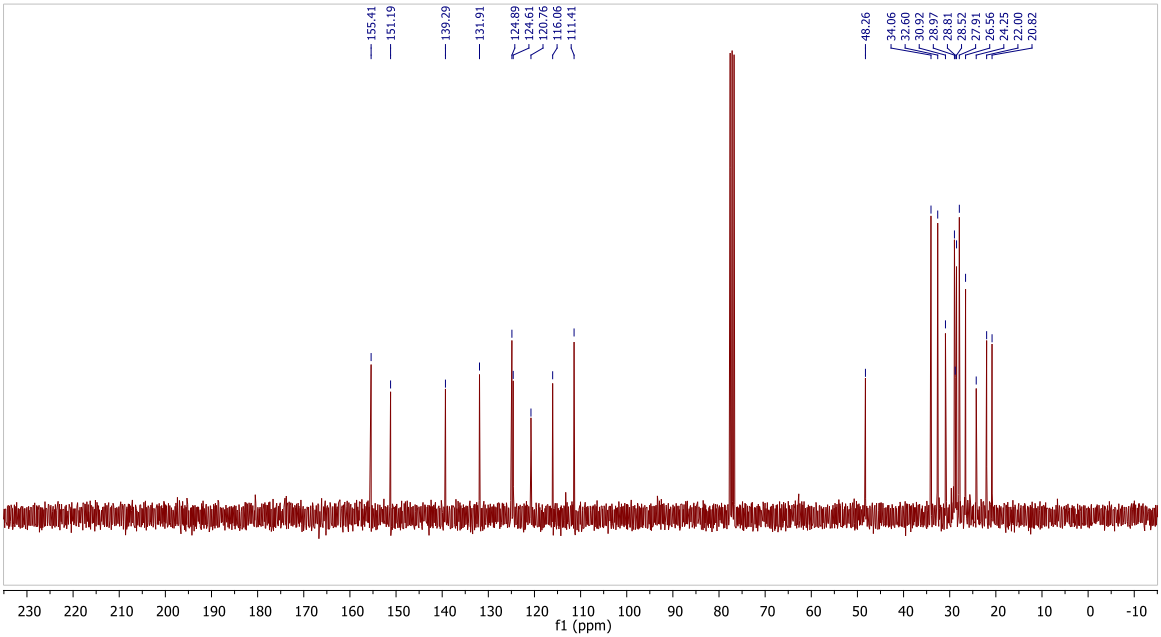

Compound 9b

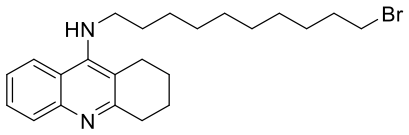

^{1}H NMR spectrum

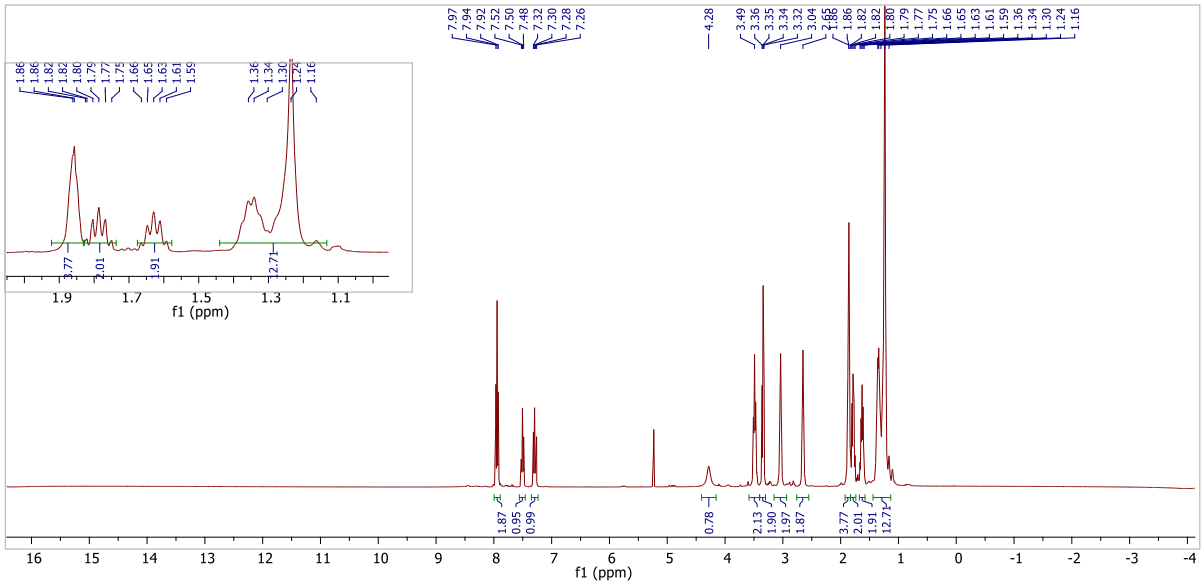

^{13}C NMR spectrum

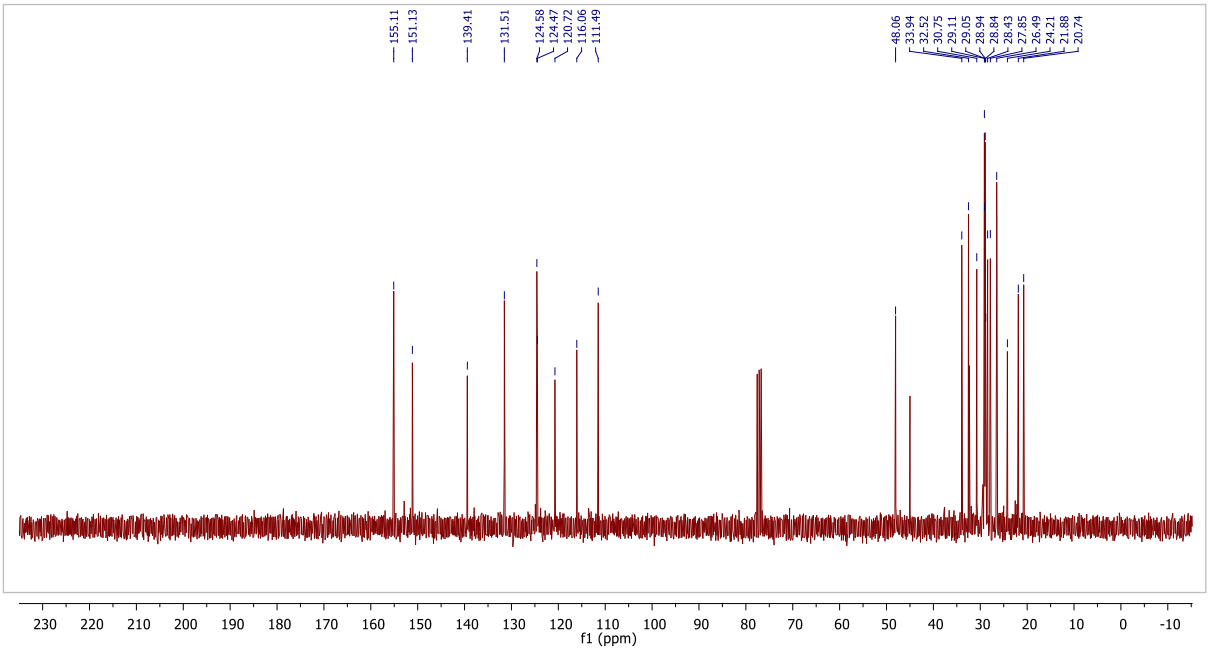

Compound 9c

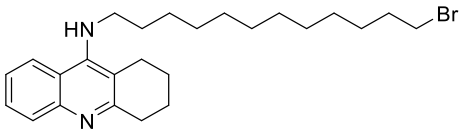

^{1}H NMR spectrum

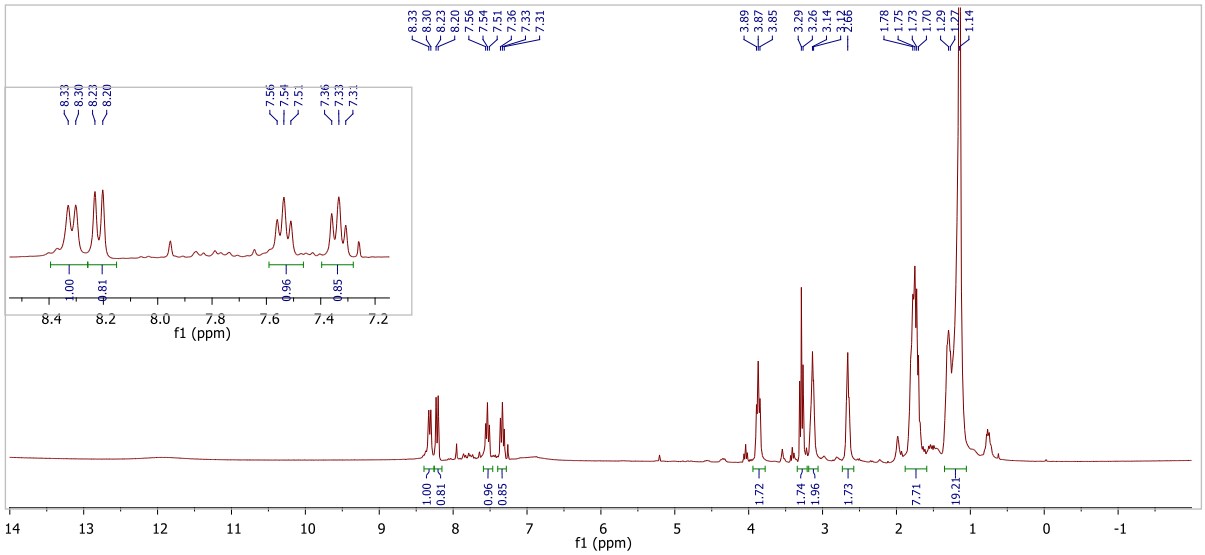

^{13}C NMR spectrum

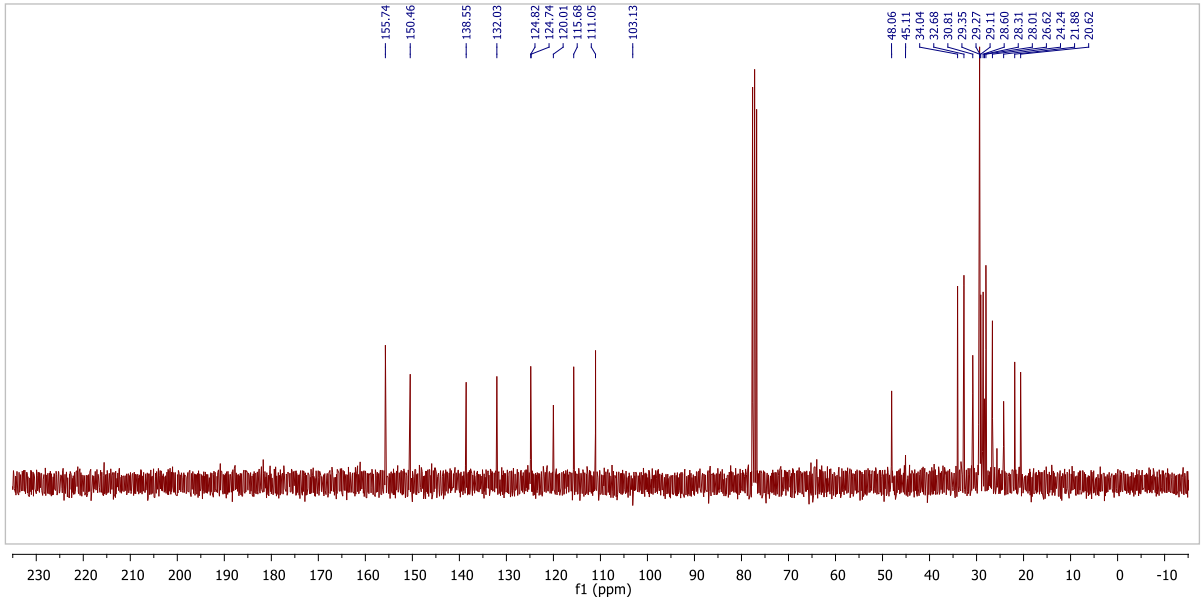

Compound 10

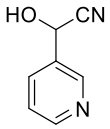

^{1}H NMR spectrum

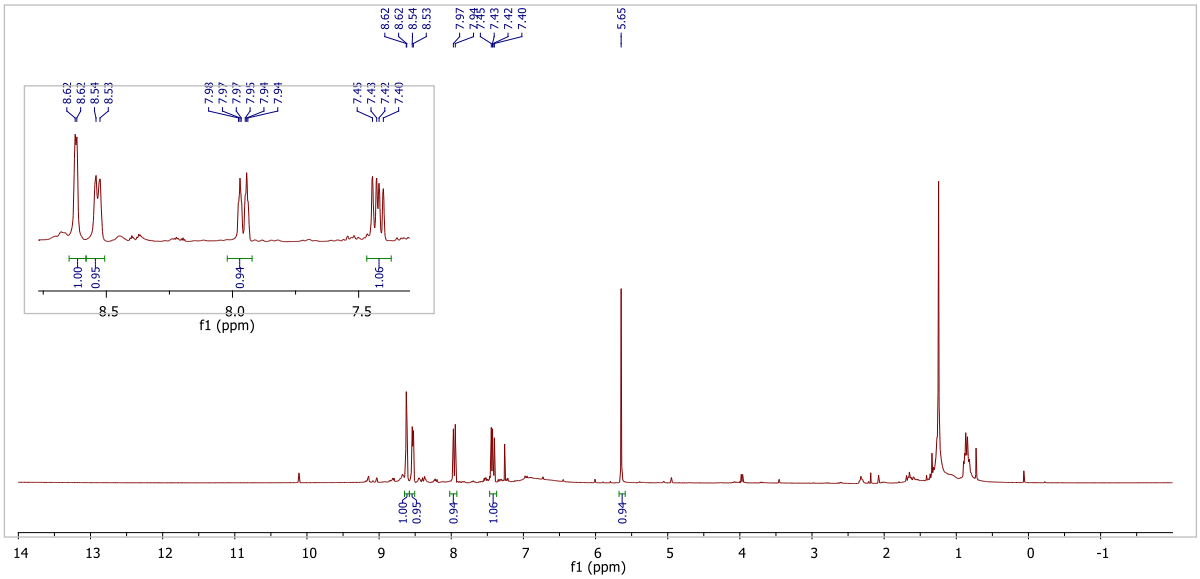

^{13}C NMR spectrum

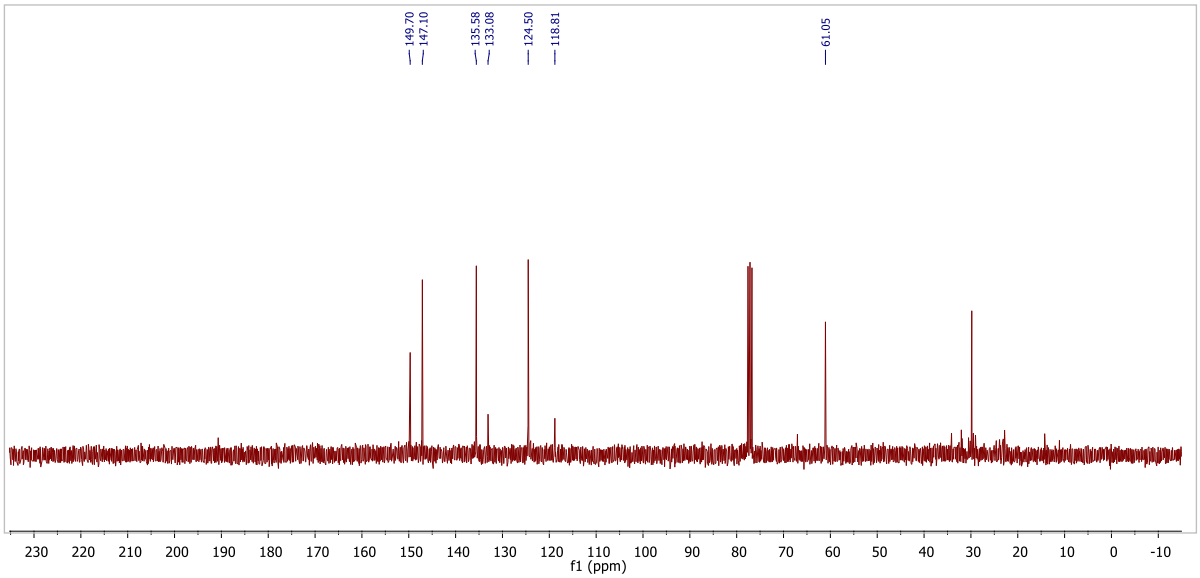

Compound 11

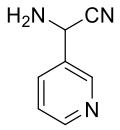

^{1}H NMR spectrum

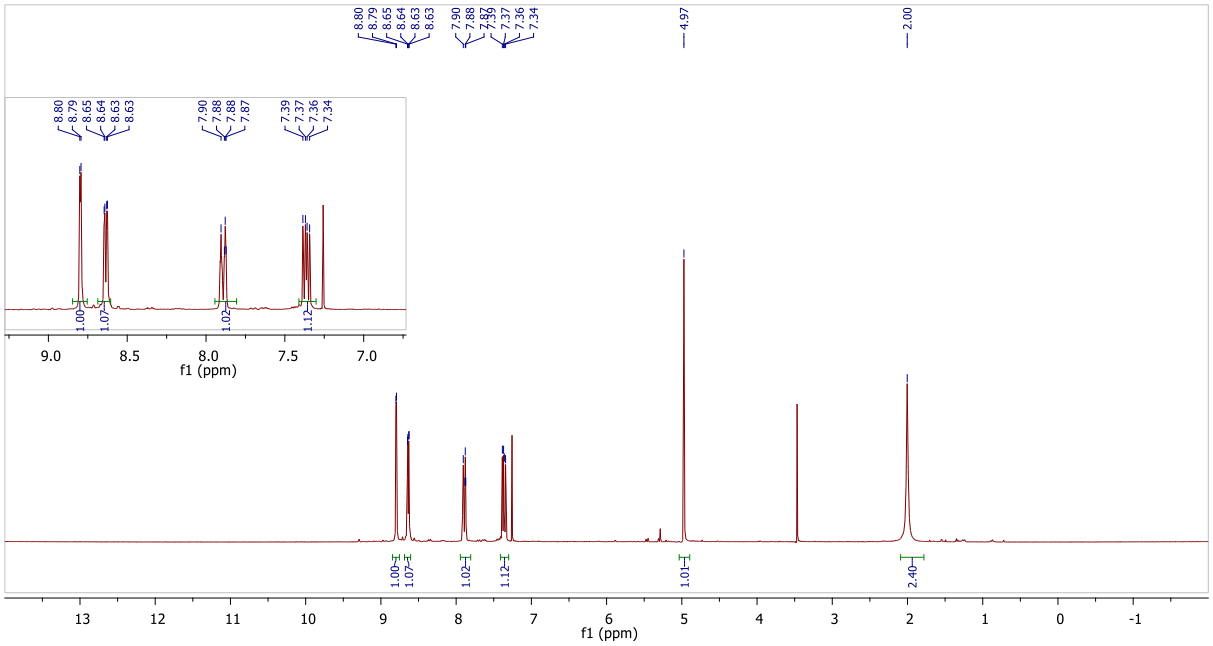

^{13}C NMR spectrum

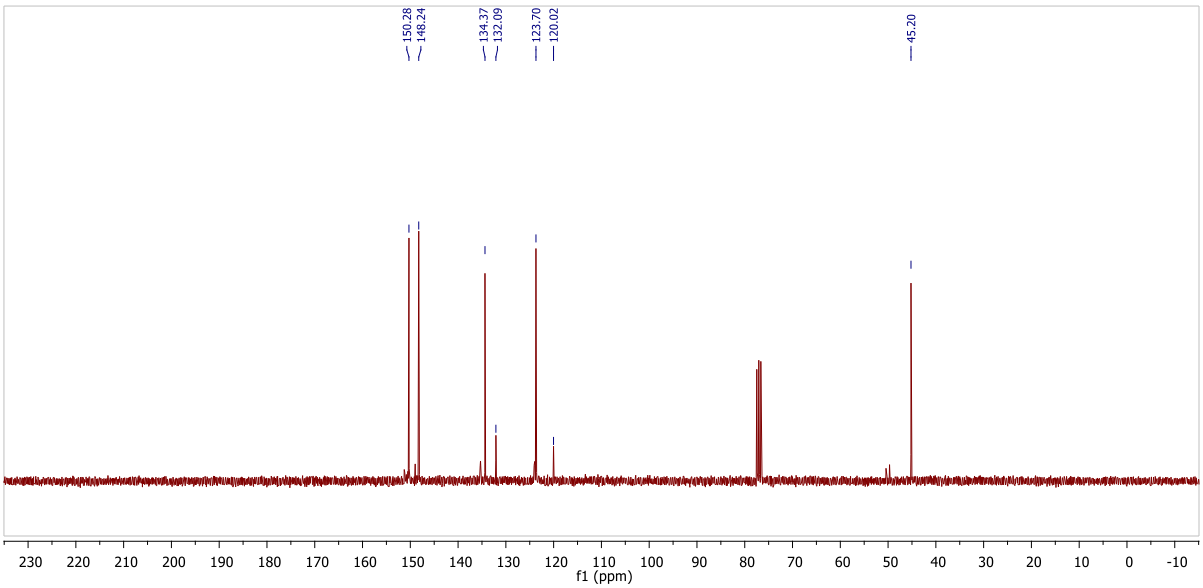

Compound 12

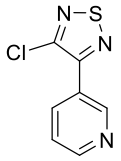

^{1}H NMR spectrum

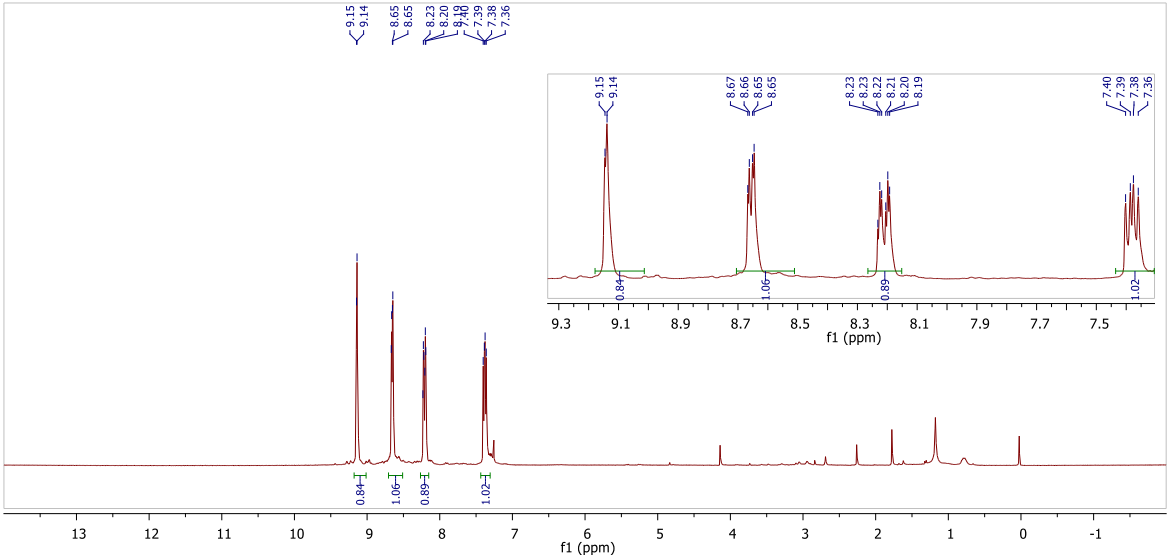

^{13}C NMR spectrum

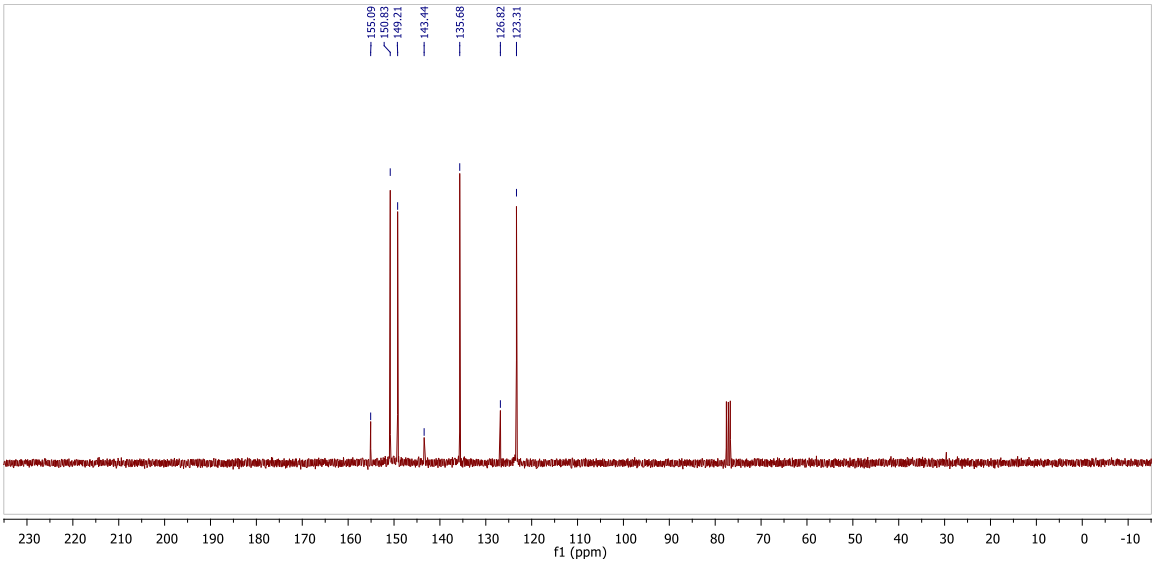

Compound 13

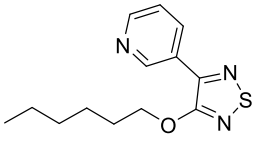

^{1}H NMR spectrum

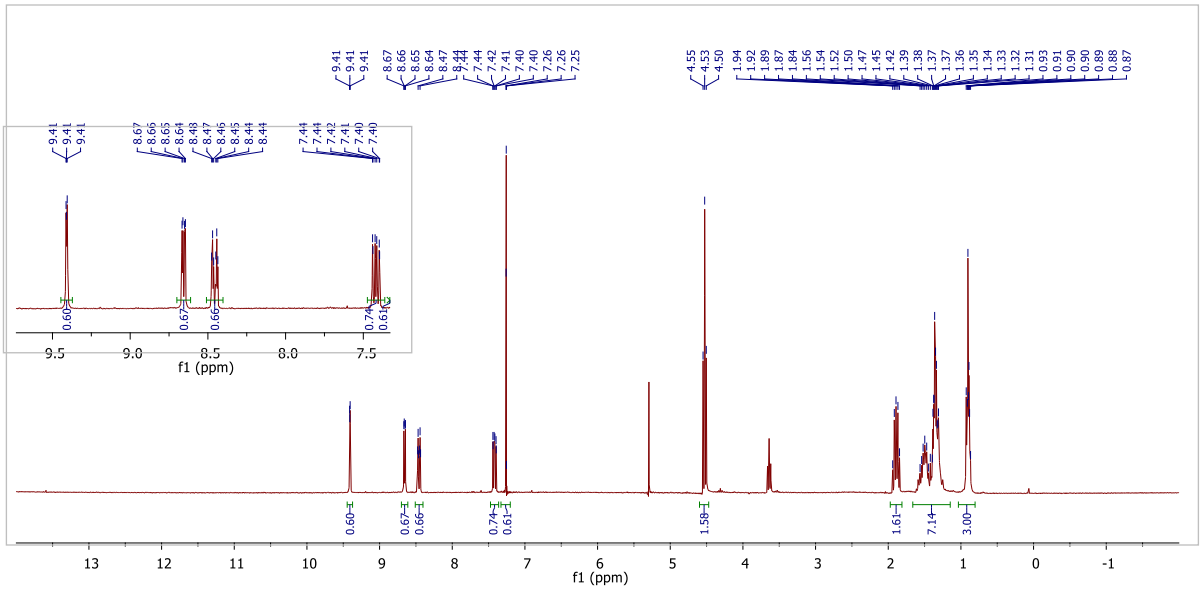

^{13}C NMR spectrum

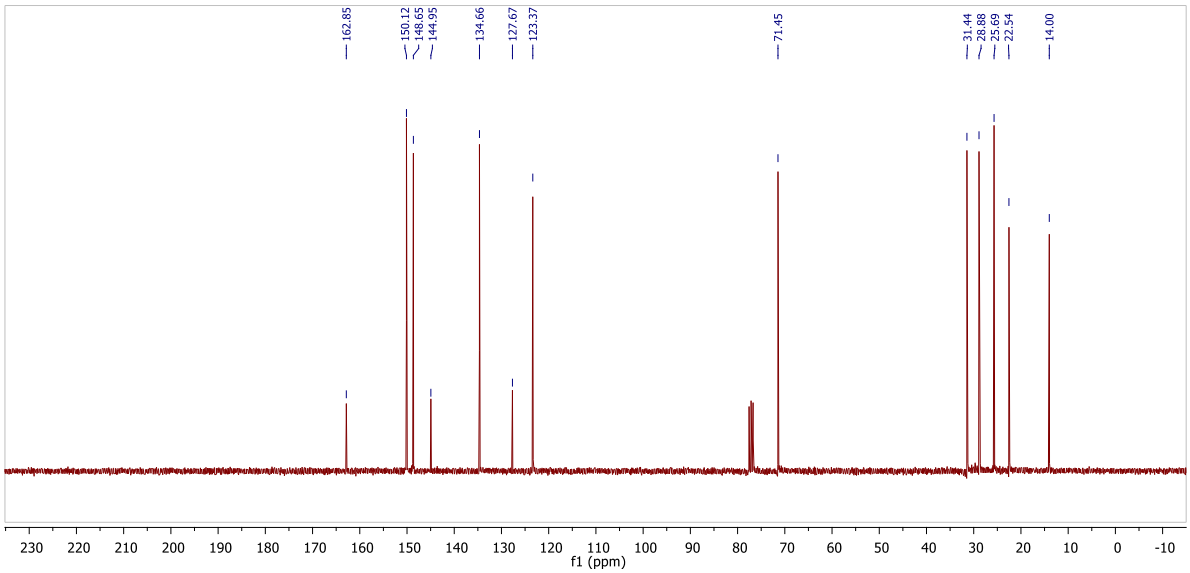

Compound 14

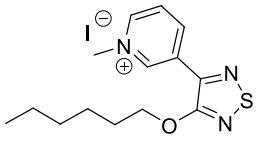

^{1}H NMR spectrum

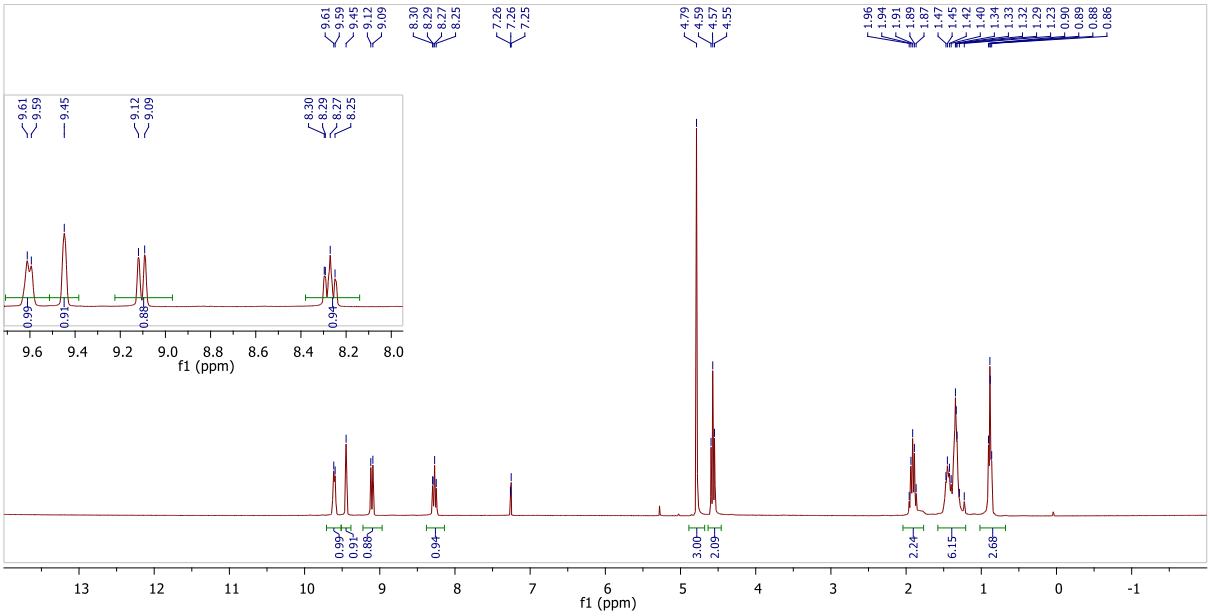

^{13}C NMR spectrum

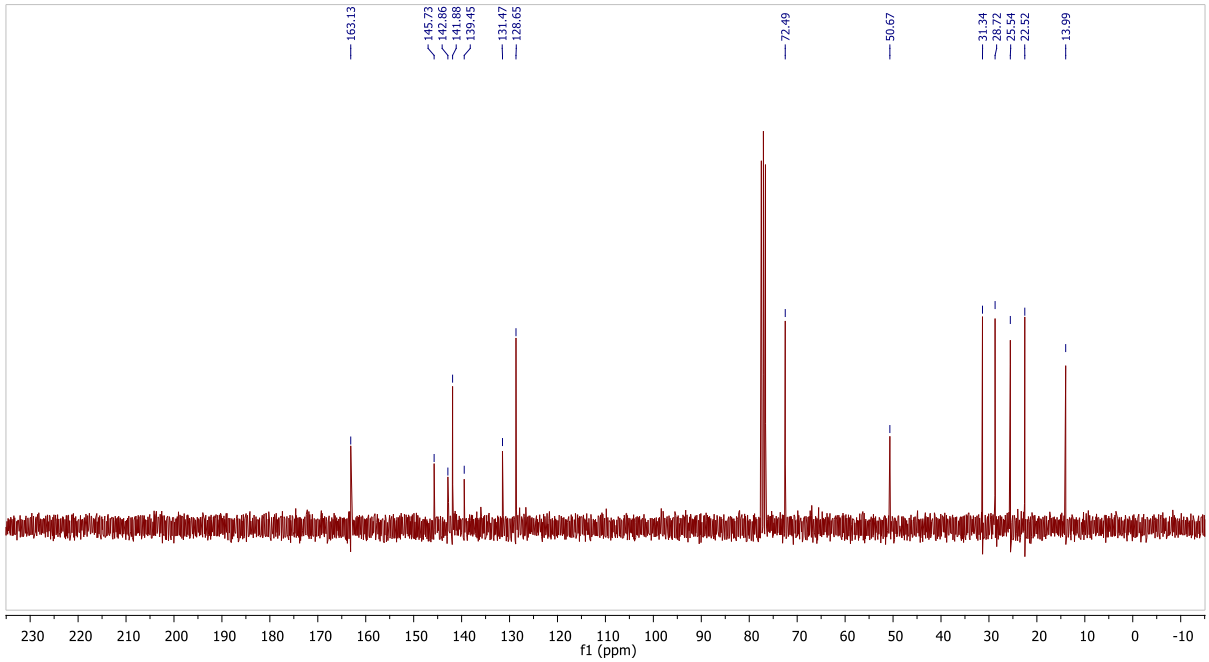

Compound 3

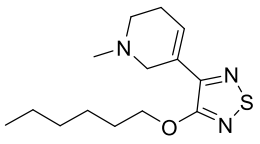

^{1}H NMR spectrum

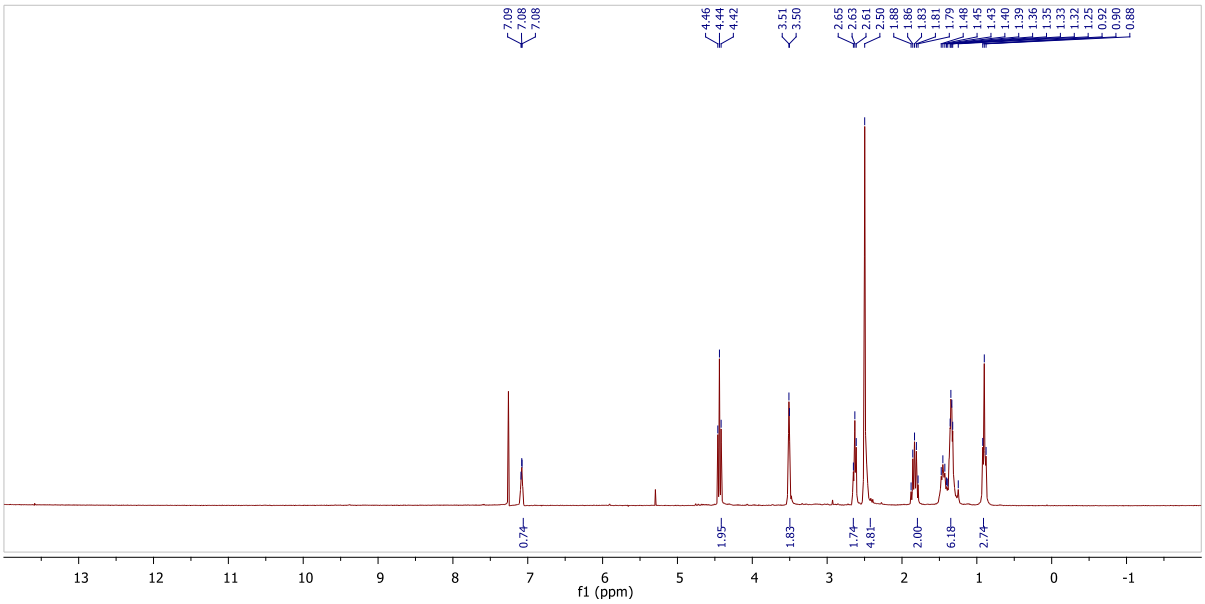

^{13}C NMR spectrum

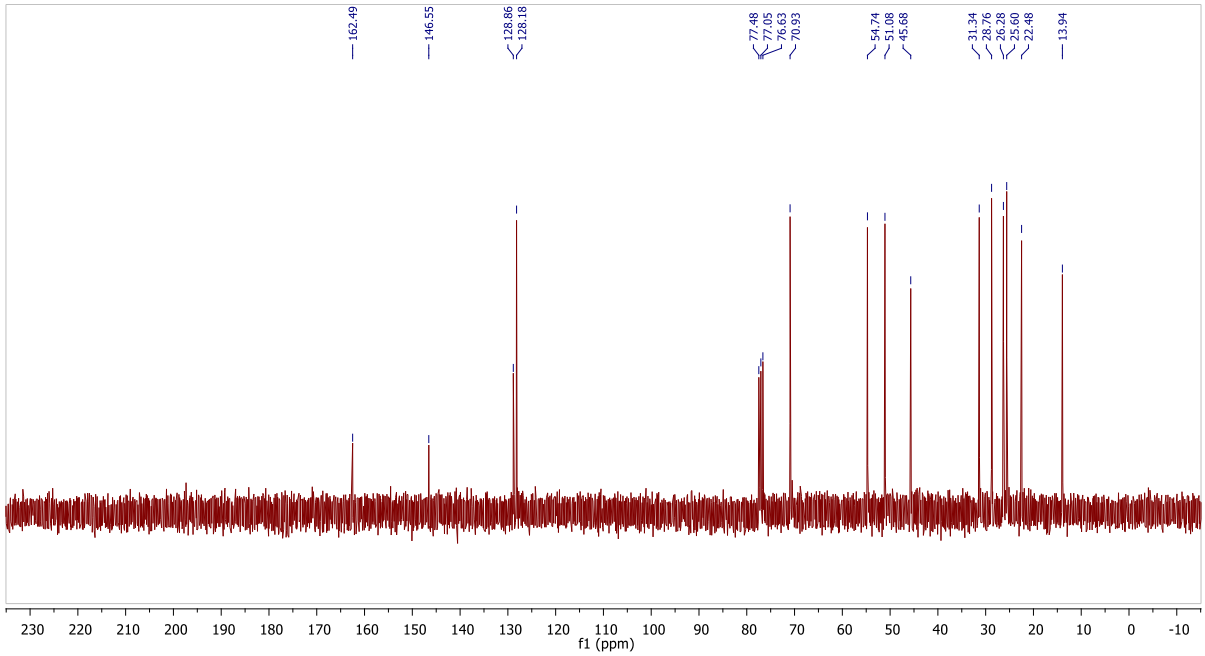

Compound 15a

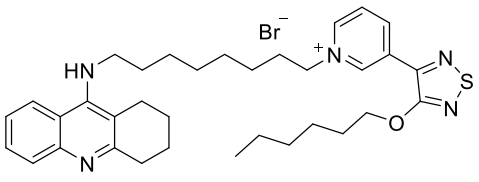

^{1}H NMR spectrum

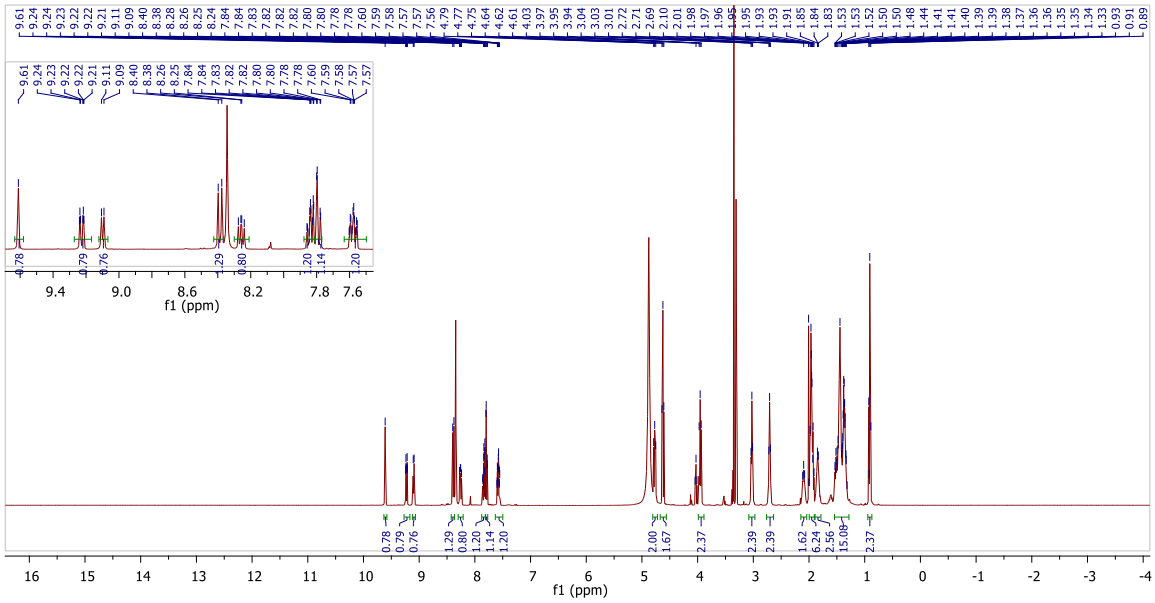

^{13}C NMR spectrum

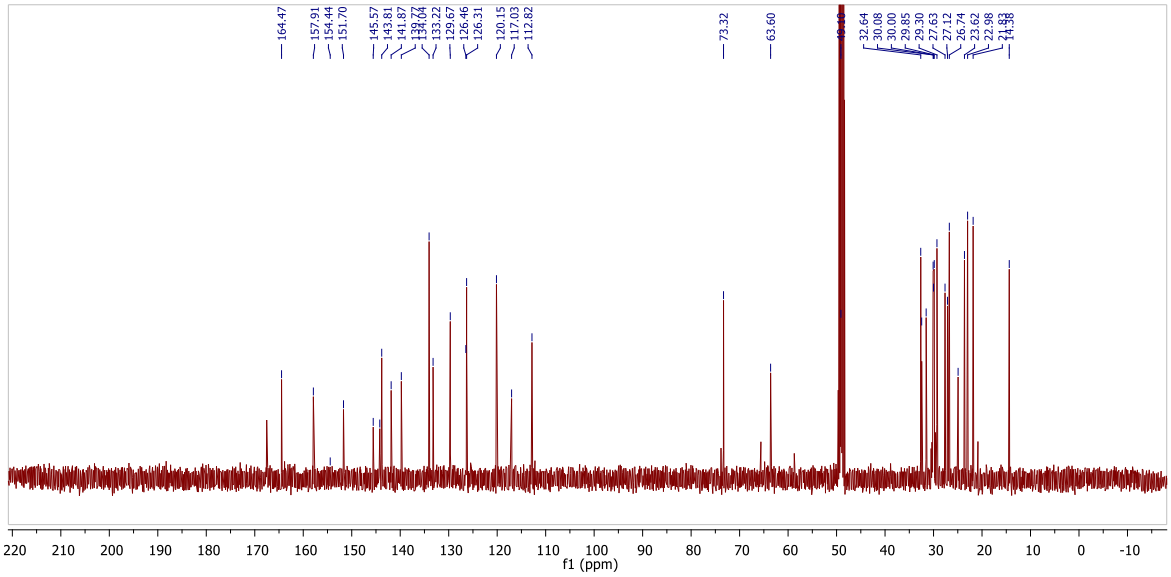

Compound 15b

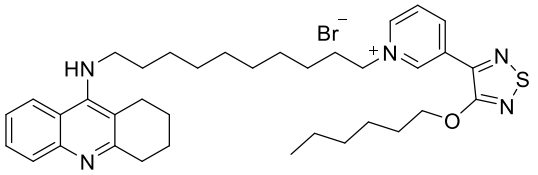

^{1}H NMR spectrum

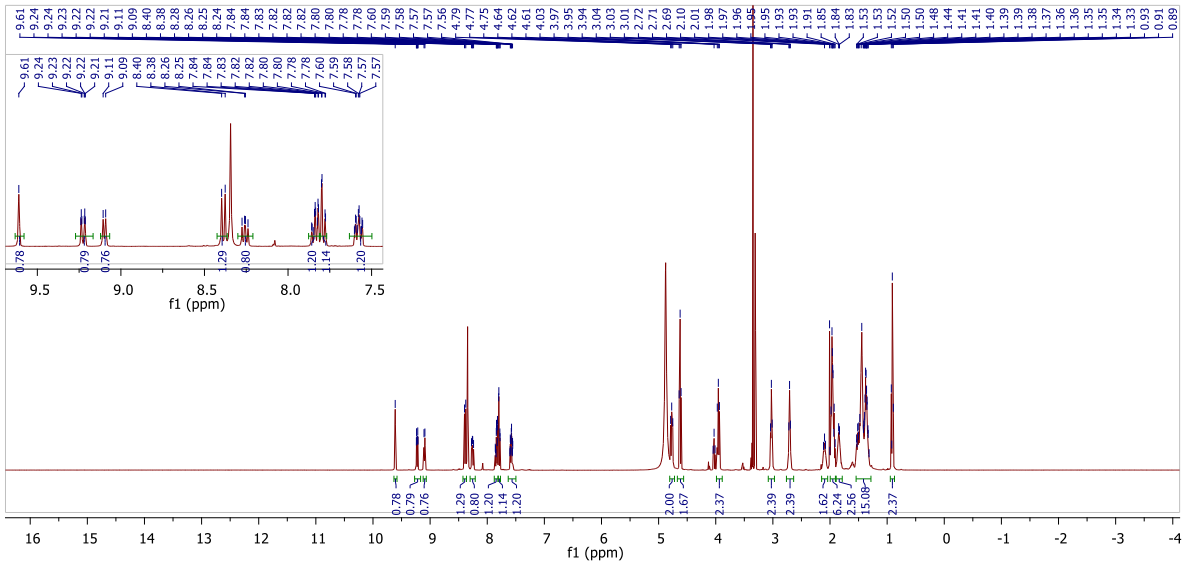

^{13}C NMR spectrum

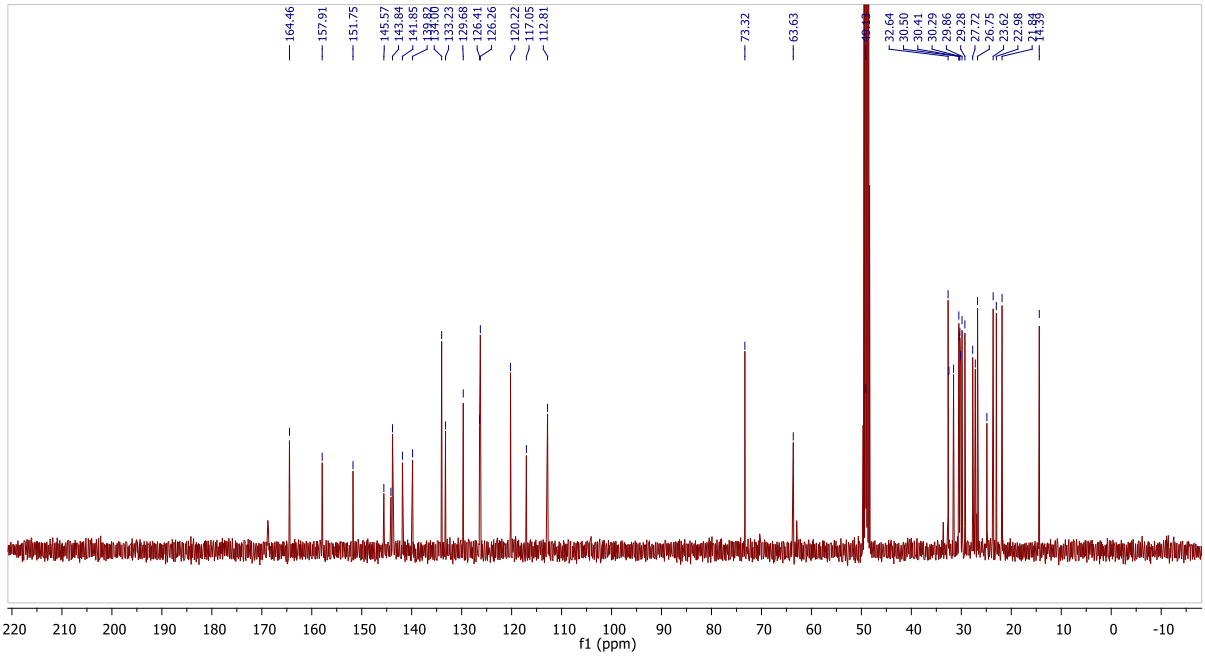

Compound 15c

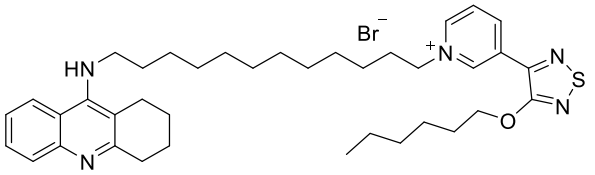

^{1}H NMR spectrum

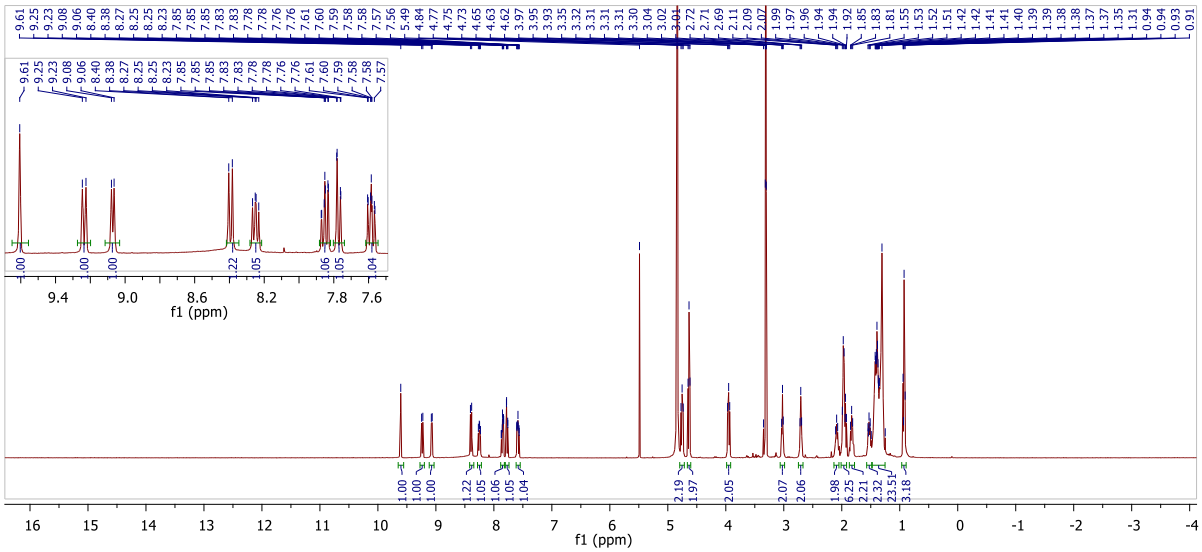

^{13}C NMR spectrum

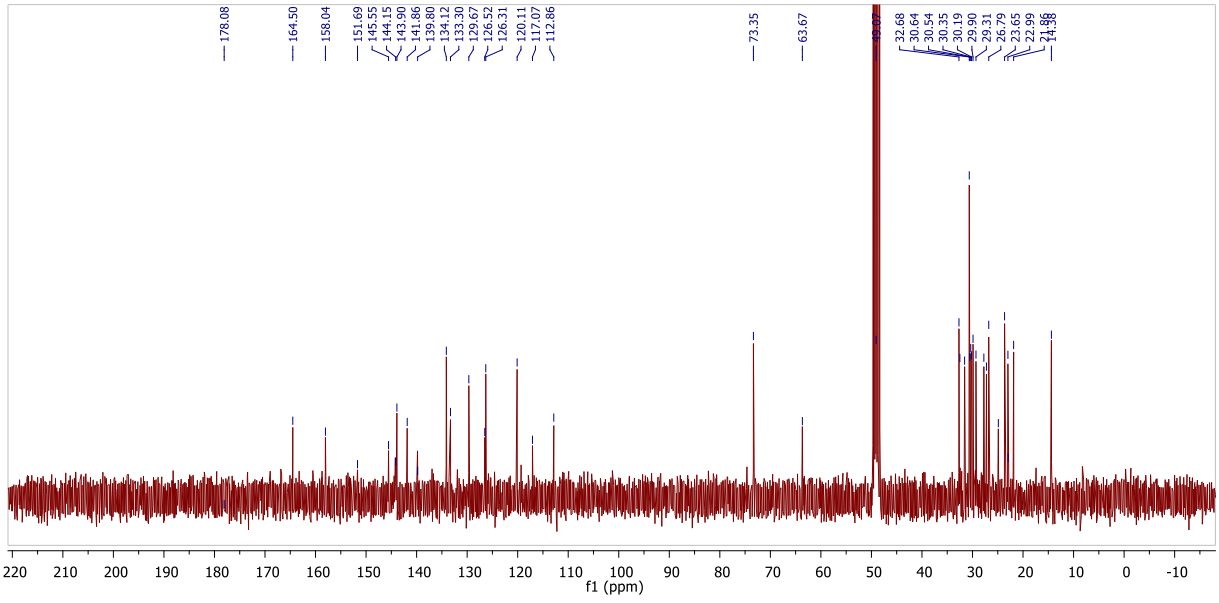

Compound 7-C8

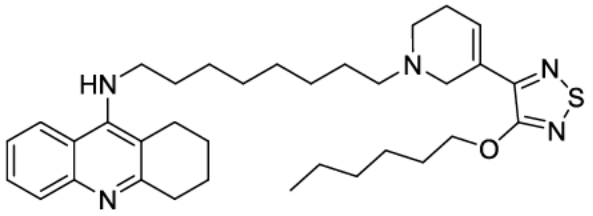

^{1}H NMR spectrum

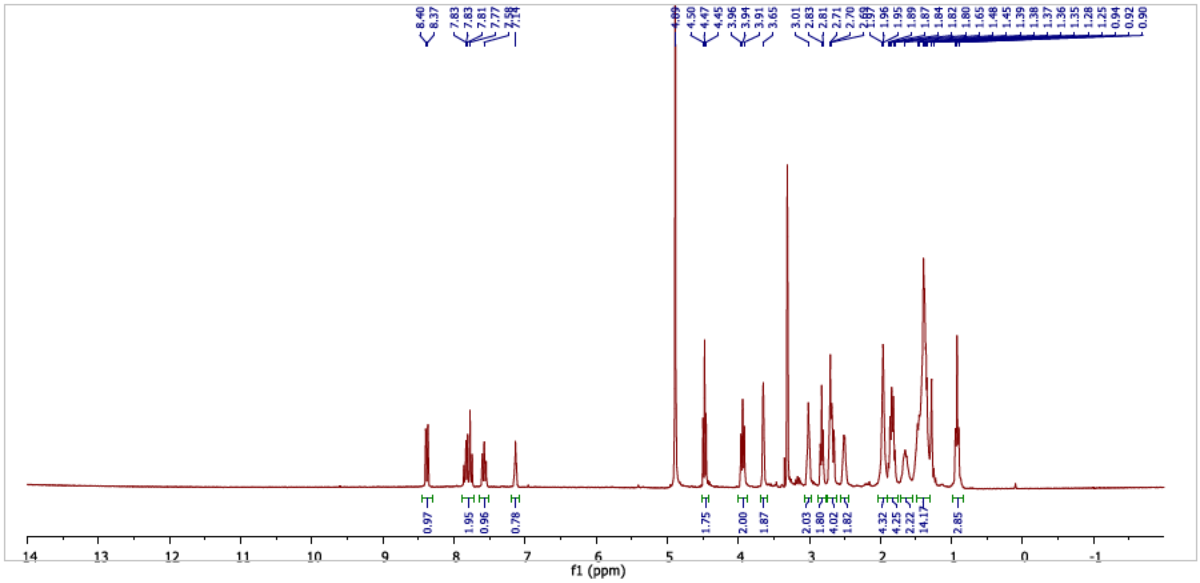

^{13}C NMR spectrum

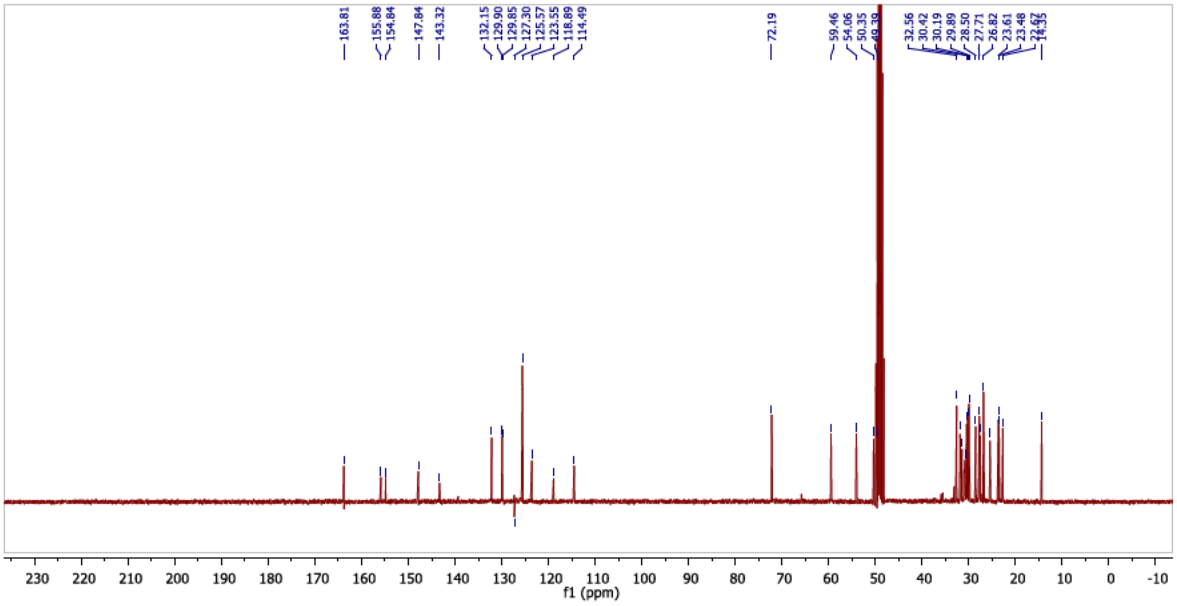

SHIMADZU LabSolutions **Analysis Report**

<Sample Information>

Sample Name	: Tac8 Xano MM6		
Sample ID	:		
Data Filename	: Tac8 Xano MM6.lcd		
Method Filename	: LCMS Analysis 15 cm 05-50 1mL_254nm.lcm		
Batch Filename	: 171220.lcb		
Vial #	: 1-78	Sample Type	: Unknown
Injection Volume	: 30 uL		
Date Acquired	: 19.01.2018 11:28:37	Acquired by	: System Administrator
Date Processed	: 19.01.2018 15:48:29	Processed by	: System Administrator

<Chromatogram>

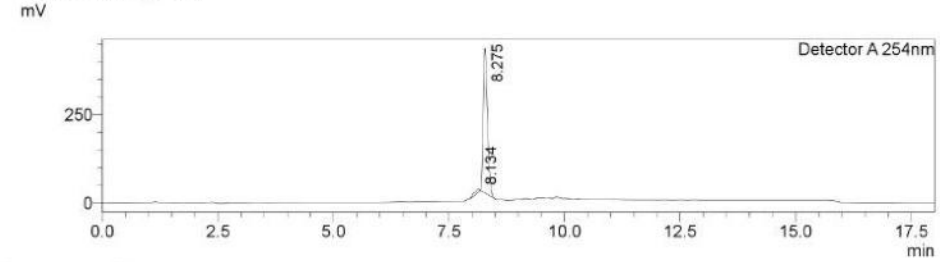

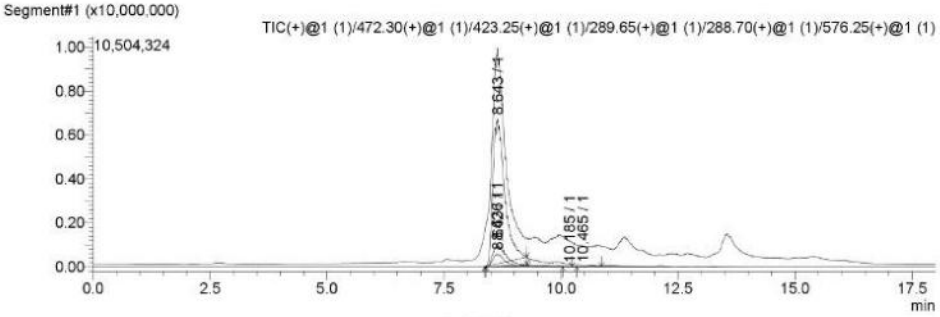

Peak Table

Detector A 254nm

Peak#	Ret. Time	Area	Height	Area%
1	8.134	83562	9235	3.095
2	8.275	2616390	408830	96.905
Total		2699952	418065	100.000

MS Spectrum

Line#:3 R.Time:8.640(Scan#:5185)
MassPeaks:384
Spectrum Mode:Averaged 8.637-8.643(5183-5187) Base Peak:288.70(6657387)
BG Mode:Calc Segment 1 - Event 1

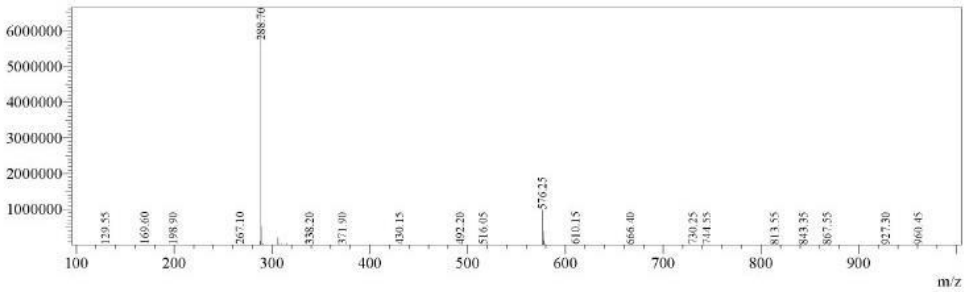

LC−MS analysis:

ESI m/z $[M+H]^+$ calculated is 575.37. It was found 288.70 as $[M+2H]^{++}$ and 576.25 as $[M+H]^+$

Retention time: 8.275

Purity: 96.91%

Compound 7-C10

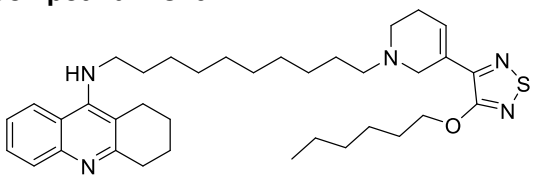

^{1}H NMR spectrum

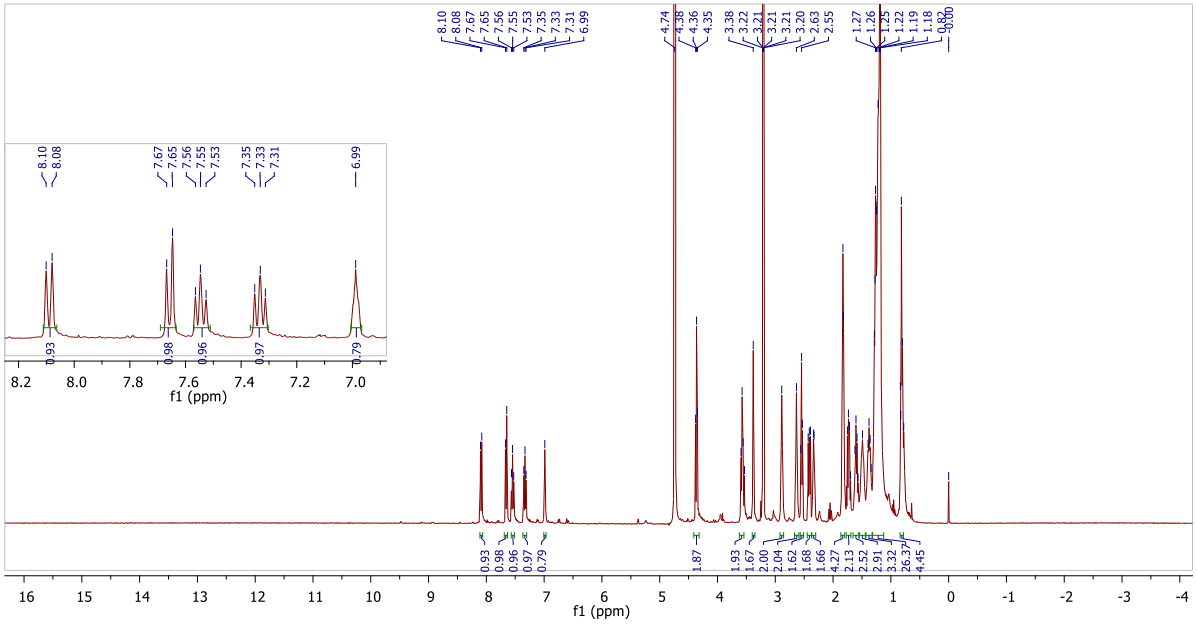

^{13}C NMR spectrum

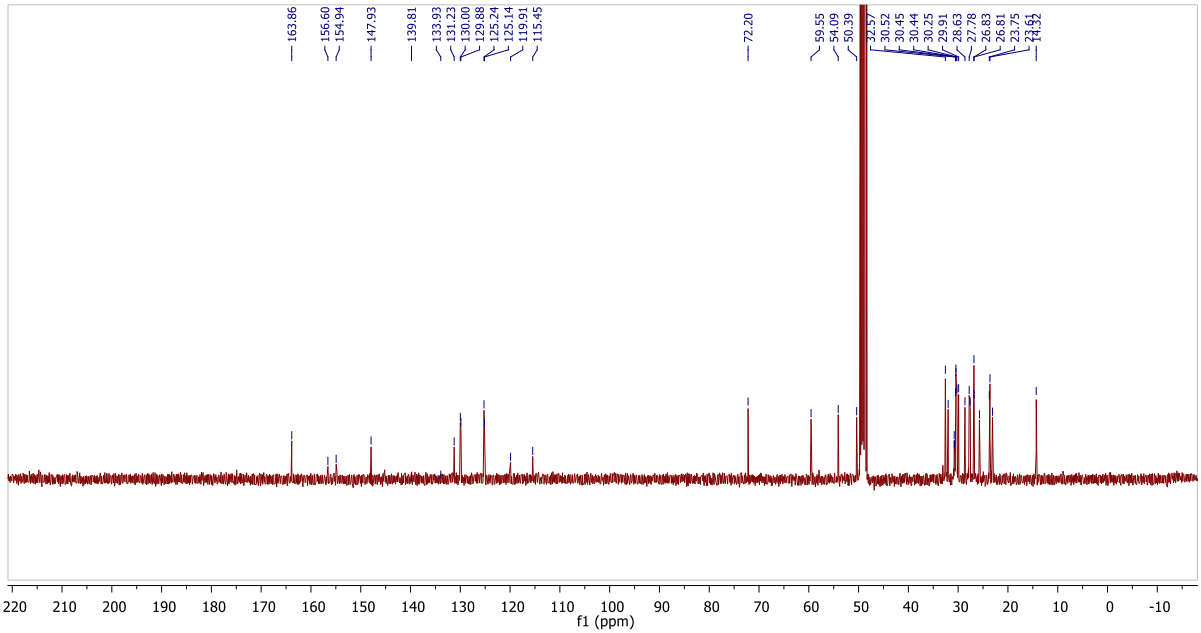

SHIMADZU LabSolutions **Analysis Report**

<Sample Information>

Sample Name	: DC T10X		
Sample ID	:		
Data Filename	: DC T10X~1.lcd		
Method Filename	: LCMS Analysis 15 cm 05-50 1mL (+) und (-).lcm		
Batch Filename	: aaa.lcb		
Vial #	: 1-78	Sample Type	: Unknown
Injection Volume	: 20 uL		
Date Acquired	: 02.09.2016 15:14:43	Acquired by	: System Administrator
Date Processed	: 02.09.2016 15:56:09	Processed by	: System Administrator

<Chromatogram>

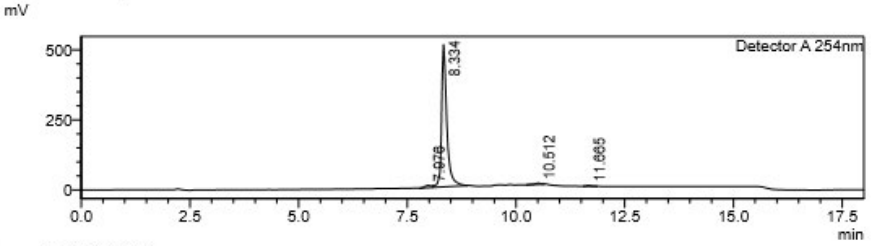

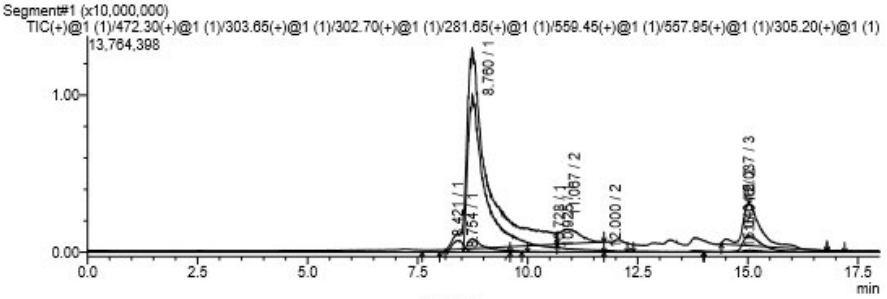

Peak Table

Detector A 254nm

Peak#	Ret. Time	Area	Height	Area%
1	7.976	84478	7704	1.923
2	8.334	4246656	505111	96.682
3	10.512	40662	4341	0.926
4	11.665	20604	2848	0.469
Total		4392400	520004	100.000

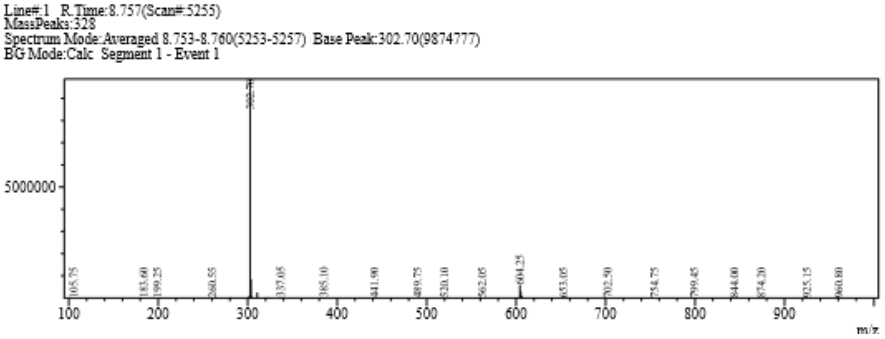

LC−MS analysis:

ESI m/z $[M+H]^+$ calculated is 603.40 It was found 302.70 as $[M+2H]^{++}$ and 604.25 as $[M+H]^+$

Retention time: 8.334

Purity: 96.68%

Compound 7-C12

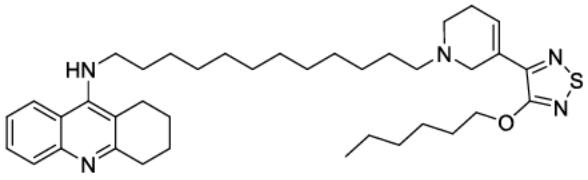

^{1}H NMR spectrum

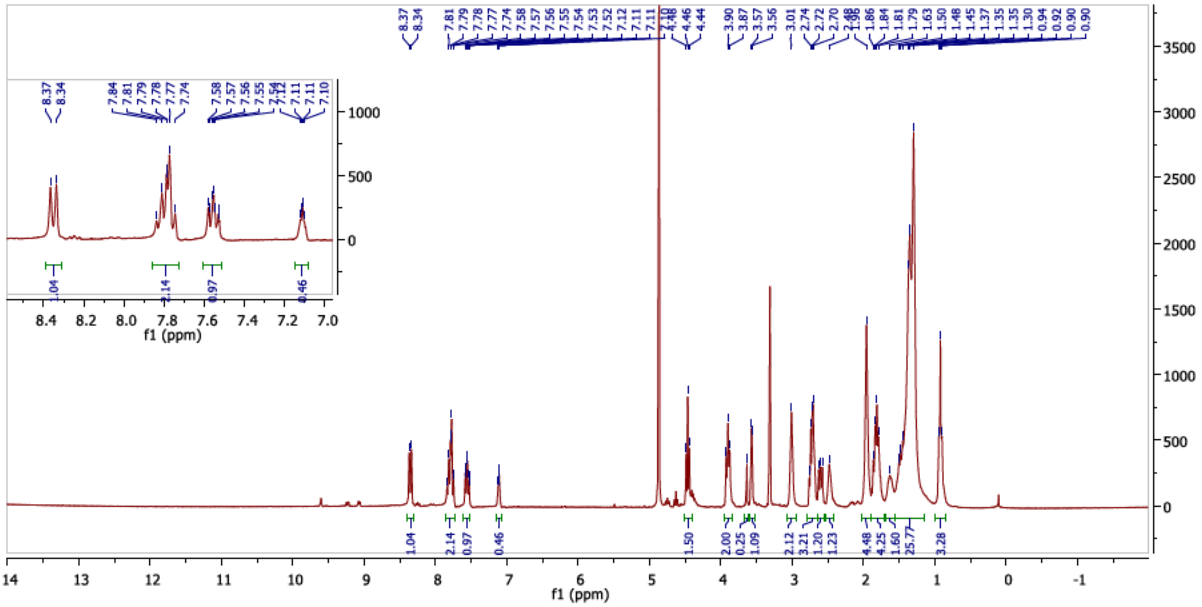

^{13}C NMR spectrum

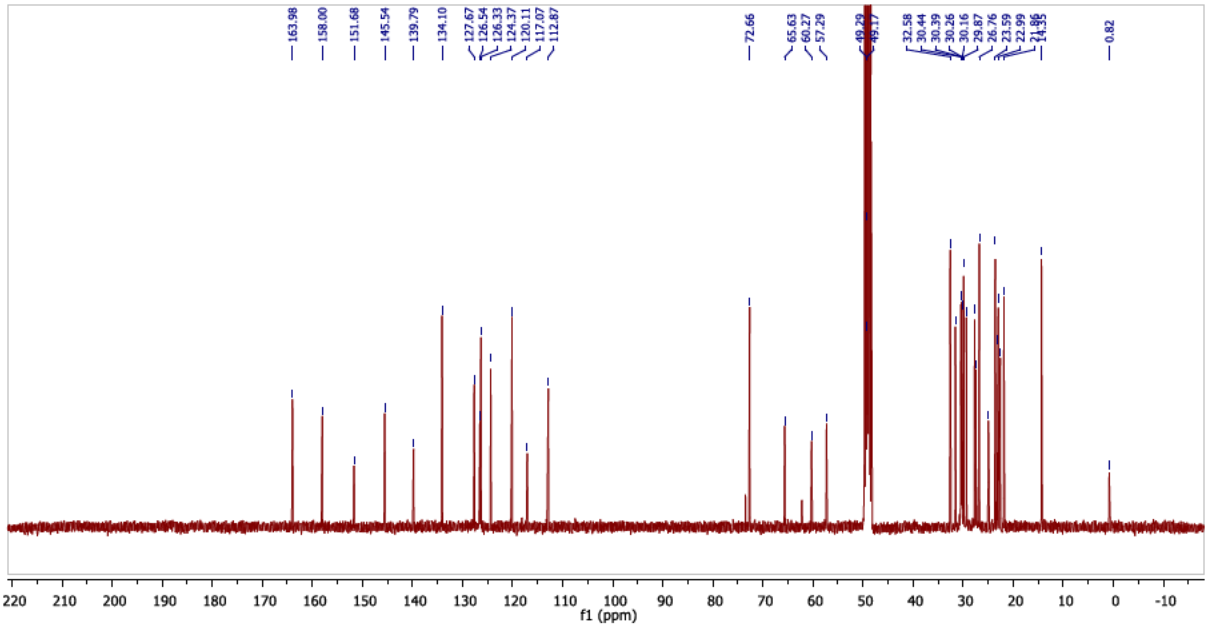

SHIMADZU LabSolutions **Analysis Report**

<Sample Information>

Sample Name	: Tac12 Xano MM8		
Sample ID	:		
Data Filename	: Tac12 Xano MM8.lcd		
Method Filename	: LCMS Analysis 15 cm 05-50 1mL_254nm.lcm		
Batch Filename	: 171220.lcb		
Vial #	: 1-79	Sample Type	: Unknown
Injection Volume	: 30 uL		
Date Acquired	: 19.01.2018 11:47:13	Acquired by	: System Administrator
Date Processed	: 19.01.2018 12:58:17	Processed by	: System Administrator

<Chromatogram>

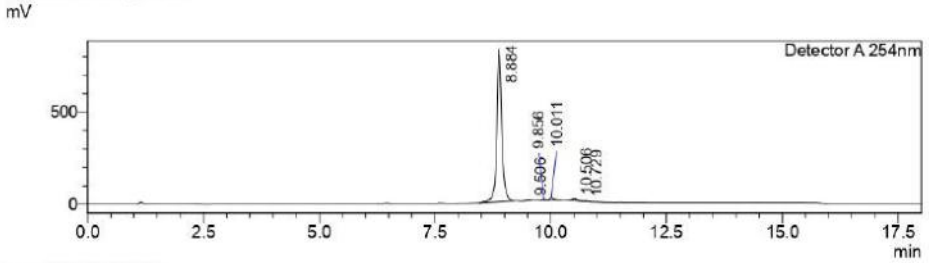

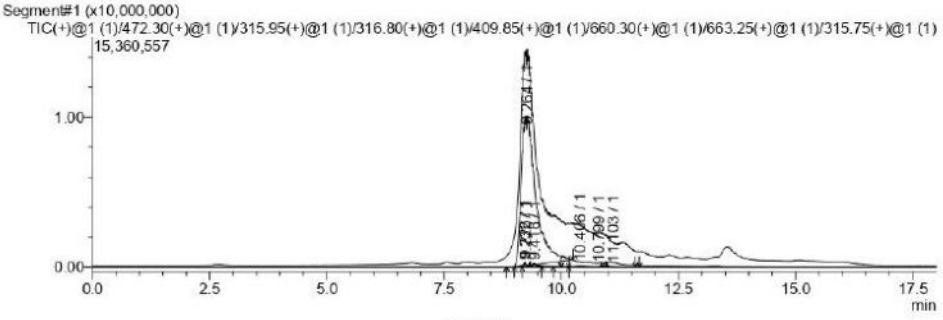

Peak Table

Detector A 254nm

Peak#	Ret. Time	Area	Height	Area%
1	8.884	6194526	820755	95.655
2	9.506	33933	5573	0.524
3	9.856	39778	5479	0.614
4	10.011	98436	12696	1.520
5	10.506	94566	10835	1.460
6	10.729	14668	2820	0.226
Total		6475907	858158	100.000

MS Spectrum

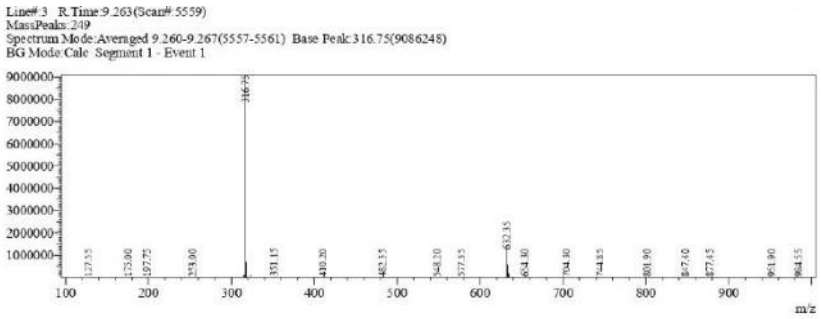

LC−MS analysis:

ESI m/z $[M]^+$ calculated is 631.42. It was found 316.75 as $[M+H]^{++}$ and 632.35 as $[M+H]^+$

Retention time: 8.884

Purity: 95.66%

Compound 8-C8

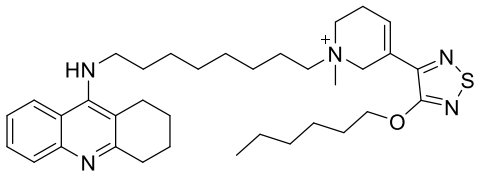

^{1}**H NMR** spectrum

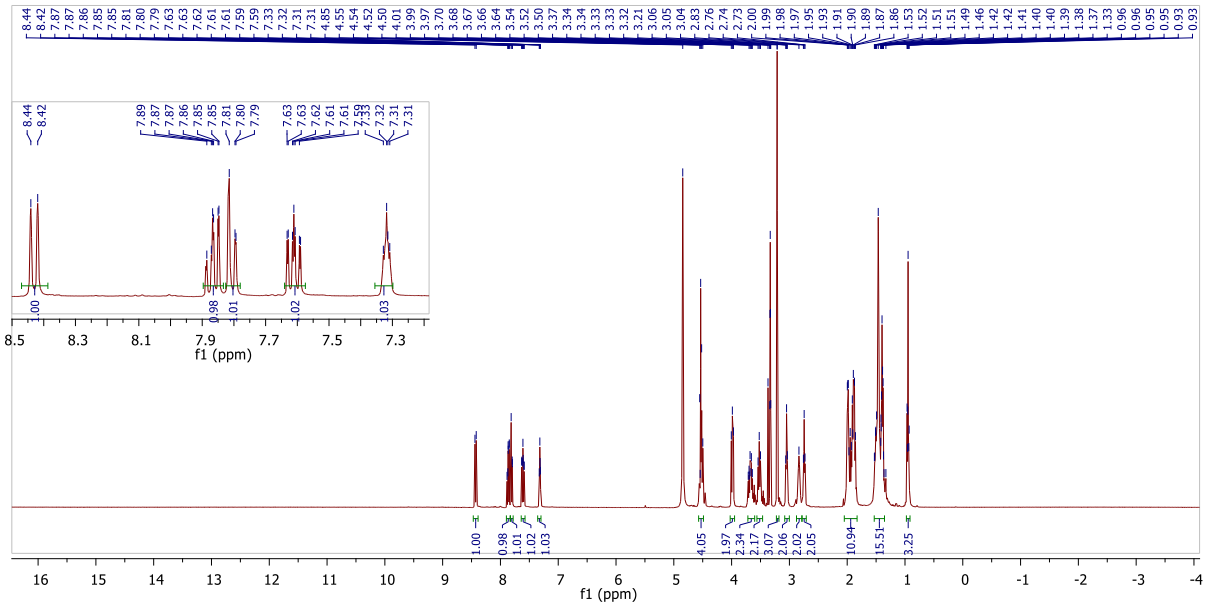

^{13}**C NMR** spectrum

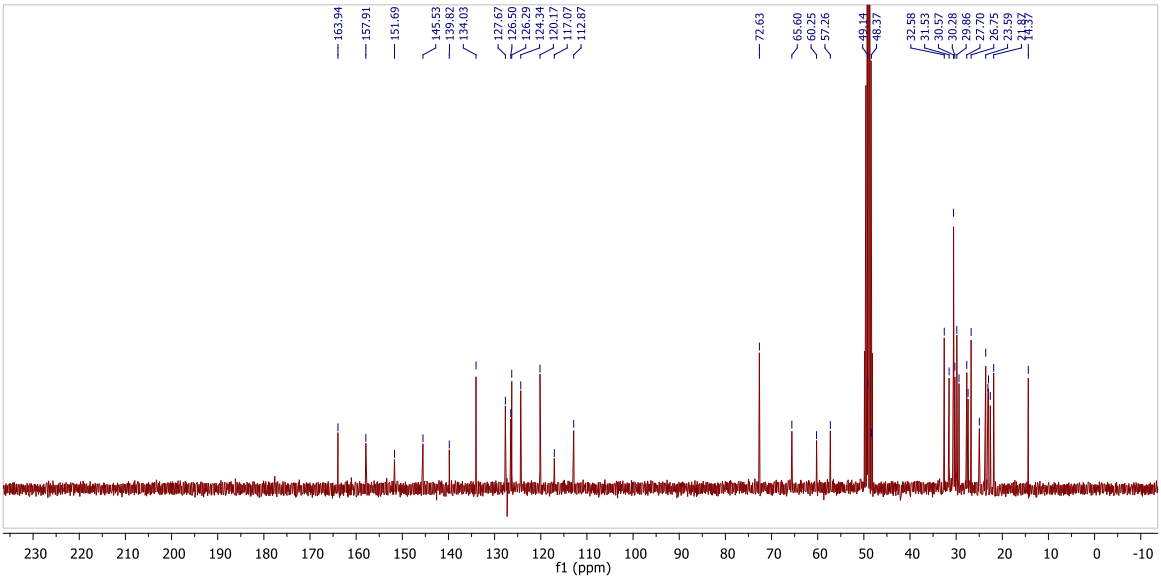

SHIMADZU LabSolutions **Analysis Report**

<Sample Information>

Sample Name	: M8		
Sample ID	:		
Data Filename	: M8.lcd		
Method Filename	: LCMS Analysis 15 cm 05-50 1mL (+) und (-).lcm		
Batch Filename	: 20.04.16.lcb		
Vial #	: 1-91	Sample Type	: Unknown
Injection Volume	: 20 uL		
Date Acquired	: 29.06.2016 12:57:12	Acquired by	: System Administrator
Date Processed	: 05.07.2016 11:34:01	Processed by	: System Administrator

<Chromatogram>

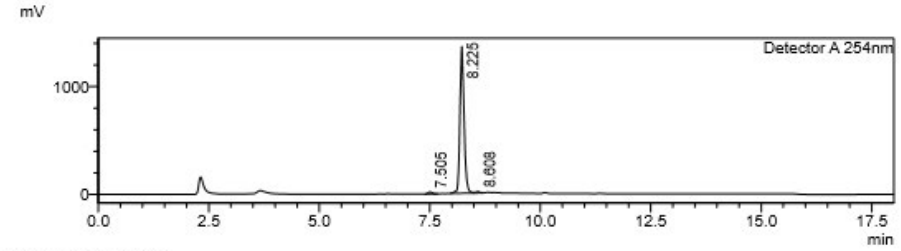

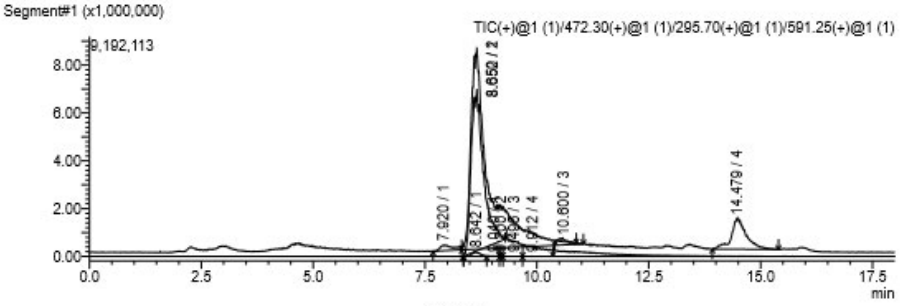

Peak Table

Detector A 254nm

Peak#	Ret. Time	Area	Height	Area%
1	7.505	116527	17465	1.284
2	8.225	8874482	1350579	97.757
3	8.608	87102	12560	0.959
Total		9078111	1380604	100.000

MS Spectrum

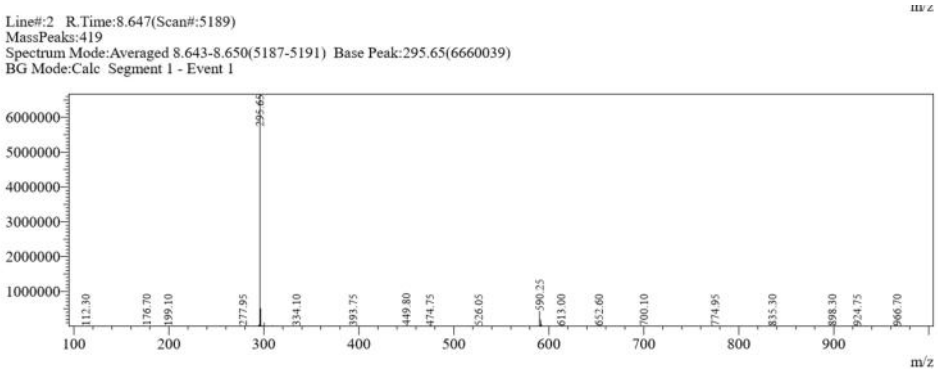

LC−MS analysis:

ESI m/z $[M]^+$ calculated is 590,39. It was found 295.65 as $[M+H]^{++}$ and 590.25 as $[M+H]^+$

Retention time: 8.225

Purity: 97.76%

Compound 8-C10

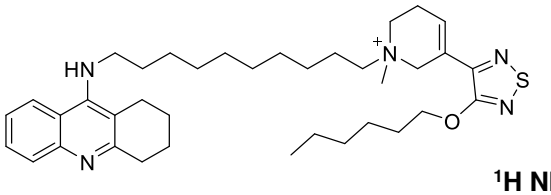

^{1}H NMR spectrum

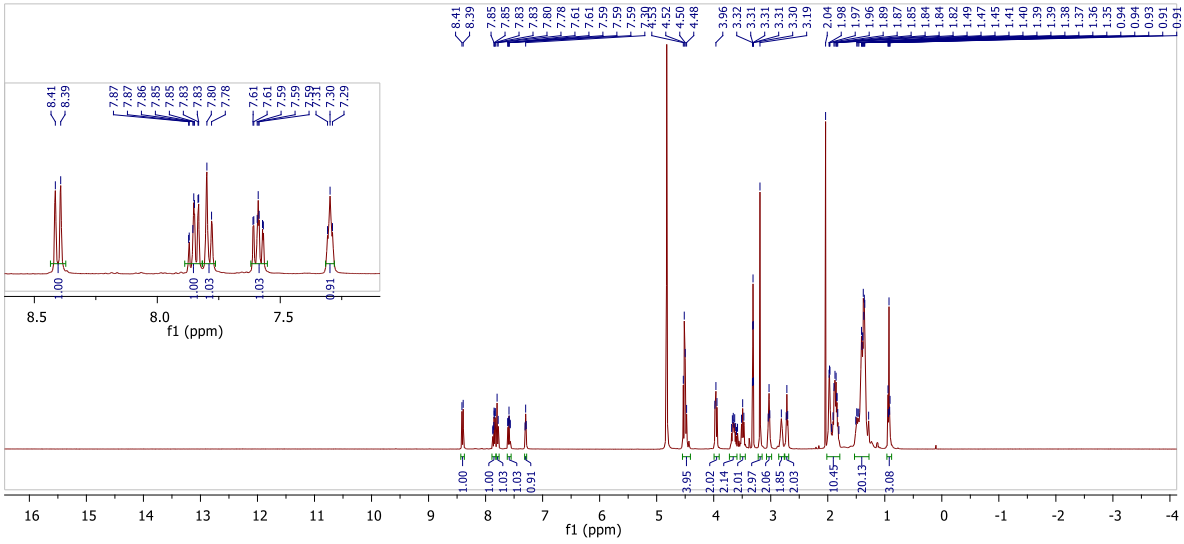

^{13}C NMR spectrum

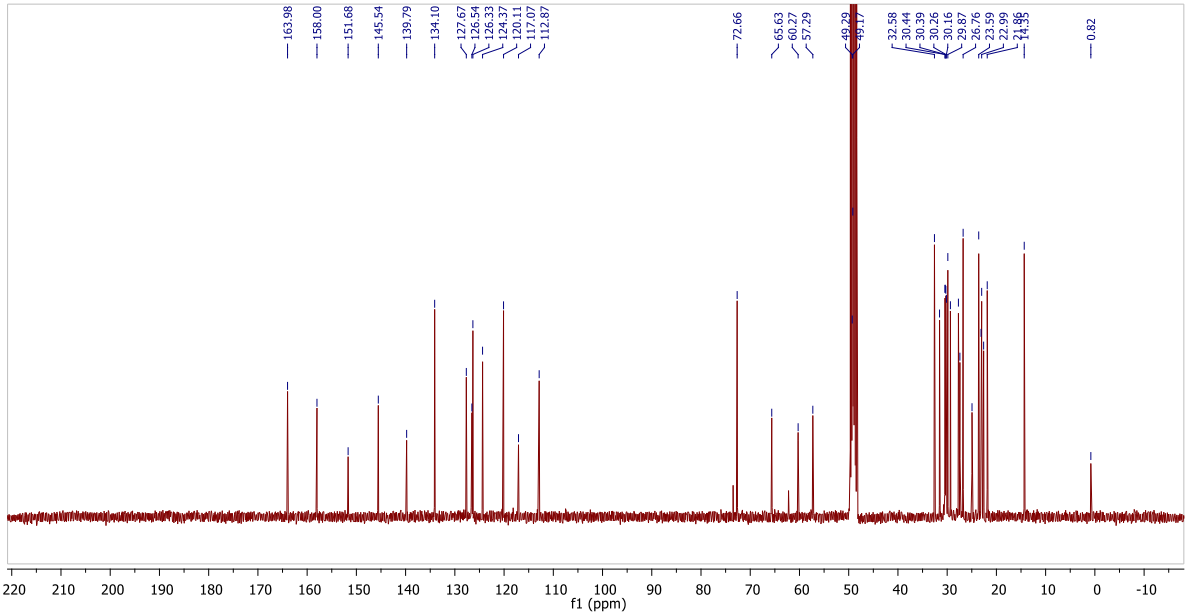

SHIMADZU LabSolutions **Analysis Report**

<Sample Information>

Sample Name	: davide		
Sample ID	:		
Data Filename	: davide~5.lcd		
Method Filename	: LCMS Analysis 15 cm 05-50 1mL (+) und (-).lcm		
Batch Filename	: 20.04.16.lcb		
Vial #	: 1-4	Sample Type	: Unknown
Injection Volume	: 20 uL		
Date Acquired	: 14.06.2016 15:20:47	Acquired by	: System Administrator
Date Processed	: 05.07.2016 11:37:39	Processed by	: System Administrator

<Chromatogram>

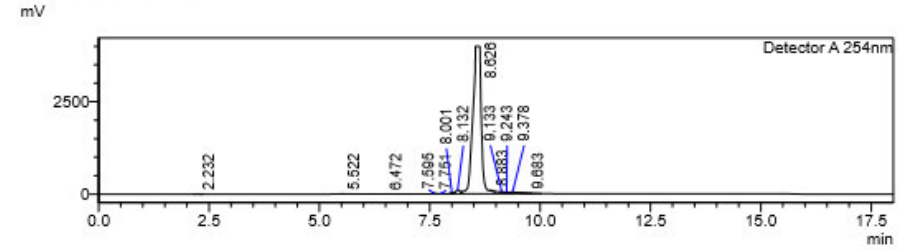

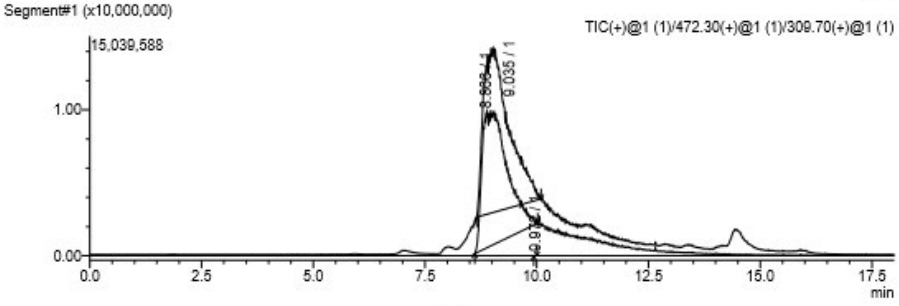

Peak Table

Detector A 254nm

Peak#	Ret. Time	Area	Height	Area%
1	2.232	16178	3805	0.029
2	5.522	63372	9404	0.114
3	6.472	22125	3976	0.040
4	7.595	162057	23976	0.292
5	7.751	42464	7518	0.076
6	8.001	236533	40105	0.426
7	8.132	747429	108123	1.346
8	8.626	54032085	3989781	97.278
9	8.883	54098	11632	0.097
10	9.133	8192	3247	0.015
11	9.243	20283	5414	0.037
12	9.378	126113	17618	0.227
13	9.685	12991	2847	0.023
Total		55543942	4227445	100.000

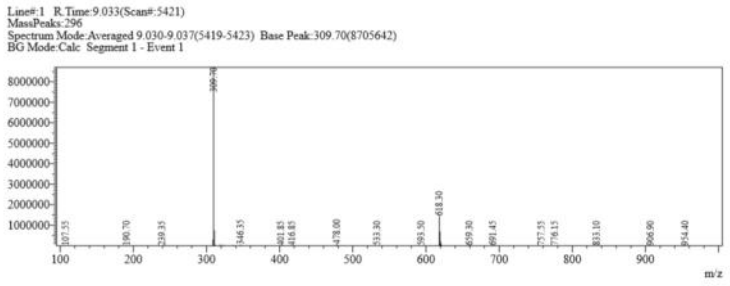

LC−MS analysis:

ESI m/z $[M+H]^+$ calculated is 618.42 It was found 309.70 as $[M+2H]^{++}$ and 618.30 as $[M+H]^+$

Retention time: 8.626

Purity: 97.28%

Compound 8-C12

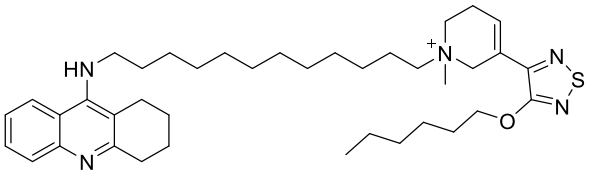

^{1}H NMR spectrum

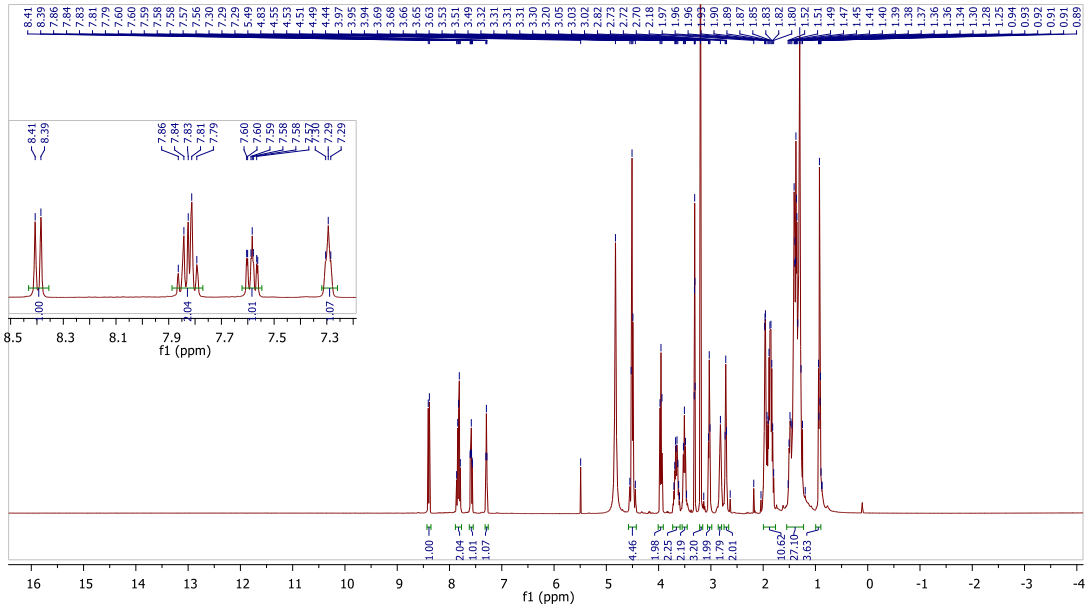

^{13}C NMR spectrum

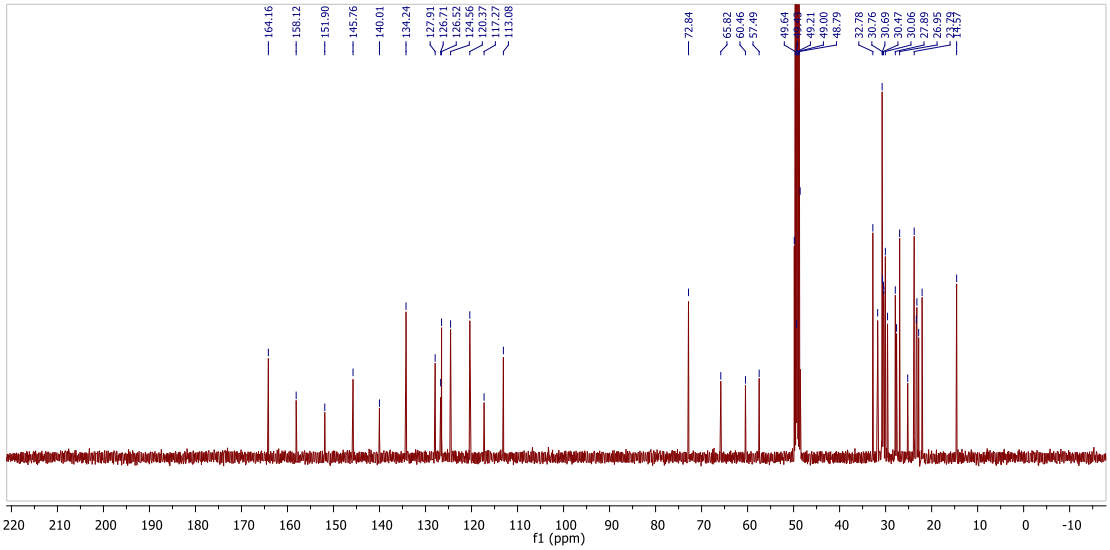

SHIMADZU LabSolutions **Analysis Report**

<Sample Information>

Sample Name	: M12		
Sample ID	:		
Data Filename	: M12.lcd		
Method Filename	: LCMS Analysis 15 cm 05-50 1mL (+) und (-).lcm		
Batch Filename	: 20.04.16.lcb		
Vial #	: 1-92	Sample Type	: Unknown
Injection Volume	: 20 uL		
Date Acquired	: 29.06.2016 13:15:54	Acquired by	: System Administrator
Date Processed	: 05.07.2016 11:35:33	Processed by	: System Administrator

<Chromatogram>

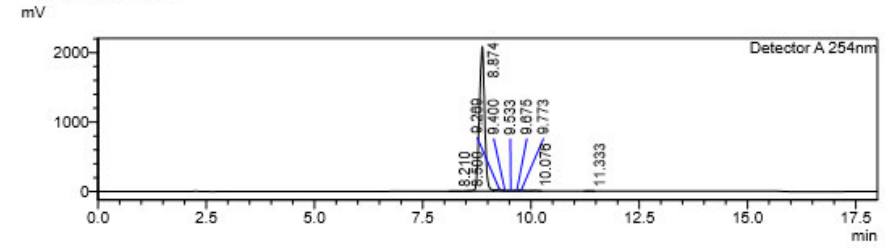

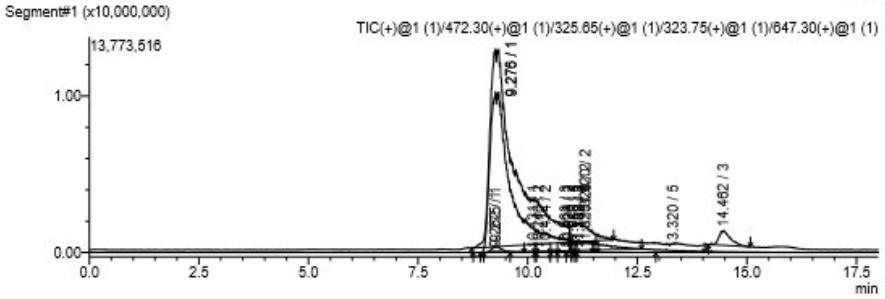

Peak Table

Detector A 254nm

Peak#	Ret. Time	Area	Height	Area%
1	8.210	21901	3038	0.121
2	8.500	29737	4769	0.164
3	8.874	17521155	2077338	96.778
4	9.269	244526	24853	1.351
5	9.400	46860	8764	0.259
6	9.533	51225	6391	0.283
7	9.675	54520	9227	0.300
8	9.773	99021	11775	0.547
9	10.076	23259	3854	0.128
10	11.333	12489	2263	0.069
Total		18104490	2151771	100.000

MS Spectrum

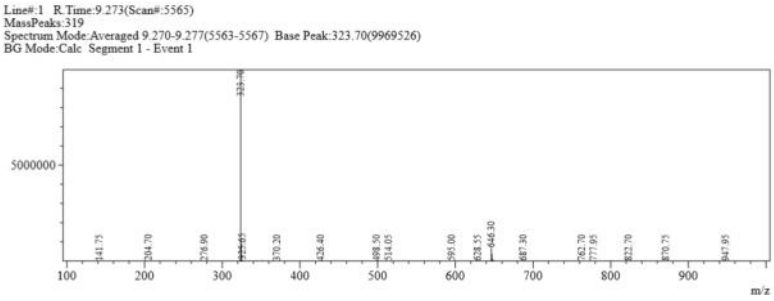

LC−MS analysis:

ESI m/z $[M+H]^+$ calculated is 646.45 It was found 323.70 as $[M+2H]^{++}$ and 646.30 as $[M+H]^+$

Retention time: 8.874

Purity: 96.78%

6. Synthesis and pharmacological investigation at M1 receptor of the BQCAd-(Iperoxo)$_2$ derivative

Introduction

Most of the body cells functions are mediated by transmembrane receptors. The majority of these receptors belong to the superfamily of G-protein-coupled receptors (GPCRs), which comprises the largest family of proteins in mammalian genomes[234,235]. Agonists, antagonists and interfering agents of GPCRs regulating these receptors are largely used as medications. GPCRs have their name because of their interaction with the heterotrimeric guanine-nucleotidebinding regulatory proteins (G proteins), and thereby regulate diverse intracellular processes through interaction with various effector systems.

Numerous studies describing the interaction of GPCRs with their G proteins classically assume the receptors as monomeric entities that function by binding to both, ligand and downstream signaling proteins, in a 1:1 stoichiometric ratio[236]. However, these classical models of receptor-G-protein coupling might be oversimplified[237] and in recent years, a growing number of studies has supported the hypothesis that these receptors can interact to form dimers and higher order oligomers[238–240]. Even M1 muscarinic acetylcholine receptors, which are often considered as monomeric structures, have been identified as dimers. Hern et al.[241] observed the transient formation and disruption of M1 receptor dimers in real time by analyzing fluorescent spot intensities and spatial trajectories. Ligand-induced receptor dimerization was examined by fluorescence correlation spectroscopy upon pirenzepine binding at the M1 receptors by Ilien et al.[242]. The assembly status of GPCRs on the cell surface is of interest because the receptors' multimerization could have pivotal roles in new cellular functions exploration and consequently in drug discovery[243]. Biochemical, biophysical and functional complementation techniques have been broadly used to examine GPCR dimerization[237]. An emerging and promising approach, used for the first time by Portoghese, for the study of receptor association at the plasma membrane targeting opioid receptor subtypes is the concept of bivalent ligands[244–247]. A bivalent ligand is a single chemical entity composed of two pharmacophores, covalently tethered by a linker. Homobivalent ligands are molecules containing two identical pharmacophoric units, whereas heterobivalent ligands contain two different pharmacophores[245,248,249]. In order to achieve improvements in affinity and selectivity, several heterobivalent/bitopic muscarinic ligands have been developed in recent years[52,81,92], such as the

hybrids composed of the superagonist iperoxo[183,189] and a phthalimid moiety related to W84[250,251] addressing the orthosteric and the allosteric site, respectively. In addition to heterobivalent molecules, several muscarinic homobivalent ligands, containing two entities of the same pharmacophore units have been explored such as the dimers of the M1 mAChR agonist NNC 11-1314[10], of xanomeline[11] or carbachol[252] as well as of the M2 selective antagonist methoctramine[253,254]. Depending on the pharmacophoric moieties and the spacer these compounds showed diverse pharmacological profiles and did not always improve in comparison to the respective monomer units alone. Carbachol homodimers linked through a methylene chain of variable length, for example, lost agonistic properties on hM1, hM2, and hM3 receptors[252]. Bitopic ligands composed of two identical pharmacophores have also been used for the discovery of a new additional GPCR transient binding pocket, termed metastable binding sites, which was revealed by computational studies[85]. This metastable site acts as a selectivity filter: molecules that do not have the required features are rejected.

Recently, homobivalent ligands of iperoxo (iperoxo-4,6,8,10-iperoxo) with different chain lengths were synthesized and pharmacologically investigated at the M1 receptor. All compounds were characterized as full agonists and a longer spacer proved to be advantageous for M1 efficacy[255]. The compounds were also tested on the muscarinic M2 receptor in [^{35}S] GTPγS binding, cAMP-formation measurements and characterization of the signaling pathway activation induced by Gi- and Gs-proteins. The iperoxo derivative iper-6-iper was found to activate the Gi pathway, whereas only weak Gs activation in similar way to the heterodimeric compound iper-6-phth was caused. (unpublished results from Regina Messerer's Thesis)[132]. To confirm the molecular dynamics simulation demonstrating that iperoxo is able to fluctuate in the 7TM receptor, escaping from the orthosteric pocket and visiting the extracellular allosteric vestibule[256], further radio ligand binding studies and molecular docking simulations are necessary.

Understanding the kind of interaction occurring between the heterodimeric/homodimer compounds, the receptor and the resulting pharmacological response, in a highly dynamic and complex environment, like that of GPCR is not trivial. Ligands must be studied in depth and different assumptions must be taken into consideration. The enhanced potencies, affinities and intrinsic selectivity observed for some bivalent GPCR ligands can be explained by different hypotheses. Firstly, the binding of the first

pharmacophoric unit increases the probability of a productive binding event of the second active moiety with another nearby receptor, increasing the local concentration of free pharmacophore. (Figure 1A). Secondly, the homodimeric ligand simultaneously interacts with two orthosteric binding sites of a dimeric or oligomeric complex of GPCRs, inducing receptor multimerization (Figure 1B); thirdly, an increased selectivity or improved functional selectivity is obtained with bitopic ligand which occupy the orthosteric and an allosteric binding site of the same receptor (Figure 1C). The last hypothesis suggests the presence of a metastable site at the entrance of the orthosteric site to which ligands bind transiently causing a conformational change of the receptor protein itself that allows the ligand to move further into the receptor cavity.[85–91] The homodimeric ligand initially binds at the metastable site providing an entry point for the second molecular portion at the orthosteric site in a thermodynamically more favorable binding interaction (Figure 1D).

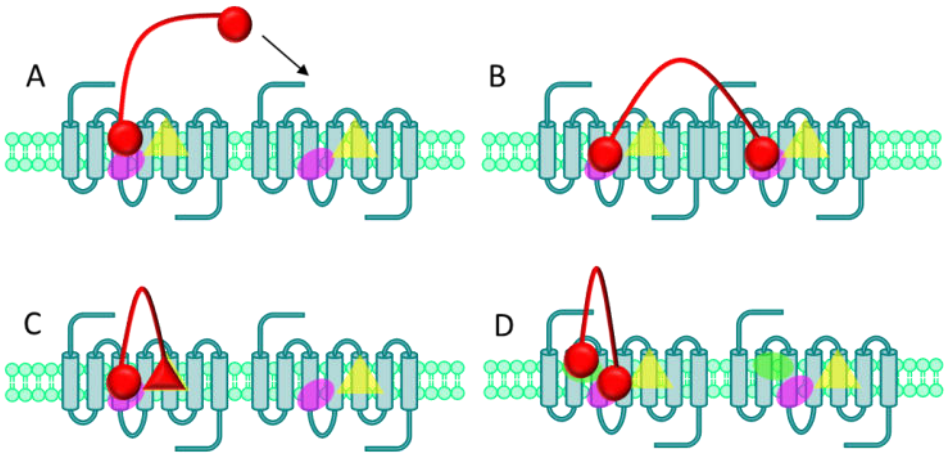

Figure 1. Purple circle: orthosteric binding site; green circle: metastable binding site; yellow triangle: allosteric binding site. Possible binding modes of bivalent ligands. (**A**) Increased local concentration of free pharmacophore. (**B**) Dimeric ligands target two separate receptors/protomers simultaneously inducing GPCR dimerization. (**C**) Simultaneous binding to an orthosteric and allosteric binding site of the same receptor molecule (bitopic or dualsteric binding mode, heterobivalent molecules). (**D**) Metastable binding sites may provide a new source of allosteric binding sites that could be targeted by homobivalent bitopic ligands. Modified from the literature.[17,8517,85]

Currently, the relationships between the dualsteric compounds' binding possibilities, GPCR activation and their dimerization states have not been analyzed well. A further contribution to study the possible form of multimerization and the most recent hypothesis of a metastable site is given with a new medicinal chemistry design strategy. Here the synthesis and some preliminary pharmacological results of a new

trimeric derivative (**3**) are reported (Figure 2). The novel trivalent ligand consists of an allosteric moiety: BQCAd (**1**) with positive allosteric modulator proprieties at the M1 receptor, which could provide receptor subtype selectivity connected through two hexamethylene linkers with two potent iperoxo fragments (**2**). The novel three-branched compound could occupy the metastable and the orthosteric binding sites of the same receptor or two orthosteric pockets of two different receptors, associated in a dimer, opening new fronts in the protein dimerization investigation and further studies on the activation pattern of the receptor. The BQCAd-(iperoxo)$_2$ compound **3** was tested for its M1 affinity in binding studies. Moreover, investigation of the signaling pathway was carried out through functional studies evaluating the degree of Ga and PLC-b3 interaction in the Split complementation assay[192192] after receptor activation. Furthermore, the mediated effect of compound **3** will be compared with the previously reported iperoxo related compounds[27,111,132] (results part 2) paying particular attention to the impact of the additional pharmacological entities and to the influence of the chain linker.

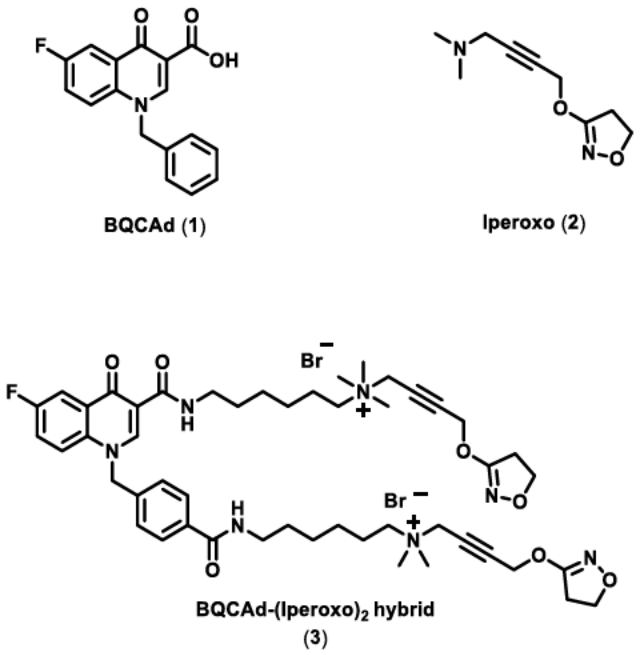

Figure 2: Structures of BQCAd (benzyl quinolone carboxylic acid derivative) (**1**), Iperoxo (**2**) and of the new hybrid trivalent derivative (**3**).

Material and Methods

Materials

Chinese hamster ovary (CHO) cell line stably expressing *h*M1 was obtained from Wyeth Research (Princeton, NJ). 384-well microplates, 96-well round bottom plates and white 96-well plates were purchased from Thermo Fisher and Greiner Bio One, Germany. Dulbecco's modified Eagle's medium (DMEM) and phosphate-buffered saline (PBS) were from Sigma (Germany). Leibovitz' L-15 medium (L-15) and Hank's balanced salt solution (HBSS) were from Gibco (Germany). Fetal calf serum (FCS), trypsin and geneticin (G418) were from Merck Biochrom (Germany). D-Luciferin was purchased as potassium salt from Pierce (Germany) and was dissolved in HBSS at a concentration of 400 mM. Puromycin was obtained from Invivogen (France). Scopolamine Methyl Chloride, [N-methyl-3H]-, 250 µCi (9.25MBq) was purchased from PerkinElmer (Rodgau, Germany) and Polyethylenimine solution (1%, PEI) from Sigma. For chromatographic applications (HPLC, LC-MS) ultrapure water produced by a Milli-Q® system (Merck, Darmstadt, Germany) was used. HPLC grade and LC-MS grade solvents were from Sigma-Aldrich (Munich, Germany). All other chemicals were purchased from Sigma-Aldrich (Schnelldorf, Germany), VWR (Darmstadt, Germany) and TCI (Eschborn, Germany) and were used without prior purification.

General Medicinal Chemistry Methods

^{1}H (400.132 MHz) and ^{13}C (100.613 MHz) NMR spectra were recorded using a Bruker AV 400 NMR spectrometer (Bruker Biospin, Ettlingen, Germany). As an internal standard, the signals of the deuterated solvents were used (DMSO-d6: 1H 2.5 ppm, 13C 39.52 ppm; CDCl3: 1H 7.26 ppm, 13C 77.16 ppm). Abbreviations for data quoted are s, singlet; d, doublet; t, triplet; q, quartet; m, multiplet; b, broad; dd, doublet of doublets; dt, doublet of triplets; tt, triplet of triplets; and tq, triplet of quartets. Coupling constants (J) are given in Hertz. The specific NMR assignments were determined by using typical techniques including polarization transfer experiments (DEPT) and two-dimensional experiments, such as ^{1}H-^{1}H correlation (COSY) and ^{1}H-^{13}C-proton-carbon heteronuclear correlation (HMQC, HMBC). TLC analyses were performed on commercial precoated plates, silica gel 60 F254, C18 silica-coated aluminum panels ALUGRAM® RP-18W / UV254 and on pre-coated TLC-plates

Alox-25/UV254 (Macherey-Nagel); detection was performed using UV spectrometry at 254 nm, intrinsic fluorescence at 366 nm or with ethanolic $KMnO_4$, Dragendorff reagent or phosphomolybdic acid ethanolic solution. For classical purification, gravity column chromatography was carried out. Silica gel with a grain size of 63-200 µm (Merck, Darmstadt, Germany) was used as stationary phase. Flash chromatography on a puriFlash®430 system (Interchim, Montlucon, France) was performed using prepacked columns (Interchim, Montluçon, France) with silica gel filling (Particle size 30 µm or 50 µm) for normal phase or with C18-silica gel filling (Particle size 15 µm) for the reverse phase. The detection was carried out by means of a UV detector and Evaporative Light Scattering Detector (ELSD). Microwave assisted reactions were carried out using either MLS-rota PREP or synthWAVE instruments (Milestone, Leutkirch, Germany).

The LC-MS analyses of all the test compounds were performed using a Shimadzu LC-MS-2020 mass spectrometer (Shimadzu Deutschland GmbH, Duisburg, Germany) consisting of a DGU-20A3R degassing unit, a LC20AB liquid chromatograph and a SPD-20A UV/Vis detector or a LC / MSD ion trap (Agilent Technologies, Waldbronn, Germany) connected to an Agilent 1100 modular system. A Synergi Fusion-RP (150 mm x 4.6 mm i.d., 4 µm; Phenomenex Ltd., Aschaffenburg, Germany) column and a mobile phase gradient using MeOH and water were utilized. Parameters of the HPLC method: solvent A: water with 0.1% formic acid; solvent B: MeOH with 0.1% formic acid. Solvent B linearly increased from 0% to 90% in 13 min, was kept at 90% for 5 min, decreased linearly from 90% to 5% in 1 min, and was kept at 5% for 4 min before the next injection. The method was run with a flow rate of 1.0 mL/min. The UV signal was recorded at 254 nm. All compounds were found to have a purity ≥ 95%. Mass spectra were recorded in ESI-positive mode and the data is reported as mass-to-charge ratio (m/z) of the corresponding positively charged molecular ions.

Cell culture

Chinese hamster ovary cells (CHO) stably expressing the hM1 receptor (CHO-hM1 cells) were cultured in Ham's nutrient mixture F-12 (HAM- F12) supplemented with 10 % (v/v) FCS (FCS), 100 U/mL penicillin, 100 µg/ml streptomycin, 0.2 mg/ml G418 and 2 mM L-glutamine at 37 °C in a 5 % CO_2 humidified atmosphere. The HEK293T cells stably co-transfected with the human M1 receptor and the $G\alpha_q$-PLC-β3 sensor were kindly provided by Timo Littmann (University of Regensburg). Cells were

cultivated in DMEM containing 10% FCS (full medium) at 37 °C in a water-saturated atmosphere containing 5% CO_2 as previously reported.[192]

Membrane Preparation

Stably transfected CHO cells overexpressing the human M1 mAChR subtype were grown adherently to a confluence of approx. 80%. The cells were harvested by gently scraping in ice-cold harvesting buffer (20 mM HEPES, 10 mM Na_2EDTA, pH= 7.4). The collected cells were homogenized on ice twice for 25 seconds using a polytron homogenizer at level 6 and the resulting cell fragments were centrifuged using the rotor JA25.50 at 40 000 g for 10 minutes (4 °C). The supernatant was aspirated and the pellet resuspended in ice-cold storage buffer (20 mM HEPES, 0.1 mM Na_2EDTA, pH= 7.4). This step was repeated twice, and finally the pellets were resuspended in ice-cold assay buffer (10 mM HEPES, 10 mM $MgCl_2$, 100 mM NaCl, pH= 7.4). Aliquots were filled in eppendorf tubes, quickly frozen and stored at -80 °C. The protein concentration was approximately 2 mg protein/ml, determined using the Pierce™ BCA Protein Assay Kit. The absorbance of the bicinchoninic acid BCA/copper complex, after completion of the biuret reaction was measured at 562 nm using a UV-Photometer (Synergy™ Neo2 Multi-Mode Microplate Reader). The obtained values were plotted in a linear calibration curve, whereby the protein content then was determined.

Radioligand Binding Experiments

Radioligand binding experiments using CHO-hM1 membranes were performed in round bottom 96-well microtiter plates applying 20 µg protein/well. Experiments were conducted at room temperature using [^{3}H]NMS as the radioactive probe (2 nM for [^{3}H]NMS dissociation and 0.2 nM for equilibrium binding experiments). The plate was incubated at room temperature using a microplate shaker (Titramax 101 Platform Shaker, Heidolph) with an incubation time ranging from 1 h for the dissociation to 24 h for the equilibrium experiments. Homologous competition assays were utilized to determine pKd at hM1 for NMS 8.88 and conformed to homologous binding assumptions.[207] Nonspecific binding was determined in the presence of atropine excess. Incubation performed in the assay buffer was terminated by filtration through glass fiber mats previously coated with a 1% polyethylenimine solution, in a cell harvester

filtration device. After filtration, the filter mats were washed with ice-cold wash water, covered with melt-on scintillator sheets on a heating block and the radioactivity was counted in a Perkin Elmer MicroBeta 2450 Microplate Counter. The inhibition constants Ki of receptors for the studied compounds were determined in competition experiments in which membranes were incubated in the presence of a fixed 0.2 nM concentration of [^{3}H]NMS and increasing concentrations of the competitor. The incubation lasted 24 h to achieve full equilibrium. Two-point kinetic experiments with measurements of [^{3}H]NMS binding at t= 0 and t= 20 min were performed. By means of two-point dissociation experiments, the dissociation rate constant k_{-1} can be determined by measuring the specific binding just before the start of the dissociation reaction (t= 0, adding a competitive antagonist in excess) and at a predetermined time t during the dissociation process (t= 20 min), as previously described.[208]

Split-Luciferase Bioluminescence Assay

Cells, expressing the developed $G\alpha_q$-PLC-β3 sensor in combination with hM_1R, were detached from a 75-cm^2 flask by trypsinization and centrifuged (700 g for 5 min). The pellet was resuspended in assay medium consisting of L-15 with 5% FCS and the density of the suspension was adjusted to $1.25 \cdot 10^6$ cells/mL. Then, 80 µL of this suspension were seeded into each well of a 96-well plate, and the plate was incubated at 37 °C in a humidified atmosphere (without additional CO_2) overnight. On the next day, 10 µL of 10 mM D-Luciferin (Pierce) were added to the cells, and the plate was transferred into a pre-heated microplate luminescence reader (Mithras LB 940 Multimode Microplate Reader, Berthold Technologies, Bad Wildbad, Germany). The cells were then allowed to equilibrate inside the reader for 10 min, before the basal luminescence was determined by recording the luminescence for the entire plate ten times with an integration time of 0.5 s per well. In the meantime, serial dilutions of agonists were prepared. The resulting solutions were also pre-heated to 37 °C and subsequently added to the cells. Afterwards, the luminescence was recorded for 15 plate repetitions amounting to a time period of 20 min. Negative controls (solvent) and positive controls (reference full agonist, carbachol (hM_1R), eliciting a maximal response (100%) were included for subsequent normalization of the data. In case of the antagonist mode, the antagonists were added 15 min prior to the initial thermal equilibration period to ensure full equilibrium between antagonists and receptors, before addition of the agonists. The pK_b values of the antagonists were determined according to the Cheng-Prusoff equation[215]. After

acquisition of the data, the peak luminescence intensities obtained after stimulation were used for quantitative analysis using GraphPad Software, San Diego, CA.

Data Treatment

The binding data from individual experiments were analyzed by computer-aided nonlinear regression analysis using Prism 5 (GraphPad Software, San Diego, CA). [^{3}H]NMS dissociation data were analyzed assuming a monoexponential decay as described previously[216216]. All sigmoidal concentration-response curves were obtained by fitting three-parameter (Hill slope constrained to 1) nonlinear regression curves (GraphPad Prism, San Diego, CA).

Results and discussion

Chemistry

The first synthetic step is the creation of the desired quinolone scaffold through the reaction of the 4-fluoroaniline with diethyl ethoxymethylenemalonate (DEEMM) to give the diethyl malonate molecule (**4**), as depicted in Scheme 1. The isolated diethyl malonate **4** was cyclized to the ethyl-4-hydroxyquinoline-3-carboxylate (**5**). As the ring cyclisation requires high temperature conditions, diphenyl ether with its high boiling point was used as solvent.*[184,227,228]* The N-1 position of compounds **5** was brought to reaction with methyl 4-(bromomethyl)benzoate in presence of K_2CO_3. The two amides of derivative **7** were formed simultaneously by conversion of the ester functions through reaction with a large excess of 6-amino-1-hexanol. The alcohol functions were then substituted with a bromine atom using HBr/H_2SO_4 and a subsequent reaction with iperoxo base at 80 °C led to the monoquaternary ammonium salts hybrids **3** in 42% yield. The schematic representation and the synthetic steps involved in the preparation of the BQCAd-(Iperoxo)$_2$ hybrid and its intermediates are shown in Scheme 1. Detailed syntheses and spectral data of target compounds are reported below.

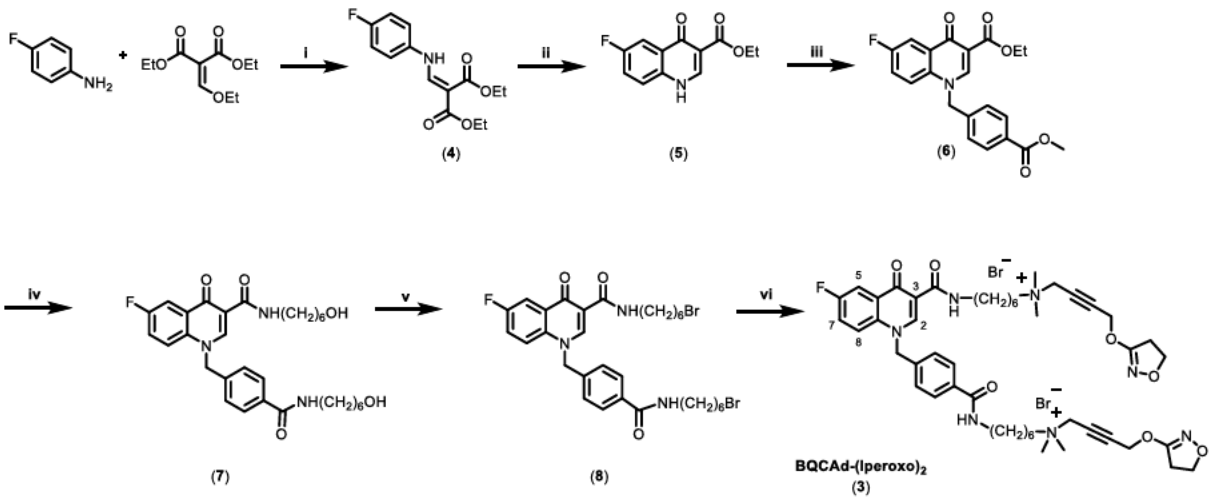

Scheme 1: Synthesis of Quinolone derivatives BQCAd-(Iperoxo)$_2$ Hybrid.-Reagents and conditions: (i) toluene, reflux; (ii) diphenyl ether, 210 °C, MW; (iii) methyl 4-(bromomethyl)benzoate, K_2CO_3, DMF, 80 °C; (iv) $H_2N(CH_2)_6OH$, 150 °C; (v) HBr (48%), H_2SO_4, reflux; (vi) iperoxo, KI/K_2CO_3, CH_3CN, 80 °C, MW.

Synthesis of the BQCAd-6-(Iperoxo)$_2$ (3)

*Ethyl 6-fluoro-1-(4-(methoxycarbonyl)benzyl)-4-oxo-1,4-dihydroquinoline-3-carboxylate **6***

2.38 mmol of the quinolone derivative (**5**) in 3 mL of DMF, 11.90 mmol of K_2CO_3 and 5.95 mmol of 4-methoxybenzyl chloride were added. The solution was kept at 80°C for 20 hours. After cooling to room temperature, the surplus of K_2CO_3 was filtered and the solvent evaporated. The oily residue was crystallized from ethanol. The precipitate was collected by filtration and dried in vacuo.

Beige solid; 75% yield; mp 198-201 °C; R_f = 0.77 (CH_2Cl_2/MeOH= 9:1); ^{1}H NMR ($CDCl_3$): 1.42 (t, 3H, J=7.1, $CH_2C\mathbf{H_3}$), 3.92 (s, 3H, $C\mathbf{H_3}$), 4.41 (q, 2H, J=7.1, $C\mathbf{H_2}CH_3$), 5.44 (s, 2H, $C\mathbf{H_{2benzyl}}$), 7.23 (m, 3H, $\mathbf{H_7}$, B_n-$C\mathbf{H_{aromat.}}$), 7.30 (d, 1H, J=5.6, $\mathbf{H_8}$), 8.06 (d, 2H, J=8.5, B_n-$C\mathbf{H_{aromat.}}$), 8.25 (dd, 1H, J_{HF}=8.9, J=2.7, $\mathbf{H_5}$), 8.59 (s, 1H, $\mathbf{H_2}$).

^{13}C NMR ($CDCl_3$): 14.71, 52.67, 57.73, 61.64, 111.75, 114.59, 118.15 (d, J_{CF}= 7.8), 120.65 (d, J_{CF}= 25.3), 126.29, 127.72 (d, J_{CF}= 20.8), 127.82, 129.50, 129.74, 131.17, 135.95 (J_{CF}= 1.6), 138.63, 150.20, 157.20, 165.51, 166.44, 173.07 (d, J_{CF}= 2.5). MS (ESI) m/z [M]$^+$ Calcd for $C_{21}H_{18}FNO_5$: 383.12. Found: 384.12. HPLC purity 96.7%.

6-fluoro-N-(6-hydroxyhexyl)-1-(4-((6-hydroxyhexyl)carbamoyl)benzyl)-4-oxo-1,4-dihydroquinoline-3-carboxamide **7**

1.3 mmol of derivative (**6**) are suspended in 6.5 mmol of 6-amino-1-hexanol and the mixture heated to 150 °C. The mixture is first liquid and finally solid again. After cooling to RT, the solid is recrystallized from ethanol and the resulting solid dried *in vacuo.*

White solid; 48% yield; mp 175-177 °C; R_f = 0.35 (CH_2Cl_2/MeOH= 9:1); ^{1}H NMR ($CDCl_3$): 0.89-0.95 (m, 4H, Alkyl), 1.27-1.51 (m, 4H, Alkyl), 1.55-1.65 (m, 4H, Alkyl), 1.65-1.71 (m, 4H, Alkyl) 3.44-3.52 (m, 4H, NHC**H$_2$**), 3.62-3.69 (m, 4H,C**H$_2$**-OH), 5.32 (s, 2H, C**H$_{2\text{benzyl}}$**), 5.52 (s, 2H,O**H**), 7.21 (d, 2H, J=8.3, B_n-C**H**$_{\text{aromat}}$), 7.36-7.34 (m, 2H, B_n-C**H**$_{\text{aromat}}$), 7.78 (d, 1H, J=8.3, **H**$_8$), 8.06-8.00 (m, 1H, **H**$_7$), 8.18 (m, 1H, **H**$_5$) 8.93 (s, 1H **H**$_2$), 9.96 (t, 1H, J=5.7, N**H**).

^{13}C NMR ($CDCl_3$): 25.82, 25.87, 25.93, 26.99, 27.17, 27.18, 30.16, 30.19, 31.57, 33.11, 33.21, 39.69, 51.48, 54.06, 63.19, 63.24, 112.51, 113.08, 126.96, 127.42, 127.71, 128.73, 137.83, 148.94, 165.31, 167.33. MS (ESI) m/z $[M]^+$ Calcd for $C_{30}H_{38}FN_3O_5$: 539.28. Found: 540.35. HPLC purity 96.7%.

N-(6-bromohexyl)-1-(4-((6-bromohexyl)carbamoyl)benzyl)-6-fluoro-4-oxo-1,4-dihydroquinoline-3-carboxamide **8**

0.95 mmol of the hydroxyl derivative (**7**) are dissolved in a large excess of HBr (conc.). Carefully, about one-tenth of H_2SO_4 (conc.) amount was added and the reaction solution was heated for 6 hours under reflux. After cooling down, the reaction mixture is poured into water and extracted several times with chloroform. The combined organic phases were neutralized with K_2CO_3. The remaining K_2CO_3 was filtered off and the solvent was removed in vacuo, finally the crude product was recrystallized from EtOH affording compound **8**.

Ochre solid; 41% yield; mp 178-180 °C; R_f = 0.84 (CH_2Cl_2/MeOH = 20:1); ^{1}H NMR ($CDCl_3$): 1.39-1.52 (m, 8H, Alkyl), 1.60-1.70 (m, 4H, NH-CH_2-C**H$_2$**), 1.82-1.92 (m, 4H, C**H$_2$**-CH_2-Br), 3.38-3.51 (m, 8H, C**H$_2$**-

Br, NH-C**H**$_2$), 5.49 (s, 2H, C**H**$_{2\text{benzyl}}$), 7.20 (d, 2H, J=8.1, C**H**$_{\text{phenyl}}$), 7.32 (d, 2H, J=4.6, B$_n$-C**H**$_{\text{aromat.}}$), 7.74 (d, 2H, J=8.4, B$_n$-C**H**$_{\text{aromat.}}$), 8.17 (d, 1H, J=8.8, J=1.4, **H**$_8$), 8.93 (s, 1H, **H**$_2$), 9.93 (t, 1H, J=5.2, N**H**).

^{13}C NMR ($CDCl_3$): 26.08, 26.30, 27.77, 27.93, 29.49, 32.54, 32.70, 33.82, 39.21, 40.00, 54.18, 112.52, 117.75, 121.67, 126.29, 128.01, 132.88, 135.61, 138.58, 148.34, 159.37, 162.53, 166.80, 177.14. MS (ESI) m/z $[M]^+$ Calcd for $C_{30}H_{36}Br_2FN_3O_3$: 665.11. Found: 665.98. HPLC purity 94.7%.

N-(4-((4,5-dihydroisoxazol-3-yl)oxy)but-2-yn-1-yl)-6-(4-((3-((6-((4-((4,5-dihydroisoxazol-3-yl)oxy)but-2-yn-1-yl)dimethylammonio)hexyl)carbamoyl)-6-fluoro-4-oxoquinolin-1(4H)-yl)methyl)benzamido)-N,N-dimethylhexan-1-aminium bromide **3**

0.40 mmol of the compound **7** are dissolved in 20 ml of abs. acetonitrile, 3 equivalents of iperoxo base (**2**), and a catalytic amount of KI/K_2CO_3 were added. The mixture was heated to 70 °C using MW assistance. After completion of the reaction, the mixture is added dropwise in Et_2O and the resulting white precipitate is filtered through a glass frit. The resulting oily crude product is washed several times with Et_2O and dried *in vacuo*. The subsequent column chromatography (basic alumina stationary phase; CH_2Cl_2/MeOH= 98:2) yielded the solid product **3**.

Ochre solid; 42% yield; mp 205-208 °C; R_f = 0.32 (CH_2Cl_2/MeOH = 85:15); ^{1}H NMR (MeOD): 1.44-1.51 (m, 8H, Alkyl), 1.68-1.62 (m, 4H, NH-CH_2-C**H**$_2$), 1.85-1.80 (m, 4H, CH_2-C**H**$_2$-N$^+$, C**H**$_2$-CH_2-N$^+$), 3.00 (dt, 4H, J=3.5, J=9.6, **H**$_{4\text{-Iperoxo}}$), 3.19 (s, 6H, N$^+$(C**H**$_3$)$_2$), 3.21 (s, 6H, N$^+$(C**H**$_3$)$_2$), 3.48-3.34 (m, 8H, NH-C**H**$_2$/C**H**$_2$-N$^+$), 4.37 (dt, 4H, J=3.1, J=9.6, **H**$_{5\text{-Iperoxo}}$), 4.45 (4H, N-C**H**$_2$-C≡), 4.89 (4H, ≡C-C**H**$_2$-O), 5.80 (s, 2H, C**H**$_{2\text{benzyl}}$), 7.34 (m, 2H, B$_n$-C**H**$_{\text{aromat}}$), 7.52 (m, 2H, B$_n$-C**H**$_{\text{aromat}}$), 7.77 (dd, 1H, J=4.2, J=9.4, **H**$_8$), 7.84 (d, 1H, J=8.4, **H**$_7$), 8.02 (dd, 1H, J=3.0, J_{HF}=8.9, **H**$_5$), 9.03 (s, 1H, **H**$_2$), 10.18 (t, 2H, J=5.7, N**H**).

^{13}C NMR (MeOD): 23.53, 23.55, 26.87, 27.37, 30.13, 30.27, 33.65, 39.95, 40.07, 40.71, 48.41, 48.62, 48.83, 49.05, 49.26, 49.47, 49.69, 51.20, 51.27, 55.08, 55.11, 58.20, 58.30, 58.32, 65.31, 65.35, 76.71, 76.73, 87.61, 87.65, 111.99, 112.11, 112.13, 112.22, 121.90, 121.98, 122-66, 122.93, 127.81, 129.21,

130.69, 130.76, 135.81, 137.43, 140.05, 150.14, 160.18, 162.63, 166.62, 168.68, 169.19, 177.22. MS (ESI) m/z $[M]^+$ Calcd for $C_{48}H_{64}FN_7O_7^+$: 434.74. Found: 434.85. HPLC purity 97.6%.

Pharmacology

Firstly, the compound was investigated for its ligand-receptor interactions in membrane hM1 homogenates in equilibrium as well as in dissociation studies**.** Afterwards, the G protein activation was measured by means of a bioluminescence split-luciferase assay. Figure 5 and Table 2 report on the Split-Luc assay investigation of the heterobivalent derivative BQCAd-iperoxo with a rigid spacer (Figure 5), which was never reported previously.

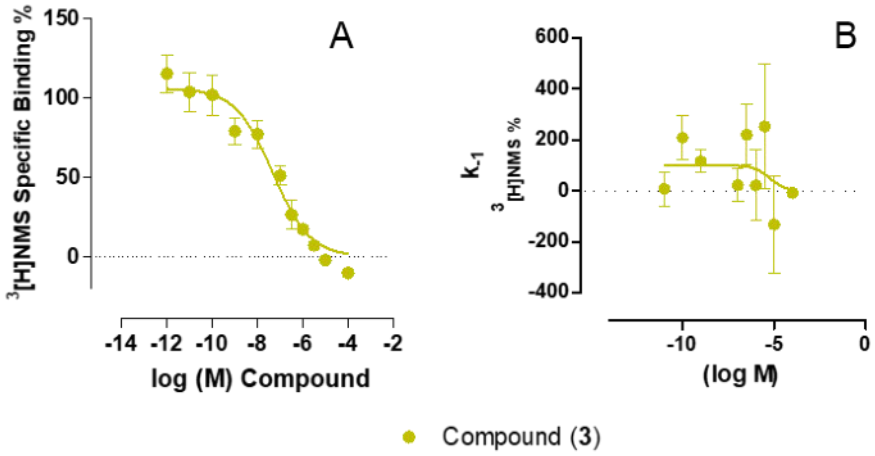

Figure 3. Effect of increasing concentrations of the hybrid compound (**3**) on specific percent equilibrium binding of [^{3}H]NMS in CHO-hM1 membranes. **B.** Allosteric effects of the hybrid (**3**) as reflected by the inhibition of [^{3}H]NMS dissociation from M1 receptors in CHO hM1 membranes. The allosteric effect is expressed as the ratio of the rate of [^{3}H]NMS dissociation in the presence of compound relative to the rate of dissociation of [3H]NMS in the absence of test compound expressed in percent k^{-1}. Data points represent the mean ± S.E.M. from three to four independent two-point kinetic experiments, conducted in quadruplicate.

In the equilibrium binding studies, the presence of two iperoxo moieties results in compound **3** having an exceptional pKi value of 7.34 (Table 1). Interestingly despite the considerable steric effect in the case the two iperoxo moiety ligands, the compound binds to the orthosteric site with an affinity even higher than iperoxo itself. It can be assumed that the ligand binds to the M1 muscarinic receptor through a

"tritopic" interaction, involving all three binding sites: metastable, orthosteric and allosteric. The accommodation of the first orthosteric portion in the metastable binding site could provide a favorable entry to the second orthosteric fragment in the orthosteric pocket. The conformational rearrangement of the receptor due to this simultaneous binding could be the cause of the extremely high affinity of compound **3**.

A second hypothesis could instead propose the dimerization event. The ligand could bind to a first receptor unit with a bitopic interaction (allo/ortho) and the second orthosteric portion protruding outside of the 7TM receptor, favoring the connection with a second receptor unit. The ligand would therefore increase the possibility of receptor dimerization.

Loss of binding at the allosteric site was measured. It seems that compound **3** prefers the active multi-topic binding pose over the purely allosteric inactive mode. This is also confirmed by functional bioluminescence studies with the derivative having a particularly high pEC_{50} value of 8.01 (Table 1). For a confirmation of the binding mode, further pharmacological studies and molecular docking simulations are needed. Yet, the trivalent ligand proves itself to be capable of receptor activation, in addition to its binding properties to the M1 receptor. The maximum efficacy of the ligand **3** is 89%. Hence, it is a partial agonist, not being able to give full receptor activation.

Table 1. Pharmacological parameters of compound **3** and the reference compounds Iperoxo and BQCAd measured by Split-Luc assay and radioligand binding assay. Affinity constants are expressed as pKi for hM1 mAChRs, expressed in CHO membranes.

Compound	Split-Luc Assay		Radioligand Binding Assay Equilibrium		Radioligand Binding Assay Dissociation
	pEC_{50}	$\%E_{max}$	pIC_{50}	pKi	pIC_{50}
Iperoxo	8.90 ± 0.01	104.60 ± 0.85	5.93±0.06	6.13	n.d.
BQCAd	n.d.	n.d.	n.d.	n.d.	5.47 ± 0.20
BQCA-(Iperoxo)$_2$	8.01 ± 0.07	89.44 ± 1.87	6.96 ± 0.14	7.34	5.23± 1.10

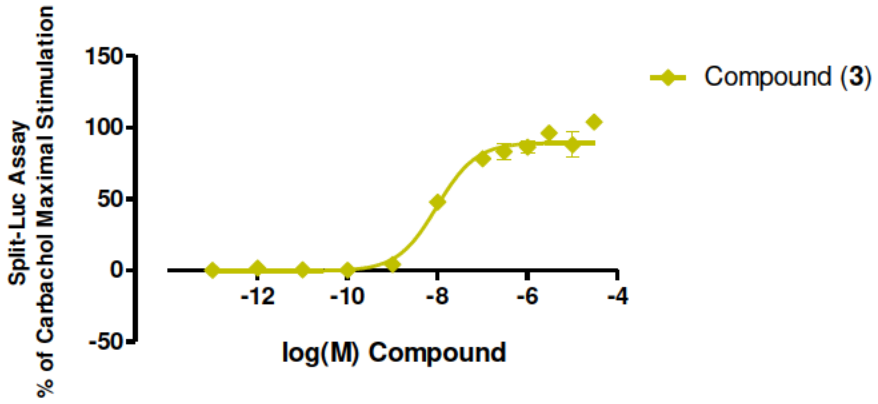

Figure 4. Dose response curve of Split-Luc assay. Data points represent the mean ± S.E.M. from three to four independent two-point kinetic experiments, conducted in triplicate.

From Iperoxo-related heterodimeric compounds to homodimeric and trimeric ones

Activation of G protein studied through the luciferase assay occurs with all series of iperoxo-hybrids considered: bivalent ligands, homobivalent as well as the trivalent compound. The trifunctional ligand **3** showed higher pIC_{50} than the bitopic ligand BQCAd-Iperoxo and even higher than all of the homobivalent iperoxo ligands. The series of homovalent ligands tends to have the highest receptor activation efficacy (E_{max} between 92.2 and 103.7%). Regardless of the spacer chain length, all the homovalent ligands give full activation of the M1 muscarinic receptor, with the exception of the derivative with 6 methylene units (92%). The 10-spacer homobivalent ligand shows the highest effect in the homovalent series with a pEC_{50} of 7.86 and an E_{max} of 103.7%. This could be the optimal distance for the design of further trivalent ligands.[255]

Table 2. Split-Luc assay pEC_{50} and $\%E_{max}$ values; RLB affinity constants of compounds **3** and, for comparison, of additional Iperoxo-Hybrids previously reported in literature.[255] The split-luc dose-response curve of the previously synthesized BQCA-rigid-Iperoxo derivative[111] is reported for the first time below.

Compound	Split-Luc Assay		Radioligand Binding Assay Equilibrium		Radioligand Binding Assay Dissociation
	pEC_{50}	$\%E_{max}$	pIC_{50}	pKi	pIC_{50}
BQCA-(Iperoxo)$_2$	8.01 ± 0.07	89.44 ± 1.87	6.96 ± 0.14	7.34	5.23± 1.10
Iperoxo-4-Iperoxo	6.49 ± 0.01[255]	103.6 ± 0.6[255]	n.d.	n.d.	n.d.
Iperoxo-6-Iperoxo	6.77 ± 0.01[255]	92.2 ± 0.6[255,255]	n.d.	n.d.	n.d.
Iperoxo-8-Iperoxo	6.89 ± 0.01[255]	101.1 ± 0.8[255]	n.d.	n.d.	n.d.
Iperoxo-10-Iperoxo	7.86 ± 0.02[255]	103.7 ± 0.7[255]	n.d.	n.d.	n.d.
BQCAd-4-Iperoxo	7.40 ± 0.08	105.10 ± 2.45	n.d.	n.d.	n.d.
BQCAd-6-Iperoxo	6.92 ± 0.13	71.23 ± 3.27	5.52 ± 0.06	5.93	5.89 ± 0.09
BQCAd-8-Iperoxo	8.09 ± 0.08	112.00 ± 2.39	n.d.	n.d.	n.d.
BQCAd-10-Iperoxo	6.01 ± 0.16	62.59 ± 4.43	5.59±0.06	6.34	6.22 ± 0.08
BQCAd-rigid-Iperoxo	7.40 ± 0.12	78.46 ± 3.25	n.d.	n.d.	n.d.

Chain linker influence in G-protein Activation of hM1 receptor

Moreover, the ligands were evaluated for an in-depth examination of the spacer chain characteristics in terms of geometry, length and physical-chemical properties with regard to the activation of the M1 receptor. A gradual increase in the pEC_{50} value occurs among the homovalent derivatives with a progressive extension of the spacer length. In the BQCAd/ iperoxo bivalent ligand series, the chain length has a considerable influence on the pEC_{50} values with a maximum value of 8.09 obtained with the 8-chain compound. By insertion of rigid spacer between the allosteric and the orthosteric portion, the pEC_{50} becomes 7.40.

Moreover, M1 receptor FRET studies on a dualsteric compound with a steric hindrance linker (in this case the azobenzene linker) showed reduced receptor activation kinetics in comparison to the related dualsteric ligands bearing a polymethylene linker. Probably the slower activation results from interactions between the voluminous linker and the aromatic lid, formed by Tyr-$104_{3.33}$, Tyr-$403_{6.51}$, and Tyr-$426_{7.39}$, located between the orthosteric and allosteric binding site.[111]

Exactly the same rigidified linker was introduced between the allosteric naphmethonium moiety and iperoxo, in the bitopic ligands of the M2 muscarinic receptor[105].[105] Introducing a longer (16.0 Å) and more

rigid linker in the iper-rigid-naph compound instead of the hexamethylene and octamethylene spacers led to a loss of binding in the M2 allosteric binding pocket. Due to multiple clashes with allosteric residues, iper-rigid-naph does not assume the purely allosteric conformation, but is forced in the purely active binding pose[109]. Computational studies and pharmacological results confirm full receptor activation.

This seems not to be the case in the corresponding M1 rigidified ligand. The ligand, despite its complete rigidification, is only able to partially activate the G protein with a maximum efficacy of 78%.

Kruse et al.[101] described the orthosteric agonist iperoxo being bound to the active state of the M2 muscarinic acetylcholine receptor. Here, the so-called tyrosine lid closes over the agonist, separating the orthosteric from the allosteric site, resulting in full receptor activation. However, the side chain conformations of these tyrosine residues appears to be very flexible in MD simulations, and the M2 receptor tolerates agonist binding within an orthosteric binding site that is not completely closed.[105] It is conceivable, that the muscarinic M1 receptor does not have the same degree of tolerance as the M2 receptor and that the rigid linker connecting the orthosteric portion to the BQCAd scaffold, oriented towards the allosteric binding pocket, hinders the closure of the tyrosine lid. The result is a restricted receptor conformational change and therefore partial agonism (E_{max} 78%).

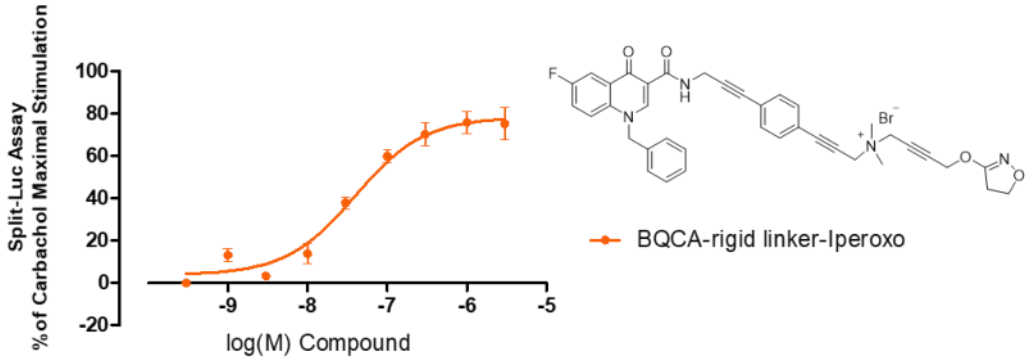

Figure 5. Dose response curve of Split-Luc assay. Data points represent the mean ± S.E.M. from three to four independent two-point kinetic experiments, conducted in triplicate.

Conclusion

Further molecular docking simulation studies are needed to elucidate the binding mode of the "tritopic" molecular-tool and its influence on the multimerization states of hM1 receptors. It could also be of interest in further studies to characterize the subtype selectivity as well as the functional selectivity of the hybrid compound. Taken together this multimer-ligand tool compound could contribute to the further exploration of the therapeutically important M1 receptor through the understanding of the fundamental interactions in the binding pocket (metastable binding site or induced multimerization), which are the key to unlocking the secrets of receptor activation. The findings concerning the influence of the spacer chain in the activation of the G protein pathway suggest that the receptor binding pose of a dualsteric ligand, the receptor activation kinetics and the structure of the connecting chain are closely related to each other. A bitopic binding mode of the rigidified M1 hybrid is presumed, but needs further studies to be confirmed.

7. Iperoxo derivatives: alkane, bis(ammonio)alkane-type and rigidified chain compounds for the study of muscarinic receptors

Introduction

Muscarinic acetylcholine receptors (mAChRs or MRs) belong to the class A GPCRs, which constitute a large superfamily of cell surface receptors. A common structural property of GPCRs is the serpentine transmembrane topology, which is composed of seven alpha-helical domains connected by intra and extracellular loops of variable structure. The GPCRs' highly dynamic structures, assuming a spectrum of conformational states[257–259], reflect the complexity of the resulting signaling mechanisms, which are not restricted to G protein binding.[260] The development of orthosteric subtype selective ligands for one of the five subtypes of muscarinic acetylcholine receptors (M1-M5) is a highly challenging task due to the high conservation of the orthosteric binding site across the subtypes of a given GPCR subfamily.

Since receptor activation is strongly influenced by the extracellular configuration of GPRCs some iperoxo derivatives with N-Alkyl residues of different lenght were synthtized and recently investigated.

Recently GPCR fluorescence resonance energy transfer (FRET) sensors were investigated as reliable detectors for conformational changes upon agonist binding[261,262]. In the research group of Carsten Hoffmann, ours collaborators use muscarinic acetylcholine receptors (MR) as model systems to study GPCR activation dynamics and created FRET-sensors for each family member. They created FRET sensors for each MR subtype were used to study activation characteristics of rationally designed iperoxo derivatives, which influence receptor activation in a subtype-specific manner. (unpublished results from Michael Kauk and Marcel Bermudez). The different size of the substituents allow a systematic exploration of steric limitations caused by an interference with the closure of the so-called tyrosine lid (aromatic lid) formed by the residues $Y^{3.33}$, $Y^{6.51}$ and $Y^{7.38}$.

To further investigate the iperoxo derivatives among the different receptor subtypes some additional derivatives have been synthesized:

- a further extension of the iperoxo N-alkyl chain (**2-C11**, **2-C12**) was provided;

- a new rigid linker iperoxo compound (**3**) was designed and synthesized to study the role of chain flexibility or stiffness in receptor activation

- and additional bis(ammonium) alkane-type iperoxo derivatives were designed (**4-Cn**) with focus on the key role of the second quaternary ammonia head.

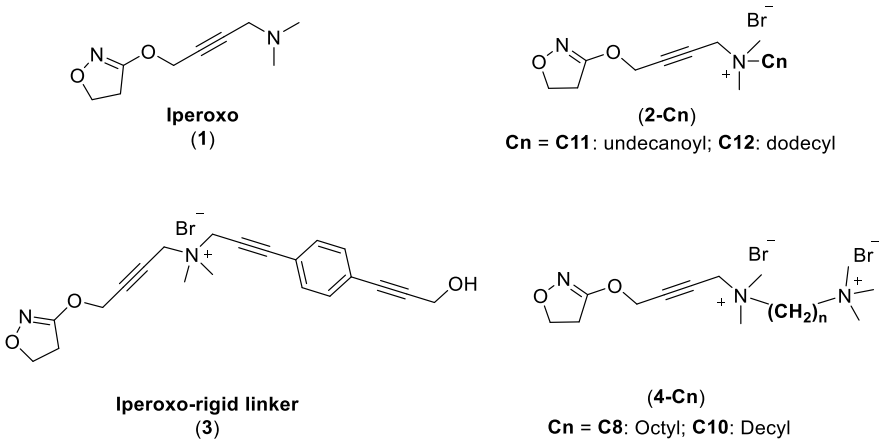

Figure 1: Structures of Iperoxo and of the new iperoxo-chain derivatives.

Material and Methods

Materials

For chromatographic applications (HPLC-MS) deionized water produced by means of a Milli-Q® system (Merck, Darmstadt, Germany) was used. HPLC grade and LC-MS grade solvents were from Sigma-Aldrich (Munich, Germany). All chemicals were purchased from Sigma-Aldrich (Schnelldorf, Germany), VWR (Darmstadt, Germany) and TCI (Eschborn, Germany) and were used without prior purification.

General Medicinal Chemistry Methods

^{1}H (400.132 MHz) and ^{13}C (100.613 MHz) NMR spectra were recorded using a Bruker AV 400 NMR spectrometer (Bruker Biospin, Ettlingen, Germany). As an internal standard, the signals of the deuterated solvents were used (DMSO-d6: ^{1}H 2.5 ppm, ^{13}C 39.52 ppm; $CDCl_3$: ^{1}H 7.26 ppm, ^{13}C 77.16 ppm). Abbreviations for data quoted are s, singlet; d, doublet; t, triplet; q, quartet; m, multiplet; b, broad; dd, doublet of doublets; dt, doublet of triplets; tt, triplet of triplets; and tq, triplet of quartets. Coupling constants (*J*) are given in Hertz. The specific NMR assignments were determined by using typical

techniques including polarization transfer experiments (DEPT) and two-dimensional experiments, such as ^{1}H-^{1}H correlation (COSY) and ^{1}H-^{13}C-proton-carbon heteronuclear correlation (HMQC, HMBC). TLC analyses were performed on commercial precoated plates, silica gel 60 F254, C18 silica-coated aluminum panels ALUGRAM® RP-18W / UV254 and on pre-coated TLC-plates Alox-25/UV254 (Macherey-Nagel); the detection was made using UV light at 254 nm, intrinsic fluorescence at 366 nm or with ethanolic $KMnO_4$, Dragendorff reagent or phosphomolybdic acid ethanolic solution. For classical purification, gravity column chromatography was carried out. Silica gel with a grain size of 63-200 µm (Merck, Darmstadt, Germany) was used as stationary phase. Flash chromatography on a puriFlash®430 system (Interchim, Montlucon, France) was performed using prepacked columns (Interchim, Montluçon, France) with silica gel filling (Particle size 30 microns or 50 microns) for normal phase or with C18-silica gel filling (Particle size 15 µm) for the reverse phase. The detection was carried out by means of a UV detector and Evaporative Light Scattering Detector (ELSD). Microwave assisted reactions were carried out by use of MLS-rota PREP or synthWAVE instruments (Milestone, Leutkirch, Germany).

The LC-MS analyses of all the test compounds were performed using a Shimadzu LC-MS-2020 mass spectrometer (Shimadzu Deutschland GmbH, Duisburg, Germany) containing a DGU-20A3R degassing unit, a LC20AB liquid chromatograph and a SPD-20A UV/Vis detector and a LC / MSD ion trap (Agilent Technologies, Waldbronn, Germany) connected to an Agilent 1100 modular system. A Synergi Fusion-RP (150 mm x 4.6 mm i.d., 4 µm; Phenomenex Ltd., Aschaffenburg, Germany) column and a gradient of MeOH/water, as a mobile phase, were used. Parameters of the HPLC method: solvent A, water with 0.1% formic acid; solvent B, MeOH with 0.1% formic acid. Solvent B was increased from 0% to 90% in 13 min, then decreased from 90% for 5 min, from 90% to 5% in 1 min, and then 5% for 4 min. The method was performed with a flow rate of 1.0 mL/min. UV detection was measured at 254 nm. All compounds were found to have a purity ≥ 95%. Mass spectrum were recorded in ESI-positive mode and the data are reported as mass-to-charge ratio (m/z) of the corresponding positively charged molecular ions. Where not possible using chromatographic methods, the purities of the final compounds individually indicated for each compound were determined by qNMR. 1,2,4,5-Tetrachloro-3-nitrobenzene or maleic acid (Sigma Aldrich, Steinheim, Germany) was chosen as internal standard.

qNMR data were acquired at 90° pulse tip angles with recovery delays of 60 s and acquisition time of 3.7 s in a non-spinning mode at a calibrated probe temperature of 300 K. Sixteen scans of 64 K data points for FID were acquired with a spectral width of 8012 Hz (16 ppm). Manuel phase and baseline correction were performed prior to integration. Preliminary data processing was carried out with Bruker software, TOPSPIN 3.0.

Integrations of the substance and the IS are used in the following formula for purity determination:

$$\mathrm{P}[\%] = \mathrm{PIC} \cdot \frac{n\mathrm{IC} \cdot \mathrm{Int} \cdot \mathrm{MWt} \cdot \mathrm{mIC}}{n\mathrm{t} \cdot \mathrm{IntIC} \cdot \mathrm{MWIC} \cdot \mathrm{ms}}$$

where Int is the integral, MW is the molecular weight, m is the mass, n is the number of protons, P is the purity (in %), IC is the internal calibrant, s is the sample, and t is the target molecule.[263]

Results

Chemistry

The reaction sequences of the iperoxo derivatives **2-C11** and **2-C12** are illustrated in Schema 1. Iperoxo-base was reacted with the corresponding bromoalkane in acetonitrile, affording the final monoquaternary ammonium salts **1-C11** and **1-C12** in 49-78% yield.

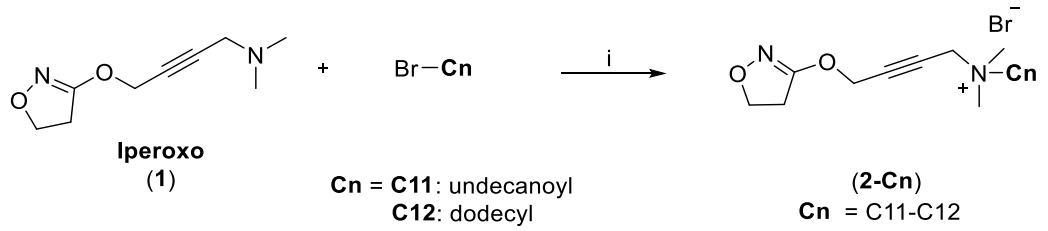

Scheme 1. Synthesis of orthosteric Iperoxo Derivatives **2-Cn**. Reagents and conditions: (i) KI/K_2CO_3, CH_3CN, 70 °C.

The reaction sequences for the synthesis of the iperoxo-rigid linker **3** are illustrated in Schema 2. For the synthesis of hybrid **3** the base of iperoxo was connected with the rigid spacer. Compound **6** was synthesized by coupling of 1,4-dibromobenzene and propargylic alcohol in a Sonogashira like reaction, followed by Appel reaction.[111] Iperoxo, was reacted with the rigid spacer in acetonitrile, affording the final monoquaternary ammonium salts **3** in 15% yield.

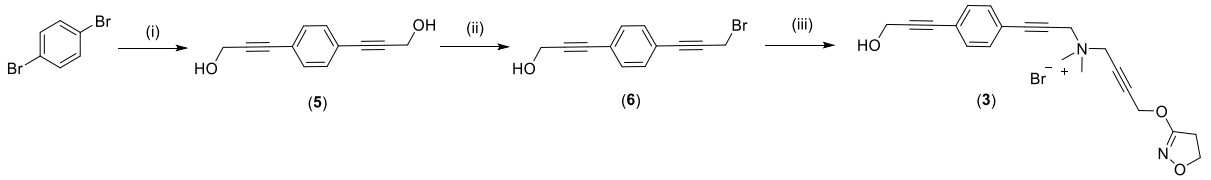

Scheme 2. Reagents and conditions: (i) propargyl alcohol, $Pd(PPh_3)_4$, propylamine, 60 °C; (ii) CBr_4, PPh_3, CH_2Cl_2, 0 °C, rt; (iii) iperoxo base, KI/K_2CO_3, CH_3CN, 80 °C, MW.

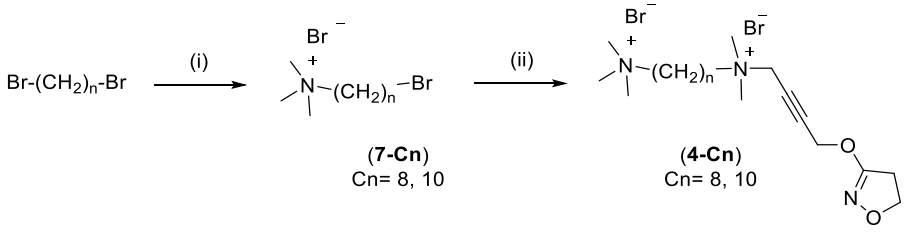

Scheme 3. Reagents and conditions: (i) trimethylammonium hydrochloride, EtOH, KOH, rt; (ii) iperoxo base, KI/K_2CO_3, CH_3CN, 80 °C, MW.

Synthesis of the Iperoxo Derivatives 2-C11, 2-C12

To a solution of iperoxo base 2.47 mmol in 10 mL of acetonitril, 10 equivalents of the corresponding 1-bromoalkane (1-Bromoundecane, 1-Bromododecane) and a catalytic amount of KI/K_2CO_3 (1:1) were added. The mixture was stirred in a sealed container at a temperature between 55 and 70 °C. The precipitate obtained was filtered and Et_2O was added to complete the precipitation. The solid was collected and washed several times with Et_2O and dried *in vacuo*.

N-(4-((4,5-Dihydroisoxazol-3-yl)oxy)but-2-yn-1-yl)-N,N-dimethylundecan-1-aminium bromide ***2-C11***

Yellow oil; 49% yield; R_f = 0.58 (CH_2Cl_2/MeOH = 8:2); ^{1}H NMR (CD_3OD): 0.90 (t, 3H, CH_2-C**H$_3$**, *J* = 6.9), 1.34 (br, 16H, CH_2-CH_2-C**H$_2$**-C**H$_2$**-C**H$_2$**-C**H$_2$**-C**H$_2$**-C**H$_2$**-C**H$_2$**-C**H$_2$**-CH_3), 1.78 (br, 2H, CH_2-C**H$_2$**-CH_2-CH_2-CH_2-CH_2-CH_2-CH_2-CH_2-CH_2-CH_3), 3.03 (t, 2H, **H**-$4_{2\text{-isox}}$, *J*=9.6), 3.16 (s, 6H, $^+$N(C**H$_3$**)$_2$), 3.43 (br, 2H, N^+-C**H$_2$**-CH_2), 4.37 (s, 2H, ≡C-C**H$_2$**-N^+), 4.40 (t, 2H, **H**-$5_{2\text{-isox}}$, *J*=9.6), 4.91 (s, 2H, O-C**H$_2$**-C≡). ^{13}C NMR (CD_3OD): 14.25, 23.50, 23.56, 27.13, 30.02, 30.28, 30.35, 30.46, 30.52, 32.89, 33.50, 50.95, 54.89, 58.06, 65.36, 71.00, 76.43, 87.55, 166.65. MS (ESI) m/z $[M]^+$ Calcd for $C_{20}H_{37}N_2O_2^+$: 337.28. Found: 337.15. qNMR purity 95.0%.

N-(4-((4,5-Dihydroisoxazol-3-yl)oxy)but-2-yn-1-yl)-N,N-dimethyldodecan-1-aminium bromide ***2-C12***

White, viscose oil; 78% yield; R_f = 0.41 (CH_2Cl_2/MeOH = 85:15); ^{1}H NMR (CD_3OD): 0.90 (t, 3H, CH_2-C**H**$_3$, *J* = 6.9), 1.28-1.38 (m, 18H, CH_2-CH_2-(C**H**$_2$)$_9$-CH_3), 1.78 (br, 2H, CH_2-C**H**$_2$-$(CH_2)_9$-CH_3), 3.03 (t, 2H, **H**-4$_{2\text{-isox}}$, *J*=9.6), 3.17 (s, 6H, $^+$N(C**H**$_3$)$_2$), 3.43 (br, 2H, N$^+$-C**H**$_2$-CH_2), 4.38 (s, 2H, ≡C-C**H**$_2$-N$^+$), 4.40 (t, 2H, **H**-5$_{2\text{-isox}}$, *J*=9.6), 4.91 (s, 2H, O-C**H**$_2$-C≡).^{13}C NMR (MeOD): 14.89, 24.14, 24.19, 27.77, 30.63, 30.93, 31.09, 31.20, 33.53, 34.13, 51.63, 55.54, 58.07, 65.99, 71.63, 77.07, 87.17, 169.15. MS (ESI) m/z [M]$^+$ Calcd for $C_{21}H_{39}N_2O_2^+$: 351.30. Found: 351.15. qNMR purity 95.6%.

Synthesis of the Iperoxo rigid linker 3

3,3'-(1,4-Phenylene)bis(prop-2-yn-1-ol) **5**

17.0 mmol of 1,4-dibromobenzene and 0.44 mmol of $Pd(PPh_3)_4$ were dissolved in 60 mL of propylamine. After addition of 2-propyn-1-ol (100 mmol), the reaction mixture was heated at 60 °C under nitrogen. The reaction was monitored via silica gel TLC (cyclohexane:ethyl acetate = 4:6, Rf = 0.48). After completion of the reaction (2 days), the mixture was quenched with 40 mL of conc. HCl. The aqueous layer was extracted three times with diethyl ether. The combined organic layers were dried over Na_2SO_4 and the solvent was removed *in vacuo*. The product was purified using column chromatography (cyclohexane:EtOAc = 7:3 to 4:6).

Yellow solid. 92%. mp 120-123 °C; R_f = 0.48 (cyclohexane/ethyl acetate = 4:6); ^{1}H NMR ($CDCl_3$): 1.64 (s, 2H, CH_2-O**H**), 4.50 (s, 4H, C**H**$_2$-OH), 7.37 (s, 4H, C**H**$_{\text{arom.}}$). ^{13}C NMR ($CDCl_3$): 51.95, 86.36, 89.57, 98.74, 122.45, 131.90.

3-(4-(3-Bromoprop-1-yn-1-yl)phenyl)prop-2-yn-1-ol **6**

3.40 mmol of 3,3'-(1,4-phenylene)bis(prop-2-yn-1-ol) **5** and 3.40 mmol of tetrabromomethane were dissolved in 20 mL dichloromethane dry under argon. 3.40 mmol of triphenylphosphine were added at 0 °C. The reaction mixture was then allowed to warm up to room temperature, stirred overnight and monitored by means of silica gel TLC (cyclohexane/ethyl acetate = 4:6, Rf = 0.73). The solvent was removed *in vacuo* and the product was purified using column chromatography (cyclohexane/EtOAc = 4:6).

Yellow solid. 20%. mp 84-86 °C; Rf = 0.73 (cyclohexane/ethyl acetate = 4:6); ^{1}H NMR ($CDCl_3$): 4.16 (s, 2H, C**H**$_2$-Br), 4.50 (s, 2H, C**H**$_2$-OH), 7.38 (s, 4H C**H**$_{arom.}$). ^{13}C NMR ($CDCl_3$): 15.0, 51.95, 85.47, 86.36, 89.57, 98.74, 122.55, 123.36, 131.88, 132.08.

4-((4,5-Dihydroisoxazol-3-yl)oxy)-N-(3-(4-(3-hydroxyprop-1-yn-1-yl)phenyl)prop-2-yn-1-yl)-N,N-dimethylbut-2-yn-1-aminium bromide **3**

Yellow oil; 15% yield; R_f = 0.45 (CH_2Cl_2/MeOH = 85:15); ^{1}H NMR ($CDCl_3$): 3.02 (t, 2H, **H**-4$_{2\text{-isox}}$), 3.31 (s, 6H, $^{+}$N(C**H**$_3$)$_2$), 4.37 (s, 2H, ≡C-C**H**$_2$-N^{+}), 4.40 (t, 2H, **H**-5$_{2\text{-isox}}$, *J*=9.6), 4.52 (s, 2H, ≡C-C**H**$_2$-N^{+}), 4.65 (s, 2H, C**H**$_2$-OH), 4.93 (s, 2H, O-C**H**$_2$-C≡), 7.45 (d, 2H, C**H**$_{phenyl}$, *J*=8.5), 7.55 (d, 2H, C**H**$_{phenyl}$, *J*=8.5), 8.25 (s, 1H, O**H**) ^{13}C NMR ($CDCl_3$): 33.47, 50.85, 50.96, 55.06, 56.72, 58.08, 71.04, 76.15, 78.25, 84.32, 88.21, 91.73, 92.35, 121.31, 126.03, 132.63, 133.10, 168.60. MS (ESI) m/z [M]$^{+}$ Calcd for $C_{21}H_{23}BrN_2O_3^{+}$: 351.17. Found: 351.05. HPLC purity 96.55%.

<u>Synthesis of the Bromo-alkane-ammonium Bromide 7-C8, 7-C10</u>

50 mmol Trimethylammonium hydrochloride and 80 mmol dibromoalkane derivatives were dissolved in ethanol. A solution of 65 mmol potassium hydroxide was added slowly dropwise and the mixture was left for three days at room temperature. The white precipitate was filtered off and the filtrate was poured into ice-cold diethyl ether. The mixture was cooled to 4 °C and the white precipitate extracted with acetone using a Soxhlet extractor. The extract was poured into diethyl ether and the precipitate filtered off and dried *in vacuo* to give **7-C8** and **7-C10**.[103]

8-Bromo-N,N,N-trimethyloctan-1-aminium bromide **7-C8**

White powder; 39% yield; mp 109-113 °C; yield; R_f = 0.45 (CH_2Cl_2/MeOH = 85:15); ^{1}H NMR (DMSO): 1.29 (br, 6H, Alkyl), 1.38 (s, 2H, C**H**$_2$-CH_2-Br), 1.80 (t, 2H, *J*=6.9, CH_2-C**H**$_2$-Br), 3.05 (s, 9H, N^{+}(C**H**$_3$)$_3$), 3.32 (s, 2H, N^{+}-C**H**$_2$), 3.53 (t, 2H, *J*=6.9, C**H**$_2$-Br). ^{13}C NMR (DMSO): 21.71, 25.36, 27.11, 27.69, 27.98, 31.84, 34.85, 51.81, 64.95.

10-Bromo-N,N,N-trimethyldecan-1-aminium bromide **7-C10**

White powder; 51% yield; mp 112-115 °C; R_f = 0.38 (CH_2Cl_2/MeOH = 9:1); ^{1}H NMR (DMSO-d_6): 1.28 (m, 10H, Alkyl), 1.38 (s, 2H, C**H**$_2$-CH_2-CH_2-Br), 1.67 (m, 2H, N^{+}-CH_2-C**H**$_2$), 1.79 (t, 2H, *J*=6.9, C**H**$_2$-CH_2-

Br), 3.05 (s, 9H, $N^+(CH_3)_3$), 3.27 (s, 2H, N^+-CH_2), 3.52 (t, 2H, *J*=6.9, CH_2-Br). ^{13}C NMR (DMSO-d_6): 21.68, 25.31, 27.21, 27.66, 27.99, 28.44, 28.49, 31.94, 34.81, 51.89, 65.15.

Synthesis of the Diammonium Compounds 4-C8, 4-C10

1 mmol of 4-((4,5-dihydroisoxazol-3-yl)oxy)-*N,N*-dimethylbut-2-yn-1-amine **1** and 1 mmol of monoquaternary bromide **7-Cn** were dissolved in acetonitrile (30 ml) and heated at 80 °C making use of the microwave assistance in the presence of a catalytic amount of KI/K_2CO_3. After the reaction was completed (TLC monitoring, eluent: 0.2 M aqueous KNO_3/CH_3OH 2:3), about one half of the solvent was evaporated and the obtained colorless solid was collected by filtration and recrystallized. The precipitate was filtered, washed with diethylether, and dried *in vacuo* to give the desired products.[103]

N^1-(4-((4,5-Dihydroisoxazol-3-yl)oxy)but-2-yn-1-yl)-N^1,N^1,N^8,N^8,N^8-pentamethyloctane-1,8-diammonium dibromide **4-C8**

Cream-colored powder; 40% yield; mp 125-129 °C; R_f = 0.47 (CH_2Cl_2/MeOH = 9:1); ^1H NMR (DMSO-d_6): 1.27-1.32 (m, 10H, Alkyl), 1.65-1.69 (m, 2H, Alkyl), 3.05 (t, 2H, *J*=11, **H**-$4_{2\text{-isox}}$), 3.12 (s, 9H, $N^+(CH_3)_3$), 3.16 (s, 6H, $N^+(CH_3)$), 3.30-3.25 (m, 4H, CH_2-N^+), 4.33 (t, 2H, J=9.6, **H**-$5_{2\text{-isox}}$), 4.46 (s, 2H, $N^+CH_2C\equiv$) 4.93 (s, 2H, $OCH_2C\equiv$). ^{13}C NMR (DMSO-d_6): 21.97, 25.58, 28.19, 28.22, 32.27, 45.49, 48.74, 52.08, 59.47, 63.87, 65.55, 77.47, 85.77, 164.17. MS (ESI) m/z $[M]^+$ Calcd for $C_{20}H_{39}N_3O_2^+$: 176.65. Found: 176.55. qNMR purity 97.39%.

N^1-(4-((4,5-Dihydroisoxazol-3-yl)oxy)but-2-yn-1-yl)-N^1,N^1,N^{10},N^{10},N^{10}-pentamethyldecan-1,10-diammonium dibromide **4-C10**

Beige powder; 37% yield; mp 127-132 °C; R_f = 0.41 (CH_2Cl_2/MeOH = 85:15); ^1H NMR (CD_3OD): 1.30 (m, 10H, Alkyl), 1.65-1.68 (m, 4H, Alkyl), 3.05 (t, 2H, *J*=11, **H**-$4_{2\text{-isox}}$), 3.12 (s, 9H, $N^+(CH_3)_3$), 3.16 (s, 6H, $N^+(CH_3)$), 3.30-3.25 (m, 4H, CH_2-N^+), 4.33 (t, 2H, J=9.6, **H**-$5_{2\text{-isox}}$), 4.46 (s, 2H, $N^+CH_2C\equiv$), 4.94 (s, 2H, $OCH_2C\equiv$). ^{13}C NMR (CD_3OD): 23.97, 27.25, 27.33, 30.07, 30.13, 30.32, 30.35, 33.73, 48.41, 48.62, 48.83, 49.05, 49.26, 49.48, 49.68, 51.23, 52.34, 53.59, 53.66, 53.67, 55.16, 58.36, 67.90, 71.22, 76.73, 87.63, 168.73. MS (ESI) m/z $[M]^+$ Calcd for $C_{22}H_{43}N_3O_2^+$: 190.67. Found: 190.60. qNMR purity 96.11%.

Discussion

Despite the high structural conservation of the muscarinic orthosteric binding site, a subtype-specific behavior of some elongated iperoxo derivatives was already observed (Unpublished results from Michael Kauk and Marcel Bermudez). Differences in the shape of the orthosteric pocket and in the dynamic activation of the receptor will be investigated upon application of the new synthetized ligands. The pharmacological investigations (performed in the working group of Carsten Hoffmann, Institute for Molecular Cell Biology, CMB-Center for Molecular Biomedicine, University Hospital Jena, Germany) concerning their subtype-selectivity and bias agonism at the muscarinic receptors are still in process.

8. FRET Studies of Rational Designed Quinolone Based Bitopic Ligands and their Derivatives: A Systematic Approach of Partial Agonism and Allosteric Modulation on the Muscarinic M1 Acetylcholine Receptor

Regina Messerer[a, ł], Michael Kauk[b, c, ł], Daniela Volpato[a], Maria Consuelo Alonso Canizal[b,c], Jessika Klöckner[a], Ulrike Zabel[b,c], Susanne Nuber[b,c], Carsten Hoffmann[b, c, *] and Ulrike Holzgrabe[a, *]

[a] *Department of Pharmaceutical and Medical Chemistry, Institute of Pharmacy, University of Würzburg, Am Hubland, 97074 Würzburg, Germany*

[b] *Department of Pharmacology and Toxicology, University of Würzburg, Versbacher Str. 9, 97078 Würzburg, Germany*

[c] *Rudolf Virchow Center for Experimental Biomedicine, University of Würzburg, Josef Schneider Straße 2, 97080 Würzburg, Germany*

Reprinted/adapted with permission from Messerer, R.; Kauk, M.; Volpato, D.; Alonso Canizal, M.C.; Kloeckner, J.; Zabel, U.; Nuber, S.; Hoffmann, C.; Holzgrabe, U. FRET Studies of Quinolone-Based Bitopic Ligands and their Structural Analogues at the Muscarinic M1 Receptor. *ACS Chem. Biol.* **2017**, doi:10.1021/acschembio.6b00828.

Author Information

ł R.M. and M.K. contributed equally.

* Corresponding author: e-mail address:

ulrike.holzgrabe@uni-wuerzburg.de (Prof. Dr. Ulrike Holzgrabe); tel.: +49 931 31-85460; fax: +49 931 31-85494.

c.hoffmann@toxi.uni-wuerzburg.de (Prof. Dr. Carsten Hoffmann); tel.: +49 931 31-48304; fax: +49 931 31-48539.

Keywords*:*

Quinolones, Bitopic ligands, Partial Agonism, Allosteric Modulation, M_1 muscarinic receptor, FRET.

Abbreviations:

ACh, acetylcholine; BQCA, benzyl quinolone carboxylic acid; CFP, cyan fluorescent protein; DAG, diacylglycerol; FlAsH, fluoresceine arsenical hairpin binder; FRET, fluorescence resonance energy transfer; GPCR, G-protein coupled receptor; IL, intracellular loop; M_1, muscarinic acetylcholine subtype

1; mAChR, muscarinic Acetylcholine receptos; NAM, negative allosteric modulator; SAM, silent allosteric modulator; PAM, positive allosteric modulator; YFP, yellow fluorescent protein.

Abstract: Aiming to design partial agonists as well as allosteric modulators for the M_1 muscarinic acetylcholine receptor, two different series of bipharmacophoric ligands and their derivatives were designed and synthesized. The hybrids were composed of the BQCA-derived subtype selective allosteric modulator **3** and the orthosteric building block iperoxo **1** or the endogenous ligand acetylcholine **2**, respectively. The two pharmacophores were linked via alkylene chains of different lengths (C4, C6, C8 and C10; **5-Cn** and **6-Cn**). Furthermore, the corresponding derivatives of acetylcholine **2**, iperoxo **1** and of modified BQCA **3** with varying alkyl chain length between C2 and C10 were investigated (**1-Cn**, **2-Cn**, and **4-Cn**). To develop an understanding how these compounds interact with a GPCR on a molecular level and how the single moieties contribute to ligand receptor interaction, FRET was the method of choice in a living single cell system. The characterization of the modified orthosteric ligands indicated that a linker attached to an orthoster rapidly attenuates the receptor response (**1-Cn** and **2-Cn**). With longer linker lengths the receptor response of bitopic ligands (**5-Cn** and **6-Cn**) increases, until reaching a maximum, followed by a gradual decrease. The optimal linker length was found to be six methylene groups (**5-C6**) at the M_1AChR. Additionally, to our knowledge a new conformational change is described that is not of inverse agonistic origin for long linker bitopic ligands. For validating the differences and for a better understanding an exceptional fragment based screening approach was developed.

Introduction

Muscarinic ACh receptors (mAChRs) belong to Class A of G-Protein-coupled receptors (GPCRs) and are divided in five M receptor subtypes (M_1-M_5). These subtypes regulate the activity of many important functions of the peripheral and central nervous system. They differ in their appearance and physiological function; e.g. the M_1 muscarinic acetylcholine receptor is mostly expressed in the central nervous system (cortex, hippocampus and striatum) and is therefore an interesting therapeutic target for the treatment of Alzheimer`s disease and schizophrenia.[1, 2]

The orthosteric binding pocket appears to be homolog among the five receptor subtypes.[3] This issue is challenging for developing subtype selective therapeutics. To our knowledge Spalding et al.[4] described for the first time an alternative - allosteric binding region at M_1 receptors. This region does not show a high sequence identity and is thus, a promising target for developing subtype selective allosteric modulators. Allosteric modulators can influence the affinity of ligands bound to the topographically distinct orthosteric site, either in a positive (PAM), neutral (SAM) or negative (NAM) manner.[5] The benzyl

quinolone carboxylic acids (BQCAs) were found to be M_1 selective positive allosteric modulators (PAMs) with respect to agonist binding, including the endogenous neurotransmitter acetylcholine **2**, and function in M_1 receptors.[6, 7, 8] These M_1-selective properties are interesting for drug research due to the avoidance of side effects associated with indiscriminate activity at other mAChRs. To combine the advantages of the two binding sites, the concept of bitopic ligands was developed.[9] These ligands address the allosteric and orthosteric site simultaneously. Recently, bipharmacophoric ligands consisting of the superagonist iperoxo **1**[10, 11] and a benzyl quinolone carboxylic acid moiety **3** were designed, and found to act as partial *h*M_1 receptor agonists.[12]

For the last two decades a series of different receptor sensors, based on fluorescence resonance energy transfer (FRET), were generated for different GPCRs.[13, 14, 15] Usually, such sensors are tagged C-terminally with CFP and in the third intracellular loop (IL) region with a YFP or a tetracysteine motif capable of binding a small soluble fluorophore called FlAsH. These receptor sensors proved to be valuable tools for pharmacological characterizations in intact cells, especially for monitoring receptor activation in real time and to investigate receptor ligand interaction on a molecular level.[16, 17]

In this study derivatives of the superagonist iperoxo **1**, orthosteric agonist acetylcholine **2**, and of the subtype selective allosteric modulator BQCA **3** were rationally designed, synthesized and characterized, resulting in modified derivatives with varying alkyl chain length between C2 and C10 (**1-Cn**, **2-Cn**, and **4-Cn**, where n give the length of the linker, i.e. the number of C-atoms, Scheme 1 and Scheme 2). Furthermore, the fluoro-substituted allosteric BQCA moieties were linked to the othosteric agonists iperoxo and acetylcholine, aiming to design bipharmacophoric M_1 receptor agonists (**5-C** and **6-C**, Scheme 2). For the pharmacological characterization of these ligands a novel M_1 FRET sensor was used. This study provides an insight into M_1 receptor activation, movement and signaling behavior.

Results and Discussion

Chemistry

The reaction sequences of the iperoxo derivatives **1-C2** to **1-C10** and of the acetylcholine derivatives **2-C4**, **2-C6**, **2-C8**, and **2-C10** are illustrated in Scheme 1. Iperoxo-base[10] **1** and acetylcholine-base **2**, respectively, were reacted with the corresponding bromoalkane in acetonitrile, affording the final

monoquaternary ammonium salts **1-C2** to **1-C10** and **2-C4**, **2-C6**, **2-C8**, and **2-C10** in 48-91% yield. The synthesis of the acetylcholine derivatives **2-C4**, **2-C6**, and **2-C8** were described previously using a different synthetic pathway.[18]

Scheme 1: Synthesis of orthosteric M_1 agonist modulators based on Iperoxo – and Acetylcholine Derivatives.

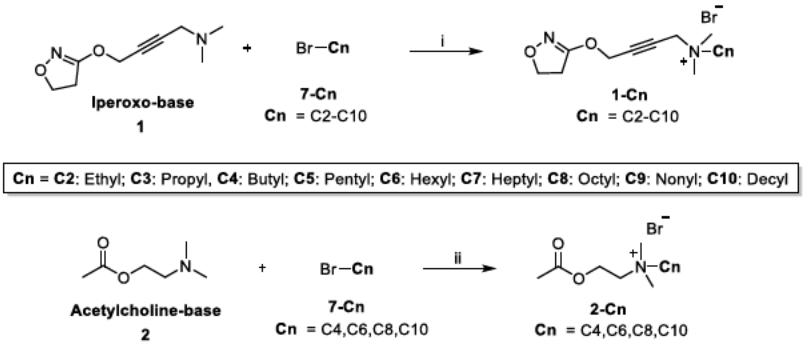

Reagents and conditions: (i) KI/K_2CO_3, $CH_3CN/CHCl_3$, 70 °C; (ii) KI/K_2CO_3, CH_3CN, 70 °C (microwave).

As already reported, the fluoro-4-oxo-quinolone skeleton of **8** was synthesized using the Gould-Jacobs procedure, starting off with the condensation of 4-fluoroaniline with diethyl 2-(ethoxymethylene)-malonate and subsequent cyclization in boiling diphenyl ether.[19, 20, 21] Ester hydrolysis led to compound **3**.[22] Conversion of the ester function (**9**) with the aminoalcohols of the corresponding spacer length (C4, C6, C8, C10), substitution of the alcohol function with a bromine atom using HBr/H_2SO_4 and subsequent reaction with trimethylamine in acetonitrile at 40 °C led to the monoquaternary ammonium salts **4-C4**, **4-C6**, **4-C8**, and **4-C10** in 53-96% yield. For the preparation of the final BQCA/iperoxo hybrids **5-C4**, **5-C6**[12], **5-C8**, and **5-C10** as well as the BQCA/ACh hybrids **6-C4**, **6-C6**, **6-C8**, and **6-C10**, the intermediate bromides were connected to iperoxo and acetylcholine, respectively, in the presence of KI/K_2CO_3 in acetonitrile (Scheme 2).

Scheme 2: Synthesis of Quinolone Derivatives, BQCA/Iperoxo Hybrids and BQCA/ACh Hybrids.

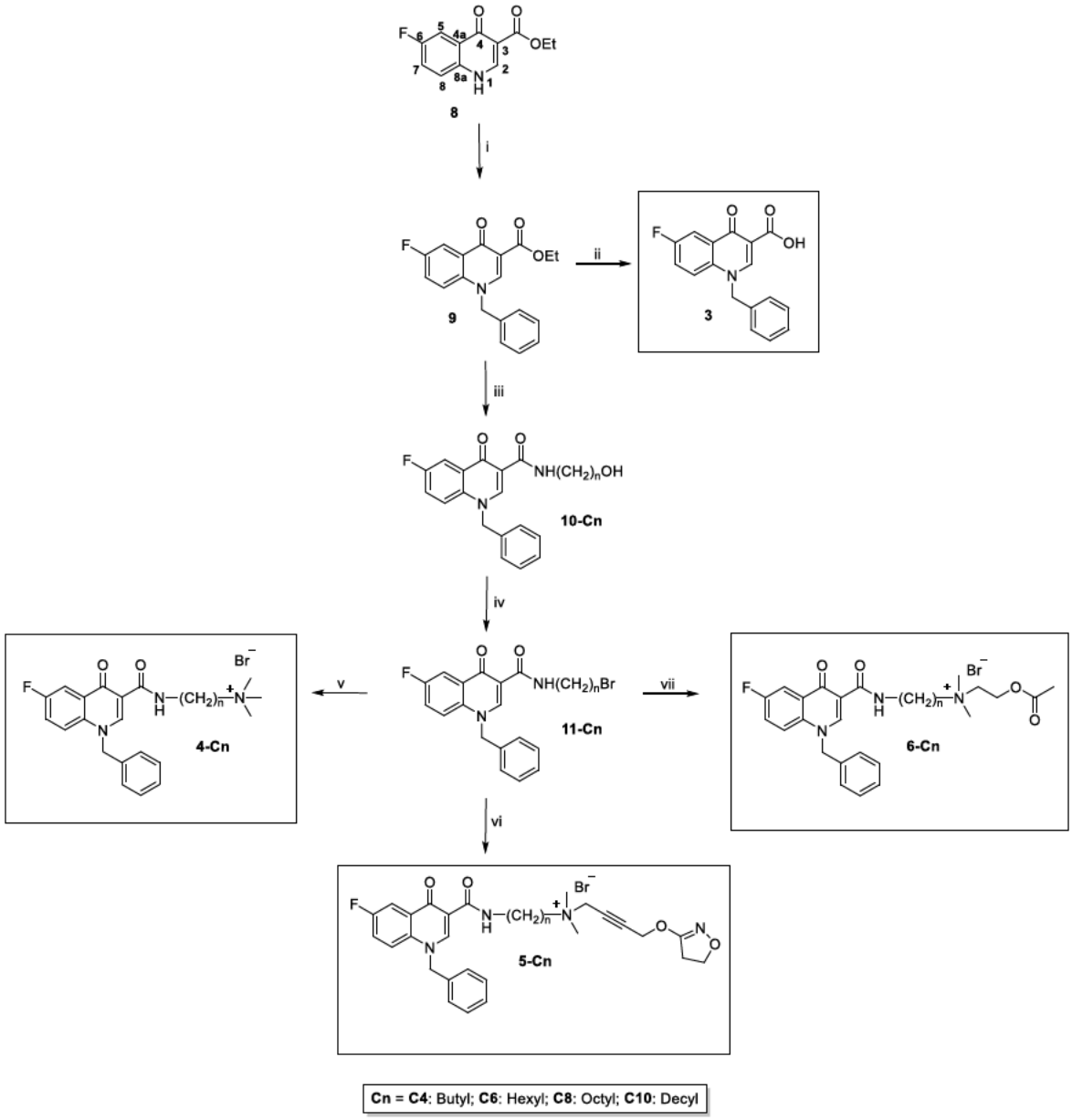

Reagents and conditions: (i) benzyl chloride, K_2CO_3, DMF, 80 °C; (ii) 6 N HCl, MeOH, reflux; (iii) $H_2N(CH_2)_nOH$, 150 °C; (iv) HBr (48%), H_2SO_4, reflux; (v) trimethylamine, CH_3CN, 40 °C (vi) iperoxo base, KI/K_2CO_3, CH_3CN, 80 °C (microwave); (vii) acetylcholine, KI/K_2CO_3, CH_3CN, 80 °C (microwave).

Pharmacology/Fret measurements

1.1.1) Receptor sensor and ligand characterization

In comparison to the previously reported M_1-, M_3-, M_5-[23] and M_2-ACh receptor FRET-sensor [24], we created a novel full length FRET sensor of the human M_1-ACh receptor which was not truncated in the 3rd intracellular loop (IL3). This novel sensor consists of the native amino acid sequence fused at the receptor C-terminus to CFP by adding the amino acids Ser/Arg encoding for an XbaI site. Additionally, a FlAsH binding motif CCPGCC was inserted between Gly^{227} and Ser^{228} (Fig. 1a) at the N-terminal part of IL3 shortly underneath transmembrane domain 5 outside of the G-protein coupling region.[25] The receptor construct M1-I3N-CFP expressed well at the cell surface as analyzed by confocal scanning laser microscopy (Fig. S1). Since the previously published truncated sensors were not different from wild-type receptors in radioligand binding,[16] we characterized only functional response of the novel sensor. To evaluate the effect of the six amino acid insertion into the M1-CFP receptor we used a dual fluorescence probe, which responds with an increase in red fluorescence intensity upon increase in Ca^{2+} and a decrease in green fluorescence upon binding to diacylglycerol (DAG). Therefore, the probe can specifically report on the activation of Gq-signalling.[26] The dual fluorescent probe was transfected in HEK293 cells either alone or co-expressed with the M1-CFP or the novel M1-I3N-CFP sensor and analyzed by confocal microscopy (see supplementary information for details). The dual probe did not respond to carbachol if no receptor was co-transfected. As shown in Figure S2 the carbachol stimulated response was indistinguishable for the M1-CFP receptor or the M1-I3N-CFP sensor. In combination with previous binding experiments on a truncated sensor version[16] it was concluded that this sensor is not disturbed in its signaling properties by insertion of the CCPGCC sequence. For further FRET experiments the M1-I3N-CFP was stably expressed in HEK293 cells and single cells were used for further analysis. To study dynamic conformational changes in real time the M1-I3n-CFP sensor was exposed to the endogenous agonist acetylcholine **2** and the synthetic full agonist iperoxo **1**. To eliminate potential artefacts from changes in flow rates, the cells were constantly superfused with buffer. Under these conditions the receptor sensor shows a constant baseline. Upon ligand addition a sharp antiparallel movement of the CFP and FlAsH signal was observed (Fig. S3), resulting in a concentration dependent change in the FRET signal of 8-12% for iperoxo (Fig. 1b). When the superfusion solution

was switched back from agonist to buffer, the signal returned to the baseline. A slight reduction of the FRET signal over time was detectable and could be due to photobleaching. To prevent artificial underestimation of ligand efficacy reference and ligand was measured in an alternating exposure regime. Thus it was able to generate concentration dependent response (Fig. 1c) curves for the endogenous agonist acetylcholine **2** (EC_{50} = 2.91 µM) and the synthetic full agonist iperoxo **1** (EC_{50} = 0.57 µM). The observed EC_{50} value for **2** is in very good agreements with previously obtained value using the truncated receptor sensor.[16] Due to a fivefold higher potency of **1** compared to **2**, iperoxo was chosen as the orthosteric building block for the studied bitopic ligands to ensure high receptor activation via the orthosteric binding site.

As allosteric building block a derivative of benzyl quinolone carboxylic acid (BQCA) origin was chosen. In 2009, BQCA was reported to be a M_1 selective positive allosteric modulator (PAM)[8] whose binding region was studied in detail.[27] However, an essential property of allosteric modulators is probe dependency. Thus, an experimental approach to show this cooperative effect of BQCA derivative (**3**) combined with **1** (Fig. 1d) was designed. To study positive modulation, a concentration of **1** which results in approximately 20% of the maximal observed signal (EC_{20}) was chosen. This way a clear signal was observed and still a large detection range to observe positive allosteric modulation was available. As seen in Figure 1d by applying the allosteric modulator **3** alone, a small conformational change was found. This small response was not clearly detectable for all cells measured. This might be explained by the very small signal that could not always be distinguished from noise. When applying saturating concentrations of **1**, a significant signal was monitored. Next **1** at 0.1 µM concentration was applied which results in 25% signal compared to saturating ligand concentrations. Now the superfusion was changed to a mix of **1** and **3** and again back to **1** alone. A clear enhanced receptor response was observed by applying **3** and **1** at the same time, compared with the appropriate iperoxo response. This enhanced response is higher than a theoretical additive effect of the conformational changes induced by **3** and **1** alone and can be described as positive allosteric modulation.

1.1.2) Linker elongation attenuates orthosteric properties

Besides their orthosteric and allosteric moieties, bitopic ligands consist of a linker region that is often not investigated in a systematic way and hence, the linker is often inappropriately treated. Until yet the

molecular effects of additional carbon atoms at an orthosteric ligand for muscarinic receptors are still unknown. Therefore, nine different derivatives of iperoxo **1** with a linker attached to the amine group were synthesized (Scheme 1, **1-C2** to **1-C10**). These compounds were investigated via FRET for their ability to induce a conformational change at the M_1 receptor. The results are summarized in Figure 2. Figure 2a shows a single FRET experiment comparing the effect of **1** and different concentrations of **1-C2** and **1-C3**. Even saturating concentrations of **1-C2** exhibit a much reduced FRET signal compared to the reference compound **1**. From these data it can be concluded, that additional carbon atoms significantly reduce the efficacy to 65% compared to iperoxo. Nontheless it was possible to generate a concentration response curve for **1-C2**. Besides the reduced efficacy a 3-fold lower affinity (EC_{50} (**1-C2**) = 1.65 µM) to the receptor sensor became evident (Fig. 2b). For **1-C3** a more than 80% reduced conformational change was found. These signals were too small to establish a reliable concentration response curve. The iperoxo derivatives (**1-C4** to **1-C10**) did not induce any conformational change at the receptor sensor (Fig. 2c). In order to test, whether the linker extended ligands were able to bind the receptor sensor at the orthosteric binding site, competition experiment were performed shown in Figure 2d. To test for binding of **1-C6** first 10 µM of **1** as a concentration which induces 80% of the maximal signal response (EC_{80}) was applied. In the first case as a single ligand to the receptor sensor (Fig 2d). Next, a 10 µM solution of **1** with 100 µM of the linker derivative **1-C6** was added. As can be seen in Figure 2d, the receptor response induced by the ligand mix was significantly reduced compared to the signal induced by **1** alone, indicating, that the two ligands compete for the orthosteric binding site and that the **1-C6** derivative shows affinity to the orthosteric binding site but does not exhibit efficacy as shown by the lack of conformational changes in Figure 2c. In Figure 2e the results for a corresponding set of ligands of ACh origin (Scheme 1) is displayed. The given FRET trace proves, that a distinct linker elongation at an orthosteric ligand attenuates orthosteric efficacy. This phenomenon could be due to a steric hindrance within the binding pocket or due to preventing an essential receptor movement like closing the aromatic lid, which was proposed before to be essential for receptor activation.[28]

1.1.3) Evaluation of Bitopic ligands

Bitopic ligands are thought to interact with both orthosteric and the allosteric binding site at the same time.[9] They are also thought to interact with the receptor in a dynamic binding mode, which consist at least of two different states.[29, 30] Abdul-Ridha et al.[27] investigated both binding sites in great detail by mutational analysis. Using this approach, it was possible to restrict the relative position of both moieties to a certain area of the receptor.[27] In combination with the crystal structure of iperoxo bound to the M_2-receptor subtype[28] and the recently published crystal structure of the M_1-receptor subtype[3], we focused on bitopic ligands with different linker length consisting of either four, six, eight or ten carbon atoms. Thus, these ligands cover a relative distance of 6 Å to 15 Å between both pharmacophore moieties and hence representing the seven transmembrane helical core.

A series of bitopic ligands consisting of iperoxo (**1**) and the BQCA derivative (**3**) were synthesized (Scheme 2). Correspondingly these ligands are called **5-Cn** with **n** reflecting the linker length (**4**, **6**, **8**, **10**) (Scheme 2). As can be seen in Figure 3a, showing a representative FRET trace of **5-C6**, clear concentration dependent increase in conformational change has taken place. This is the largest conformational change at this FRET sensor compared to all other derivatives in this series. All other ligands were also able to induce a conformational change at the M_1 receptor sensor. Figure 3b shows the maximal ligand induced chances in comparison to **1**. The dashed line indicates the maximal observed signal for the allosteric moiety **3** when tested alone. Since all corresponding iperoxo linker derivatives (**1-C4** to **1-C10**) alone did not induce a conformational change (cf. Fig. 2c), the difference in conformational changes of the hybrids above the dashed line should result from the positive cooperativity between the orthosteric and allosteric moieties. Moreover, for the M_1 receptor the optimal linker length for the combination of **1** and **3** is in the range of six methylene groups (see Fig. 3b), whereas for the M_2-receptor subtype longer linker lengths are necessary to improve bitopic ligand efficacy.[29] Thus, the optimal linker length for every receptor subtype might be different for each receptor subtype, depending on their tertiary structure.

Furthermore, after reaching an optimal linker length, the efficacy of bitopic ligands decline by further linker elongation (Fig. 3b). Surprisingly, when investigating compound **5-C10** a concentration dependent signal with opposite signal direction compared to iperoxo (**1**) was found (Fig. 3C). Since changes in

FRET signals in general represent a relative distance change this property was used as a readout for conformational changes at GPCRs. The opposite FRET signal induced by **5-C10** was not observed before for any bitopic ligand at M-receptors. Comparable inverse FRET signals were reported for inverse agonistic responses at constitutively active mutants of the α_{2a} adrenergic receptor[31] and the M_3 mutant[32]. At constitutively active M_3 receptors, atropine behaves as an inverse agonist. Hence, to compare the effect found for **5-C10** at the M1-I3N-CFP with eventual constitutive activity, the effect of atropine at this construct was studied. However, atropine does not induce any conformational change (see Fig. 3d), arguing against constitutive activity as an explanation for the behavior of **5-C10**. Of note, the high receptor affinity of atropine becomes visible by the fact, that it was almost impossible to induce a second signal for **1** after the first application of 10 µM atropine. To further study the surprising effect of **5-C10**, a series of bitopic ligands based on acetylcholine as orthosteric building block **6-C4** to **6-C10** (Scheme 2) was investigated. Figure 3e displays a representative FRET trace of acetylcholine based bitopic ligands and the bar graph in Figure 3f summarizes the measured FRET-signals. Again a linker length dependent receptor response was found. Moreover, again inverse FRET-signals for bitopic ligands of longer chain length were detected. Interestingly, for this compound series a FRET-signal with similar direction as observed for ACh (**2**) was never detected.

1.1.4) Linker fusion at the allosteric building block

In order to find out, why bitopic ligands with longer linkers produce an inverse FRET signal it was of interest to unravel the moiety of the ligands contributing to the observed signals. Additionally, the question arised whether it would be possible to reconstruct the signal derived by different bitopic ligands by combining the individual components in a fragment-based screening approach in a single cell. Therefore, the ligands **5-C6** and **5-C10** who showed the most extreme signals were studied. As shown in Figure 1d the BQCA derivative (**3**) induces a small conformational change but the corresponding linker extended iperoxo derivative (**1-C6**) did not exhibit a detectable effect at our receptor sensor (Fig. 2c), but **1-C6** binds to the receptor (Fig. 2d). Both effects are shown in Figure 4a, this time measured at the same cell. By applying both compounds (**3** and **1-C6**) at the same time a receptor response was observed that was on the one hand significantly different to the BQCA response but on the other hand similar in the maximal signal intensity as reported before for the bitopic ligand **5-C6** (Fig. 3a), indicating

first that it is possible to reconstruct the effect of a bitopic ligand interacting with a receptor by applying the fragments at the same time to the receptor sensor, and second that there is cooperativity between the allosteric modulator BQCA (**3**) and the orthosteric ligand **1-C6**.

Comparable experiments were performed with the ligand **5-C10** and its respective building blocks (Fig. 4b). Interestingly in this case it was impossible to reconstruct the signal of the bitopic ligand by applying the single fragments, suggesting, that the inverse signal is likely mechanistically different to the agonistic signal. Interestingly at the M_2 mAChR, iperoxo-based bitopic ligands have been shown to bind in at least two different binding poses[30] and one of them was shown to be purely allosteric. This has recently been further investigated by molecular modeling.[33] In an attempt to further investigate the inverse FRET signal mechanistically, the set of compounds **4-C4** to **4-C10**, consisting of the allosteric moiety, was investigated. Here a linker moiety of different length and a tertiary amine are combined to imitate the positively charged amine of the orthosteric ligand (Scheme 2) in the presence of the allosteric moiety. Figure 4c displays a representative FRET trace recorded for a single cell that was super-fused with the indicated ligands. Increasing linker length lead to the appearance of an inverse signal for compound **4-C8** and **4-C10** even in the absence of the orthosteric moiety similar to the signal observed for compound **5-C10** or **6-C10**. This result supports the notion of an alternative second binding pose for the linker extended bitopic ligands at the M_1 receptor, as recently described for the M_2 receptor.[33]

Concluding remarks

Bitopic ligands are molecular entities, which bind to more than one pharmacological interesting region of membrane proteins and are thought to have an impact on further drug development. This study provides a molecular insight of the interactions between GPCRs and bitopic ligands for a better understanding of ligand receptor interactions on a molecular level. Here, linker dependent responses of bitopic ligands at a M_1 receptor FRET sensor were investigated. The findings indicate an optimal linker length of the bitopic ligands for conformational changes at the M_1 mAChR. This optimal linker length is probably different for each receptor subtype and is likely dependent on the individual receptor architecture. Furthermore, a previously unknown conformational change for GPCRs induced by bitopic

ligands of long linker length was observed. Furthermore, an understanding of the origin of different conformational changes of GPCRs is provided. The influences of the reported movements on the downstream signaling of GPCRs are subjects of current studies. Bitopic ligands were discussed critically due to the fact, whether the lipophilic linker can pass the aromatic lid of muscarinic receptors. Here, it could be shown that an increased linker first hampers the orthoster to induce a conformational change although there is a distinct affinity to the orthosteric binding region. This phenomenon might be due to a steric clash with the aromatic lid structure in muscarinic acetylcholine receptors. Moreover, the findings indicate, that this fact is no longer true for the bitopic derivatives indicating that here the linker is able to pass through this lid like structure.

Methods

Chemistry

Melting points were determined with a Stuart melting point apparatus SMP3 (Bibby Scientific, UK) and are uncorrected. ^{1}H (400.132 MHz) and ^{13}C (100.613 MHz) NMR spectra were recorded on a Bruker AV 400 instrument (Bruker Biospin, Ettlingen, Germany). As internal standard, the signals of the deuterated solvents were used (DMSO-d_6: ^{1}H 2.5 ppm, ^{13}C 39.52 ppm; $CDCl_3$: ^{1}H 7.26 ppm, ^{13}C 77.16 ppm). Abbreviation for data quoted are: s, singlet; d, doublet; t, triplet; q, quartet; m, multiplet; b, broad; dd, doublet of doublets; dt, doublet of triplets; tt, triplet of triplets; tq, triplet of quartets. Coupling constants (*J*) are given in Hz. TLC analyses were performed on commercial pre-coated plates, silica gel 60 F_{254} (Macherey-Nagel, Düren, Germany); spots were further evidenced by spraying with Dragendorff reagent[, 35] for amines. ESI mass spectra of the compounds were obtained on an Agilent LC/MSD Trap G2445D instrument (Waldbronn, Germany). Data are reported as mass-to-charge ratio (*m/z*) of the corresponding positively charged molecular ions. Microwave assisted reactions were carried out on a MLS-rotaPREP instrument (Milestone, Leutkirch, Germany). Chemicals were of analytical grade and purchased from Aldrich (Steinheim, Germany) and Merck (Darmstadt, Germany).

The purities of the compounds (**2-C4**, **2-C6**, **2-C8**, and **2-C10**) were determined using qNMR and were found to be $\geq$95% (method see supporting information). Purity of compounds **1-C2**, **1-C6**, **1-C7**, **1-C8**, **1-C9**, **1-C10**, **5-C4**, and **6-C6** were determined using capillary electrophoresis and were found to be

≥95% (method see supporting information). Compounds **1-C4** and **6-C4** (confirming purity ≥95%) and compounds **5-C8** and **5-C10** (confirming purity ≥90%) were measured on a HPLC system (Agilent 1100 series system with UV detector, Waldbronn, Germany) using a C18 reversed-phase (Knauer, Germany) (150 x 4.6 mm) column. The mobile phase (MeOH/phosphate buffer = 70/30) was used at a flow rate of 1.5 mL/min, detecting at 254 nm. The HPLC analyses of compounds **4-C4** (confirming purity ≥90%) **4-C6**, **4-C8**, **4-C10**, **6-C8**, and **6-C10** (confirming purity >95%) were performed on a LCMS 2020 Shimadzu (Duisburg, Germany). The LCMS-system from Shimadzu Products, contained a DGU-20A3R degassing unit, a LC20AB liquid chromatograph and a SPD-20A UV/Vis detector. Mass spectra were obtained by a LCMS 2020. As stationary phase a Synergi 4U fusion-RP (150 * 4.6 mm) column and as mobile phase a gradient of MeOH/water was used. Parameters for method: Solvent A: water with 0.1% formic acid, solvent B: MeOH with 0.1% formic acid. Solvent B from 0% to 90% in 13 min, then 90% for 5 min, from 90% to 5% in 1 min, then 5% for 4 min. The method was performed with a flow rate of 1.0 mL/min. UV detection was measured at 254 nm.

The compounds **1-C3**, **1-C5**,[11] and **3**[22] as well as **9**, **10-C6**, **11-C6**, and **5-C6**[12] were prepared according to previously reported procedures. The synthesis of the 4-oxo-quinoline skeleton **8**[36, 37] was performed in analogy to the Gould-Jacobs procedure, using diethyl 2-(ethoxymethylene)-malonate for the condensation with 4-fluoroaniline followed by microwave assisted cyclization in diphenyl ether.[19, 20, 21]

3.1.1) General Procedure for the Synthesis of the Iperoxo Derivatives **1-C2**, **1-C4**, **1-C6**, **1-C7**, **1-C8**, **1-C9**, and **1-C10**

To a solution of iperoxo base[10] 0.45 g (2.47 mmol) in 10 mL of acetonitril or chloroform, 5 - 10 equivalents of the corresponding 1-bromoalkane **7-C2** to **7-C10** and a catalytic amount of KI/K_2CO_3 (1:1) were added. The mixture was stirred in a sealed container at a temperature between 55 and 70 °C. The precipitate obtained was filtered and Et_2O was added to complete the precipitation. The solid was washed several times with Et_2O, and dried over P_2O_5 in vacuo.

3.1.2) General Procedure for the Synthesis of the Acetylcholine Derivatives **2-C4**, **2-C6**, **2-C8**, and **2-C10**

To a solution of acetylcholine base 0.50 g (3.81 mmol) in acetonitrile (10 mL), 2 equiv. of the corresponding bromoalkane **7-C4**, **7-C6**, **7-C8**, and **7-C10** and a catalytic amount of KI/K_2CO_3 (1:1) were

added. The reaction mixture was heated in the microwave (500 W, 70 °C) for 4 h. After cooling to room temperature the surplus of KI/K_2CO_3 was filtered and the filtrate was evaporated to the half of the volume. After addition of Et_2O, a viscose oil was formed. The solvent was decanted and the product obtained was dried in vacuo.

3.1.3) General Procedure for the Synthesis of the Quinolone Derivatives **4-C4**, **4-C6**, **4-C8**, and **4-C10**

To a solution of bromoalkyl 4-oxo-quinoline-3-carboxamides **11-C4**, **11-C6**, **11-C8**, and **11-C10** (0.11 mmol) in acetonitrile (5 mL), trimethylamine (45% in H_2O, 0.22 mmol) was added. The reaction was heated at 40 °C. After completion of the reaction (5 h) controlled by TLC (CH_2Cl_2/MeOH = 85:15, R_f = 0.10 – 0.45), the mixture was cooled to room temperature. The solvent was distilled off. The so obtained solid was crystallized from acetonitrile, filtered and dried in vacuo.

*3.1.4) General Procedure for the Synthesis of the Quinolone-Iperoxo Hybrids **5-C4**, **5-C8**, and **5-C10***

To a solution of 1 equiv. of the bromoalkyl 4-oxo-quinoline-3-carboxamides **11-C4**, **11-C8**, and **11-C10** in 20 mL acetonitrile, 2 equiv. iperoxo base[10] and a catalytic amount of KI/K_2CO_3 (1:1) were added. The reaction mixture was heated in the microwave (500 W, 80 °C) for 4 h. The reaction was monitored by TLC (MeOH/NH_4NO_2 (0.2 M) = 3:2, R_f = 0.54 – 0.68). After cooling to room temperature the surplus of KI/K_2CO_3 was filtered. Et_2O was added to the filtrate to obtain a precipitation. The solid was filtered, washed with Et_2O and dried in vacuo.

3.1.5) General Procedure for the Synthesis of the Quinolone-Acetylcholine Hybrids **6-C4**, **6-C6**, **6-C8**, and **6-C10**

To a solution of 1 equiv. of the bromoalkyl 4-oxo-quinoline-3-carboxamides **11-C4**, **11-C8**, and **11-C10** in 15 mL acetonitrile, 2 equiv. acetylcholine base and a catalytic amount of KI/K_2CO_3 (1:1) were added. The reaction mixture was heated in the microwave (500 W, 80 °C) for 4.0 – 6.5 h. After cooling to room temperature the surplus of KI/K_2CO_3 was filtered and Et_2O was added to the filtrate. The solid obtained was filtered, washed with Et_2O and dried in vacuo.

Pharmacology

3.2.1) Construction of the *h*M_1 receptor FRET sensor

Muscarinic ACh receptor construct was C-terminally fused to the enhanced variants of cyan fluorescent protein (eCFP) (BD Bioscience Clontech, Heidelberg, Germany) by standard PCR extension overlap technique.[38] The amino acid sequence SR, coding for an Xba I restriction site, was inserted as a linker sequence between receptor and fluorescent protein. In the third intracellular loop (IL3) an amino acid motif was introduced, thus the novel sequence reads QG227CCPGCCSGS228E. It specifically binds the fluorescein arsenical hairpin binder (FlAsH) and codes for a restriction site. The construct was cloned into pcDNA3 (Invitrogen) and verified by sequencing, done by Eurofins Genomics (Ebersberg, Germany).

3.2.2) Stable cell line generation

Cells were seeded into a culture dish with a confluency of 30% three hours before transfecting the cells with the Effectene® reagent ordered from Quiagene. Reagent concentration and incubation times were applied in accordance with the manufacturer's instructions. 24 hours after transfecting the normal culture medium was replaced by culture medium supplemented with 400 µg/mL G-418. After that the medium was refreshed every day until all untransfected cells died. Now the cells were counted, diluted and applied to 48-well plates resulting in a one cell to well distribution. This homogenous cell population were characterized with fluorescence microscopy and were investigated concerning their cDNA content.

3.2.3) Cell culture

HEK293 cells stably expressing the *h*M_1 receptor FRET sensor were maintained in DMEM with 4.5 g l 1, 10% (v/v) FCS, 100 U mL-1 penicillin, 100 µg mL-1 streptomycin sulfate and 2 mM L-glutamine and 200 µg mL 1 G-418. The cells were kept at 37 °C in a humidified 7% CO_2 atmosphere and were routinely passaged every two to three days. Untransfected HEK cells maintained in cell culture medium without G-418.

3.2.4) FlAsH labeling

A labeling protocol was applied as described previously.[14, 39, 40] In brief, cells were grown to near confluency on Poly-D-lysin coated glass coverslips. Initially cells were washed with labeling buffer

(150 mM NaCl, 10 mM HEPES, 2.5 mM KCl, 4 mM $CaCl_2$, 2mM $MgCl_2$ supplemented with 10 mM glucose (pH 7.3)). After that cells were incubated with labeling buffer containing 500 nM FlAsH and 12.5 µM 1,2-ethanedithiol (EDT) for 1 h at 37 °C followed by flushing with labeling buffer. To reduce non-specific FlAsH binding, the cells were incubated for 10 min with labeling buffer containing 250 µM EDT. After flushing with labeling buffer the cells were held in cell culture medium.

3.2.5) Ligand application

The reference ligands were prepared from 1 mM stock solutions that were stored at -20 °C, taking into consideration, that at least acetylcholine remains instable in solution.[41] Used stock solutions have not been older than a couple of weeks. Bitopic ligands or derivatives were stored at 4 °C and were weighed out directly before the experiment. Than the ligands were solubilized in measuring buffer (140 mM NaCl, 10 mM HEPES, 5.4 mM KCl, 2 mM $CaCl_2$, 1 mM $MgCl_2$ (pH 7.3)) to a final concentration of 100 µM.

3.2.6) Single cell FRET experiments

FRET measurements were performed using a Zeiss Axiovert 200 inverted microscope endued with a PLAN-Neoflar oil immersion 100-objective, a dual emission photometric system and a Polychrome IV light source (Till Photonica, Gräfelfig, Germany) as described previously.[14, 13] Experiments were conducted at 25 °C using live HEK293 cells stably expressing the *h*M_1 receptor FRET-sensor that were maintained in assay buffer. Single cells were excited at 436 nm (dichroic 460 nm) with a frequency of 10 Hz. Emitted light was recorded using 535/30 nm and 480/40 nm emission filters and a DCLP 505 nm beam splitter for FlAsH and CFP, respectively. FRET was observed as the ratio of FlAsH/CFP, which was corrected offline for bleed through, direct FlAsH excitation and photo bleaching using the 2015 version of the Origin software as described recently. To investigate changes in FRET on ligand addition, cells were continuously super fused with FRET buffer complemented with various ligands in saturating concentrations as indicated. Superfusion was done using the ALA-VM8 (ALA Scientifi Instruments).

3.2.7) Data processing

Data are shown as means ± s.e.m. for n independent observations. Fluorescence intensities were acquired using Clampex (Axon Instruments). Statistical analysis and curve fitting were performed using Origin (OriginLab).

Supporting Information

More detailed syntheses, elemental analyses data and spectral data of intermediate and target compounds as well as calcium measurement procedure description and supporting figures.

Acknowledgements

K.M. and V.D. were supported by the international doctoral college “Receptor Dynamics: Emerging Paradigms for Novel Drugs” funded within the framework of the Elite Network of Bavaria. M.C.A.C. was supported by the Marie Curie Initial Training Networks (ITN) “WntsApp” grant agreement number 608180. We thank Montana Molecular and Dr. Anne Marie Quinn for technical support and help to use the dual sensor

Supporting Information

FRET Studies of Rational Designed Quinolone Based Bitopic Ligands and their Derivatives: A Systematic Approach of Partial Agonism and Allosteric Modulation on the Muscarinic M_1 Acetylcholine Receptor

Regina Messerer[a, ǂ], Michael Kauk[b, c, ǂ], Daniela Volpato[a], Maria Consuelo Alonso Canizal[b, c], Jessika Klöckner[a], Ulrike Zabel[b, c], Susanne Nuber[b, c], Carsten Hoffmann[b, c, *] and Ulrike Holzgrabe[a, *]

[a] Department of Pharmaceutical Chemistry, Institute of Pharmacy, University of Würzburg, Am Hubland, 97074 Würzburg, Germany

[b] Department of Pharmacology and Toxicology, University of Würzburg, Versbacher Str. 9, 97078 Würzburg, Germany

[c] Rudolf Virchow Center for Experimental Biomedicine, University of Würzburg, Josef Schneider Straße 2, 97080 Würzburg, Germany

Table of Contents

Methods

The purities of the compounds (2-C4, 2-C6, 2-C8, and 2-C10) were determined using qNMR and were found to be $\geq$95%. 1,2,4,5-Tetrachloro-3-nitrobenzene (Sigma Aldrich, Steinheim, Germany) was chosen as internal standard. qNMR data were acquired at 90° pulse tip angles with recovery delays of 60 s and acquisition time of 3.7 s in a non-spinning mode at a calibrated probe temperature of 300 K. Sixteen scans of 64 K data points for FID were acquired with a spectral width of 8012 Hz (16 ppm). Manuel phase and baseline correction were performed prior to integration. Preliminary data processing was carried out with Bruker software, TOPSPIN 3.0. Purity of compounds 1-C2, 1-C6, 1-C7, 1-C8, 1-C9, 1-C10, 5-C4, and 6-C6 were determined using capillary electrophoresis and were found to be $\geq$95%. The CE measurements were performed by means of a Beckman Coulter P/ACE System MDQ

(Fullerton, CA, USA), equipped with a diode array detector measuring at wavelengths of 210 nm and 254 nm. A fused silica capillary (effective length 50.0 cm, total length 60.2 cm, inner diameter 50 µm) was used for the separation. A new capillary was conditioned by rinsing for 30 min with 0.1 mol/L NaOH, 2 min with H_2O, 10 min with 0.1 mol/L HCl and 2 min with H_2O. Before each run the capillary was rinsed for 2 min with H_2O and 5 min with the running buffer. All rinsing steps were performed with a pressure of 30.0 psi. The samples were injected with a pressure of 0.5 psi for 5.0 s at the anodic side of the capillary. The capillary was kept at 25 °C and a voltage of +25 kV was applied. A 50 mM aqueous sodium borate, pH 10.5, was prepared as running buffer, using ultrapure Milli-Q water (Millipore, Milford, MA, USA). The aqueous solutions were filtered through a 0.22 µm pore-size CME (cellulose mix ester) filter (Carl Roth GmbH, Karlsruhe, Germany). Purity of all other target compounds were determined on two HPLC systems.

Chemistry

4-((4,5-Dihydroisoxazol-3-yl)oxy)-N-ethyl-N,N-dimethylbut-2-yn-1-aminium bromide ***1-C2***

Beige powder; 89% yield; mp 108-110 °C; ^{1}H NMR (DMSO): 1.26 (t, 3H, CH_2-C**H$_3$**, *J* = 7.2), 3.02 (t, 2H, **H**-4$_{2\text{-isox}}$, *J* = 9.6), 3.08 (s, 6H, $^+$N(C**H$_3$**)$_2$), 3.45 (m, 2H, N$^+$-C**H$_2$**-CH_3), 4.32 (t, 2H, **H**-5$_{2\text{-isox}}$, *J* = 9.6), 4.50 (s, 2H, ≡C-C**H$_2$**-N$^+$), 4.93 (s, 2H, O-C**H$_2$**-C≡). ^{13}C NMR (DMSO): 7.8, 32.1, 49.1, 52.8, 57.1, 58.7, 69.5, 76.1, 85.7, 166.6. MS (ESI) m/z [M]$^+$ Calcd for $C_{11}H_{20}BrN_2O_2^+$ 211.3. Found: 221.2. CE purity 99.1%.

N-Butyl-4-((4,5-Dihydroisoxazol-3-yl)oxy)-N,N-dimethylbut-2-yn-1-aminium bromide ***1-C4***

White solid; 65% yield; mp 110-112 °C; ^{1}H NMR (DMSO): 0.93 (t, 3H, CH_2-C**H$_3$**, *J* = 7.5), 1.27-1.36 (m, 2H, CH_2-CH_2-C**H$_2$**-CH_3), 1.62-1.70 (m, 2H, CH_2-C**H$_2$**-CH_2-CH_3), 3.02 (t, 2H, **H**-4$_{2\text{-isox}}$, *J* = 9.5), 3.09 (s, 6H, $^+$N(C**H$_3$**)$_2$), 3.36-3.39 (m, 2H, N$^+$-C**H$_2$**-CH_2), 4.32 (t, 2H, **H**-5$_{2\text{-isox}}$, *J* = 9.47), 4.49 (s, 2H, ≡C-C**H$_2$**-N$^+$), 4.93 (s, 2H, O-C**H$_2$**-C≡). ^{13}C NMR (DMSO): 13.4, 19.1, 23.8, 32.2, 49.8, 53.3, 57.2, 63.0, 69.6, 76.2, 86.0, 166.7. MS (ESI) m/z [M]$^+$ Calcd for $C_{13}H_{23}N_2O_2^+$: 239.2. Found: 239.2. HPLC purity 96.1%.

N-(4-((4,5-Dihydroisoxazol-3-yl)oxy)but-2-yn-1-yl)-N,N-dimethylhexan-1-aminium bromide ***1-C6***

White solid, 85% yield; mp 121-122 °C; ^{1}H NMR (DMSO): 0.88 (t, 3H, CH_2-C**H$_3$**, *J* = 6.6), 1.30 (br, 6H, CH_2-CH_2-C**H$_2$**-C**H$_2$**-C**H$_2$**-CH_3), 1.62-1.73 (m, 2H, CH_2-C**H$_2$**-CH_2-CH_2-CH_2-CH_3), 3.01 (t, 2H, **H**-4$_{2\text{-isox}}$, *J* = 9.6), 3.09 (s, 6H, $^+$N(C**H$_3$**)$_2$), 3.33-3.38 (m, 2H, N$^+$-C**H$_2$**-CH_2), 4.32 (t, 2H, **H**-5$_{2\text{-isox}}$, *J* = 9.6), 4.48 (s, 2H, ≡C-C**H$_2$**-N$^+$), 4.93 (s, 2H, O-C**H$_2$**-C≡). ^{13}C NMR (DMSO): 13.7, 21.6, 21.7, 25.2, 30.5, 32.1, 49.7, 53.1, 57.1, 63.1, 69.5, 76.1, 85.8, 166.6. MS (ESI) m/z [M]$^+$ Calcd for $C_{15}H_{27}N_2O_2^+$: 267.2. Found: 267.3. CE purity 99.5%.

N-(4-((4,5-Dihydroisoxazol-3-yl)oxy)but-2-yn-1-yl)-N,N-dimethylheptan-1-aminium bromide ***1-C7***

White solid; 74% yield; mp 121-122 °C; ^{1}H NMR (DMSO): 0.87 (t, 3H, CH_2-C**H$_3$**, *J* = 6.8), 1.25-1.33 (br, 8H, CH_2-CH_2-C**H$_2$**-C**H$_2$**-C**H$_2$**-C**H$_2$**-CH_3), 1.63-1.72 (m, 2H, CH_2-C**H$_2$**-CH_2-CH_2-CH_2-CH_2-CH_3), 3.01 (t, 2H, **H**-4$_{2\text{-isox}}$, *J* = 9.6), 3.07 (s, 6H, $^+$N(C**H$_3$**)$_2$), 3.34-3.37 (m, 2H, N$^+$-C**H$_2$**-CH_2), 4.32 (t, 2H, **H**-5$_{2\text{-isox}}$, *J* = 9.6), 4.45 (s, 2H, ≡C-C**H$_2$**-N$^+$), 4.93 (s, 2H, O-C**H$_2$**-C≡). ^{13}C NMR (DMSO): 13.8, 20.8, 21.7, 21.9, 25.5, 28.0, 32.2, 49.7, 53.2, 57.1, 63.1, 69.5, 76.1, 85.9, 166.6. MS (ESI) m/z [M]$^+$ Calcd for $C_{16}H_{29}N_2O_2^+$: 281.2. Found: 281.3. CE purity 99.5%.

N-(4-((4,5-Dihydroisoxazol-3-yl)oxy)but-2-yn-1-yl)-N,N-dimethyloctan-1-aminium bromide ***1-C8***

White solid; 48% yield; mp 130-133 °C; ^{1}H NMR (DMSO): 0.87 (t, 3H, CH_2-C**H$_3$**, *J* = 6.9) , 1.23-1.33 (br, 10H, CH_2-CH_2-C**H$_2$**-C**H$_2$**-C**H$_2$**-C**H$_2$**-C**H$_2$**-CH_3), 1.63-1.71 (m, 2H, CH_2-C**H$_2$**-CH_2-CH_2-CH_2-CH_2-CH_2-CH_3), 3.01 (t, 2H, **H**-4$_{2\text{-isox}}$, *J* = 9.6), 3.07 (s, 6H, $^+$N(C**H$_3$**)$_2$), 3.33-3.37 (m, 2H, N$^+$-C**H$_2$**-CH_2), 4.32 (t, 2H, **H**-5$_{2\text{-isox}}$, *J* = 9.6), 4.45 (s, 2H, ≡C-C**H$_2$**-N$^+$), 4.93 (s, 2H, O-C**H$_2$**-C≡). ^{13}C NMR (DMSO): 13.8, 21.7, 21.9, 25.6, 28.3, 31.0, 32.1, 49.7, 53.2, 57.1, 63.1, 69.5, 76.1, 85.9, 166.6. MS (ESI) m/z [M]$^+$ Calcd for $C_{17}H_{31}N_2O_2^+$: 295,2. Found: 295.3. CE purity 99.1%.

N-(4-((4,5-Dihydroisoxazol-3-yl)oxy)but-2-yn-1-yl)-N,N-dimethylnonan-1-aminium bromide ***1-C9***

White solid; 80% yield; mp 130-132 °C; ^{1}H NMR (DMSO): 0.86 (t, 3H, CH_2-C**H$_3$**, *J* = 6.7), 1.26 (br, 12H, CH_2-CH_2-C**H$_2$**-C**H$_2$**-C**H$_2$**-C**H$_2$**-C**H$_2$**-C**H$_2$**-CH_3), 1.62-1.71 (m, 2H, CH_2-C**H$_2$**-CH_2-CH_2-CH_2-CH_2-CH_2-CH_2-CH_3), 3.01 (t, 2H, **H**-4$_{2\text{-isox}}$, *J* = 9.6), 3.08 (s, 6H, $^+$N(C**H$_3$**)$_2$), 3.33-3.37 (m, 2H, N$^+$-C**H$_2$**-CH_2), 4.32 (t, 2H, **H**-5$_{2\text{-isox}}$, *J* = 9.6), 4.48 (s, 2H, ≡C-C**H$_2$**-N$^+$), 4.93 (s, 2H, O-C**H$_2$**-C≡). ^{13}C NMR (DMSO): 13.8, 21.7, 22.0, 25.6, 28.3, 28.6, 31.1, 32.1, 49.7, 53.2, 57.1, 63.1, 69.5, 76.1, 85.8, 166.6. MS (ESI) m/z [M]$^+$ Calcd for $C_{18}H_{33}N_2O_2^+$: 309.3. Found: 309.4. CE purity 98.8%.

N-(4-((4,5-Dihydroisoxazol-3-yl)oxy)but-2-yn-1-yl)-N,N-dimethyldecan-1-aminium bromide ***1-C10***

White solid; 83% yield; mp 135-137 °C; ^{1}H NMR (DMSO): 0.86 (t, 3H, CH_2-C**H$_3$**, *J* = 6.9), 1.26 (br, 14H, CH_2-CH_2-C**H$_2$**-C**H$_2$**-C**H$_2$**-C**H$_2$**-C**H$_2$**-C**H$_2$**-C**H$_2$**-CH_3), 1.67 (br, 2H, CH_2-C**H$_2$**-CH_2-CH_2-CH_2-CH_2-CH_2-CH_2-CH_2-CH_3), 3.01 (t, 2H, **H**-4$_{2\text{-isox}}$, *J* = 9.6), 3.08 (s, 6H, $^+$N(C**H$_3$**)$_2$), 3.33-3.37(m, 2H, N$^+$-C**H$_2$**-CH_2), 4.32 (t, 2H, **H**-5$_{2\text{-isox}}$, *J* = 9.6), 4.47 (s, 2H, ≡C-C**H$_2$**-N$^+$), 4.93 (s, 2H, O-C**H$_2$**-C≡). ^{13}C NMR (DMSO): 13.8, 21.7, 22.0, 25.6, 28.3, 28.5, 28.6, 28.7, 31.2, 32.1, 49.7, 53.1, 57.1, 63.1, 69.5, 76.1, 85.8, 166.6. MS (ESI) m/z [M]$^+$ Calcd for $C_{19}H_{35}N_2O_2^+$: 323.3. Found: 323.3 CE purity 99.8%.

N-(2-Acetoxyethyl)-N,N-dimethylbutan-1-aminium bromide ***2-C4***

White, viscose oil; yield 71%; ^{1}H NMR (DMSO): 0.93 (t, 3H, CH_2-C**H$_3$**, *J* = 7.2), 1.26-1.35 (m, 2H, CH_2-CH_2-C**H$_2$**-CH_3), 1.62-1.70 (m, 2H, CH_2-C**H$_2$**-CH_2-CH_3), 2.06 (s, 3H, CO-C**H$_3$**), 3.08 (s, 6H, $^+$N(C**H$_3$**)$_2$),

3.33-3.37 (m, 2H, $^{+}$N-C**H$_2$**-CH$_2$), 3.63-3.65 (m, 2H, C**H$_2$**-N^{+}), 4.42 (t, 2H, O-C**H$_2$**, *J* = 4.4). ^{13}C NMR (DMSO): 13.4, 19.1, 20.6, 23.6, 50.5, 57.4, 61.2, 63.6, 169.7. MS (ESI) m/z [M]$^{+}$ Calcd for $C_{10}H_{22}NO_2^{+}$: 188.2. Found: 188.2. qNMR purity 98.0%.

N-(2-Acetoxyethyl)-N,N-dimethylhexan-1-aminium bromide ***2-C6***

Transparent, viscose oil; yield 65%; ^{1}H NMR (DMSO): 0.88 (t, 3H, CH$_2$-C**H$_3$**, *J* = 6.8), 1.25-1.32 (m, 6H, CH$_2$-CH$_2$-C**H$_2$**-C**H$_2$**-C**H$_2$**-CH$_3$), 1.63-1.70 (m, 2H, CH$_2$-C**H$_2$**-CH$_2$-CH$_2$-CH$_2$-CH$_3$), 2.06 (s, 3H, CO-C**H$_3$**), 3.07 (s, 6H, $^{+}$N(C**H$_3$**)$_2$), 3.34-3.39 (m, 2H, $^{+}$N-C**H$_2$**-CH$_2$), 3.62-3.65 (m, 2H, C**H$_2$**-N^{+}), 4.41 (t, 2H, O-C**H$_2$**, *J* = 4,6). ^{13}C NMR (DMSO): 13.7, 20.6, 21.6, 21.7, 25.3, 30.6, 50.5, 57.4, 61.2, 63.8, 169.7. MS (ESI) m/z [M]$^{+}$ Calcd for $C_{12}H_{26}NO_2^{+}$: 216.2. Found: 216.2. qNMR purity 96.0%.

N-(2-Acetoxyethyl)-N,N-dimethyloctan-1-aminium bromide ***2-C8***

White, viscose oil; yield 91%; ^{1}H NMR (DMSO): 0.86 (t, 3H, CH$_2$-C**H$_3$**, *J* = 6.8), 1.26-1.29 (m, 10H, CH$_2$-CH$_2$-C**H$_2$**-C**H$_2$**-C**H$_2$**-C**H$_2$**-C**H$_2$**-CH$_3$), 1.63-1.70 (m, 2H, CH$_2$-C**H$_2$**-CH$_2$-CH$_2$-CH$_2$-CH$_2$-CH$_2$-CH$_3$), 2.05 (s, 3H, CO-C**H$_3$**), 3.08 (s, 6H, $^{+}$N(C**H$_3$**)$_2$), 3.33-3.37 (m, 2H, $^{+}$N-C**H$_2$**-CH$_2$), 3.63-3.66 (m, 2H, C**H$_2$**-N^{+}), 4.41 (t, 2H, O-C**H$_2$**, *J* = 4,6 Hz). ^{13}C NMR (DMSO): 13.8, 20.6, 21.6, 21.9, 25.6, 28.3, 31.0, 50.5, 57.4, 61.2, 63.8, 169.7. MS (ESI) m/z [M]$^{+}$ Calcd for $C_{14}H_{30}NO_2^{+}$: 244.2. Found: 244.3. qNMR purity 96.0%.

N-(2-Acetoxyethyl)-N,N-dimethyldecan-1-aminium bromide ***2-C10***

White, viscose oil; yield 88%; ^{1}H NMR (DMSO): 0.86 (t, 3H, CH$_2$-C**H$_3$**, *J* = 6.8), 1.26-1.28 (m, 14H, CH$_2$-CH$_2$-C**H$_2$**-C**H$_2$**-C**H$_2$**-C**H$_2$**-C**H$_2$**-C**H$_2$**-C**H$_2$**-CH$_3$), 1.63-1.70 (m, 2H, CH$_2$-C**H$_2$**-CH$_2$-CH$_2$-CH$_2$-CH$_2$-CH$_2$-CH$_2$-CH$_2$-CH$_3$), 2.05 (s, 3H, CO-C**H$_3$**), 3.07 (s, 6H, $^{+}$N(C**H$_3$**)$_2$), 3.32-3.35 (m, 2H, $^{+}$N-C**H$_2$**-CH$_2$), 3.62-3.64 (m, 2H, C**H$_2$**-N^{+}), 4.41 (t, 2H, O-C**H$_2$**, *J* = 4.6). ^{13}C NMR (DMSO): 13.8, 20.5, 21.6, 22.0, 25.6, 28.4, 28.5, 28.7, 28.8, 31.2, 50.5, 57.4, 61.2, 63.8, 169.7. MS (ESI) m/z [M]$^{+}$ Calcd for $C_{16}H_{34}NO_2^{+}$: 272.3. Found: 272.3. qNMR purity 96.0%.

General Procedure for the Amidation of **10-C4**, **10-C8**, and **10-C10**

1 equiv. of ethyl 1-benzyl-6-fluoro-4-oxo-1,4-dihydroquinoline-3-carboxylate **9**[1] was reacted with 3 equiv. of 4-aminobutanol, 8-aminooctanol and 10-aminodecanol, respectively, and heated to 150 °C to melt the ester. The reaction was followed up by TLC (CH_2Cl_2/MeOH = 20:1, R_f = 0.35 – 0.54). After completion of the reaction (1.0 – 3.5 h), the mixture was cooled to room temperature. The so obtained solid was crystallized in ethanol and recrystallized from methanol.

1-Benzyl-6-fluoro-N-(4-hydroxybutyl)-4-oxo-1,4-dihydroquinoline-3-carboxamide ***10-C4***

White solid; yield 28%; mp 163-165 °C; R_f = 0.35 (CH_2Cl_2/MeOH = 20:1); ^{1}H NMR (DMSO): 1.47-1.61 (m, 4H, NH-CH$_2$-C**H$_2$**-C**H$_2$**), 3.34-3.46 (m, 4H, NH-C**H$_2$**/C**H$_2$**-OH), 4.42 (t, 1H, O**H**, *J* = 5.2), 5.80 (s, 2H, C**H$_2$**$_{benzyl}$), 7.21-7.24 (m, 2H, C**H**$_{phenyl}$), 7.27-7.37 (m, 3H, C**H**$_{phenyl}$), 7.67 (ddd, 1H, **H**-7, *J* = 3.1, J_{HF} = 8.0, *J* = 9.4), 7.84 (dd, 1H, **H**-8, J_{HF} = 4.3, *J* = 9.4), 7.99 (dd, 1H, **H**-5, *J* = 3.1, J_{HF} = 9.1), 9.08 (s, 1H, **H**-2),

9.88 (t, 1H, N**H**, J = 5.7). ^{13}C NMR (DMSO): 25.9, 29.9, 38.2, 56.0, 60.3, 110.5 (d, J_{CF} = 22.7), 110.7, 120.9 (d, J_{CF} = 8.4), 121.3 (d, J_{CF} = 25.0), 126.4, 127.9, 128.9, 128.9 (d, J_{CF} = 6.9), 135.7, 135.9, 148.7, 159.1 (d, J_{CF} = 245.3), 163.6, 174.7 (d, J_{CF} = 2.6).

1-Benzyl-6-fluoro-N-(8-hydroxyoctyl)-4-oxo-1,4-dihydroquinoline-3-carboxamide ***10-C8***

White solid; yield 28%; mp 154-156 °C; R_f = 0.54 (CH_2Cl_2/MeOH = 20:1); ^{1}H NMR (DMSO): 1.28-1.37 (m, 8H, NH-CH_2-CH_2-C**H₂**-C**H₂**-C**H₂**-C**H₂**), 1.39-1.42 (m, 2H, NH-CH_2-C**H₂**), 1.50-1.57 (m, 2H, C**H₂**-CH_2-OH), 3.33-3.39 (m, 4H, NH-C**H₂**/C**H₂**-OH), 4.30 (t, 1H, O**H**, J = 5.0), 5.80 (s, 2H, C**H₂**$_{benzyl}$), 7.21-7.23 (m, 2H, C**H**$_{phenyl}$), 7.27-7.37 (m, 3H, C**H**$_{phenyl}$), 7.67 (ddd, 1H, **H**-7, J = 3.1, J_{HF} = 8.0, J = 9.4), 7.84 (dd, 1H, **H**-8, J_{HF} = 4.4, J = 9.4), 7.99 (dd, 1H, **H**-5, J = 3.1, J_{HF} = 9.05), 9.08 (s, 1H, **H**-2), 9.87 (t, 1H, N**H**, ^3J = 5.6). ^{13}C NMR (DMSO): 25.4, 26.4, 28.7, 28.8, 29.2, 32.4, 38.3, 56.0, 60.6, 110.5 (d, J_{CF} = 22.4), 110.7, 120.9 (d, J_{CF} = 8.4), 121.3 (d, J_{CF} = 24.8), 126.4, 127.8, 128.9, 128.9 (d, J_{CF} = 7.2), 135.7, 135.8, 148.7, 159.1 (d, J_{CF} = 245.0), 163.6, 174.7 (d, J_{CF} = 2.5).

1-Benzyl-6-fluoro-N-(10-hydroxydecyl)-4-oxo-1,4-dihydroquinoline-3-carboxamide ***10-C10***

White solid; yield 31%; mp 152-154 °C; R_f = 0.37 (CH_2Cl_2/MeOH = 20:1); ^{1}H NMR (DMSO): 1.25-1.40 (m, 14H, NH-CH_2-C**H₂**-C**H₂**-C**H₂**-C**H₂**-C**H₂**-C**H₂**-C**H₂**), 1.50-1.55 (m, 2H, C**H₂**-CH_2-OH), 3.35-3.38 (m, 4H, NH-C**H₂**/C**H₂**-OH), 4.30 (t, 1H, O**H**, J = 5.0), 5.80 (s, 2H, C**H₂**$_{benzyl}$), 7.21-7.23 (m, 2H, C**H**$_{phenyl}$), 7.27-7.37 (m, 3H, C**H**$_{phenyl}$), 7.66 (ddd, 1H, **H**-7, J = 3.1, J_{HF} = 8.0, J = 9.4), 7.84 (dd, 1H, **H**-8, J_{HF} = 4.4, J = 9.4), 7.99 (dd, 1H, **H**-5, J = 3.1, J_{HF} = 9.05), 9.08 (s, 1H, **H**-2), 9.87 (t, 1H, N**H**, J = 5.6). ^{13}C NMR (DMSO): 25.4, 26.4, 28.6, 28.8, 28.9, 29.0, 29.1, 32.4, 38.3, 56.0, 60.6, 110.5 (d, J_{CF} = 22.9), 110.7, 120.9 (d, J_{CF} = 8.0), 121.3 (d, J_{CF} = 25.3), 126.4, 127.8, 128.9, 128.9 (d, J_{CF} = 6.8), 135.7, 135.8, 148.7, 159.1 (d, J_{CF} = 245.1), 163.6, 174.7 (d, J_{CF} = 2.6).

General Procedure for the Substitution of the Alcohol group with a Bromine group, Compounds **11-C4**, **11-C8**, and **11-C10**

1 equiv. of hydroxyalkyl fluoro substituted 4-oxo-quinolinecarboxamides **10-C4**, **10-C8**, and **10-C10**, respectively, were dissolved in 10 equiv. of aqueous HBr (48%). Then, 4.2 equiv. of conc. sulfuric acid was carefully added, and the reaction mixture was heated to reflux. The reaction was followed up by TLC (CH_2Cl_2/MeOH = 20:1, R_f = 0.81 – 0.95). After completion of the reaction (3.0 – 6.0 h), the solution was poured into water and extracted several times with chloroform. The combined organic phases were neutralized with K_2CO_3 and the solvent was evaporated to obtain the desired products.

1-Benzyl-N-(4-bromobutyl)-6-fluoro-4-oxo-1,4-dihydroquinoline-3-carboxamide ***11-C4***

White solid; yield 93%; mp 165-167 °C; R_f = 0.84 (CH_2Cl_2/MeOH = 20:1); ^{1}H NMR (DMSO): 1.64-1.71 (m, 2H, NH-CH_2-C**H₂**), 1.85-1.92 (m, 2H, NH-CH_2-CH_2-C**H₂**), 3.39 (dd, 2H, NH-C**H₂**, J = 6.9, J = 12.9), 3.59 (t, 2H, C**H₂**-Br, J = 6.7), 5.80 (s, 2H, C**H₂**$_{benzyl}$), 7.21-7.37 (m, 5H, C**H**$_{phenyl}$), 7.67 (ddd, 1H, **H**-7, J = 3.1, J_{HF} = 7.9, J = 9.4), 7.84 (dd, 1H, **H**-8, J_{HF} = 4.4, J = 9.4), 7.99 (dd, 1H, **H**-5, J = 3.1, J_{HF} = 9.1), 9.08

(s, 1H, **H**-2), 9.90 (t, 1H, N**H**, *J* = 5.8). ^{13}C NMR (DMSO): 28.0, 29.8, 34.7, 37.4, 56.0, 110.5 (d, J_{CF} = 22.7), 110.7, 120.9 (d, J_{CF} = 7.6), 121.3 (d, J_{CF} = 24.5), 126.4, 127.9, 128.9, 128.9 (d, J_{CF} = 7.0), 135.7, 135.9, 148.8, 159.1 (d, J_{CF} = 245.2), 163.8, 174.7 (d, J_{CF} = 2.5 Hz).

1-Benzyl-N-(8-bromooctyl)-6-fluoro-4-oxo-1,4-dihydroquinoline-3-carboxamide ***11-C8***

White solid; yield 88%; mp 168-171 °C; R_f = 0.81 (CH_2Cl_2/MeOH = 20:1); ^{1}H NMR (DMSO): 1.28-1.41 (m, 8H, NH-CH_2-CH_2-C**H$_2$**-C**H$_2$**-C**H$_2$**-C**H$_2$**), 1.51-1.57 (m, 2H, NH-CH_2-C**H$_2$**), 1.75-1.82 (m, 2H, C**H$_2$**-CH_2-Br), 3.33-3.37 (m, 2H, NH-C**H$_2$**), 3.51 (t, 2H, C**H$_2$**-Br, *J* = 6.8), 5.80 (s, 2H, C**H$_{2\text{benzyl}}$**), 7.21-7.37 (m, 5H, C**H**$_{\text{phenyl}}$), 7.66 (ddd, 1H, **H**-7, *J* = 3.1, J_{HF} = 8.0, *J* = 9.4), 7.84 (dd, 1H, **H**-8, J_{HF} = 4.4, *J* = 9.4), 7.99 (dd, 1H, **H**-5, *J* = 3.1, J_{HF} = 9.1), 9.08 (s, 1H, **H**-2), 9.87 (t, 1H, N**H**, *J* = 5.6 Hz). ^{13}C NMR (DMSO): 26.3, 27.4, 27.9, 28.4, 29.1, 33.1, 35.1, 38.2, 56.0, 110.4 (d, J_{CF} = 22.6), 110.7, 120.9 (d, J_{CF} = 8.4), 121.3 (d, J_{CF} = 24.9), 126.4, 127.8, 128.8, 128.9 (d, J_{CF} = 7.0), 135.7, 135.8, 148.7, 159.1 (d, J_{CF} = 245.2), 163.6, 174.7 (d, J_{CF} = 2.6).

1-Benzyl-N-(10-bromodecyl)-6-fluoro-4-oxo-1,4-dihydroquinoline-3-carboxamide ***11-C10***

White solid; yield 73%; mp 147-150 °C; R_f = 0.95 (CH_2Cl_2/MeOH = 20:1); ^{1}H NMR (DMSO): 1.26-1.35 (m, 12H, NH-CH_2-CH_2-C**H$_2$**-C**H$_2$**-C**H$_2$**-C**H$_2$**-C**H$_2$**-C**H$_2$**), 1.50-1.57 (m, 2H, NH-CH_2-C**H$_2$**), 1.73-1.80 (m, 2H, C**H$_2$**-CH_2-Br), 3.35-3.37 (m, 2H, NH-C**H$_2$**), 3.49 (t, 2H, C**H$_2$**-Br, *J* = 6.8), 5.80 (s, 2H, C**H$_{2\text{benzyl}}$**), 7.21-7.37 (m, 5H, C**H**$_{\text{phenyl}}$), 7.66 (ddd, 1H, **H**-7, *J* = 3.1, J_{HF} = 8.0, *J* = 9.4), 7.84 (dd, 1H, **H**-8, J_{HF} = 4.4, *J* = 9.4), 7.99 (dd, 1H, **H**-5, *J* = 3.1, J_{HF} = 9.1), 9.08 (s, 1H, **H**-2), 9.87 (t, 1H, N**H**, *J* = 5.6). ^{13}C NMR (DMSO): 26.4, 27.4, 28.0, 28.5, 28.7, 28.7, 29.1, 32.1, 35.0, 38.3, 56.0, 110.5 (d, J_{CF} = 22.8), 110.7, 120.9 (d, J_{CF} = 8.4), 121.3 (d, J_{CF} = 25.2), 126.4, 127.8, 128.8, 128.9 (d, J_{CF} = 6.9), 135.7, 135.8, 148.7, 159.1 (d, J_{CF} = 244.9), 163.6, 174.7 (d, J_{CF} = 2.7).

4-(1-Benzyl-6-fluoro-4-oxo-1,4-dihydroquinoline-3-carboxamido)-N,N,N-trimethylbutan-1-aminium bromide ***4-C4***

White solid; 53% yield; mp 176-179 °C; R_f = 0.18 (CH_2Cl_2/MeOH = 85:15); ^{1}H NMR (DMSO): 1.58-1.60 (m, 2H, NH-CH_2-C**H$_2$**), 1.74-1.78 (m, 2H, NH-CH_2-CH_2-C**H$_2$**), 3.06 (s, 9H, $^+$N(C**H$_3$**)$_3$), 3.33-3.45 (m, 4H, NH-C**H$_2$**/C**H$_2$**-N^+), 5.81 (s, 2H, C**H$_{2\text{benzyl}}$**), 7.23-7.21 (m, 2H, C**H**$_{\text{phenyl}}$), 7.28-7.37 (m, 3H, C**H**$_{\text{phenyl}}$), 7.69 (ddd, 1H, **H**-7, *J* = 3.1, J_{HF} = 8.0, *J* = 9.4), 7.86 (dd, 1H, **H**-8, J_{HF} = 4.3, *J* = 9.4), 7.99 (dd, 1H, **H**-5, *J* = 3.1, J_{HF} = 9.0), 9.08 (s, 1H, **H**-2), 9.93 (t, 1H, N**H**, *J* = 5.8). ^{13}C NMR: (DMSO) 19.7, 26.2, 37.7, 52.1, 56.0, 64.8, 110.5, 110.6 (d, J_{CF} = 22.7), 121.0 (d, J_{CF} = 8.9), 121.5 (d, J_{CF} = 25.5), 126.4, 127.9, 128.9, 128.9, 135.6, 135.8, 148.7, 163.9, 169.7, 174.7 (d, J_{CF} = 2.5). MS (ESI) m/z $[M]^+$ Calcd for $C_{24}H_{29}FN_3O_2^+$: 410.2. Found: 410.1. LC purity 92.2%.

6-(1-Benzyl-6-fluoro-4-oxo-1,4-dihydroquinoline-3-carboxamido)-N,N,N-trimethylhexan-1-aminium bromide ***4-C6***

Ochre solid; 96% yield; mp 179-182 °C; R_f = 0.26 (CH_2Cl_2/MeOH = 85:15); ^{1}H NMR ($CDCl_3$): 1.48-1.49 (m, 4H, NH-CH_2-C**H$_2$**-C**H$_2$**), 1.64-1.68 (m, 2H, NH-CH_2-CH_2-CH_2-C**H$_2$**), 1.80-1.82 (m, 2H, C**H$_2$**-CH_2-N^+), 3.45 (s, 9H, $^+$N(C**H$_3$**)$_3$), 3.47-3.49 (m, 2H, NH-C**H$_2$**), 3.56-3.60 (m, 2H, C**H$_2$**-N^+), 5.51 (s, 2H, C**H$_2$**$_{benzyl}$), 7.14 (dd, 2H, C**H**$_{phenyl}$, *J* = 1.6, *J* = 7.7), 7.31-7.36 (m, 4H, C**H**$_{phenyl}$, **H**-8), 7.43 (dd, 1H, **H**-7, *J* = 4.2, J_{HF} = 9.4), 8.12 (dd, 1H, **H**-5, *J* = 3.0, J_{HF} = 8.8), 8.92 (s, 1H, **H**-2), 9.95 (t, 1H, N**H**, *J* = 5.7).^{13}C NMR: ($CDCl_3$) 22.9, 25.6, 26.3, 29.7, 38.7, 53.5, 58.1, 67.0, 111.9, 112.2 (d, J_{CF} = 22.8), 119.3 (d, J_{CF} = 7.9), 121.6 (d, J_{CF} = 25.4), 126.1, 128.8, 129.4, 134.0, 135.9, 148.4, 164.8, 167.2, 176.0 (d, J_{CF} = 2.7). MS (ESI) m/z $[M]^+$ Calcd for $C_{26}H_{33}FN_3O_2^+$: 438.3. Found: 438.1. LC purity 95.5%.

*8-(1-Benzyl-6-fluoro-4-oxo-1,4-dihydroquinoline-3-carboxamido)-N,N,N-trimethyloctan-1-aminium bromide **4-C8***

White solid; 53% yield; mp 185-187 °C; R_f = 0.10 (CH_2Cl_2/MeOH = 85:15); ^{1}H NMR (DMSO): 1.29-1.39 (m, 8H, NH-CH_2-CH_2-C**H$_2$**-C**H$_2$**-C**H$_2$**-C**H$_2$**), 1.55-1.58 (m, 2H, NH-CH_2-C**H$_2$**), 1.66-1.69 (m, 2H, C**H$_2$**-CH_2-N^+), 3.03 (s, 9H, N^+(C**H$_3$**)$_3$), 3.25-3.27 (m, 2H, NH-C**H$_2$**), 3.40-3.45 (m, 2H, C**H$_2$**-N^+), 5.81 (s, 2H, C**H$_2$**$_{benzyl}$), 7.20-7.24 (m, 2H, C**H**$_{phenyl}$), 7.30-7.38 (m, 3H, C**H**$_{phenyl}$), 7.69 (ddd, 1H, **H**-7, *J* = 3.1, J_{HF} = 8.0, *J* = 9.4), 7.86 (dd, 1H, **H**-8, J_{HF} = 4.4, *J* = 9.4), 7.99 (dd, 1H, **H**-5, *J* = 3.1, J_{HF} = 9.0), 9.07 (s, 1H, **H**-2), 9.89 (t, 1H, N**H**, *J* = 5.7). ^{13}C NMR (DMSO): 21.3, 25.0, 25.7, 27.7, 27.7, 28.5, 37.7, 51.5, 55.4, 64.6, 109.9, 110.1 (d, J_{CF} = 23.0), 120.4 (d, J_{CF} =8.1), 120.9 (d, J_{CF} = 24.8), 125.8, 127.3, 128.3, 128.3, 135.0, 135.2, 148.1, 163.1, 170.4, 174.2 (d, J_{CF} = 2.5). MS (ESI) m/z $[M]^+$ Calcd for $C_{28}H_{37}FN_3O_2^+$: 466.3. Found: 466.1. LC purity 95.5%.

*10-(1-Benzyl-6-fluoro-4-oxo-1,4-dihydroquinoline-3-carboxamido)-N,N,N-trimethyldecan-1-aminium bromide **4-C10***

White solid; 64% yield; mp 178-180 °C; R_f = 0.45 (CH_2Cl_2/MeOH = 8:2); ^{1}H NMR ($CDCl_3$) 1.31-1.42 (m, 12H, NH-CH_2-CH_2-C**H$_2$**-C**H$_2$**-C**H$_2$**-C**H$_2$**-C**H$_2$**-C**H$_2$**), 1.63-1.65 (m, 2H, NH-CH_2-C**H$_2$**), 1.73-1.76 (m, 2H, C**H$_2$**-CH_2-N^+), 3.46 (s, 9H, $^+$N(C**H$_3$**)$_3$), 3.47-3.55 (m, 4H, NH-C**H$_2$**/C**H$_2$**-N^+), 5.49 (s, 2H, C**H$_2$**$_{benzyl}$), 7.13-7.15 (dd, 2H, C**H**$_{phenyl}$, *J* = 1.7, *J* = 7.7), 7.31-7.35 (m, 4H, C**H**$_{phenyl}$/**H**-8), 7.40-7.44 (dd, 1H, **H**-7, *J* = 4.2, J_{HF} = 9.3), 8.15 (dd, 1H, **H**-5, *J* = 2.9, J_{HF} = 8.9), 8.93 (s, 1H, **H**-2), 9.92 (t, 1H, N**H**, *J* = 4.5). ^{13}C NMR ($CDCl_3$): 23.4, 26.4, 27.3, 29.3, 29.4, 29.5, 29.9, 30.0, 39.6, 53.8, 58.4, 67.6, 112.1, 112.5 (d, J_{CF} = 23.1), 119.5 (d, J_{CF} = 8.0), 121.8 (d, J_{CF} = 24.8), 126.4, 129.1, 129.7, 134.3, 136.1, 148.7, 164.9, 169.6, 176.3 (d, J_{CF} = 2.8). MS (ESI) m/z $[M]^+$ Calcd for $C_{30}H_{41}FN_3O_2^+$: 494.3. Found: 494.2. LC purity 97.8%.

*N-(4-(1-Benzyl-6-fluoro-4-oxo-1,4-dihydroquinoline-3-carboxamido)butyl)-4-((4,5-dihydroisoxazol-3-yl)oxy)-N,N-dimethylbut-2-yn-1-aminium bromide **5-C4***

Beige solid; yield 37%; mp 94-101 °C; R_f = 0.54 (MeOH/NH_4NO_2 (0.2 M) = 3:2); ^{1}H NMR (DMSO): 1.57-1.63 (m, 2H, NH-CH_2-C**H$_2$**), 1.74-1.82 (m, 2H, NH-CH_2-CH_2-C**H$_2$**), 3.01 (t, 2H, **H**-4$_{2\text{-isox}}$, *J* = 9.6), 3.09 (s, 6H, $^+$N(C**H$_3$**)$_2$), 3.36-3.45 (m, 4H, NH-C**H$_2$**/C**H$_2$**-N^+), 4.31 (t, 2H, **H**-5$_{2\text{-isox}}$, *J* = 9.6), 4.45 (s, 2H, $^+$N-C**H$_2$**-C≡), 4.94 (s, 2H, ≡C-C**H$_2$**-O), 5.81 (s, 2H, C**H$_2$**$_{benzyl}$), 7.21-7.23 (m, 2H, C**H**$_{phenyl}$), 7.28-7.38 (m, 3H,

C**H**$_{phenyl}$), 7.69 (ddd, 1H, **H**-7, J = 9.3, J_{HF} = 8.0, J = 3.1), 7.86 (dd, 1H, **H**-8, J_{HF} = 4.3, J = 9.5), 7.99 (dd, 1H, **H**-5, J = 3.0, J_{HF} = 9.0), 9.07 (s, 1H, **H**-2), 9.93 (t, 1H, N**H**, J = 5.7). ^{13}C NMR (DMSO): 19.5, 26.1, 32.1, 37.6, 49.8, 53.3, 56.0, 57.1, 62.8, 69.5, 76.0, 86.0, 110.4 (d, J_{CF} = 22.6), 110.6, 121.1 (d, J_{CF} = 8.4), 121.5 (d, J_{CF} = 24.8), 126.4, 127.9, 128.8, 128.9, 135.6, 135.9, 148.7, 159.1 (d, J_{CF} = 244.8), 163.9, 166.6, 175.4. MS (ESI) m/z [M]$^+$ Calcd for $C_{30}H_{34}FN_4O_4^+$: 533.3. Found: 533.4. CE purity 95.0%.

8-(1-Benzyl-6-fluoro-4-oxo-1,4-dihydroquinoline-3-carboxamido)-N-(4-((4,5-dihydroisoxazol-3-yl)oxy)but-2-yn-1-yl)-N,N-dimethyloctan-1-aminium bromide ***5-C8***

Beige solid; yield 60%; mp 112-118 °C; R_f = 0.56 (MeOH/NH_4NO_2 (0.2 M) = 3:2); ^{1}H NMR (DMSO): 1.28-1.39 (m, 8H, NH-CH_2-CH_2-C**H$_2$**-C**H$_2$**-C**H$_2$**-C**H$_2$**), 1.52-1.59 (m, 2H, NH-CH_2-C**H$_2$**), 1.67-1.73 (m, 2H, C**H$_2$**-CH_2-N$^+$), 3.00 (t, 2H, **H**-4$_{2\text{-isox}}$, J = 9.6), 3.08 (s, 6H, $^+$N(C**H$_3$**)$_2$), 3.35-3.37 (m, 4H, NH-C**H$_2$**/C**H$_2$**-N$^+$), 4.31 (t, 2H, **H**-5$_{2\text{-isox}}$, J = 9.6), 4.45 (s, 2H, $^+$N-C**H$_2$**-C≡), 4.93 (s, 2H, ≡C-C**H$_2$**-O), 5.81 (s, 2H, C**H$_2$**$_{benzyl}$), 7.21-7.38 (m, 5H, C**H**$_{phenyl}$), 7.68 (ddd, 1H, **H**-7, J = 9.3, J_{HF} = 8.0, J = 3.1), 7.85 (dd, 1H, **H**-8, J_{HF} = 4.0, J = 9.4), 7.98 (dd, 1H, **H**-5, J = 3.1, J_{HF} = 9.0), 9.07 (s, 1H, **H**-2), 9.88 (t, 1H, N**H**, J = 5.6). ^{13}C NMR (DMSO): 21.7, 25.5, 26.3, 28.2, 29.1, 32.2, 38.3, 49.7, 53.2, 56.0, 57.1, 64.8, 69.5, 76.0, 85.9, 110.4 (d, J_{CF} = 22.8), 110.7, 121.0, 121.5, 126.4, 127.9, 128.9, 128.9, 135.8, 148.7, 159.1 (d, J_{CF} = 245.3), 163.6, 166.6, 174.7. MS (ESI) m/z [M]$^+$ Calcd for $C_{34}H_{42}FN_4O_4^+$: 589.7. Found: 589.6. HPLC purity 91.1%.

10-(1-Benzyl-6-fluoro-4-oxo-1,4-dihydroquinoline-3-carboxamido)-N-(4-((4,5-dihydroisoxazol-3-yl)oxy)but-2-yn-1-yl)-N,N-dimethyldecan-1-aminium bromide ***5-C10***

Beige solid; yield 44%; mp 107-109 °C; R_f = 0.68 (MeOH/NH_4NO_2 (0.2 M) = 3:2); ^{1}H NMR (DMSO): 1.22-1.39 (m, 12H, NH-CH_2-CH_2-C**H$_2$**-C**H$_2$**-C**H$_2$**-C**H$_2$**-C**H$_2$**-C**H$_2$**), 1.53-1.56 (m, 2H, NH-CH_2-C**H$_2$**), 1.65-1.67 (m, 2H, C**H$_2$**-CH_2-N$^+$), 3.00 (t, 2H, **H**-4$_{2\text{-isox}}$, J = 9.6), 3.07 (s, 6H, $^+$N(C**H$_3$**)$_2$), 3.35-3.37 (m, 4H, NH-C**H$_2$**/C**H$_2$**-N$^+$), 4.31 (t, 2H, **H**-5$_{2\text{-isox}}$, J = 9.6), 4.44 (s, 2H, $^+$N-C**H$_2$**-C≡), 4.93 (s, 2H, ≡C-C**H$_2$**-O), 5.81 (s, 2H, C**H$_2$**$_{benzyl}$), 7.21-7.37 (m, 5H, C**H**$_{phenyl}$), 7.68 (ddd, 1H, **H**-7, J = 9.3, J_{HF} = 8.0, J = 3.1), 7.85 (dd, 1H, **H**-8, J_{HF} = 4.0, J = 9.4), 7.98 (dd, 1H, **H**-5, J = 3.1, J_{HF} = 9.0), 9.07 (s, 1H, **H**-2), 9.87 (t, 1H, N**H**, J = 5.6). ^{13}C NMR (DMSO): 21.7, 25.5, 26.5, 28.3, 28.6, 28.7, 29.1, 32.2, 38.3, 49.7, 53.2, 56.0, 57.1, 63.1, 69.5, 76.0, 85.9, 110.7, 110.8, 121.0, 121.2, 126.4, 127.9, 128.9, 128.9, 135.7, 135.8, 148.7, 160.3, 163.6, 166.6, 174.7. MS (ESI) m/z [M]$^+$ Calcd for $C_{36}H_{46}FN_4O_4^+$: 617.8. Found: 617.7. HPLC purity 93.1%.

N-(2-Acetoxyethyl)-4-(1-benzyl-6-fluoro-4-oxo-1,4-dihydroquinoline-3-carboxamido)-N,N-dimethylbutan-1-aminium bromide ***6-C4***

White solid; yield 73%; mp 153-156 °C; ^{1}H NMR (DMSO): 1.56-1.63 (m, 2H, NH-CH_2-C**H$_2$**), 1.73-1.81 (m, 2H, NH-CH_2-CH_2-C**H$_2$**), 2.06 (s, 3H, C**H$_3$**), 3.09 (s, 6H, $^+$N(C**H$_3$**)$_2$), 3.40-3.44 (m, 4H, NH-C**H$_2$**/C**H$_2$**-N$^+$), 3.63-3.66 (m, 2H, C**H$_2$**-CH_2-O), 4.43 (t, 2H, C**H$_2$**-O, J = 4.6), 5.81 (s, 2H, C**H$_2$**$_{benzyl}$), 7.21-7.38 (m, 5H, C**H**$_{phenyl}$), 7.69 (ddd, 1H, **H**-7, J = 3.1, J = 8.0, J = 9.4), 7.86 (dd, 1H, **H**-8, J = 4.3, J = 9.4), 7.98 (dd, 1H, **H**-5, J = 3.0, J = 9.0), 9.08 (s, 1H, **H**-2), 9.93 (t, 1H, N**H**, J = 5.8). ^{13}C NMR (DMSO): 19.4, 20.5, 26.2, 37.7, 50.6, 56.0, 57.4, 61.4, 63.4, 110.4 (d, J_{CF} = 22.6), 110.6, 121.0 (d, J_{CF} = 8.2), 121.5, 126.4,

127.9, 128.9, 128.9, 135.6, 135.8, 148.7, 159.1 (d, J_{CF} = 245.6), 163.9, 169.7, 174.7 (d, J_{CF} = 2.3). MS (ESI) m/z $[M]^+$ Calcd for $C_{27}H_{33}FN_3O_4^+$: 482.2. Found: 482.2. HPLC purity 95.0%.

N-(2-Acetoxyethyl)-6-(1-benzyl-6-fluoro-4-oxo-1,4-dihydroquinoline-3-carboxamido)-N,N-dimethylhexan-1-aminium bromide ***6-C6***

White solid; yield 19%; mp 184-188 °C; ^{1}H NMR (DMSO): 1.34-1.46 (m, 4H, NH-CH_2-CH_2-C**H$_2$**-C**H$_2$**), 1.55-1.62 (m, 2H, NH-CH_2-C**H$_2$**), 1.67-1.75 (m, 2H, C**H$_2$**-CH_2-N^+), 2.05 (s, 3H, C**H$_3$**), 3.08 (s, 6H, $^+$N(C**H$_3$**)$_2$), 3.33-3.39 (m, 4H, NH-C**H$_2$**/C**H$_2$**-N^+), 3.64 (t, 2H, C**H$_2$**-CH_2-O, *J* = 4.8), 4.42 (t, 2H, C**H$_2$**-O, *J* = 4.4), 5.81 (s, 2H, C**H$_2$**$_{benzyl}$), 7.22-7.37 (m, 5H, C**H**$_{phenyl}$), 7.68 (ddd, 1H, **H**-7, *J* = 3.1, *J* = 8.0, *J* = 9.3), 7.86 (dd, 1H, **H**-8, *J* = 4.3, *J* = 9.4), 7.98 (dd, 1H, **H**-5, *J* = 3.0, *J* = 9.0), 9.07 (s, 1H, **H**-2), 9.89 (t, 1H, N**H**, *J* = 5.6). ^{13}C NMR (DMSO): 20.6, 21.6, 25.4, 25.9, 28.9, 38.1, 50.5, 56.0, 57.4, 61.3, 63.8, 110.4 (d, J_{CF} = 22.8), 110.7, 121.0 (d, J_{CF} = 8.1), 121.4 (d, J_{CF} = 24.8), 126.4, 127.9, 128.9, 128.9, 135.6, 135.8, 148.7, 159.1 (d, J_{CF} = 245.0), 163.7, 169.7, 174.7 (d, J_{CF} = 2.3). MS (ESI) m/z $[M]^+$ Calcd for $C_{29}H_{37}FN_3O_4^+$: 510.3. Found: 510.4. CE purity 95.3%.

N-(2-Acetoxyethyl)-8-(1-benzyl-6-fluoro-4-oxo-1,4-dihydroquinoline-3-carboxamido)-N,N-dimethyloctan-1-aminium bromide ***6-C8***

White solid; yield 39%; mp 163-166 °C; ^{1}H NMR (DMSO): 1.29-1.35 (m, 8H, NH-CH_2-CH_2-C**H$_2$**-C**H$_2$**-C**H$_2$**-C**H$_2$**), 1.54-1.55 (m, 2H, NH-CH_2-C**H$_2$**), 1.65-1.72 (m, 2H, C**H$_2$**-CH_2-N^+), 2.05 (s, 3H, C**H$_3$**), 3.08 (s, 6H, $^+$N(C**H$_3$**)$_2$), 3.34-3.37 (m, 4H, NH-C**H$_2$**/C**H$_2$**-N^+), 3.64 (t, 2H, C**H$_2$**-CH_2-O, *J* = 4.8), 4.42 (t, 2H, C**H$_2$**-O, *J* = 4.6), 5.81 (s, 2H, C**H$_2$**$_{benzyl}$), 7.22-7.37 (m, 5H, C**H**$_{phenyl}$), 7.67 (ddd, 1H, **H**-7, *J* = 3.1, *J* = 8.0, *J* = 9.4), 7.86 (dd, 1H, **H**-8, *J* = 4.4, *J* = 9.4), 7.98 (dd, 1H, **H**-5, *J* = 3.1, *J* = 9.0), 9.07 (s, 1H, **H**-2), 9.88 (t, 1H, N**H**, *J* = 5.6). ^{13}C NMR (DMSO): 20.6, 21.6, 25.6, 26.3, 28.3, 28.4, 29.1, 38.2, 50.5, 56.0, 57.4, 61.3, 63.8, 110.4 (d, J_{CF} = 22.8), 110.7, 121.0 (d, J_{CF} = 7.8), 121.3 (d, J_{CF} = 25.1), 126.4, 127.9, 128.8, 128.9, 135.6, 135.8, 148.7, 159.1 (d, J_{CF} = 245.2), 163.6, 169.7, 174.7 (d, J_{CF} = 2.4). MS (ESI) m/z $[M]^+$ Calcd for $C_{31}H_{41}FN_3O_4^+$: 538.3. Found: 538.5. LC purity 97.6%.

N-(2-Acetoxyethyl)-10-(1-benzyl-6-fluoro-4-oxo-1,4-dihydroquinoline-3-carboxamido)-N,N-dimethyldecan-1-aminium bromide ***6-C10***

White solid; yield 63%; mp 122-126 °C; ^{1}H NMR (DMSO): 1.27-1.33 (m, 12H, NH-CH_2-CH_2-C**H$_2$**-C**H$_2$**-C**H$_2$**-C**H$_2$**-C**H$_2$**-C**H$_2$**), 1.51-1.58 (m, 2H, NH-CH_2-C**H$_2$**), 1.63-1.71 (m, 2H, C**H$_2$**-CH_2-N^+), 2.05 (s, 3H, C**H$_3$**), 3.06 (s, 6H, $^+$N(C**H$_3$**)$_2$), 3.31-3.37 (m, 4H, NH-C**H$_2$**/C**H$_2$**-N^+), 3.60-3.63 (m, 2H, C**H$_2$**-CH_2-O), 4.41 (t, 2H, C**H$_2$**-O, *J* = 4.6), 5.81 (s, 2H, C**H$_2$**$_{benzyl}$), 7.21-7.38 (m, 5H, C**H**$_{phenyl}$), 7.68 (ddd, 1H, **H**-7, *J* = 3.1, *J* = 7.9, *J* = 9.4), 7.85 (dd, 1H, **H**-8, *J* = 4.4, *J* = 9.4), 7.98 (dd, 1H, **H**-5, *J* = 3.1, *J* = 9.0), 9.07 (s, 1H, **H**-2), 9.87 (t, 1H, N**H**, *J* = 5.6). ^{13}C NMR (DMSO): 20.5, 21.6, 25.6, 26.5, 28.4, 28.6, 28.6, 28.7, 29.1, 38.3, 50.5, 56.0, 57.4, 61.2, 63.8, 110.3, 110.5 (d, J_{CF} = 23.0), 110.7, 120.9 (d, J_{CF} = 6.9), 121.3 (d, J_{CF} = 24.4), 126.4, 127.9, 128.9, 128.9, 135.6, 135.8, 148.7, 157.9 (d, J_{CF} = 243.8), 163.7, 169.7, 174.7 (d, J_{CF} = 2.4). MS (ESI) m/z $[M]^+$ Calcd for $C_{33}H_{45}FN_3O_4^+$: 566.3. Found: 566.5. LC purity 100.0%.

Pharmacology

Description of Calcium/DAG determination using confocal microscopy

To evaluate the effect of the six amino acid insertion into the M1-CFP receptor we used a dual fluorescence probe from Montana Molecular (downward DAG2/R Geco). This fluorescence probe is composed of two sensors, fused in frame on both sides of a 2A peptide sequence: first, a DAG sensor, which consist of a cpGFP fused to the C1 domain of a PKC; second, the red calcium sensor R-GECO. This dual sensor responds with an increase in red fluorescence intensity upon increase in Ca^{2+} and a decrease in green fluorescence upon binding to diacylglycerol (DAG). Therefore, the probe can specifically report on the activation of the Gq-signalling pathway. The dual fluorescent probe was used in HEK293 cells either alone or co-expressed with the M1-CFP or the novel M1-I3N-CFP sensor. In brief, round 24 mm cover slips were placed in six-well plates and coated for 20 min using 200µl of poly-d-lysine (1 mg/ml). After washing with sterile PBS, HEK293 cells stably expressing the calcium sensor were seeded onto these cover slips. Cells were transfected 3-4 hours later using Effectene (Quiagen), according to the manufacturer's instructions. For transfection, 500 ng DNA per well of each receptor construct were used, and cell culture medium was exchanged 16–18 h later. Analysis of the cells was done 48 h after transfection.

Confocal microscopy analysis and quantification of cell responses

48 h after transfection cells were placed in an Attofluor holder (Molecular probes), maintained in imaging buffer and analyzed using LeicaSP8 microscope equipped with four detection channels. CFP was excited using 440 nm line and emission was detected from 470-530nm; GFP was excited using the 488 nm line and detected from 510-560 nm; R-GECO was excited at 562 nm and detected from 610-660 nm. Time series were taken using 512*512 resolution and sequential scan mode, leading to total image acquisition times of 1.290 sec. Cells were monitored for 200 frames. After 15 seconds cells were stimulated by addition of 100 µM carbachol and analyzed for their agonist response. The dual probe did not respond to carbachol if no receptor was co-transfected. Fluorescence data were acquired using the Leica software. Only cell expressing CFP tagged receptors were used for analysis. Off line analysis was performed using Origin software. To account for none homogenous cell response due to bath application

of carbachol, individual cell responses were manually aligned to the first time frame showing an increase in R-GECO and averaged after alignment.

Supporting Figures

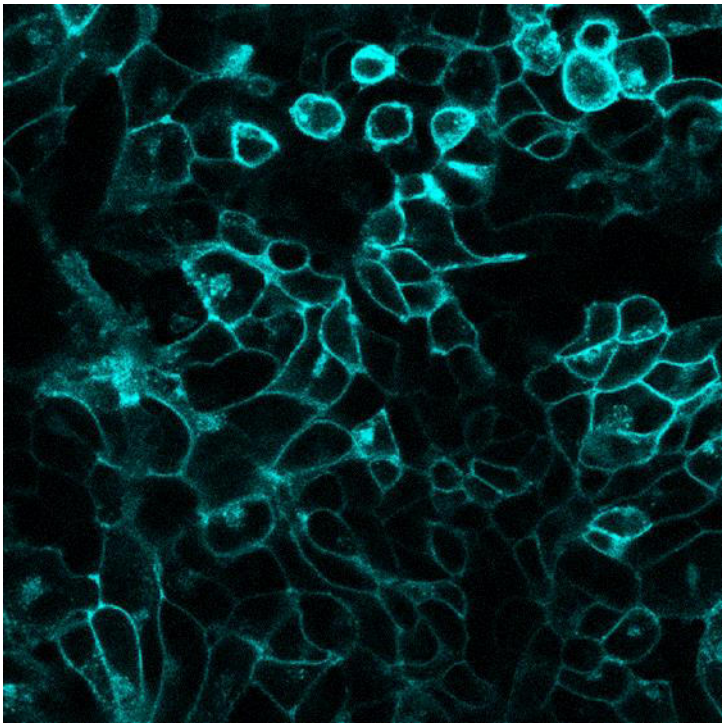

Supporting figure 1 Confocal microscopy analysis of the M1-I3N-CFP receptor sensor in HEK 293 cells. Cell surface expression studies were performed with confocal scanning laser microscopy

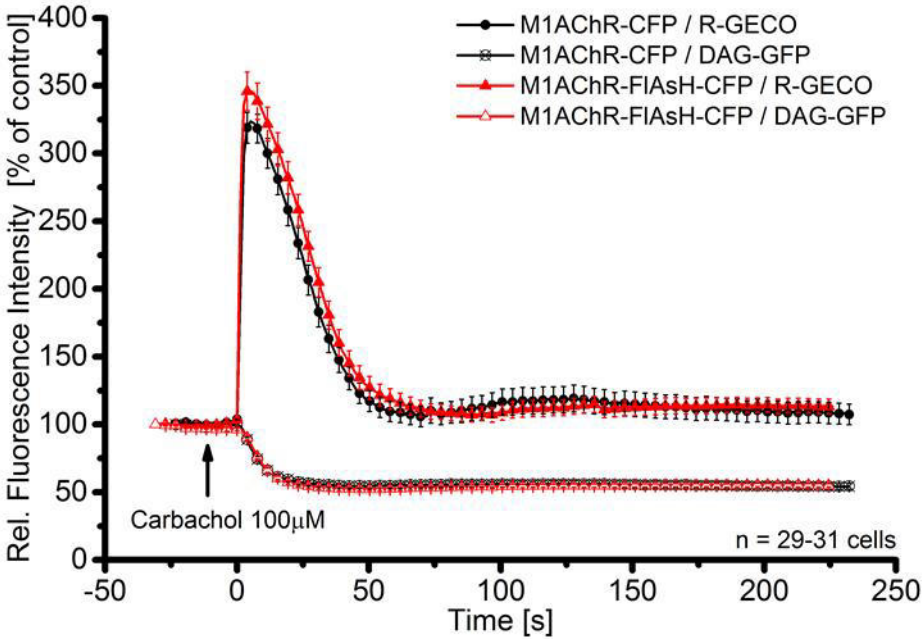

Supporting figure 2 M1-I3N-CFP receptor sensor characterization was performed with a dual fluorescence probe from Molecular Montana. With the help of this fluorescence tool it is possible to monitor DAG formation and Ca2+ release. The stimulated response was indistinguishable for the M1-CFP receptor or the M1I3N-CFP

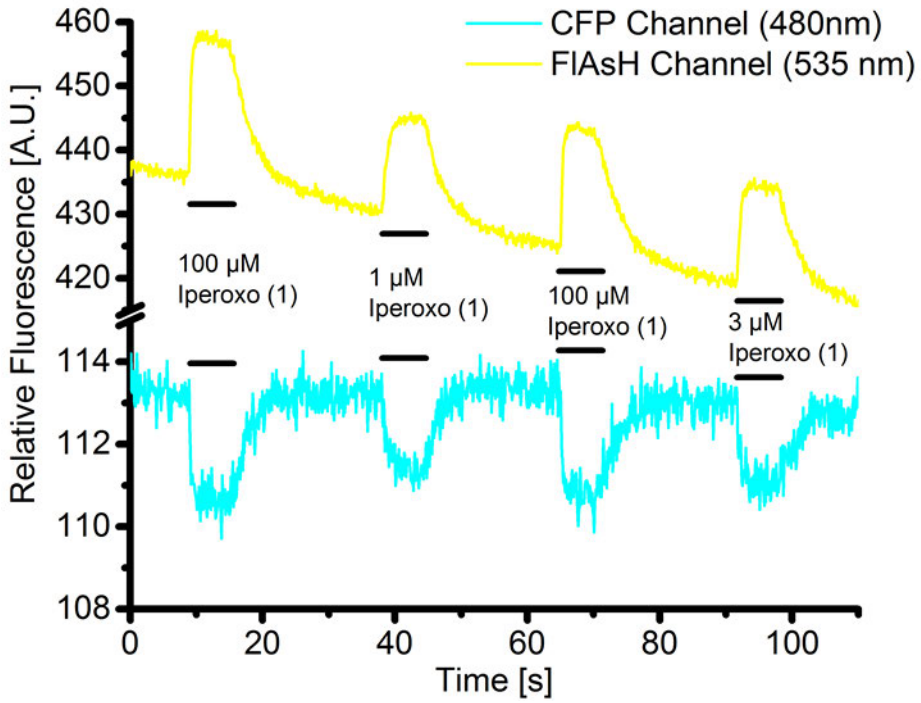

Supporting figure 3 Effect of agonist addition to the receptor sensor. Upon ligand exposure sharp concentration dependent, antiparallel movements of the different FRET channels were detectable. Constant superfusion of buffer results in a constant baseline.

D. Discussion

In literature many types of multifunctional compounds are reported: merged, linked and fused ligands, bitopic, dualsteric, multitarget compounds, message-adress derivatives, heterobivalent or homobivalent hybrids.[26,54,92,264] All display one common characteristic: they covalently combine multiple pharmacophores in a single structure. The rationales for exploiting the hybrid approach stem from the opportunity to increase subtype-selectivity, modulate the activity of a protein as well as to address several targets simultaneously, through the integration of multiple pharmacophoric units in a single chemical structure. These useful medicinal chemistry tools could help to promise properties for future therapeutic application in GPCR pharmacology and in the role of cholinergic system in AD. All the hybrid compounds synthetized in this work could expand, with auxiliary and significant information, the knowledge regarding the cholinergic system in AD, showing the importance of applying novel strategies and offering new pharmacological perspectives. Because of the wide range of possible interactions, the study of multifunctional ligands is a complicated issue which needs to interpret clues coming from a set of highly interdisciplinary sciences, by integrating drug design, medicinal chemistry, pharmacology, computational studies, molecular biology, biochemistry into the observations. The common goal is to understand small essential details at the biological interface of the target proteins that can open new approaches for future therapeutic development.

The aim of this thesis was to investigate the molecular mechanism and the pharmacological response of some multifunctional or dualsteric ligands using innovative medicinal chemistry strategies, ranging from bitopic and tritopic ligands to their molecular fragment and abandoning the one-drug one-target concept for the field of multitarget hybrids. An advantage of the hybrid approach is the rationality of the design. With the due attention regarding the connection position between the different pharmacophores and the chemical nature of the spacer, a molecule that already shows activity at a target is very likely to reveal similar activity when it's combined with another entity over a linker. The poor drugability is the direct disadvantage of such hybrids because of their physicochemical properties, which do not comply with Lipinski's rule of five[265], the progression of the derivatives in drug development is prevented. Especially for diseases of the central nervous system (CNS), the compounds should reach the brain through the blood brain barrier (BBB). Therefore, the permanent charge, the high molecular weight and

the moderate lipophilicity of the studied compounds limit their use as pharmacological tools. Further modification trying to overcome the physicochemical limits but maintaining the potential achieved are necessary for future therapeutic applications.

The idea of combining high affinity (via orthosteric sites) with high selectivity (via allosteric sites) in dualsteric ligands was already studied by Chen et al.[82], which investigate the ligand-receptor activation at the M1 muscarinic GPCR. The iperoxo/BQCAd hybrids turn out to be partial agonists. The spacer length has a role in controlling the probability of switch, between the inactive purely allosteric and the active bitopic orthosteric/allosteric binding pose, in the dynamic ligand binding model.[105] FRET experiments were subsequently performed in order to obtain information about interactions between GPCRs and bitopic ligands for a better understanding of ligand receptor interactions on a molecular level. The studies confirmed that the linker attached to an orthoster attenuates the receptor response. The maximal positive FRET signal was reached with the 6-linker chain iperoxo/BQCAd compound. Interestingly, hybrids consisting of longer linker chains showed an inverse previously undiscovered FRET signal indicating a different receptor movement in comparison to shorter linked hybrids and to the reference compounds.[83] For the purpose of further investigation of this new conformational change in the intracellular signaling cascade and to obtain a more detailed picture of the structure-functional selectivity relationships of the M1 muscarinic receptor agonism, seven series of BQCAd hybrid analogs were synthetized and further studied (Figure 1).

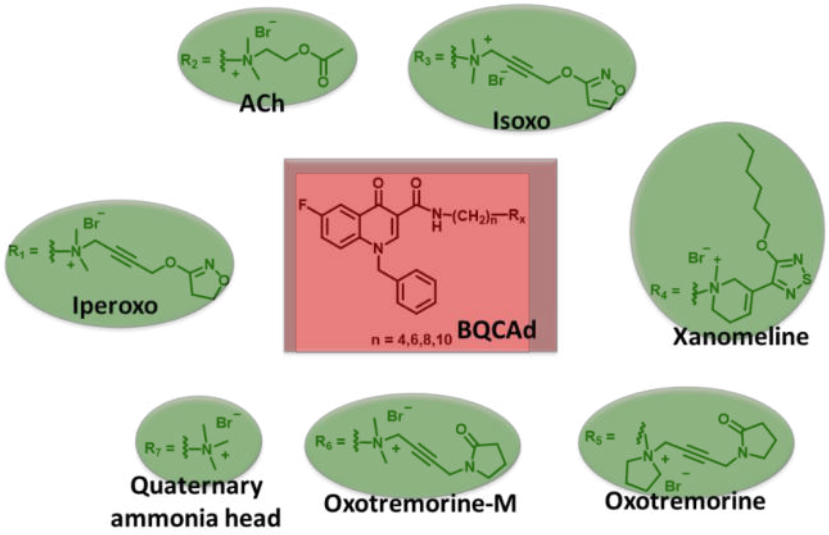

Figure 1. Overview of the BQCAd dualsteric derivetives.

It was found that all the hybrids bind to the muscarinic M1 receptor and with exception of the BQCAd-Oxotremorine derivatives all the hybrids can activate the G protein. Not only the Oxotremorine derivatives suppress the activation of the G protein, but they turn out to be antagonists. Exceptionally the mere introduction of the pyrrolidine ring, when compared to oxotremorine-hybrids, blocks the M1 muscarinic receptor, probably due to its steric hindrance. However, β-arrestins recruitment was observed only for the three hybrids BQCAd-6-Iperoxo, BQCAd-8-Iperoxo and BQCAd-8-Isoxo among all the hybrids. The compounds are therefore characterized by functional selectivity inducing GPCR conformational states related to G-proteins activation sacrificing β-arrestins recruitment. Shrinking the orthosteric moiety down to the essential ammonium head (as TMA) the hybrids surprisingly revealed a very active response regarding the G protein activation, however also these bitopic ligands fail to stimulate β-arrestins recruitment. The fragment is composed of a quaternary ammonia head at the end of the flexible alkyl chain connected with the BQCAd portion and its high efficacy, supported by molecular modeling studies reveal that the overall binding mode is mainly determined by their allosteric building block, which may also lead to better subtype receptor selectivityof other bitopic ligands. In all the series of compounds the 4 and 8 methylenic spacer chain is tolerated best, probably the linker length plays a key role in positioning the interaction within the binding pocket of the M1 muscarinic receptor. Several muscarinic receptor agonists which have thus far been tested in AD have not proven to be therapeutically useful, because of a lack of selectivity at the M1 receptors. An efficacious and more selective M1 agonist might be expected to provide a more appropriate test of the cholinergic hypothesis of dementia. Therefore, the M1/M4 Xanomeline preferring receptor agonist was also incorporated in the dualsteric ligands by connection with the BQCAd allosteric fragment, trying to further investigate the bases of receptor selectivity. The Xanomeline-hybrids bind to the M1 receptor and are capable of delaying the dissociation of the [^{3}H] NMS radioactive probe from the receptor indicating a dualsteric interaction. In literature the Xanomeline binding at the M1 receptor is described as atypical, since it does not fully overlap with the acetylcholine orthosteric site. The atypical binding nature seems to be maintained even in the dualsteric hybrids. In fact, the xanomeline-derivatives are the only series in which, even for the with the 10-chain compound, inositol monophosphate accumulation, a stable

downstream metabolite of IP3, is measured. A diverse binding orientation and a different activation mechanism at the molecular level it could be the cause and it will be further studied. The understanding of supplemental interaction of xanomeline with the M1 mAChR indeed makes the basis for the development of new muscarinic agonist in the treatment of AD.[232] Subtype selective M1 agonists were found to be a beneficial therapeutic opportunity against the neurodegenerative Alzheimer diseases. The current treatment uses Acetylcholinesterase inhibitors since disfunction of the cholinergic system in distinct brain areas and reduction of ACh-mediated signal transduction was found to be the causes of memory deficits.[220,266–268] Thus, inhibition of AChE increases the cholinergic tone relieving the cognitive symptoms[34], without preventing the progression of the disease. By means of a multifunctional strategy a direct activation of the target neuronal receptors and a simultaneous indirect enhance of the ACh concentration in the synaptic cleft could reveal promising candidates for the treatment of AD. For this reason, Tacrine, a well-known AChE inhibitor withdrawn from the market due to its hepatotoxicity and the muscarinic agonist Xanomeline, have been combined in the two new hybrid series (Figure 2).

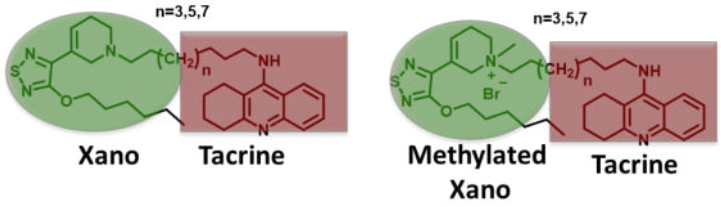

Figure 2. Tacrine/Xanomeline multifunctional derivatives.

Regarding the AChE inhibition the new Tacrine-Xanomeline hybrids show a higher (Tac/Xano Hybrids) or similar (Methylated-Tac/Xano Hybrids) potency compared to the reference compound Tacrine. In docking studies, the selected representative positions in the AChE model for the methylated and non-methylated series are similar, hence their inhibition differences could be attributed to a higher desolvation cost. On the other hand, the compounds investigation in terms of both, G protein activation and the second messenger inositol trisphosphate using the IP1 Cisbio assay, were inactive.

A binding pose completely shifted in favor of the inactive allosteric at the expense of the active dualsteric one could be hypothesized. Conversely, M1 receptor activation occurs for the hybrids connecting tacrine and the iperoxo moieties through an heptyl or decyl spacer chain.

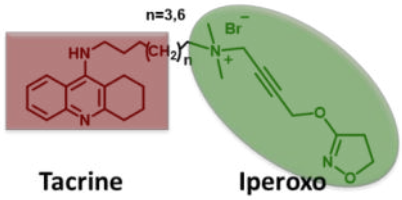

Figure 3. Tacrine/Iperoxo bifunctional hybrids.

These hybrid derivatives previously studied in terms of M1 and M2 binding and inhibition of AChE and BChE, result capable of binding and inhibition with subnanomolar IC_{50} values.[131] Their ability to bind to the M1 muscarinic receptor was further investigated in terms of intracellular M1 signalling cascade. Dose-response curves were recorded with both compounds in bioluminescence assays measuring G protein activation and even in experiments quantifying the IP1 concentration. Additionally, their reduced toxicity makes these dual-targeting compounds extremely attractive for future AD drug investigations and development.

Further studies open new horizons in the GPCR dynamic activation demonstrating that not only the helical core region of GPCRs is involved in ligand binding and stimulation, but also the extracellular receptor domain which contribute to ligand-specific pharmacological effects. In this regard some iperoxo elongated derivatives, with chains of different lengths, were used to probe the space around the orthosteric binding pocket. By means of FRET sensors measurements all muscarinic receptor subtypes were investigated. Incredibly, despite the high conservation of the orthosteric site among the five receptor subtypes, the heptyl, octyl and nonyl linker derivatives turn out to be selective partial agonists at the M3 receptor. Computational studies help in unravelling the secrets of M3-selectivity opening new avenues in the pharmacology of type II diabetes (unpublished results).

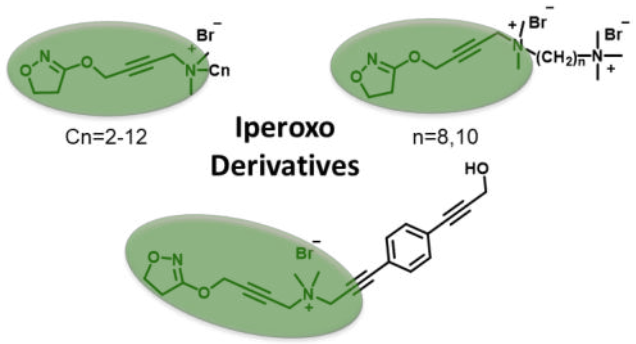

Figure 4. Iperoxo-chain derivatives

Besides Iperoxo-derivatives with flexible alkyl chains, an iperoxo-compound with a rigidified linker and additional compounds having a quaternary ammonic head at the end of the flexible chains were designed and synthesized. Such ligands are still under investigation in the working group of Carsten Hoffmann, Institute for Molecular Cell Biology, CMB-Center for Molecular Biomedicine, University Hospital Jena, Germany.

The possibility of hybrid structures to be capable of bridging independent recognition sites (i.e. two recognition sites on a receptor dimer or one receptor and an accessory site) has been exploited to design the tritopic compound BQCAd-(iperoxo)$_2$. This may result in thermodynamically more favorable binding interaction than the binding of two monovalent molecules, giving enhanced activity or selectivity. Exists also the possibility that the binding of the first pharmacophore would increase the binding of the second pharmacophore to the dimer partner or to the receptor itself. Or again, that the first pharmacophore would help the entry of the second molecular portion in the binding pocket ones the molecular filter, represented by the metastable site, is exceeded. All these possibilities can be investigated through the study of multi-functional ligands. For now, it has been shown that, despite the considerable steric effect, the trivalent ligand BQCAd-(iperoxo)$_2$ binds to the M1 receptor with an higher affinity iperoxo. In the activation of the protein G the compound shows partial agonism. This ligand was also compared with numerous other iperoxo-homobivalent ligands in order to delineate some SARs regarding the influence of the spacer chain on the activation of the G protein at the M1 receptor.

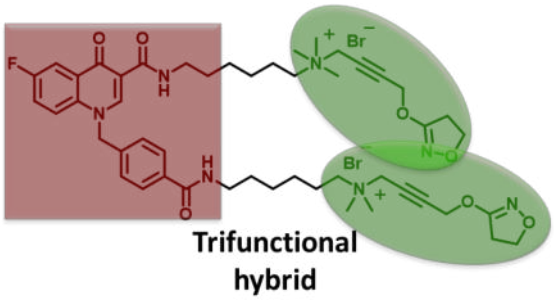

Figure 5. BQCAd/iperoxo tritopic ligand.

Taken together some examples are reported here, showing how the multifunctional-ligand tool compound could help the development of bioactive molecules and new pharmacological tools as well as novel approaches for collect new information related to cellular drug targets.

E. Summary

As population get older, diseases associated with ageing, in particular neurodegenerative diseases such as Alzheimer's Disease (AD) have become more common, being moreover an imminent economic problem for the society[28,269]. AD is a severe age-dependent neurodegenerative brain disorder associated with memory loss and a decrease of cognitive functions which starts slowly and gradually worsens over time[270]. The absence of a cure so far and the expected dramatic incidence increase in the coming years has led to current intensive studies aimed at preventing and treating AD. Today the primary goal is understanding the causes and mechanisms of these disabling disease through innovative basic research. AD is a complicated and interconnected network of various pathological hallmarks[51,269]. These distinguished characteristics of the disease, which occur concomitantly, must be investigated and targeted simultaneously for the development of powerful and selective drugs.

Thus, this work focuses on two different targets of the AD cholinergic hypothesis: the muscarinic M1 receptor[27,83] and the AChE[22] by use of the hybridization approach. Firstly, hybrid putative selective M1 agonist molecules were designed and synthesized, resulting in enhanced cholinergic transmission, as an approach to increase cholinergic function in Alzheimer patients. The hybridization process in this case result from the covalent union in a single molecule of an allosteric portion and an orthosteric portion.

Previously considerable efforts were made to obtain selective agonists for M1 receptor but their off-target effects preclude the therapeutic use[32,57]. The M1 muscarinic receptor is a G protein coupled receptor predominantly expressed in the Central Nervous System (CNS), where it is responsible for essential cognitive functions such as memory and learning. The M1 subtype has long been identified as the preferred target among the five-different subtypes of muscarinic receptors for the treatment of AD. Unfortunately, until now the drugs on the market, only provide a symptomatic relief without preventing the progression of the disease[28]. Progress through clinical trials is limited by poor selectivity of candidate molecule. Thus, there is a desperate need to find selective and powerful drugs. The difficulty in obtaining selective molecules is due to the high conservation among the five different receptor types at the orthosteric active site, this is the binding site of the endogenous ligand acetylcholine which triggers the physiological response[200]. Alternative allosteric sites, whose name derives from the ancient greek word

“ἄλλος”, which means "other", can be regulatory sites too. The allosteric modulators fits into the additional sites. Its binding results in a conformational change of the protein, in particular a rearrangement in the shape of the active site which causes an alteration (enhancement or reduction) of the protein's activity itself. Allosters can modulate the receptor's activation induced by the orthosteric probe and can be thought to act like a dimmer switch in an electrical circuit, able to regulate the intensity of response.

Hence the idea of merging the moieties of allosteric modulators and orthosteric ligands in a bitopic compound follows the message-address concept[2,3,5]. The approach may result in a subtype-selective full or partial agonism because the bitopic compounds occupies both binding sites. Here the BQCAd allosteric M1 modulator and some iperoxo-derivatives fragments were used to compose dualsteric ligands. Thanks to the proximity of the two binding sites in the receptor, the dualsteric hybrids can be addressed from the same bitopic molecule, in which the allosteric and orthosteric moieties are connected through an appropriate spacer.

The system in consideration is however more complicated than a simple fixed electrical circuit. The second messenger activation at the M1 receptor is transient and part of a dynamic and complex systems. Once the signal is ‘switched on’ at the G-protein complex, further proteins and molecules amplify the original signal and produce a complex cascade of interactions. A series of bipharmacophoric ligands composed of the positive allosteric modulators (BQCA-derived compounds) linked with chain of various lengths to different orthosteric building blocks was synthesized and pharmacologically investigated in a broad spectrum of assays, in order to study different aspects of receptor activation, signaling cascades, receptor movement, binding affinity and dissociation rates (Results parts 1,2, 3 and 8).

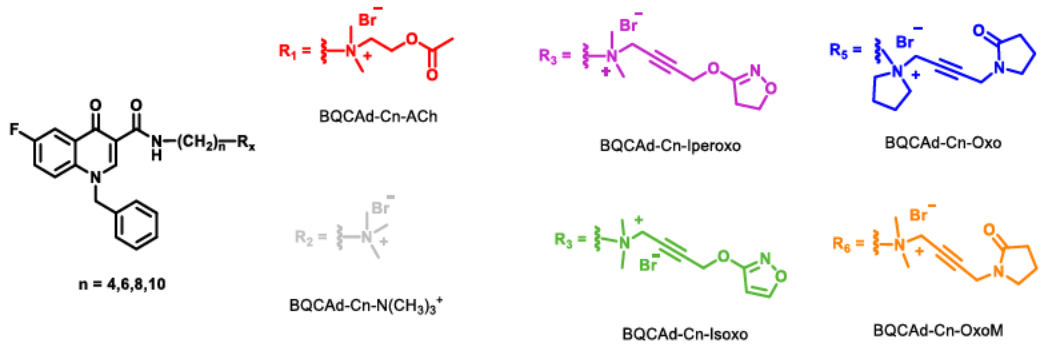

Figure 1. Structures of the M1 agonist dualsteric hybrid composed by the positive allosteric modulator (PAM) benzyl quinolone carboxylic acid derivative (BQCAd) and several various non-selective muscarinic agonist fragments (Acetylcholine (red), quaternary ammonium head (gray), iperoxo (purple), isoxo (green), Oxotremorine (blue), Oxotremorine-M (orange)).

All the hybrids analyzed in radioligand binding studies are able to bind to both the orthosteric and the allosteric binding sites. In terms of G protein activation, the compounds analyzed with a split-bioluminescent assay are all agonists with exception, surprisingly, of oxotremorine- derivatives (Result part 2).

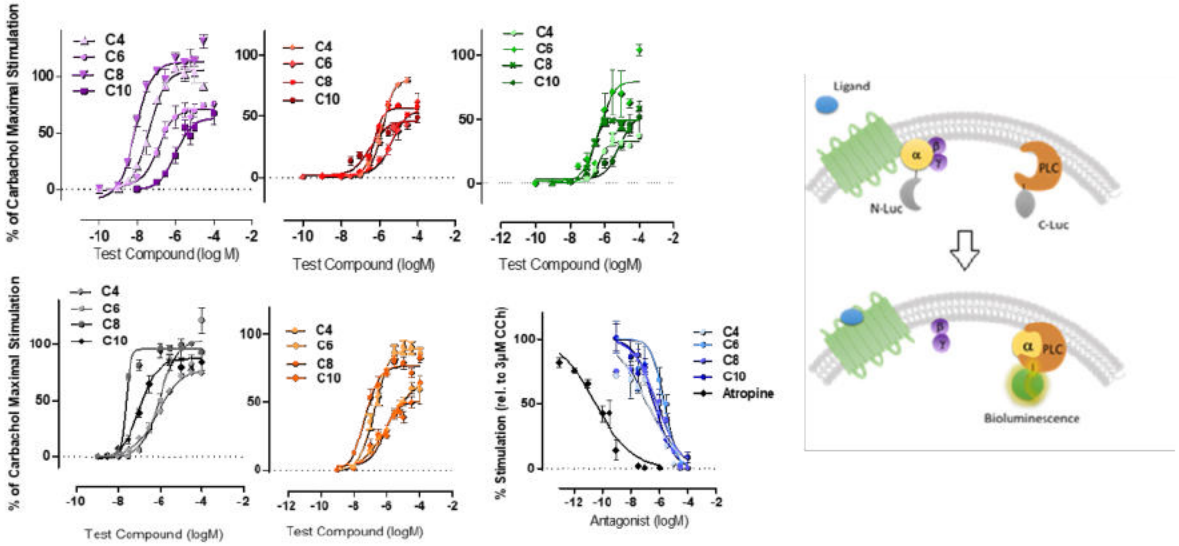

Figure 2. Split/assay studies of six series of bitopic compounds. A concentration dependent G protein activation is observed, with exception of the Oxotremorine derivatives. In this case an antagonist response is measured.

On the other hand, only 3 hybrids (BQCAd-6-Iperoxo, BQCAd-8-Iperoxo, BQCAd-6-Isoxo) were able to recruit β-arrestins[27]. Detailed analyses of the structure-activity relationship were carried out in order to

elucidate the role of the different orthosteric moieties in affecting M1 muscarinic receptor affinity as well as efficacy of the dualsteric ligands. The functional selectivity associated with the bitopic compounds can be further studied to deepen the structure-bias-relationships of the new ligands.

Subsequently, the structure of xanomeline was incorporated in the BQCAd hybrid derivatives using an alkyl chain (Result part 4). The starting hypothesis to obtain dualsteric compounds acting directly at the M1 receptor proved correct, demonstrating the hybrids' binding mode and their functional activity at the M1 receptor.

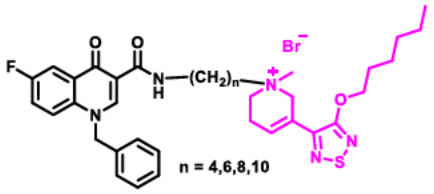

Figure 3. BQCAd-Xanomeline derivatives

Because of a special binding pose of xanomeline in the orthosteric binding site of the M1 receptor, being defined as atypical, the bitopic ligands can provide important information about key residues involved in the orthosteric/allosteric interactions.

Additionally, new Tacrine-Xanomeline hybrids aiming to improve the inhibitory potency of the acetylcholinesterase and simultaneously to increase the cholinergic tone, via the xanomelinic portion acting on the M1 receptor were design and synthetized[22] (Result part 5).

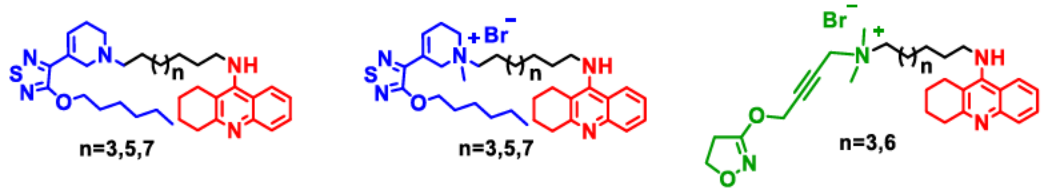

Figure 4. Structures of Tac/Xano hybrids and Tac/Iperoxo compunds

Unfortunately, Tac/Xano hybrids did not activate M1 receptors. In contrast, some previously synthesized derivatives, combining tacrine with iperoxo through a heptyl or decyl linker chain, cause G protein stimulation and IP1 accumulation. Demonstrating that bitopic research can provide excellent starting points to further drug development studies.

Moreover, a new tritopic approach is presented for the first time to deepen the study of the M1 muscarinic receptor (Result part 6). The three-branched compound (two orthosteric moieties and one allosteric

portion connected covalently) could occupy the metastable and the orthosteric binding sites of the same receptor or two orthosteric pockets of different receptors, leading to dimeric association.

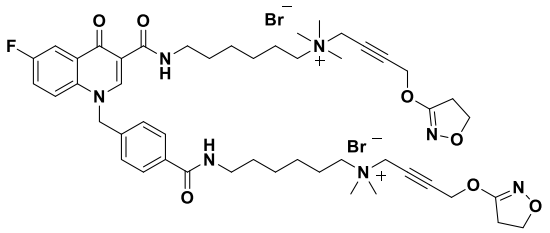

Figure 5. Structures of the new hybrid trivalent derivative.

Interestingly despite the considerable steric effect in the case the two iperoxo moiety ligands, the compound binds to the orthosteric site with an affinity even higher than iperoxo itself. The compound, currently only investigated on the M1 muscarinic receptor in terms of radioligand binding (equilibrium and dissociation) and G protein activation, could be used as molecular tool for the investigation of metastable binding or multimerization states of hM1 receptors.

Furthermore, a series of iperoxo-derived alkane, bis(ammonio)alkane-type and rigidified chain ligands were prepared (Result part 7). The probes will be used to investigate the orthosteric pocket environment in terms of flexibility, physical-chemical properties and space at all muscarinic receptor subtypes.

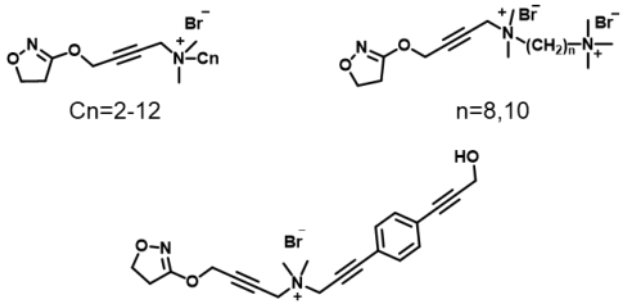

Figure 6. Structures of the new iperoxo-derivative.

The multi-targeting compounds, bitopic compounds and their molecular fragments can provide new useful information to fully understand how the M1 receptor produce specific effects and, hopefully, learn to modulate its function for therapeutic intentions in ways that are currently not possible with the available drugs. Poor drugability is the immediate consequence of the size of these molecules, often

also positively charged. But this strategy provides essential information for further considerations and developments in the cholinergic field, since a multiple-targeting approach appears to be the right innovation for the multifactorial nature of the AD disease.

F. Zusammenfassung

Mit zunehmendem Alter der Bevölkerung werden altersbedingte Krankheiten, insbesondere neurodegenerative Erkrankungen wie die Alzheimer-Krankheit (AD), häufiger und stellen darüber hinaus ein soziales und wirtschaftliches Problem für die Gesellschaft dar[1,2]. AD ist eine schwere altersabhängige neurodegenerative Erkrankung des Gehirns, die mit Gedächtnisverlust und einer Abnahme der kognitiven Funktionen verbunden ist und immer weiter fortschreitet. Die Krankheit ist derzeit unheilbar und aufgrund des demographischen Wandels wird ein starker Anstieg an Betroffenen erwartet. Daher beschäftigt sich eine Vielzahl wissenschaftlicher Studien mit der Prävention und der Behandlung von AD. Derzeit besteht das Hauptziel darin, die Ursachen und Mechanismen dieser Krankheit durch innovative Grundlagenforschung zu verstehen. AD ist ein komplexes Zusammenspiel verschiedener pathologischer Merkmale[2,4]. Diese besonderen Merkmale der Krankheit, die gleichzeitig auftreten, müssen untersucht und gleichzeitig untersucht werden, um wirksame und selektive Medikamente zu entwickeln.

Diese Arbeit beschäftigt sich daher mit zwei Zielstrukturen der cholinergen Hypothese zur Entstehung von AD: dem muskarinischen M1-Rezeptor[5,6] und der AChE[7] unter Verwendung des Hybridisierungsansatzes. Zunächst wurden vermeintlich selektive M1 Agonisten entwickelt und synthetisiert. Diese sollten die cholinerge Transmission verstärken um die cholinerge Funktion in Alzheimer Patienten zu verbessern. Hierbei wurde die Hybridisierung durch die kovalente Verbindung einer allosterischen und einer orthosterischen Einheit in einem Molekül durchgeführt.

Selektive Agonisten des M1 Rezeptors aus vorherigen Arbeiten konnten aufgrund ihrer off-target Effekte keine therapeutische Verwendung finden[8,9]. Der M1-Muskarinrezeptor ist ein G-Protein-gekoppelter Rezeptor, der überwiegend im Zentralnervensystem (ZNS) exprimiert wird und dort für wesentliche kognitive Funktionen wie Gedächtnis und Lernen verantwortlich ist. Innerhalb der fünf unterschiedlichen Rezeptor-Subtypen gilt der M1 Subtyp als bevorzugte Zielstruktur für die Behandlung von AD. Die derzeitig verfügbaren Therapien von AD sind rein symptomatisch und können den Fortschritt der Krankheit weder aufhalten noch verhindern. Der Erfolg von klinische Studien wird durch eine schlechte Selektivität des Kandidatenmoleküls begrenzt. Es besteht daher ein dringender Bedarf, selektive und wirksame Medikamente zu finden. Die Schwierigkeit selektive Verbindungen für die fünf Rezeptor-

Subtypen zu finden liegt in der hochkonservierten orthosterischen Bindestelle der Rezeptoren, an der der endogene Ligand Acetylcholin bindet und somit die physiologische Antwort auslöst. [10]. Alternative allosterische Bindestellen, deren Name vom altgriechischen Wort „ἄλλος“ = „andere“ abgeleitet ist, können ebenfalls regulatorische Bindestellen sein für sogenannte allosterische. Modulatoren. Die Bindung allosterischer Modulatoren führt zu einer Konformationsänderung des Rezeptors, insbesondere im aktiven Zentrum, was zu einer Veränderung der Rezeptoraktivität(Verstärkung oder Verringerung) führt. Allostere können die Rezpetorantwort durch die orthosterische Bindung modulieren, vergleichbar mit einem Dimmer in einem elektrischen Stromkreis, der die Intenstität reguliert.

Nach dem "message-address"-Konzept sollen daher bitopische Verbindungen entwickelt werden, in der ein allosterischer Modulator mit einem orthosteren Liganden vereint wird. [−13]. Dieser Ansatz kann zu einem subtypselektiven, vollständigen oder partiellen Agonismus führen, da die bitopischen Verbindungen beide Bindestellen besetzen. Für diese Arbeit wurden der allosterische B1CAd-M1-Modulator und einige Fragmente von Iperoxoderivaten verwendet, um dualsterische Liganden zu synthetisieren. Aufgrund der räumlichen Nähe der beiden Bindstellen im Rezeptor können die dualsterischen Hybride mit einem bitopischen Molekül adressiert werden, in dem die allosterische und orthosterische Einheit über einen geeigneten Linker verbunden werden.

Das zu betrachtende System ist jedoch komplizierter als ein statischer elektrischer Stromkreis. Die Aktivierung des sekundären Botenstoffs am M1-Rezeptor ist transient und Teil eines dynamischen und komplexen Systems. Sobald das Signal am G-Protein-Komplex "eingeschaltet" ist, verstärken weitere Proteine und Moleküle das ursprüngliche Signal und erzeugen eine komplexe Kaskade von Wechselwirkungen. Daher wurde in dieser Arbeit eine Reihebipharmakophorischer Liganden synthetisiert. Hierzu wurden positive allosterische Modulatoren (BQCA-Derivate) über Linker verschiedener Kettenlängen mit orthosterischen Einheiten gekoppelt und pharmakologisch in einer Vielzahl von Assays untersucht um unterschiedliche Aspekte der Rezeptoraktivierung, Rezeptordynamik, Signalkaskaden, Bindungsaffinitäten und Dissoziationseraten zu bestimmen (Ergebnisse Teile 1,2, 3 und 8).

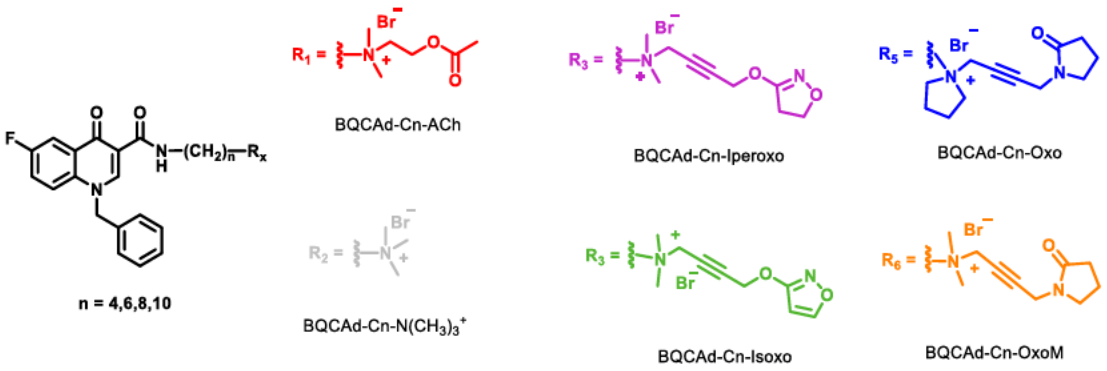

Abbildung 1. Strukturen derdualsterischen M1-Agonisten-Hybride, bestehend aus dem Benzylchinoloncarbonsäurederivat (BQCAd) und mehreren verschiedenen Bausteinen unselektiver Muskarinagonisten (Acetylcholin (rot), quaternärer Ammoniumkopf (grau), Iperoxo (lila)). Isoxo (grün), Oxotremorin (blau), Oxotremorin-M (orange)).

In Radioligand-Bindungsstudien haben alle synthetisierten Hybride sowohl an die orthosterische als auch an die allosterische Bindestelle gebunden. In einem Split-Biolumineszenz-Assay wurden alle Verbindungen in Bezug auf die G-Protein-Aktivierung als Agonisten charakterisiert, mit Ausnahme von den Oxotremorinderivaten (Ergebnis Teil 2).

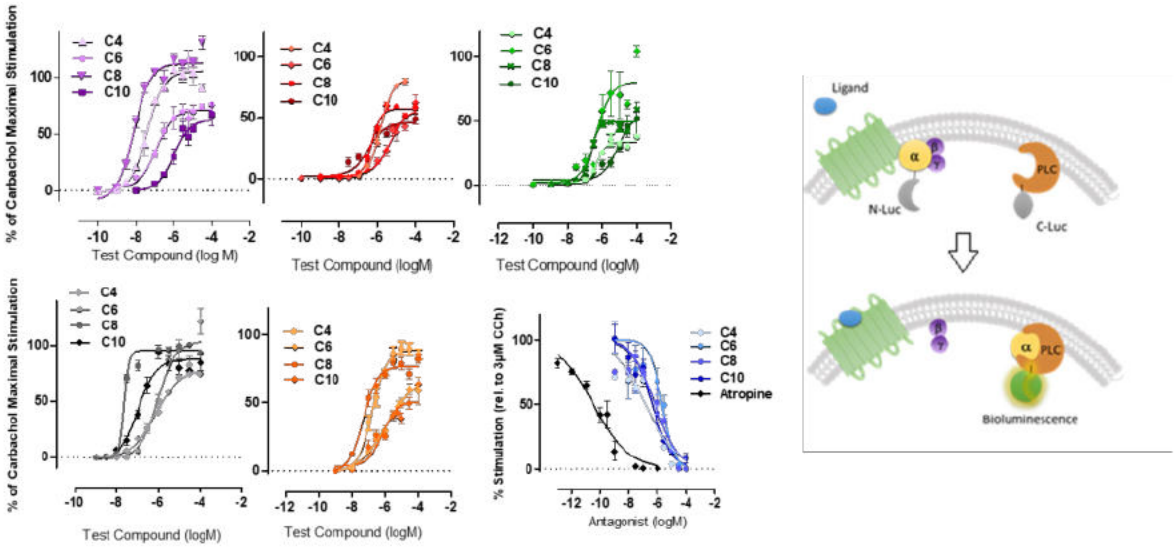

Abbildung 2. Split / Assay-Studien von sechs Serien bitopischer Verbindungen. Mit Ausnahme der Oxotremorinderivate wird eine konzentrationsabhängige G-Protein-Aktivierung beobachtet. Für diese wird eine Antagonistenantwort gemessen.

Allerdings konnten nur drei Hybride (BQCAd-6-Iperoxo, BQCAd-8-Iperoxo, BQCAd-6-Isoxo) β-Arrestine rekrutieren5. Detaillierte Analysen/Untersuchungen der Struktur-Aktivitäts-Beziehung wurden durchgeführt, um den Einfluss der verschiedenen orthosterischen Einheiten auf die M1-

Muskarinrezeptoraffinität, sowie die Wirksamkeit der dualsterischen Liganden aufzuklären. Die mit den bitopischen Verbindungen verbundene funktionelle Selektivität kann weiter untersucht werden, um die Struktur-Bias-Beziehungen der neuen Liganden zu analysieren.

Hierzu wurde Xanomelin über eine Alkylkette in die BQCAd-Hybridderivate eingebaut (Ergebnisteil 4). Dualsterische Verbindungen, die direkt am M1-Rezeptor wirken, konnten erfolgreich synthetisiert werden. Es konnte der Bindungsmodus der Hybride und ihre funktionelle Aktivität am M1-Rezeptor gezeigt werden.

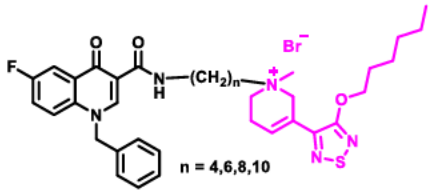

Abbildung 3. BQCAd-Xanomeline-Derivate

Aufgrund der besonderen Bindungsposition von Xanomeline an der orthosterischen Bindestelle des M1-Rezeptors, die als atypisch definiert ist, können die bitopischen Liganden wichtige Informationen über chemische Einheiten liefern, die an den orthosterischen / allosterischen Wechselwirkungen beteiligt sind.

Zusätzlich/Außerdem wurden neue Tacrine-Xanomeline-Hybride entwickelt und synthetisiert, die darauf abzielen, die Inhibition der Acetylcholinesterase zu verbessern und gleichzeitig den cholinergen Tonus über den xanomelinischen Anteil, der auf den M1-Rezeptor einwirkt, zu erhöhen7 (Ergebnis Teil 5).

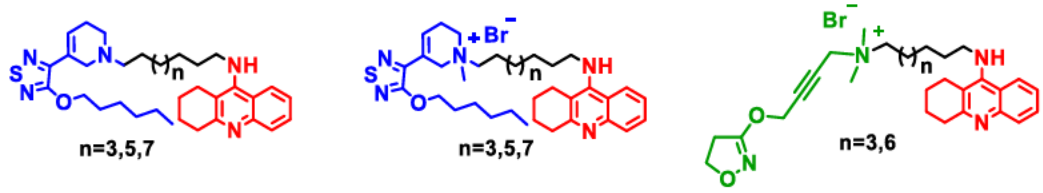

Abbildung 4. Strukturen von Tac / Xano-Hybriden und Tac / Iperoxo-Verbindungen

Leider waren Tac / Xano-Hybride nicht in der Lage M1-Rezeptoren zu aktivieren. Allerdings haben einige zuvor synthetisierte Derivate, in denen Tacrin mit Iperoxo über eine Heptyl- oder Decyllinkerkettegekoppelt wurde, eine G-Protein-Stimulation und eine IP1-Akkumulation gezeigt. Dies

ist ein Beweis dafür, dass dieForschung an bitopische Liganden ein hervorragenderAusgangspunkt für die Arzneimittelentwicklung ist.

Darüber hinaus wird in dieser Arbeit erstmals ein neuer tritopischer Ansatz vorgestellt, um die Untersuchung des M1-Muskarinrezeptors zu vertiefen (Ergebnis Teil 6). Die dreifach verzweigte Verbindung (zwei orthosterische Einheiten und ein kovalent gebundener allosterischer Teil) könnte die metastabilen und die orthosterischen Bindestellen desselben Rezeptors oder zwei orthosterische Taschen verschiedener Rezeptoren besetzen, was zu Dimerisierung führt.

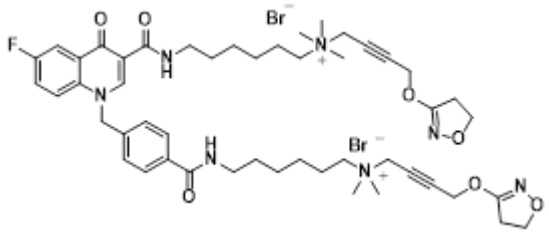

Abbildung 5. Strukturen des neuen dreiwertiger Hybridderivats

Interessanterweise bindet die Verbindung trotz der beträchtlichen sterischen Wirkung der beiden Iperoxo-Ligandeneinheiten an die orthosterische Stelle mit einer Affinität, die sogar höher ist als die von Iperoxo selbst. Die Verbindung, die derzeit nur am M1-Muskarinrezeptor im Hinblick auf Radioligandenbindung (Gleichgewicht und Dissoziation) und G-Protein-Aktivierung untersucht wird, könnte als molekulares Instrument zur Untersuchung metastabiler Bindungs- oder Multimerisierungszustände von hM1-Rezeptoren verwendet werden.

Außerdem wurde eine Reihe von Liganden vom Iperoxo-abgeleiteten Alkan-, Bis (ammonium) alkan-Typ und versteiften Ketten hergestellt (Ergebnisteil 7). Die Sonden werden verwendet, um die orthosterische Bindetasche hinsichtlich Flexibilität, physikalisch-chemischer Eigenschaften und räumlicher Beschaffenheitbei allen Muskarinrezeptor-Subtypen zu untersuchen.

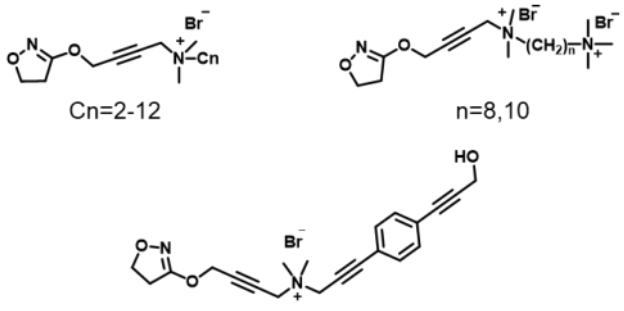

Abbildung 6. Strukturen des neuen Iperoxo-derivats.

Die Multi-Target-Verbindungen, die bitopischen Verbindungen und ihre molekularen Fragmente können wichtige Informationen liefern, um die spezifische Wirkung des M1 Rezeptors vollständig zu verstehen, und seine Funktion für therapeutische Anwendungen zu modulieren, was mit den derzeit verfügbaren Arzneimitteln nicht möglich ist. Aufgrund der Größe dieser Moleküle und die häufig positiveLadung haben die Verbindungen eine schlechte Arzneitauglichkeit. Die Ergebnisse dieser Arbeitliefern jedoch wichtige Informationen für weitere Überlegungen und Entwicklungen im cholinergen Bereich, da ein multi-target Ansatz die richtige Herangehensweise für die multifaktorielle Natur der AD-Krankheit zu sein scheint.

References

(1) May, L. T.; Leach, K.; Sexton, P. M.; Christopoulos, A. Allosteric modulation of G protein-coupled receptors. *Annual review of pharmacology and toxicology* **2007**, *47*, 1–51.

(2) Valant, C.; Sexton, P. M.; Christopoulos, A. Orthosteric/allosteric bitopic ligands: going hybrid at GPCRs. *Molecular interventions* **2009**, *9*, 125–135.

(3) Mohr, K.; Trankle, C.; Kostenis, E.; Barocelli, E.; Amici, M. de; Holzgrabe, U. Rational design of dualsteric GPCR ligands: quests and promise. *British journal of pharmacology* **2010**, *159*, 997–1008.

(4) Schwyzer, R. Acth: A short introductory review. *Ann NY Acad Sci* **1977**, *297*, 3–26.

(5) Portoghese, P. S. Bivalent ligands and the message-address concept in the design of selective opioid receptor antagonists. *Trends in pharmacological sciences* **1989**, *10*, 230–235.

(6) Messer, W. S. Bivalent ligands for G protein-coupled receptors. *Current pharmaceutical design* **2004**, *10*, 2015–2020.

(7) Berque-Bestel, I.; Lezoualc'h, F.; Jockers, R. Bivalent Ligands as Specific Pharmacological Tools for G Protein-Coupled Receptor Dimers. *CDDT* **2008**, *5*, 312–318.

(8) Peng, X.; Neumeyer, J. L. Kappa receptor bivalent ligands. *Current topics in medicinal chemistry* **2007**, *7*, 363–373.

(9) Portoghese, P. S. The bivalent ligand approach in the design of highly selective opioid receptor antagonists. *NIDA research monograph* **1990**, *96*, 3–20.

(10) Christopoulos, A.; Grant, M. K.; Ayoubzadeh, N.; Kim, O. N.; Sauerberg, P.; Jeppesen, L.; El-Fakahany, E. E. Synthesis and pharmacological evaluation of dimeric muscarinic acetylcholine receptor agonists. *The Journal of pharmacology and experimental therapeutics* **2001**, *298*, 1260–1268.

(11) Rajeswaran, W. G.; Cao, Y.; Huang, X. P.; Wroblewski, M. E.; Colclough, T.; Lee, S.; Liu, F.; Nagy, P. I.; Ellis, J.; Levine, B. A.*; et al.* Design, synthesis, and biological characterization of bivalent 1-methyl-1,2,5,6-tetrahydropyridyl-1,2,5-thiadiazole derivatives as selective muscarinic agonists. *J. Med. Chem.* **2001**, *44*, 4563–4576.

(12) Bonifazi, A.; Yano, H.; Del Bello, F.; Farande, A.; Quaglia, W.; Petrelli, R.; Matucci, R.; Nesi, M.; Vistoli, G.; Ferre, S.*; et al.* Synthesis and biological evaluation of a novel series of heterobivalent muscarinic ligands based on xanomeline and 1-3-(4-butylpiperidin-1-yl)propyl-1,2,3,4-tetrahydroquinolin-2-one (77-LH-28-1). *Journal of medicinal chemistry* **2014**, *57*, 9065–9077.

(13) Piergentili, A.; Quaglia, W.; Tayebati, S. K.; Paparelli, F.; Malmusi, L.; Brasili, L. Synthesis and muscarinic receptors affinity of a series of antagonist bivalent ligands. *Farmaco (Societa chimica italiana : 1989)* **1994**, *49*, 83–87.

(14) Lezoualc'h, F.; Jockers, R.; Berque-Bestel, I. Multivalent-based drug design applied to serotonin 5-HT(4) receptor oligomers. *Current pharmaceutical design* **2009**, *15*, 719–729.

(15) Soulier, J.-L.; Russo, O.; Giner, M.; Rivail, L.; Berthouze, M.; Ongeri, S.; Maigret, B.; Fischmeister, R.; Lezoualc'h, F.; Sicsic, S.*; et al.* Design and synthesis of specific probes for human 5-HT4 receptor dimerization studies. *J. Med. Chem.* **2005**, *48*, 6220–6228.

(16) Liu, J.; Brahimi, F.; Saragovi, H. U.; Burgess, K. Bivalent diketopiperazine-based tropomysin receptor kinase C (TrkC) antagonists. *Journal of medicinal chemistry* **2010**, *53*, 5044–5048.

(17) Bonger, K. M.; van den Berg, R. J. B. H. N.; Heitman, L. H.; IJzerman, A. P.; Oosterom, J.; Timmers, C. M.; Overkleeft, H. S.; van der Marel, G. A. Synthesis and evaluation of homo-bivalent GnRHR ligands. *Bioorganic & medicinal chemistry* **2007**, *15*, 4841–4856.

(18) Simoni, E.; Bartolini, M.; Abu, I. F.; Blockley, A.; Gotti, C.; Bottegoni, G.; Caporaso, R.; Bergamini, C.; Andrisano, V.; Cavalli, A.*; et al.* Multitarget drug design strategy in Alzheimer's disease: Focus on cholinergic transmission and amyloid-β aggregation. *Future medicinal chemistry* **2017**, *9*, 953–963.
(19) Haydar, S. N.; Ghiron, C.; Bettinetti, L.; Bothmann, H.; Comery, T. A.; Dunlop, J.; La Rosa, S.; Micco, I.; Pollastrini, M.; Quinn, J.*; et al.* SAR and biological evaluation of SEN12333/WAY-317538: Novel alpha 7 nicotinic acetylcholine receptor agonist. *Bioorganic & medicinal chemistry* **2009**, *17*, 5247–5258.
(20) Cavalli, A.; Bolognesi, M. L.; Capsoni, S.; Andrisano, V.; Bartolini, M.; Margotti, E.; Cattaneo, A.; Recanatini, M.; Melchiorre, C. A small molecule targeting the multifactorial nature of Alzheimer's disease. *Angewandte Chemie (International ed. in English)* **2007**, *46*, 3689–3692.
(21) Rosini, M.; Simoni, E.; Bartolini, M.; Cavalli, A.; Ceccarini, L.; Pascu, N.; McClymont, D. W.; Tarozzi, A.; Bolognesi, M. L.; Minarini, A.*; et al.* Inhibition of acetylcholinesterase, beta-amyloid aggregation, and NMDA receptors in Alzheimer's disease: A promising direction for the multi-target-directed ligands gold rush. *Journal of medicinal chemistry* **2008**, *51*, 4381–4384.
(22) Maspero, M.; Volpato, D.; Cirillo, D.; Yuan Chen, N.; Messerer, R.; Sotriffer, C.; Amici, M. de; Holzgrabe, U.; Dallanoce, C. Tacrine-xanomeline and tacrine-iperoxo hybrid ligands: Synthesis and biological evaluation at acetylcholinesterase and M1 muscarinic acetylcholine receptors. *Bioorganic chemistry* **2020**, *96*, 103633.
(23) Ma, H.-J.; Xie, R.-L.; Zhao, Q.-F.; Mei, X.-D.; Ning, J. Synthesis and insecticidal activity of novel carbamate derivatives as potential dual-binding site acetylcholinesterase inhibitors. *Journal of agricultural and food chemistry* **2010**, *58*, 12817–12821.
(24) Brahimi, F.; Liu, J.; Malakhov, A.; Chowdhury, S.; Purisima, E. O.; Ivanisevic, L.; Caron, A.; Burgess, K.; Saragovi, H. U. A monovalent agonist of TrkA tyrosine kinase receptors can be converted into a bivalent antagonist. *Biochimica et biophysica acta* **2010**, *1800*.
(25) Lane, J. R.; Sexton, P. M.; Christopoulos, A. Bridging the gap: bitopic ligands of G-protein-coupled receptors. *Trends in pharmacological sciences* **2013**, *34*, 59–66.
(26) Volpato, D.; Holzgrabe, U. Designing Hybrids Targeting the Cholinergic System by Modulating the Muscarinic and Nicotinic Receptors: A Concept to Treat Alzheimer's Disease. *Molecules (Basel, Switzerland)* **2018**, *23*.
(27) Volpato, D.; Kauk, M.; Messerer, R.; Bermudez, M.; Wolber, G.; Bock, A.; Hoffmann, C.; Holzgrabe, U. The Role of Orthosteric Building Blocks of Bitopic Ligands for Muscarinic M1 Receptors. *ACS Omega* **2020.** DOI: 10.1021/acsomega.0c04220.
(28) Anand, A.; Patience, A. A.; Sharma, N.; Khurana, N. The present and future of pharmacotherapy of Alzheimer's disease: A comprehensive review. *European journal of pharmacology* **2017**, *815*, 364–375.
(29) Davie, B. J.; Christopoulos, A.; Scammells, P. J. Development of M1 mAChR allosteric and bitopic ligands: Prospective therapeutics for the treatment of cognitive deficits. *ACS chemical neuroscience* **2013**, *4*, 1026–1048.
(30) Verma, S.; Kumar, A.; Tripathi, T.; Kumar, A. Muscarinic and nicotinic acetylcholine receptor agonists: Current scenario in Alzheimer's disease therapy. *The Journal of pharmacy and pharmacology* **2018**, *70*, 985–993.
(31) Li, J. J.; Dolios, G.; Wang, R.; Liao, F.-F. Soluble beta-amyloid peptides, but not insoluble fibrils, have specific effect on neuronal microRNA expression. *PloS one* **2014**, *9*, e90770.
(32) Langmead, C. J.; Watson, J.; Reavill, C. Muscarinic acetylcholine receptors as CNS drug targets. *Pharmacology & therapeutics* **2008**, *117*, 232–243.

(33) Mikiciuk-Olasik, E.; Szymański, P.; Zurek, E. Diagnostics and therapy of Alzheimer's disease. *Indian journal of experimental biology* **2007**, *45*, 315–325.
(34) Hassan, M.; Abbas, Q.; Seo, S.-Y.; Shahzadi, S.; Al Ashwal, H.; Zaki, N.; Iqbal, Z.; Moustafa, A. A. Computational modeling and biomarker studies of pharmacological treatment of Alzheimer's disease (Review). *Molecular medicine reports* **2018**, *18*, 639–655.
(35) Francis, P. T. The Interplay of Neurotransmitters in Alzheimer's Disease. *CNS Spectr.* **2005**, *10*, 6–9.
(36) Giacobini, E. Cholinergic function and Alzheimer's disease. *International journal of geriatric psychiatry* **2003**, *18*, S1-5.
(37) Decker, M., Ed. *Design of Hybrid Molecules for Drug Development*; Elsevier, **2017**.
(38) Greig, N. H.; Utsuki, T.; Ingram, D. K.; Wang, Y.; Pepeu, G.; Scali, C.; Yu, Q.-S.; Mamczarz, J.; Holloway, H. W.; Giordano, T.*; et al.* Selective butyrylcholinesterase inhibition elevates brain acetylcholine, augments learning and lowers Alzheimer beta-amyloid peptide in rodent. *Proceedings of the National Academy of Sciences of the United States of America* **2005**, *102*, 17213–17218.
(39) Hamley, I. W. The amyloid beta peptide: A chemist's perspective. Role in Alzheimer's and fibrillization. *Chemical reviews* **2012**, *112*, 5147–5192.
(40) Lambert, M. P.; Barlow, A. K.; Chromy, B. A.; Edwards, C.; Freed, R.; Liosatos, M.; Morgan, T. E.; Rozovsky, I.; Trommer, B.; Viola, K. L.*; et al.* Diffusible, nonfibrillar ligands derived from Abeta1-42 are potent central nervous system neurotoxins. *Proceedings of the National Academy of Sciences of the United States of America* **1998**, *95*, 6448–6453.
(41) Wang, H.-W.; Pasternak, J. F.; Kuo, H.; Ristic, H.; Lambert, M. P.; Chromy, B.; Viola, K. L.; Klein, W. L.; Stine, W. B.; Krafft, G. A.*; et al.* Soluble oligomers of beta amyloid (1-42) inhibit long-term potentiation but not long-term depression in rat dentate gyrus. *Brain research* **2002**, *924*, 133–140.
(42) Dahlgren, K. N.; Manelli, A. M.; Stine, W. B.; Baker, L. K.; Krafft, G. A.; LaDu, M. J. Oligomeric and fibrillar species of amyloid-beta peptides differentially affect neuronal viability. *The Journal of biological chemistry* **2002**, *277*, 32046–32053.
(43) Nussbaum, J. M.; Schilling, S.; Cynis, H.; Silva, A.; Swanson, E.; Wangsanut, T.; Tayler, K.; Wiltgen, B.; Hatami, A.; Rönicke, R.*; et al.* Prion-like behaviour and tau-dependent cytotoxicity of pyroglutamylated amyloid-β. *Nature* **2012**, *485*, 651–655.
(44) Walsh, D. M.; Klyubin, I.; Fadeeva, J. V.; Cullen, W. K.; Anwyl, R.; Wolfe, M. S.; Rowan, M. J.; Selkoe, D. J. Naturally secreted oligomers of amyloid beta protein potently inhibit hippocampal long-term potentiation in vivo. *Nature* **2002**, *416*, 535–539.
(45) Cleary, J. P.; Walsh, D. M.; Hofmeister, J. J.; Shankar, G. M.; Kuskowski, M. A.; Selkoe, D. J.; Ashe, K. H. Natural oligomers of the amyloid-beta protein specifically disrupt cognitive function. *Nature neuroscience* **2005**, *8*, 79–84.
(46) Lesné, S.; Koh, M. T.; Kotilinek, L.; Kayed, R.; Glabe, C. G.; Yang, A.; Gallagher, M.; Ashe, K. H. A specific amyloid-beta protein assembly in the brain impairs memory. *Nature* **2006**, *440*, 352–357.
(47) Esparza, T. J.; Wildburger, N. C.; Jiang, H.; Gangolli, M.; Cairns, N. J.; Bateman, R. J.; Brody, D. L. Soluble Amyloid-beta Aggregates from Human Alzheimer's Disease Brains. *Scientific reports* **2016**, *6*, 38187.
(48) Tasker, A.; Perry, E. K.; Ballard, C. G. Butyrylcholinesterase: Impact on symptoms and progression of cognitive impairment. *Expert review of neurotherapeutics* **2005**, *5*, 101–106.
(49) Giacobini, E. Cholinesterase inhibitors: New roles and therapeutic alternatives. *Pharmacological research* **2004**, *50*, 433–440.
(50) Geula, C.; Darvesh, S. Butyrylcholinesterase, cholinergic neurotransmission and the pathology of Alzheimer's disease. *Drugs Today* **2004**, *40*, 711.

(51) Auld, D. S.; Kar, S.; Quirion, R. β-Amyloid peptides as direct cholinergic neuromodulators: A missing link? *Trends in Neurosciences* **1998**, *21*, 43–49.
(52) Valant, C.; Robert Lane, J.; Sexton, P. M.; Christopoulos, A. The best of both worlds? Bitopic orthosteric/allosteric ligands of g protein-coupled receptors. *Annual review of pharmacology and toxicology* **2012**, *52*, 153–178.
(53) Wermuth, C. G. Multitargeted drugs: The end of the 'one-target-one-disease' philosophy? *Drug discovery today* **2004**, *9*, 826–827.
(54) Muñoz-Torrero, D. Multitarget Anti-Alzheimer Hybrid Compounds. *Design of Hybrid Molecules for Drug Development*; Elsevier, **2017**; pp 167–192.
(55) Gregory, K. J.; Sexton, P. M.; Christopoulos, A. Overview of receptor allosterism. *Current protocols in pharmacology* **2010**, *Chapter 1*, Unit 1.21.
(56) Burger, W. A. C.; Sexton, P. M.; Christopoulos, A.; Thal, D. M. Toward an understanding of the structural basis of allostery in muscarinic acetylcholine receptors. *The Journal of general physiology* **2018.** DOI: 10.1085/jgp.201711979.
(57) Bock, A.; Schrage, R.; Mohr, K. Allosteric modulators targeting CNS muscarinic receptors. *Neuropharmacology* **2017.** DOI: 10.1016/j.neuropharm.2017.09.024.
(58) Mohr, K.; Schmitz, J.; Schrage, R.; Trankle, C.; Holzgrabe, U. Molecular alliance-from orthosteric and allosteric ligands to dualsteric/bitopic agonists at G protein coupled receptors. *Angewandte Chemie (International ed. in English)* **2013**, *52*, 508–516.
(59) Conn, P. J.; Christopoulos, A.; Lindsley, C. W. Allosteric modulators of GPCRs: a novel approach for the treatment of CNS disorders. *Nature reviews. Drug discovery* **2009**, *8*, 41–54.
(60) Kenakin, T.; Christopoulos, A. Signalling bias in new drug discovery: detection, quantification and therapeutic impact. *Nature reviews. Drug discovery* **2013**, *12*, 205–216.
(61) Bock, A.; Kostenis, E.; Trankle, C.; Lohse, M. J.; Mohr, K. Pilot the pulse: controlling the multiplicity of receptor dynamics. *Trends in pharmacological sciences* **2014**, *35*, 630–638.
(62) Wild, C.; Cunningham, K. A.; Zhou, J. Allosteric Modulation of G Protein-Coupled Receptors: An Emerging Approach of Drug Discovery. *Austin journal of pharmacology and therapeutics* **2014**, *2*.
(63) Ehlert, F. J. Estimation of the affinities of allosteric ligands using radioligand binding and pharmacological null methods. *Molecular pharmacology*, **1988**, 33(2):187-94.
(64) Lazareno, S.; Dolezal, V.; Popham, A.; Birdsall, N. J. M. Thiochrome enhances acetylcholine affinity at muscarinic M4 receptors: Receptor subtype selectivity via cooperativity rather than affinity. *Molecular pharmacology* **2004**, *65*, 257–266.
(65) Decker, M.; Holzgrabe, U. M1 muscarinic cetylcholine receptor allosteric modulators as potential therapeutic opportunities for treating Alzheimer's disease. *Med. Chem. Commun.* **2012**, *3*, 752.
(66) Matera, C.; Tata, A. Pharmacological Approaches to Targeting Muscarinic Acetylcholine Receptors. *RPCN* **2014**, *9*, 85–100.
(67) Sánchez-Fernández, G.; Cabezudo, S.; García-Hoz, C.; Tobin, A. B.; Mayor, F.; Ribas, C. ERK5 activation by Gq-coupled muscarinic receptors is independent of receptor internalization and β-arrestin recruitment. *PloS one* **2013**, *8*, e84174.
(68) Kenakin, T. Signaling bias in drug discovery. *Expert opinion on drug discovery* **2017**, *12*, 321–333.
(69) Keller, M.; Tränkle, C.; She, X.; Pegoli, A.; Bernhardt, G.; Buschauer, A.; Read, R. W. M2 Subtype preferring dibenzodiazepinone-type muscarinic receptor ligands: Effect of chemical homo-dimerization on orthosteric (and allosteric?) binding. *Bioorganic & medicinal chemistry* **2015**, *23*, 3970–3990.

(70) Pegoli, A.; She, X.; Wifling, D.; Hübner, H.; Bernhardt, G.; Gmeiner, P.; Keller, M. Radiolabeled Dibenzodiazepinone-Type Antagonists Give Evidence of Dualsteric Binding at the M2 Muscarinic Acetylcholine Receptor. *Journal of medicinal chemistry* **2017**, *60*, 3314–3334.
(71) She, X.; Pegoli, A.; Mayr, J.; Hübner, H.; Bernhardt, G.; Gmeiner, P.; Keller, M. Heterodimerization of Dibenzodiazepinone-Type Muscarinic Acetylcholine Receptor Ligands Leads to Increased M 2 R Affinity and Selectivity. *ACS Omega* **2017**, *2*, 6741–6754.
(72) Narlawar, R.; Lane, J. R.; Doddareddy, M.; Lin, J.; Brussee, J.; Ijzerman, A. P. Hybrid ortho/allosteric ligands for the adenosine A(1) receptor. *Journal of medicinal chemistry* **2010**, *53*, 3028–3037.
(73) Aurelio, L.; Valant, C.; Flynn, B. L.; Sexton, P. M.; Christopoulos, A.; Scammells, P. J. Allosteric modulators of the adenosine A1 receptor: Synthesis and pharmacological evaluation of 4-substituted 2-amino-3-benzoylthiophenes. *Journal of medicinal chemistry* **2009**, *52*, 4543–4547.
(74) Steinfeld, T.; Mammen, M.; Smith, J. A. M.; Wilson, R. D.; Jasper, J. R. A novel multivalent ligand that bridges the allosteric and orthosteric binding sites of the M2 muscarinic receptor. *Molecular pharmacology* **2007**, *72*, 291–302.
(75) Lane, J. R.; Donthamsetti, P.; Shonberg, J.; Draper-Joyce, C. J.; Dentry, S.; Michino, M.; Shi, L.; López, L.; Scammells, P. J.; Capuano, B.*; et al.* A new mechanism of allostery in a G protein-coupled receptor dimer. *Nature chemical biology* **2014**, *10*, 745–752.
(76) Stemp, G.; Ashmeade, T.; Branch, C. L.; Hadley, M. S.; Hunter, A. J.; Johnson, C. N.; Nash, D. J.; Thewlis, K. M.; Vong, A. K. K.; Austin, N. E.*; et al.* Design and Synthesis of trans - N -[4-[2-(6-Cyano-1,2,3,4-tetrahydroisoquinolin-2- yl)ethyl]cyclohexyl]-4-quinolinecarboxamide (SB-277011): A Potent and Selective Dopamine D 3 Receptor Antagonist with High Oral Bioavailability and CNS Penetration in the Rat. *J. Med. Chem.* **2000**, *43*, 1878–1885.
(77) Rossi, M.; Fasciani, I.; Marampon, F.; Maggio, R.; Scarselli, M. The First Negative Allosteric Modulator for Dopamine D2 and D3 Receptors, SB269652 May Lead to a New Generation of Antipsychotic Drugs. *Molecular pharmacology* **2017**, *91*, 586–594.
(78) Kopinathan, A.; Scammells, P. J.; Lane, J. R.; Capuano, B. Multivalent approaches and beyond: Novel tools for the investigation of dopamine D2 receptor pharmacology. *Future medicinal chemistry* **2016**, *8*, 1349–1372.
(79) Jo, E.; Bhhatarai, B.; Repetto, E.; Guerrero, M.; Riley, S.; Brown, S. J.; Kohno, Y.; Roberts, E.; Schürer, S. C.; Rosen, H. Novel selective allosteric and bitopic ligands for the S1P(3) receptor. *ACS chemical biology* **2012**, *7*, 1975–1983.
(80) Sanna, M. G.; Vincent, K. P.; Repetto, E.; Nguyen, N.; Brown, S. J.; Abgaryan, L.; Riley, S. W.; Leaf, N. B.; Cahalan, S. M.; Kiosses, W. B.*; et al.* Bitopic Sphingosine 1-Phosphate Receptor 3 (S1P3) Antagonist Rescue from Complete Heart Block: Pharmacological and Genetic Evidence for Direct S1P3 Regulation of Mouse Cardiac Conduction. *Molecular pharmacology* **2016**, *89*, 176–186.
(81) Antony, J.; Kellershohn, K.; Mohr-Andra, M.; Kebig, A.; Prilla, S.; Muth, M.; Heller, E.; Disingrini, T.; Dallanoce, C.; Bertoni, S.*; et al.* Dualsteric GPCR targeting: a novel route to binding and signaling pathway selectivity. *FASEB journal : official publication of the Federation of American Societies for Experimental Biology* **2009**, *23*, 442–450.
(82) Chen, X.; Klockner, J.; Holze, J.; Zimmermann, C.; Seemann, W. K.; Schrage, R.; Bock, A.; Mohr, K.; Tränkle, C.; Holzgrabe, U.*; et al.* Rational design of partial agonists for the muscarinic m1 acetylcholine receptor. *Journal of medicinal chemistry* **2015**, *58*, 560–576.
(83) Messerer, R.; Kauk, M.; Volpato, D.; Alonso Canizal, M. C.; Kloeckner, J.; Zabel, U.; Nuber, S.; Hoffmann, C.; Holzgrabe, U. FRET Studies of Quinolone-Based Bitopic Ligands and their Structural Analogues at the Muscarinic M1 Receptor. *ACS chemical biology* **2017.** DOI: 10.1021/acschembio.6b00828.

(84) Schmitz, J.; van der Mey, D.; Bermudez, M.; Klockner, J.; Schrage, R.; Kostenis, E.; Trankle, C.; Wolber, G.; Mohr, K.; Holzgrabe, U. Dualsteric muscarinic antagonists--orthosteric binding pose controls allosteric subtype selectivity. *Journal of medicinal chemistry* **2014**, *57*, 6739–6750.
(85) Fronik, P.; Gaiser, B. I.; Sejer Pedersen, D. Bitopic Ligands and Metastable Binding Sites: Opportunities for G Protein-Coupled Receptor (GPCR) Medicinal Chemistry. *Journal of medicinal chemistry* **2017**, *60*, 4126–4134.
(86) Paoletta, S.; Sabbadin, D.; Kügelgen, I. von; Hinz, S.; Katritch, V.; Hoffmann, K.; Abdelrahman, A.; Straßburger, J.; Baqi, Y.; Zhao, Q.*; et al.* Modeling ligand recognition at the P2Y12 receptor in light of X-ray structural information. *J Comput Aided Mol Des* **2015**, *29*, 737–756.
(87) Sabbadin, D.; Ciancetta, A.; Deganutti, G.; Cuzzolin, A.; Moro, S. Exploring the recognition pathway at the human A 2A adenosine receptor of the endogenous agonist adenosine using supervised molecular dynamics simulations. *Med. Chem. Commun.* **2015**, *6*, 1081–1085.
(88) Sabbadin, D.; Ciancetta, A.; Moro, S. Bridging Molecular Docking to Membrane Molecular Dynamics To Investigate GPCR–Ligand Recognition: The Human A 2A Adenosine Receptor as a Key Study. *J. Chem. Inf. Model.* **2013**, *54*, 169–183.
(89) Buch, I.; Giorgino, T.; Fabritiis, G. de. Complete reconstruction of an enzyme-inhibitor binding process by molecular dynamics simulations. *Proceedings of the National Academy of Sciences of the United States of America* **2011**, *108*, 10184–10189.
(90) González, A.; Perez-Acle, T.; Pardo, L.; Deupi, X.; van Veen, H. W. Molecular Basis of Ligand Dissociation in β-Adrenergic Receptors. *PloS one* **2011**, *6*, e23815.
(91) Dror, R. O.; Pan, A. C.; Arlow, D. H.; Borhani, D. W.; Maragakis, P.; Shan, Y.; Xu, H.; Shaw, D. E. Pathway and mechanism of drug binding to G-protein-coupled receptors. *Proceedings of the National Academy of Sciences of the United States of America* **2011**, *108*, 13118–13123.
(92) Disingrini, T.; Muth, M.; Dallanoce, C.; Barocelli, E.; Bertoni, S.; Kellershohn, K.; Mohr, K.; Amici, M. de; Holzgrabe, U. Design, synthesis, and action of oxotremorine-related hybrid-type allosteric modulators of muscarinic acetylcholine receptors. *Journal of medicinal chemistry* **2006**, *49*, 366–372.
(93) Abrams, P.; Andersson, K.-E.; Buccafusco, J. J.; Chapple, C.; Groat, W. C. de; Fryer, A. D.; Kay, G.; Laties, A.; Nathanson, N. M.; Pasricha, P. J.*; et al.* Muscarinic receptors: Their distribution and function in body systems, and the implications for treating overactive bladder. *British journal of pharmacology* **2006**, *148*, 565–578.
(94) Bradley, S. J.; Bourgognon, J.-M.; Sanger, H. E.; Verity, N.; Mogg, A. J.; White, D. J.; Butcher, A. J.; Moreno, J. A.; Molloy, C.; Macedo-Hatch, T.*; et al.* M1 muscarinic allosteric modulators slow prion neurodegeneration and restore memory loss. *The Journal of clinical investigation* **2017**, *127*, 487–499.
(95) Caccamo, A.; Oddo, S.; Billings, L. M.; Green, K. N.; Martinez-Coria, H.; Fisher, A.; LaFerla, F. M. M1 receptors play a central role in modulating AD-like pathology in transgenic mice. *Neuron* **2006**, *49*, 671–682.
(96) Fisher, A. Cholinergic treatments with emphasis on m1 muscarinic agonists as potential disease-modifying agents for Alzheimer's disease. *Neurotherapeutics : the journal of the American Society for Experimental NeuroTherapeutics* **2008**, *5*, 433–442.
(97) Fisher, A.; Brandeis, R.; Bar-Ner, R. H. N.; Kliger-Spatz, M.; Natan, N.; Sonego, H.; Marcovitch, I.; Pittel, Z. AF150(S) and AF267B: M1 muscarinic agonists as innovative therapies for Alzheimer's disease. *Journal of molecular neuroscience : MN* **2002**, *19*, 145–153.
(98) Sams, A. G.; Hentzer, M.; Mikkelsen, G. K.; Larsen, K.; Bundgaard, C.; Plath, N.; Christoffersen, C. T.; Bang-Andersen, B. Discovery of N-{1-3-(3-oxo-2,3-dihydrobenzo1,4oxazin-4-yl)propylpiperidin-4-yl}-2-phenylacetamide (Lu AE51090): An allosteric muscarinic M1 receptor agonist with unprecedented selectivity and procognitive potential. *Journal of medicinal chemistry* **2010**, *53*, 6386–6397.

(99) Budzik, B.; Garzya, V.; Shi, D.; Foley, J. J.; Rivero, R. A.; Langmead, C. J.; Watson, J.; Wu, Z.; Forbes, I. T.; Jin, J. 2' biaryl amides as novel and subtype selective M1 agonists. Part I: Identification, synthesis, and initial SAR. *Bioorganic & medicinal chemistry letters* **2010**, *20*, 3540–3544.
(100) Budzik, B.; Garzya, V.; Shi, D.; Walker, G.; Woolley-Roberts, M.; Pardoe, J.; Lucas, A.; Tehan, B.; Rivero, R. A.; Langmead, C. J.*; et al.* Novel N-Substituted Benzimidazolones as Potent, Selective, CNS-Penetrant, and Orally Active M1 mAChR Agonists. *ACS medicinal chemistry letters* **2010**, *1*, 244–248.
(101) Kruse, A. C.; Ring, A. M.; Manglik, A.; Hu, J.; Hu, K.; Eitel, K.; Hubner, H.; Pardon, E.; Valant, C.; Sexton, P. M.*; et al.* Activation and allosteric modulation of a muscarinic acetylcholine receptor. *Nature* **2013**, *504*, 101–106.
(102) Matera, C.; Flammini, L.; Quadri, M.; Vivo, V.; Ballabeni, V.; Holzgrabe, U.; Mohr, K.; Amici, M. de; Barocelli, E.; Bertoni, S.*; et al.* Bis(ammonio)alkane-type agonists of muscarinic acetylcholine receptors: synthesis, in vitro functional characterization, and in vivo evaluation of their analgesic activity. *European journal of medicinal chemistry* **2014**, *75*, 222–232.
(103) Bock, A.; Merten, N.; Schrage, R.; Dallanoce, C.; Batz, J.; Klockner, J.; Schmitz, J.; Matera, C.; Simon, K.; Kebig, A.*; et al.* The allosteric vestibule of a seven transmembrane helical receptor controls G-protein coupling. *Nature communications* **2012**, *3*, 1044.
(104) Valant, C.; Gregory, K. J.; Hall, N. E.; Scammells, P. J.; Lew, M. J.; Sexton, P. M.; Christopoulos, A. A novel mechanism of G protein-coupled receptor functional selectivity. Muscarinic partial agonist McN-A-343 as a bitopic orthosteric/allosteric ligand. *The Journal of biological chemistry* **2008**, *283*, 29312–29321.
(105) Bock, A.; Bermudez, M.; Krebs, F.; Matera, C.; Chirinda, B.; Sydow, D.; Dallanoce, C.; Holzgrabe, U.; Amici, M. de; Lohse, M. J.*; et al.* Ligand Binding Ensembles Determine Graded Agonist Efficacies at a G Protein-coupled Receptor. *The Journal of biological chemistry* **2016**, *291*, 16375–16389.
(106) Ma, L.; Seager, M. A.; Seager, M.; Wittmann, M.; Jacobson, M.; Bickel, D.; Burno, M.; Jones, K.; Graufelds, V. K.; Xu, G.*; et al.* Selective activation of the M1 muscarinic acetylcholine receptor achieved by allosteric potentiation. *Proceedings of the National Academy of Sciences of the United States of America* **2009**, *106*, 15950–15955.
(107) Wess, J. Allosteric binding sites on muscarinic acetylcholine receptors. *Molecular pharmacology* **2005**, *68*, 1506–1509.
(108) Felder, C. C.; Goldsmith, P. J.; Jackson, K.; Sanger, H. E.; Evans, D. A.; Mogg, A. J.; Broad, L. M. Current status of muscarinic M1 and M4 receptors as drug targets for neurodegenerative diseases. *Neuropharmacology* **2018**, *136*, 449–458.
(109) Bock, A.; Chirinda, B.; Krebs, F.; Messerer, R.; Batz, J.; Muth, M.; Dallanoce, C.; Klingenthal, D.; Trankle, C.; Hoffmann, C.*; et al.* Dynamic ligand binding dictates partial agonism at a G protein-coupled receptor. *Nature chemical biology* **2014**, *10*, 18–20.
(110) Choi, M.; Staus, D. P.; Wingler, L. M.; Ahn, S.; Pani, B.; Capel, W. D.; Lefkowitz, R. J. G protein-coupled receptor kinases (GRKs) orchestrate biased agonism at the β2-adrenergic receptor. *Science signaling* **2018**, *11*.
(111) Agnetta, L.; Kauk, M.; Canizal, M. C. A.; Messerer, R.; Holzgrabe, U.; Hoffmann, C.; Decker, M. A Photoswitchable Dualsteric Ligand Controlling Receptor Efficacy. *Angewandte Chemie (International ed. in English)* **2017**, *56*, 7282–7287.
(112) Watt, M. L.; Schober, D. A.; Hitchcock, S.; Liu, B.; Chesterfield, A. K.; McKinzie, D.; Felder, C. C. Pharmacological characterization of LY593093, an M1 muscarinic acetylcholine receptor-selective partial orthosteric agonist. *The Journal of pharmacology and experimental therapeutics* **2011**, *338*, 622–632.

(113) Avlani, V. A.; Langmead, C. J.; Guida, E.; Wood, M. D.; Tehan, B. G.; Herdon, H. J.; Watson, J. M.; Sexton, P. M.; Christopoulos, A. Orthosteric and allosteric modes of interaction of novel selective agonists of the M1 muscarinic acetylcholine receptor. *Molecular pharmacology* **2010**, *78*, 94–104.
(114) Langmead, C. J.; Fry, V. A. H.; Forbes, I. T.; Branch, C. L.; Christopoulos, A.; Wood, M. D.; Herdon, H. J. Probing the molecular mechanism of interaction between 4-n-butyl-1-4-(2-methylphenyl)-4-oxo-1-butyl-piperidine (AC-42) and the muscarinic M(1) receptor: Direct pharmacological evidence that AC-42 is an allosteric agonist. *Molecular pharmacology* **2006**, *69*, 236–246.
(115) Thomas, R. L.; Mistry, R.; Langmead, C. J.; Wood, M. D.; Challiss, R. A. J. G protein coupling and signaling pathway activation by m1 muscarinic acetylcholine receptor orthosteric and allosteric agonists. *The Journal of pharmacology and experimental therapeutics* **2008**, *327*, 365–374.
(116) Spalding, T. A.; Ma, J.-N.; Ott, T. R.; Friberg, M.; Bajpai, A.; Bradley, S. R.; Davis, R. E.; Brann, M. R.; Burstein, E. S. Structural requirements of transmembrane domain 3 for activation by the M1 muscarinic receptor agonists AC-42, AC-260584, clozapine, and N-desmethylclozapine: Evidence for three distinct modes of receptor activation. *Molecular pharmacology* **2006**, *70*, 1974–1983.
(117) Zhang, S.; Saathoff, J. M.; He, L. Molecular Hybridization: An Emerging Tool for the Design of Novel Therapeutics for Alzheimer's Disease. *Design of Hybrid Molecules for Drug Development*; Elsevier, **2017**; pp 219–237.
(118) Carvajal, F. J.; Inestrosa, N. C. Interactions of AChE with Aβ Aggregates in Alzheimer's Brain: Therapeutic Relevance of IDN 5706. *Frontiers in molecular neuroscience* **2011**, *4*, 19.
(119) Sussman, J.; Harel, M.; Frolow, F.; Oefner, C.; Goldman, A.; Toker, L.; Silman, I. Atomic structure of acetylcholinesterase from Torpedo californica: A prototypic acetylcholine-binding protein. *Science (New York, N.Y.)* **1991**, *253*, 872–879.
(120) Colletier, J.-P.; Fournier, D.; Greenblatt, H. M.; Stojan, J.; Sussman, J. L.; Zaccai, G.; Silman, I.; Weik, M. Structural insights into substrate traffic and inhibition in acetylcholinesterase. *The EMBO journal* **2006**, *25*, 2746–2756.
(121) Zheng, Z.-H.; Dong, Y.-S.; Zhang, H.; Lu, X.-H.; Ren, X.; Zhao, G.; He, J.-G.; Si, S.-Y. Isolation and characterization of N98-1272 A, B and C, selective acetylcholinesterase inhibitors from metabolites of an actinomycete strain. *Journal of enzyme inhibition and medicinal chemistry* **2007**, *22*, 43–49.
(122) Bullock, R.; Bergman, H.; Touchon, J.; Gambina, G.; He, Y.; Nagel, J.; Lane, R. Effect of age on response to rivastigmine or donepezil in patients with Alzheimer's disease. *Current medical research and opinion* **2006**, *22*, 483–494.
(123) Bullock, R.; Touchon, J.; Bergman, H.; Gambina, G.; He, Y.; Rapatz, G.; Nagel, J.; Lane, R. Rivastigmine and donepezil treatment in moderate to moderately-severe Alzheimer's disease over a 2-year period. *Current medical research and opinion* **2005**, *21*, 1317–1327.
(124) Mueller, B.; Adler, G. Prevalence of Wild-Type Butyrylcholinesterase Genotype in Patients with Alzheimer's Dementia. *WJNS* **2015**, *05*, 175–179.
(125) Munoz-Torrero, D. Acetylcholinesterase Inhibitors as Disease-Modifying Therapies for Alzheimers Disease. *CMC* **2008**, *15*, 2433–2455.
(126) Mehta, M.; Adem, A.; Sabbagh, M. New acetylcholinesterase inhibitors for Alzheimer's disease. *International journal of Alzheimer's disease* **2012**, *2012*, 728983.
(127) Stepankova, S.; Komers, K. Cholinesterases and Cholinesterase Inhibitors. *CEI* **2008**, *4*, 160–171.
(128) Colović, M. B.; Krstić, D. Z.; Lazarević-Pašti, T. D.; Bondžić, A. M.; Vasić, V. M. Acetylcholinesterase inhibitors: Pharmacology and toxicology. *Current neuropharmacology* **2013**, *11*, 315–335.

(129) McGleenon; Dynan; Passmore. Acetylcholinesterase inhibitors in Alzheimer's disease. *British Journal of Clinical Pharmacology* **1999**, *48*, 471–480.
(130) Pang, Y.-P.; Hong, F.; Quiram, P.; Jelacic, T.; Brimijoin, S. Synthesis of alkylene linked bis-THA and alkylene linked benzyl-THA as highly potent and selective inhibitors and molecular probes of acetylcholinesterase. *J. Chem. Soc., Perkin Trans. 1* **1997**, 171–176.
(131) Messerer, R.; Dallanoce, C.; Matera, C.; Wehle, S.; Flammini, L.; Chirinda, B.; Bock, A.; Irmen, M.; Tränkle, C.; Barocelli, E.*; et al.* Novel bipharmacophoric inhibitors of the cholinesterases with affinity to the muscarinic receptors M 1 and M 2. *Med. Chem. Commun.* **2017**, *8*, 1346–1359.
(132) Regina Messerer. Synthesis of Dualsteric Ligands for Muscarinic Acetylcholine Receptors and Cholinesterase Inhibitors, Würzburg, **2017**.
(133) Campiani, G.; Fattorusso, C.; Butini, S.; Gaeta, A.; Agnusdei, M.; Gemma, S.; Persico, M.; Catalanotti, B.; Savini, L.; Nacci, V.*; et al.* Development of molecular probes for the identification of extra interaction sites in the mid-gorge and peripheral sites of butyrylcholinesterase (BuChE). Rational design of novel, selective, and highly potent BuChE inhibitors. *J. Med. Chem.* **2005**, *48*, 1919–1929.
(134) Carlier, P. R.; Han, Y. F.; Chow, E. S.-H.; Li, C. P.-L.; Wang, H.; Xuan Lieu, T.; Sum Wong, H.; Pang, Y.-P. Evaluation of short-tether Bis-THA AChE inhibitors. A further test of the dual binding site hypothesis. *Bioorganic & medicinal chemistry* **1999**, *7*, 351–357.
(135) Fang, L.; Jumpertz, S.; Zhang, Y.; Appenroth, D.; Fleck, C.; Mohr, K.; Tränkle, C.; Decker, M. Hybrid molecules from xanomeline and tacrine: enhanced tacrine actions on cholinesterases and muscarinic M1 receptors. *Journal of medicinal chemistry* **2010**, *53*, 2094–2103.
(136) Bymaster, F. P.; Whitesitt, C. A.; Shannon, H. E.; DeLapp, N.; Ward, J. S.; Calligaro, D. O.; Shipley, L. A.; Buelke-Sam, J. L.; Bodick, N. C.; Farde, L.*; et al.* Xanomeline: A selective muscarinic agonist for the treatment of Alzheimer's disease. *Drug Dev. Res.* **1997**, *40*, 158–170.
(137) Farrell, M.; Roth, B. L. Allosteric antipsychotics: M4 muscarinic potentiators as novel treatments for schizophrenia. *Neuropsychopharmacology : official publication of the American College of Neuropsychopharmacology* **2010**, *35*, 851–852.
(138) Mirza, N. R.; Peters, D.; Sparks, R. G. Xanomeline and the Antipsychotic Potential of Muscarinic Receptor Subtype Selective Agonists. *CNS Drug Reviews* **2003**, *9*, 159–186.
(139) Jakubík, J.; El-Fakahany, E. E.; Dolezal, V. Differences in kinetics of xanomeline binding and selectivity of activation of G proteins at M(1) and M(2) muscarinic acetylcholine receptors. *Molecular pharmacology* **2006**, *70*, 656–666.
(140) Jakubík, J.; Tucek, S.; El-Fakahany, E. E. Role of receptor protein and membrane lipids in xanomeline wash-resistant binding to muscarinic M1 receptors. *The Journal of pharmacology and experimental therapeutics* **2004**, *308*, 105–110.
(141) Kane, B. E.; Grant, M. K. O.; El-Fakahany, E. E.; Ferguson, D. M. Synthesis and evaluation of xanomeline analogs--probing the wash-resistant phenomenon at the M1 muscarinic acetylcholine receptor. *Bioorganic & medicinal chemistry* **2008**, *16*, 1376–1392.
(142) Randáková, A.; Dolejší, E.; Rudajev, V.; Zimčík, P.; Doležal, V.; El-Fakahany, E. E.; Jakubík, J. Classical and atypical agonists activate M1 muscarinic acetylcholine receptors through common mechanisms. *Pharmacological research* **2015**, *97*, 27–39.
(143) Kruse, A. C.; Kobilka, B. K.; Gautam, D.; Sexton, P. M.; Christopoulos, A.; Wess, J. Muscarinic acetylcholine receptors: novel opportunities for drug development. *Nature reviews. Drug discovery* **2014**, *13*, 549–560.
(144) Lombardo, S.; Maskos, U. Role of the nicotinic acetylcholine receptor in Alzheimer's disease pathology and treatment. *Neuropharmacology* **2015**, *96*, 255–262.
(145) Miwa, J. M.; Freedman, R.; Lester, H. A. Neural systems governed by nicotinic acetylcholine receptors: Emerging hypotheses. *Neuron* **2011**, *70*, 20–33.

(146) Rosini, M.; Simoni, E.; Bartolini, M.; Tarozzi, A.; Matera, R.; Milelli, A.; Hrelia, P.; Andrisano, V.; Bolognesi, M. L.; Melchiorre, C. Exploiting the lipoic acid structure in the search for novel multitarget ligands against Alzheimer's disease. *European journal of medicinal chemistry* **2011**, *46*, 5435–5442.
(147) Bolognesi, M. L.; Bartolini, M.; Tarozzi, A.; Morroni, F.; Lizzi, F.; Milelli, A.; Minarini, A.; Rosini, M.; Hrelia, P.; Andrisano, V.*; et al.* Multitargeted drugs discovery: Balancing anti-amyloid and anticholinesterase capacity in a single chemical entity. *Bioorganic & medicinal chemistry letters* **2011**, *21*, 2655–2658.
(148) Hampel, H.; Mesulam, M.-M.; Cuello, A. C.; Farlow, M. R.; Giacobini, E.; Grossberg, G. T.; Khachaturian, A. S.; Vergallo, A.; Cavedo, E.; Snyder, P. J.*; et al.* The cholinergic system in the pathophysiology and treatment of Alzheimer's disease. *Brain : a journal of neurology* **2018**, *141*, 1917–1933.
(149) Francis, P. T.; Palmer, A. M.; Snape, M.; Wilcock, G. K. The cholinergic hypothesis of Alzheimer's disease: A review of progress. *Journal of Neurology, Neurosurgery & Psychiatry* **1999**, *66*, 137–147.
(150) Selkoe, D. J. The molecular pathology of Alzheimer's disease. *Neuron* **1991**, *6*, 487–498.
(151) Hardy, J. A.; Higgins, G. A. Alzheimer's disease: The amyloid cascade hypothesis. *Science (New York, N.Y.)* **1992**, *256*, 184–185.
(152) Kennedy, R. H.; Wyeth, R. P.; Gerner, P.; Liu, S.; Fontenot, H. J.; Seifen, E. Tetramethylammonium is a muscarinic agonist in rat heart. *The American journal of physiology* **1995**, *268*, C1414-7.
(153) Zakharov, S. I.; Overholt, J. L.; Wagner, R. A.; Harvey, R. D. Tetramethylammonium activation of muscarinic receptors in cardiac ventricular myocytes. *The American journal of physiology* **1993**, *264*, C1625-30.
(154) Bonner, T. I.; Buckley, N. J.; Young, A. C.; Brann, M. R. Identification of a family of muscarinic acetylcholine receptor genes. *Science (New York, N.Y.)* **1987**, *237*, 527–532.
(155) Bonner, T. I. The molecular basis of muscarinic receptor diversity. *Trends in Neurosciences* **1989**, *12*, 148–151.
(156) Wess, J. Molecular biology of muscarinic acetylcholine receptors. *Critical reviews in neurobiology* **1996**, *10*, 69–99.
(157) Thal, D. M.; Sun, B.; Feng, D.; Nawaratne, V.; Leach, K.; Felder, C. C.; Bures, M. G.; Evans, D. A.; Weis, W. I.; Bachhawat, P.*; et al.* Crystal structures of the M1 and M4 muscarinic acetylcholine receptors. *Nature* **2016**, *531*, 335–340.
(158) Jakubík, J.; Zimčík, P.; Randáková, A.; Fuksová, K.; El-Fakahany, E. E.; Doležal, V. Molecular mechanisms of methoctramine binding and selectivity at muscarinic acetylcholine receptors. *Molecular pharmacology* **2014**, *86*, 180–192.
(159) Bradley, S. R.; Lameh, J.; Ohrmund, L.; Son, T.; Bajpai, A.; Nguyen, D.; Friberg, M.; Burstein, E. S.; Spalding, T. A.; Ott, T. R.*; et al.* AC-260584, an orally bioavailable M(1) muscarinic receptor allosteric agonist, improves cognitive performance in an animal model. *Neuropharmacology* **2010**, *58*, 365–373.
(160) Dror, R. O.; Green, H. F.; Valant, C.; Borhani, D. W.; Valcourt, J. R.; Pan, A. C.; Arlow, D. H.; Canals, M.; Lane, J. R.; Rahmani, R.*; et al.* Structural basis for modulation of a G-protein-coupled receptor by allosteric drugs. *Nature* **2013**, *503*, 295–299.
(161) Gnagey, A. L.; Seidenberg, M.; Ellis, J. Site-directed mutagenesis reveals two epitopes involved in the subtype selectivity of the allosteric interactions of gallamine at muscarinic acetylcholine receptors. *Molecular pharmacology* **1999**, *56*, 1245–1253.
(162) Venkatakrishnan, A. J.; Deupi, X.; Lebon, G.; Tate, C. G.; Schertler, G. F.; Babu, M. M. Molecular signatures of G-protein-coupled receptors. *Nature* **2013**, *494*, 185–194.

(163) Spalding, T. A. Discovery of an Ectopic Activation Site on the M1 Muscarinic Receptor. *Molecular pharmacology* **2002**, *61*, 1297–1302.
(164) Buckley, N. J.; Bonner, T. I.; Brann, M. R. Localization of a family of muscarinic receptor mRNAs in rat brain. *The Journal of neuroscience : the official journal of the Society for Neuroscience* **1988**, *8*, 4646–4652.
(165) Levey, A. I.; Edmunds, S. M.; Koliatsos, V.; Wiley, R. G.; Heilman, C. J. Expression of m1-m4 muscarinic acetylcholine receptor proteins in rat hippocampus and regulation by cholinergic innervation. *The Journal of neuroscience : the official journal of the Society for Neuroscience* **1995**, *15*, 4077–4092.
(166) Anagnostaras, S. G.; Murphy, G. G.; Hamilton, S. E.; Mitchell, S. L.; Rahnama, N. P.; Nathanson, N. M.; Silva, A. J. Selective cognitive dysfunction in acetylcholine M1 muscarinic receptor mutant mice. *Nature neuroscience* **2003**, *6*, 51–58.
(167) Bodick, N. C.; Offen, W. W.; Shannon, H. E.; Satterwhite, J.; Lucas, R.; van Lier, R.; Paul, S. M. The selective muscarinic agonist xanomeline improves both the cognitive deficits and behavioral symptoms of Alzheimer disease. *Alzheimer disease and associated disorders* **1997**, *11 Suppl 4*, S16-22.
(168) Bartus, R. T. On neurodegenerative diseases, models, and treatment strategies: Lessons learned and lessons forgotten a generation following the cholinergic hypothesis. *Experimental neurology* **2000**, *163*, 495–529.
(169) Fisher, A. M1 muscarinic agonists target major hallmarks of Alzheimer's disease--the pivotal role of brain M1 receptors. *Neuro-degenerative diseases* **2008**, *5*, 237–240.
(170) Bender, A. M.; Jones, C. K.; Lindsley, C. W. Classics in Chemical Neuroscience: Xanomeline. *ACS chemical neuroscience* **2017**, *8*, 435–443.
(171) Lange, H. S.; Cannon, C. E.; Drott, J. T.; Kuduk, S. D.; Uslaner, J. M. The M1 Muscarinic Positive Allosteric Modulator PQCA Improves Performance on Translatable Tests of Memory and Attention in Rhesus Monkeys. *The Journal of pharmacology and experimental therapeutics* **2015**, *355*, 442–450.
(172) Puri, V.; Wang, X.; Vardigan, J. D.; Kuduk, S. D.; Uslaner, J. M. The selective positive allosteric M1 muscarinic receptor modulator PQCA attenuates learning and memory deficits in the Tg2576 Alzheimer's disease mouse model. *Behavioural brain research* **2015**, *287*, 96–99.
(173) Vardigan, J. D.; Cannon, C. E.; Puri, V.; Dancho, M.; Koser, A.; Wittmann, M.; Kuduk, S. D.; Renger, J. J.; Uslaner, J. M. Improved cognition without adverse effects: Novel M1 muscarinic potentiator compares favorably to donepezil and xanomeline in rhesus monkey. *Psychopharmacology* **2015**, *232*, 1859–1866.
(174) Sako, Y.; Kurimoto, E.; Mandai, T.; Suzuki, A.; Tanaka, M.; Suzuki, M.; Shimizu, Y.; Yamada, M.; Kimura, H. TAK-071, a novel M1 positive allosteric modulator with low cooperativity, improves cognitive function in rodents with few cholinergic side effects. *Neuropsychopharmacology : official publication of the American College of Neuropsychopharmacology* **2019**, *44*, 950–960.
(175) Kurimoto, E.; Matsuda, S.; Shimizu, Y.; Sako, Y.; Mandai, T.; Sugimoto, T.; Sakamoto, H.; Kimura, H. An Approach to Discovering Novel Muscarinic M1 Receptor Positive Allosteric Modulators with Potent Cognitive Improvement and Minimized Gastrointestinal Dysfunction. *The Journal of pharmacology and experimental therapeutics* **2018**, *364*, 28–37.
(176) Bock, A.; Mohr, K. Dualsteric GPCR targeting and functional selectivity: The paradigmatic M(2) muscarinic acetylcholine receptor. *Drug discovery today. Technologies* **2013**, *10*, e245-52.
(177) Amici, M. de; Dallanoce, C.; Holzgrabe, U.; Trankle, C.; Mohr, K. Allosteric ligands for G protein-coupled receptors: a novel strategy with attractive therapeutic opportunities. *Medicinal research reviews* **2010**, *30*, 463–549.

(178) Smith, J. S.; Lefkowitz, R. J.; Rajagopal, S. Biased signalling:From simple switches to allosteric microprocessors. *Nature reviews. Drug discovery* **2018.** DOI: 10.1038/nrd.2017.229.
(179) Wootten, D.; Christopoulos, A.; Marti-Solano, M.; Babu, M. M.; Sexton, P. M. Mechanisms of signalling and biased agonism in G protein-coupled receptors. *Nature reviews. Molecular cell biology* **2018**, *19*, 638–653.
(180) Kuduk, S. D.; Di Marco, C. N.; Saffold, J. R.; Ray, W. J.; Ma, L.; Wittmann, M.; Koeplinger, K. A.; Thompson, C. D.; Hartman, G. D.; Bilodeau, M. T.*; et al.* Identification of a methoxynaphthalene scaffold as a core replacement in quinolizidinone amide M(1) positive allosteric modulators. *Bioorganic & medicinal chemistry letters* **2014**, *24*, 1417–1420.
(181) Kuduk, S. D.; Chang, R. K.; Di Marco, C. N.; Ray, W. J.; Ma, L.; Wittmann, M.; Seager, M. A.; Koeplinger, K. A.; Thompson, C. D.; Hartman, G. D.*; et al.* Quinolizidinone carboxylic acids as CNS penetrant, selective m1 allosteric muscarinic receptor modulators. *ACS medicinal chemistry letters* **2010**, *1*, 263–267.
(182) Schrage, R.; Seemann, W. K.; Klockner, J.; Dallanoce, C.; Racke, K.; Kostenis, E.; Amici, M. de; Holzgrabe, U.; Mohr, K. Agonists with supraphysiological efficacy at the muscarinic M2 ACh receptor. *British journal of pharmacology* **2013**, *169*, 357–370.
(183) Dallanoce, C.; Amici, M. de; Barocelli, E.; Bertoni, S.; Roth, B. L.; Ernsberger, P.; Micheli, C. de. Novel oxotremorine-related heterocyclic derivatives: Synthesis and in vitro pharmacology at the muscarinic receptor subtypes. *Bioorganic & medicinal chemistry* **2007**, *15*, 7626–7637.
(184) Gould, R. G.; Jacobs, W. A. The Synthesis of Certain Substituted Quinolines and 5,6-Benzoquinolines. *J. Am. Chem. Soc.* **1939**, *61*, 2890–2895.
(185) Niedermeier, S.; Singethan, K.; Rohrer, S. G.; Matz, M.; Kossner, M.; Diederich, S.; Maisner, A.; Schmitz, J.; Hiltensperger, G.; Baumann, K.*; et al.* A small-molecule inhibitor of Nipah virus envelope protein-mediated membrane fusion. *Journal of medicinal chemistry* **2009**, *52*, 4257–4265.
(186) Microwave assisted Gould-Jacob reaction: Sinthesis of 4-quinolones under solvent free reactions.
(187) Dallanoce, C.; Conti, P.; Amici, M. de; Micheli, C. de; Barocelli, E.; Chiavarini, M.; Ballabeni, V.; Bertoni, S.; Impicciatore, M. Synthesis and functional characterization of novel derivatives related to oxotremorine and oxotremorine-M. *Bioorganic & medicinal chemistry* **1999**, *7*, 1539–1547.
(188) Bebbington, A.; Shakeshaft, D. An Improved Synthesis of Oxotremorine. *J. Med. Chem.* **1965**, *8*, 274–275.
(189) Kloeckner, J.; Schmitz, J.; Holzgrabe, U. Convergent, short synthesis of the muscarinic superagonist iperoxo. *Tetrahedron Letters* **2010**, *51*, 3470–3472.
(190) Kliewer, A.; Gillis, A.; Hill, R.; Schmiedel, F.; Bailey, C.; Kelly, E.; Henderson, G.; Christie, M. J.; Schulz, S. Morphine-induced respiratory depression is independent of β-arrestin2 signalling. *British journal of pharmacology* **2020**, *177*, 2923–2931.
(191) Bradley, S. J.; Molloy, C.; Valuskova, P.; Dwomoh, L.; Scarpa, M.; Rossi, M.; Finlayson, L.; Svensson, K. A.; Chernet, E.; Barth, V. N.*; et al.* Biased M1-muscarinic-receptor-mutant mice inform the design of next-generation drugs. *Nature chemical biology* **2020**, *16*, 240–249.
(192) Littmann, T.; Ozawa, T.; Hoffmann, C.; Buschauer, A.; Bernhardt, G. A split luciferase-based probe for quantitative proximal determination of Gαq signalling in live cells. *Scientific reports* **2018**, *8*, 17179.
(193) Holze, J.; Bermudez, M.; Pfeil, E. M.; Kauk, M.; Bödefeld, T.; Irmen, M.; Matera, C.; Dallanoce, C.; Amici, M. de; Holzgrabe, U.*; et al.* Ligand-Specific Allosteric Coupling Controls G-Protein-Coupled Receptor Signaling. *ACS pharmacology & translational science* **2020**, *3*, 859–867.

(194) Bermudez, M.; Bock, A.; Krebs, F.; Holzgrabe, U.; Mohr, K.; Lohse, M. J.; Wolber, G. Ligand-Specific Restriction of Extracellular Conformational Dynamics Constrains Signaling of the M2 Muscarinic Receptor. *ACS chemical biology* **2017**, *12*, 1743–1748.
(195) Vass, M.; Podlewska, S.; Esch, I. J. P. de; Bojarski, A. J.; Leurs, R.; Kooistra, A. J.; Graaf, C. de. Aminergic GPCR-Ligand Interactions: A Chemical and Structural Map of Receptor Mutation Data. *Journal of medicinal chemistry* **2019**, *62*, 3784–3839.
(196) Matsui, H.; Lazareno, S.; Birdsall, N. J. Probing of the location of the allosteric site on m1 muscarinic receptors by site-directed mutagenesis. *Molecular pharmacology* **1995**, *47*, 88–98.
(197) Keov, P.; Lopez, L.; Devine, S. M.; Valant, C.; Lane, J. R.; Scammells, P. J.; Sexton, P. M.; Christopoulos, A. Molecular mechanisms of bitopic ligand engagement with the M1 muscarinic acetylcholine receptor. *The Journal of biological chemistry* **2014**, *289*, 23817–23837.
(198) Abdul-Ridha, A.; Lopez, L.; Keov, P.; Thal, D. M.; Mistry, S. N.; Sexton, P. M.; Lane, J. R.; Canals, M.; Christopoulos, A. Molecular determinants of allosteric modulation at the M1 muscarinic acetylcholine receptor. *The Journal of biological chemistry* **2014**, *289*, 6067–6079.
(199) Bermudez, M.; Rakers, C.; Wolber, G. Structural Characteristics of the Allosteric Binding Site Represent a Key to Subtype Selective Modulators of Muscarinic Acetylcholine Receptors. *Molecular informatics* **2015**, *34*, 526–530.
(200) Decker, M., Ed. *Design of Hybrid Molecules for Drug Development*; Elsevier, **2017**.
(201) Bradley, S. J.; Molloy, C.; Bundgaard, C.; Mogg, A. J.; Thompson, K. J.; Dwomoh, L.; Sanger, H. E.; Crabtree, M. D.; Brooke, S. M.; Sexton, P. M.*; et al.* Bitopic Binding Mode of an M1 Muscarinic Acetylcholine Receptor Agonist Associated with Adverse Clinical Trial Outcomes. *Molecular pharmacology* **2018**, *93*, 645–656.
(202) Machleidt, T.; Woodroofe, C. C.; Schwinn, M. K.; Méndez, J.; Robers, M. B.; Zimmerman, K.; Otto, P.; Daniels, D. L.; Kirkland, T. A.; Wood, K. V. NanoBRET--A Novel BRET Platform for the Analysis of Protein-Protein Interactions. *ACS chemical biology* **2015**, *10*, 1797–1804.
(203) Jones, G.; Willett, P.; Glen, R. C.; Leach, A. R.; Taylor, R. Development and validation of a genetic algorithm for flexible docking. *Journal of molecular biology* **1997**, *267*, 727–748.
(204) Wolber, G.; Seidel, T.; Bendix, F.; Langer, T. Molecule-pharmacophore superpositioning and pattern matching in computational drug design. *Drug discovery today* **2008**, *13*, 23–29.
(205) Humphrey, W.; Dalke, A.; Schulten, K. VMD: Visual molecular dynamics. *Journal of Molecular Graphics* **1996**, *14*, 33–38.
(206) Schaller, D.; Šribar, D.; Noonan, T.; Deng, L.; Nguyen, T. N.; Pach, S.; Machalz, D.; Bermudez, M.; Wolber, G. Next generation 3D pharmacophore modeling. *WIREs Comput Mol Sci* **2020**, *1*, 30.
(207) Hulme, E. C.; Trevethick, M. A. Ligand binding assays at equilibrium: Validation and interpretation. *British journal of pharmacology* **2010**, *161*, 1219–1237.
(208) Kostenis, E.; Mohr, K. Two-point kinetic experiments to quantify allosteric effects on radioligand dissociation. *Trends in pharmacological sciences* **1996**, *17*, 280–283.
(209) Jakubík, J.; Bacáková, L.; El-Fakahany, E. E.; Tucek, S. Positive cooperativity of acetylcholine and other agonists with allosteric ligands on muscarinic acetylcholine receptors. *Molecular pharmacology* **1997**, *52*, 172–179.
(210) Dong, G. Z.; Kameyama, K.; Rinken, A.; Haga, T. Ligand binding properties of muscarinic acetylcholine receptor subtypes (m1-m5) expressed in baculovirus-infected insect cells. *The Journal of pharmacology and experimental therapeutics* **1995**, *274*, 378–384.
(211) Wood, M. D.; Murkitt, K. L.; Ho, M.; Watson, J. M.; Brown, F.; Hunter, A. J.; Middlemiss, D. N. Functional comparison of muscarinic partial agonists at muscarinic receptor subtypes hM1, hM2, hM3, hM4 and hM5 using microphysiometry. *British journal of pharmacology* **1999**, *126*, 1620–1624.

(212) Mistry, S. N.; Valant, C.; Sexton, P. M.; Capuano, B.; Christopoulos, A.; Scammells, P. J. Synthesis and pharmacological profiling of analogues of benzyl quinolone carboxylic acid (BQCA) as allosteric modulators of the M1 muscarinic receptor. *Journal of medicinal chemistry* **2013**, *56*, 5151–5172.
(213) Schrage, R.; Holze, J.; Klockner, J.; Balkow, A.; Klause, A. S.; Schmitz, A.-L.; Amici, M. de; Kostenis, E.; Trankle, C.; Holzgrabe, U.*; et al.* New insight into active muscarinic receptors with the novel radioagonist (3)Hiperoxo. *Biochemical pharmacology* **2014**, *90*, 307–319.
(214) Hoffmann, C.; Gaietta, G.; Zürn, A.; Adams, S. R.; Terrillon, S.; Ellisman, M. H.; Tsien, R. Y.; Lohse, M. J. Fluorescent labeling of tetracysteine-tagged proteins in intact cells. *Nature protocols* **2010**, *5*, 1666–1677.
(215) Yung-Chi Cheng and Willim H. Prusoff. Relationship between the inhibition constant and the concentration of inhibitor which causes 50 percent inhibition of an enzymatic reaction, Cheng Y. and Prusoff W. H. Biochem Pharmacol. *22*: 3099-3108, **1973**.
(216) Tränkle, C.; Weyand, O.; Voigtländer, U.; Mynett, A.; Lazareno, S.; Birdsall, N. J. M.; Mohr, K. Interactions of orthosteric and allosteric ligands with 3Hdimethyl-W84 at the common allosteric site of muscarinic M2 receptors. *Molecular pharmacology* **2003**, *64*, 180–190.
(217) Dallanoce, C.; Conti, P.; Amici, M. de; Micheli, C. de; Barocelli, E.; Chiavarini, M.; Ballabeni, V.; Bertoni, S.; Impicciatore, M. Synthesis and functional characterization of novel derivatives related to oxotremorine and oxotremorine-M. *Bioorganic & medicinal chemistry* **1999**, *7*, 1539–1547.
(218) Schirmer, B.; Giehl, K.; Kubatzky, K. F. Report of the Signal Transduction Society Meeting 2018-Signaling: From Past to Future. *International journal of molecular sciences* **2019**, *20*.
(219) Burford, N. T.; Nahorski, S. R. Muscarinic m1 receptor-stimulated adenylate cyclase activity in Chinese hamster ovary cells is mediated by Gs alpha and is not a consequence of phosphoinositidase C activation. *The Biochemical journal* **1996**, *315 (Pt 3)*, 883–888.
(220) Bartus, R. T.; Dean, R. L.; Beer, B.; Lippa, A. S. The cholinergic hypothesis of geriatric memory dysfunction. *Science (New York, N.Y.)* **1982**, *217*, 408–414.
(221) Kenakin, T. Biased Receptor Signaling in Drug Discovery. *Pharmacological reviews* **2019**, *71*, 267–315.
(222) Abdul-Ridha, A.; Lane, J. R.; Sexton, P. M.; Canals, M.; Christopoulos, A. Allosteric modulation of a chemogenetically modified G protein-coupled receptor. *Molecular pharmacology* **2013**, *83*, 521–530.
(223) Yeatman, H. R.; Lane, J. R.; Choy, K. H. C.; Lambert, N. A.; Sexton, P. M.; Christopoulos, A.; Canals, M. Allosteric modulation of M1 muscarinic acetylcholine receptor internalization and subcellular trafficking. *The Journal of biological chemistry* **2014**, *289*, 15856–15866.
(224) Khajehali, E.; Valant, C.; Jörg, M.; Tobin, A. B.; Conn, P. J.; Lindsley, C. W.; Sexton, P. M.; Scammells, P. J.; Christopoulos, A. Probing the binding site of novel selective positive allosteric modulators at the M1 muscarinic acetylcholine receptor. *Biochemical pharmacology* **2018**, *154*, 243–254.
(225) Bodick, N. C.; Offen, W. W.; Levey, A. I.; Cutler, N. R.; Gauthier, S. G.; Satlin, A.; Shannon, H. E.; Tollefson, G. D.; Rasmussen, K.; Bymaster, F. P.*; et al.* Effects of xanomeline, a selective muscarinic receptor agonist, on cognitive function and behavioral symptoms in Alzheimer disease. *Archives of Neurology* **1997**, *54*, 465–473.
(226) Sauerberg, P.; Olesen, P. H.; Nielsen, S.; Treppendahl, S.; Sheardown, M. J.; Honore, T.; Mitch, C. H.; Ward, J. S.; Pike, A. J. Novel functional M1 selective muscarinic agonists. Synthesis and structure-activity relationships of 3-(1,2,5-thiadiazolyl)-1,2,5,6-tetrahydro-1-methylpyridines. *J. Med. Chem.* **1992**, *35*, 2274–2283.

(227) Shindikar, A. V.; Viswanathan, C. L. Novel fluoroquinolones: Design, synthesis, and in vivo activity in mice against Mycobacterium tuberculosis H37Rv. *Bioorganic & medicinal chemistry letters* **2005**, *15*, 1803–1806.
(228) La Cruz, A. de; Elguero, J.; Goya, P.; Martínez, A.; Pfleiderer, W. Tautomerism and acidity in 4-quinolone-3-carboxylic acid derivatives. *Tetrahedron* **1992**, *48*, 6135–6150.
(229) Trinquet, E.; Fink, M.; Bazin, H.; Grillet, F.; Maurin, F.; Bourrier, E.; Ansanay, H.; Leroy, C.; Michaud, A.; Durroux, T.*; et al.* D-myo-inositol 1-phosphate as a surrogate of D-myo-inositol 1,4,5-tris phosphate to monitor G protein-coupled receptor activation. *Analytical biochemistry* **2006**, *358*, 126–135.
(230) Zhang, J. Y.; Kowal, D. M.; Nawoschik, S. P.; Dunlop, J.; Pausch, M. H.; Peri, R. Development of an improved IP(1) assay for the characterization of 5-HT(2C) receptor ligands. *Assay and drug development technologies* **2010**, *8*, 106–113.
(231) Prilla, S.; Schrobang, J.; Ellis, J.; Holtje, H.-D.; Mohr, K. Allosteric interactions with muscarinic acetylcholine receptors: complex role of the conserved tryptophan M2422Trp in a critical cluster of amino acids for baseline affinity, subtype selectivity, and cooperativity. *Molecular pharmacology* **2006**, *70*, 181–193.
(232) Christopoulos, A.; Pierce, T. L.; Sorman, J. L.; El-Fakahany, E. E. On the unique binding and activating properties of xanomeline at the M1 muscarinic acetylcholine receptor. *Molecular pharmacology* **1998**, *53*, 1120–1130.
(233) Christopoulos, A.; El-Fakahany, E. E. Novel persistent activation of muscarinic M1 receptors by xanomeline. *European journal of pharmacology* **1997**, *334*, R3-R4.
(234) Lander, E. S.; Linton, L. M.; Birren, B.; Nusbaum, C.; Zody, M. C.; Baldwin, J.; Devon, K.; Dewar, K.; Doyle, M.; FitzHugh, W.*; et al.* Initial sequencing and analysis of the human genome. *Nature* **2001**, *409*, 860–921.
(235) Brink, C. B.; Harvey, B. H.; Bodenstein, J.; Venter, D. P.; Oliver, D. W. Recent advances in drug action and therapeutics: Relevance of novel concepts in G-protein-coupled receptor and signal transduction pharmacology. *British Journal of Clinical Pharmacology* **2004**, *57*, 373–387.
(236) Felce, J. H.; Latty, S. L.; Knox, R. G.; Mattick, S. R.; Lui, Y.; Lee, S. F.; Klenerman, D.; Davis, S. J. Receptor Quaternary Organization Explains G Protein-Coupled Receptor Family Structure. *Cell reports* **2017**, *20*, 2654–2665.
(237) Devi, L. A. Heterodimerization of G-protein-coupled receptors: Pharmacology, signaling and trafficking. *Trends in pharmacological sciences* **2001**, *22*, 532–537.
(238) Marsango, S.; Ward, R. J.; Alvarez-Curto, E.; Milligan, G. Muscarinic receptor oligomerization. *Neuropharmacology* **2017.** DOI: 10.1016/j.neuropharm.2017.11.023.
(239) Birdsall, N. J.M. Can different receptors interact directly with each other? *Trends in Neurosciences* **1982**, *5*, 137–138.
(240) Gomes, I.; Jordan, B. A.; Gupta, A.; Rios, C.; Trapaidze, N.; Devi, L. A. G protein coupled receptor dimerization: Implications in modulating receptor function. *J Mol Med* **2001**, *79*, 226–242.
(241) Hern, J. A.; Baig, A. H.; Mashanov, G. I.; Birdsall, B.; Corrie, J. E. T.; Lazareno, S.; Molloy, J. E.; Birdsall, N. J. M. Formation and dissociation of M1 muscarinic receptor dimers seen by total internal reflection fluorescence imaging of single molecules. *Proceedings of the National Academy of Sciences of the United States of America* **2010**, *107*, 2693–2698.
(242) Ilien, B.; Glasser, N.; Clamme, J.-P.; Didier, P.; Piemont, E.; Chinnappan, R.; Daval, S. B.; Galzi, J.-L.; Mely, Y. Pirenzepine promotes the dimerization of muscarinic M1 receptors through a three-step binding process. *The Journal of biological chemistry* **2009**, *284*, 19533–19543.

(243) Nomura, W.; Koseki, T.; Ohashi, N.; Mizuguchi, T.; Tamamura, H. Trivalent ligands for CXCR4 bearing polyproline linkers show specific recognition for cells with increased CXCR4 expression. *Organic & biomolecular chemistry* **2015**, *13*, 8734–8739.
(244) Portoghese, P. S. From models to molecules: Opioid receptor dimers, bivalent ligands, and selective opioid receptor probes. *J. Med. Chem.* **2001**, *44*, 2259–2269.
(245) Bhushan, R. G.; Sharma, S. K.; Xie, Z.; Daniels, D. J.; Portoghese, P. S. A bivalent ligand (KDN-21) reveals spinal delta and kappa opioid receptors are organized as heterodimers that give rise to delta(1) and kappa(2) phenotypes. Selective targeting of delta-kappa heterodimers. *J. Med. Chem.* **2004**, *47*, 2969–2972.
(246) Daniels, D. J.; Kulkarni, A.; Xie, Z.; Bhushan, R. G.; Portoghese, P. S. A bivalent ligand (KDAN-18) containing delta-antagonist and kappa-agonist pharmacophores bridges delta2 and kappa1 opioid receptor phenotypes. *J. Med. Chem.* **2005**, *48*, 1713–1716.
(247) Zhang, S.; Yekkirala, A.; Tang, Y.; Portoghese, P. S. A bivalent ligand (KMN-21) antagonist for mu/kappa heterodimeric opioid receptors. *Bioorganic & medicinal chemistry letters* **2009**, *19*, 6978–6980.
(248) Perez, M.; Jorand-Lebrun, C.; Pauwels, P. J.; Pallard, I.; Halazy, S. Dimers of 5HT 1 ligands preferentially bind to 5HT1b1d receptor subtypes. *Bioorganic & medicinal chemistry letters* **1998**, *8*, 1407–1412.
(249) Portoghese, P. S.; Larson, D. L.; Sayre, L. M.; Yim, C. B.; Ronsisvalle, G.; Tam, S. W.; Takemori, A. E. Opioid agonist and antagonist bivalent ligands. The relationship between spacer length and selectivity at multiple opioid receptors. *J. Med. Chem.* **1986**, *29*, 1855–1861.
(250) Mohr, K.; Tränkle, C.; Holzgrabe, U. Structure/Activity Relationships of M 2 Muscarinic Allosteric Modulators. *Receptors and Channels* **2011**, *9*, 229–240.
(251) Mohr, M.; Heller, E.; Ataie, A.; Mohr, K.; Holzgrabe, U. Development of a new type of allosteric modulator of muscarinic receptors: hybrids of the antagonist AF-DX 384 and the hexamethonio derivative W84. *Journal of medicinal chemistry* **2004**, *47*, 3324–3327.
(252) Matucci, R.; Nesi, M.; Martino, M. V.; Bellucci, C.; Manetti, D.; Ciuti, E.; Mazzolari, A.; Dei, S.; Guandalini, L.; Teodori, E.*; et al.* Carbachol dimers as homobivalent modulators of muscarinic receptors. *Biochemical pharmacology* **2016**, *108*, 90–101.
(253) Melchiorre, C.; Cassinelli, A.; Quaglia, W. Differential blockade of muscarinic receptor subtypes by polymethylene tetraamines. Novel class of selective antagonists of cardiac M-2 muscarinic receptors. *J. Med. Chem.* **1987**, *30*, 201–204.
(254) Melchiorre, C.; Angeli, P.; Lambrecht, G.; Mutschler, E.; Picchio, M. T.; Wess, J. Antimuscarinic action of methoctramine, a new cardioselective M-2 muscarinic receptor antagonist, alone and in combination with atropine and gallamine. *European journal of pharmacology* **1987**, *144*, 117–124.
(255) Agnetta, L.; Bermudez, M.; Riefolo, F.; Matera, C.; Claro, E.; Messerer, R.; Littmann, T.; Wolber, G.; Holzgrabe, U.; Decker, M. Fluorination of Photoswitchable Muscarinic Agonists Tunes Receptor Pharmacology and Photochromic Properties. *J. Med. Chem.* **2019.** DOI: 10.1021/acs.jmedchem.8b01822.
(256) Miao, Y.; McCammon, J. A. Graded activation and free energy landscapes of a muscarinic G-protein-coupled receptor. *Proceedings of the National Academy of Sciences of the United States of America* **2016**, *113*, 12162–12167.
(257) Kobilka, B. K.; Deupi, X. Conformational complexity of G-protein-coupled receptors. *Trends in pharmacological sciences* **2007**, *28*, 397–406.
(258) Rasmussen, S. G. F.; DeVree, B. T.; Zou, Y.; Kruse, A. C.; Chung, K. Y.; Kobilka, T. S.; Thian, F. S.; Chae, P. S.; Pardon, E.; Calinski, D.*; et al.* Crystal structure of the β2 adrenergic receptor-Gs protein complex. *Nature* **2011**, *477*, 549–555.

(259) Cherezov, V.; Rosenbaum, D. M.; Hanson, M. A.; Rasmussen, S. G. F.; Thian, F. S.; Kobilka, T. S.; Choi, H.-J.; Kuhn, P.; Weis, W. I.; Kobilka, B. K.*; et al.* High-resolution crystal structure of an engineered human beta2-adrenergic G protein-coupled receptor. *Science (New York, N.Y.)* **2007**, *318*, 1258–1265.
(260) Lefkowitz, R. J. Seven transmembrane receptors: A brief personal retrospective. *Biochimica et biophysica acta* **2007**, *1768*, 748–755.
(261) Kauk, M.; Hoffmann, C. Intramolecular and Intermolecular FRET Sensors for GPCRs - Monitoring Conformational Changes and Beyond. *Trends in pharmacological sciences* **2017.** DOI: 10.1016/j.tips.2017.10.011.
(262) Stumpf, A. D.; Hoffmann, C. Optical probes based on G protein-coupled receptors - added work or added value? *British journal of pharmacology* **2016**, *173*, 255–266.
(263) Pauli, G. F.; Chen, S.-N.; Simmler, C.; Lankin, D. C.; Gödecke, T.; Jaki, B. U.; Friesen, J. B.; McAlpine, J. B.; Napolitano, J. G. Importance of purity evaluation and the potential of quantitative ^{1}H NMR as a purity assay. *Journal of medicinal chemistry* **2014**, *57*, 9220–9231.
(264) Uliassi, E.; Prati, F.; Bongarzone, S.; Bolognesi, M. L. Medicinal Chemistry of Hybrids for Neurodegenerative Diseases. In *Design of Hybrid Molecules for Drug Development*; Decker, M., Ed.; Elsevier, 2017; pp 259–277.
(265) Lipinski, C. A.; Lombardo, F.; Dominy, B. W.; Feeney, P. J. Experimental and computational approaches to estimate solubility and permeability in drug discovery and development settings. *Advanced Drug Delivery Reviews* **1997**, *23*, 3–25.
(266) Davies, P.; Maloney, A. J. Selective loss of central cholinergic neurons in Alzheimer's disease. *Lancet (London, England)* **1976**, *2*, 1403.
(267) Perry, E. K.; Perry, R. H.; Blessed, G.; Tomlinson, B. E. Necropsy evidence of central cholinergic deficits in senile dementia. *Lancet (London, England)* **1977**, *1*, 189.
(268) Terry, A. V.; Buccafusco, J. J. The cholinergic hypothesis of age and Alzheimer's disease-related cognitive deficits: Recent challenges and their implications for novel drug development. *The Journal of pharmacology and experimental therapeutics* **2003**, *306*, 821–827.
(269) Fisher, A.; Pittel, Z.; Haring, R.; Bar-Ner, N.; Kliger-Spatz, M.; Natan, N.; Egozi, I.; Sonego, H.; Marcovitch, I.; Brandeis, R. M_1 Muscarinic Agonists Can Modulate Some of the Hallmarks in Alzheimer's Disease: Implications in Future Therapy. *JMN* **2003**, *20*, 349–356.
(270) Becker, R. E.; Giacobini, E.; Barton, J. M.; Brown, M., Eds. *Alzheimer Disease*; Birkhäuser Boston: Boston, MA, **1996**.

G. Appendix

A. Abbreviations

abs	absolute
ACh	acetylcholine
AChE	acetylcholinesterase
AD	Alzheimer disease
BBB	blood brain barrier
BChE	butyrylcholinesterase
BQCA	benzyl quinolone carboxylic acid
BQCAd	benzyl quinolone carboxylic acid derivative
Ca^{2+}	intracellular calcium ion concentration
calcd.	calculated
cAMP	cyclic adenosine monophosphate
CAS	catalytic active site
CFP	cyan fluorescent protein
CH_2Cl_2	dichloromethane
$CHCl_3$	chloroform
CH_3CN	acetonitrile
CHO-cells	Chinese hamster ovary cells
CNS	central nervous system
COSY	correlated spectroscopy
d	day(s) or doublet
dd	doublet of doublets
dt	doublet of triplets
DAG	diacylglycerol
DCM	dichloromethane
dd	doublet of doublets
DMF	dimethylformamide
DMSO	dimethylsulfoxide
ELSD	evaporative light scattering detector
ESI	electrospray ionization
EtOAc	ethylacetate
Et_2O	diethylether
EtOH	ethanol
FlAsH	fluoresceine arsenical hairpin binder
FRET	fluorescence resonance energy transfer
GDP	guanosindiphosphat
GTP	guanosine triphosphate
Gi	inhibitory G-protein
Gq	G-protein activating phospholipase C
GPCR	G protein-coupled receptor
GTP	guanosintriphosphat
h	hour(s) or human
HEK293	Human embryonic kidney 293 cells
HMBC	Heteronuclear Multiple Bond Correlation
HMQC	Heteronuclear Multiple-Quantum Correlation
HPLC	high-performance liquid chromatography
IL	intracellular loop
IP1	inositol monophosphate
IP3	ionositol-1,4,5-triphosphate
J	coupling constant

L15	Leibovitz medium without phenol red
LCMS	liquid chromatography mass spectrometry
m	multiplet
M1-M5	muscarininc acetylcholine subtype 1-5
mAChR	muscarinic acetylcholine receptor
nAChR	nicotinic acetylcholine receptor
MW	microwave
NAL	neutral allosteric modulator
NAM	negative allosteric modulator
NMR	nuclear magnetic resonance
NMS	N-methylscopolamine
PAM	positive allosteric modulator
PAS	peripheral anionic site
PLC	phospholipase C
PTX	pertussis toxin
q	quartet
t	triplet
tq	triplet of quartets
tt	triplet of triplets
TLC	thin layer chromatography
TM	transmembrane
UV-VIS	ultraviolet-visible
YFP	yellow fluorescent protein

C. Publications list and documentation of authorship

Volpato D., Kauk M., Messerer R., Bermudez M., Wolber G., Bock A., Hoffmann C. and Holzgrabe U. The role of orthosteric building blocks of bitopic ligands for muscarinic M1 receptors *ACS Omega*, **2020**. DOI: 10.1021/acsomega.0c04220.

Maspero, M.; **Volpato, D.;** Cirillo, D.; Yuan Chen, N.; Messerer, R.; Sotriffer, C.; Amici, M. de; Holzgrabe, U.; Dallanoce, C. Tacrine-xanomeline and tacrine-iperoxo hybrid ligands. *Bioorganic chemistry*, ***2020***, *96*, 103633.

Volpato, D.; Holzgrabe, U. Designing Hybrids Targeting the Cholinergic System by Modulating the Muscarinic and Nicotinic Receptors: A Concept to Treat Alzheimer's Disease. *Molecules (Basel, Switzerland)* **2018**, *23,* doi: 10.3390/molecules23123230.

Messerer, R.; Kauk, M.; **Volpato, D**.; Alonso Canizal, M.C.; Kloeckner, J.; Zabel, U.; Nuber, S.; Hoffmann, C.; Holzgrabe, U. FRET Studies of Quinolone-Based Bitopic Ligands and their Structural Analogues at the Muscarinic M1 Receptor. *ACS Chem. Biol.* **2017,** doi:10.1021/acschembio.6b00828.

This section contains a list of individual contribution for each author to the publications reprinted in this thesis.

Statement of individual author contributions

Volpato D., Kauk M., Messerer R., Bermudez M., Wolber, G., Bock A., Hoffmann C.and Holzgrabe U. **The role of orthosteric building blocks of bitopic ligands for muscarinic M1 receptors** ACS Omega, 2020, 10.1021/acsomega.0c04220.

Participated in	**Author Initials,** Responsibility decreasing from left to right				
Study Design Methods Development	DV, AB, UH	MB, CH	MK, RM		
Data Collection	DV	MK, RM, BM			
Data Analysis and Interpretation	DV, AB, UH	MB, BW, CH			
Manuscript Writing Writing of Introduction Writing of Materials & Methods Writing of Discussion Writing of First Draft	DV, UH DV, UH DV, AB, UH DV, UH	 MK, RM, BM, CH BM			

Explanations: Compound synthesis and characterization (DV, RM), Split-luciferase assay and radioligand binding experiments (DV, AB), BRET-based assay (MK), Computational studies (MB), Study design/concept development (DV, MB, GW, AB, CH, UH), Data analysis and interpretation (DV, MK, RM, MB, GW, AB, CH, UH), Manuscript planning, (DV, MB, AB, UH), Manuscript writing (DV, AB, UH), Correction of manuscript (DV, AB, UH), Supervision of Daniela Volpato (UH).

Maspero, M.; Volpato, D.; Cirillo, D.; Yuan Chen, N.; Messerer, R.; Sotriffer, C.; Amici, M. de; Holzgrabe, U.; Dallanoce, C. **Tacrine-xanomeline and tacrine-iperoxo hybrid ligands.** *Bioorganic chemistry*, *2020*, *96*, 103633.

Participated in	**Author Initials,** Responsibility decreasing from left to right				
Study Design Methods Development	DV, MM, UH, CD	MDA, CS			
Data Collection	DV, MM, DC	CY, RM			
Data Analysis and Interpretation	DV, MM, CS, MDA, UH, CD	CY			
Manuscript Writing Writing of Introduction Writing of Materials & Methods Writing of Discussion Writing of First Draft	DV, MM, CD, DV, MM, CD, DV, MM, CD,	MDA, CY, MDA, UH MDA, UH			

Explanations: Compound synthesis and characterization (DV, MM, DC), Acetylcholinesterase inhibitory activity investigation (DV, MM, DC, RM), Split Luciferase Bioluminescence and IP1 Accumulation Assay (DV), Molecular modeling investigations (CY, CS), Study design/concept development (DV, MM, CS, MD, UH, CD), Data analysis and interpretation (DV, MM, CS, MD, UH, CD), Manuscript planning (DV, MM, UH, CD), Manuscript writing (DV, MM, CD, UH), Correction of manuscript (DV, MM, UH, CD, MDA),Supervision of Daniela Volpato (UH).

Messerer, R.; Kauk, M.; Volpato, D.; Alonso Canizal, M.C.; Kloeckner, J.; Zabel, U.; Nuber, S.; Hoffmann, C.; Holzgrabe, U. **FRET Studies of Quinolone-Based Bitopic Ligands and their Structural Analogues at the Muscarinic M1 Receptor**. *ACS Chem. Biol.* 2017.

Participated in	**Author Initials,** Responsibility decreasing from left to right				
Study Design Methods Development	MR, MK				
Data Collection	MR, MK,	DV, JK, UZ, SN			
Data Analysis and Interpretation	RM, MK, CH, UH				
Manuscript Writing Writing of Introduction Writing of Materials & Methods Writing of Discussion Writing of First Draft	RM, MK, CH, UH RM, MK, CH, UH RM, MK CH, UH RM, MK CH, UH	DV, JK, UZ, SN			

Explanations: Compound synthesis and characterization (RM, DV), FRET studies (MK, MCAC), FRET-sensor characterization (UZ, SN), Study design/concept development (RM, MK, CH, UH), Data analysis and interpretation (RM, MK, CH, UH), Manuscript planning (RM, MK, CH, UH), Manuscript writing (MR, MK, CH, UH), Correction of manuscript (RM, MK, CH, UH), Supervision of Daniela Volpato (UH).

Volpato, D.; Holzgrabe, U. **Designing Hybrids Targeting the Cholinergic System by Modulating the Muscarinic and Nicotinic Receptors: A Concept to Treat Alzheimer's Disease.** *Molecules (Basel, Switzerland)* 2018, *23*.					
Participated in	**Author Initials,** Responsibility decreasing from left to right				
Study Design Methods Development	DV, UH				
Data Collection	--				
Data Analysis and Interpretation	--				
Manuscript Writing Writing of Introduction Writing of Materials & Methods Writing of Discussion Writing of First Draft	 DV, UH -- DV, UH DV, UH				

Explanations: Study design (DV, UH), Manuscript planning (DV, UH) Manuscript writing (DV, UH), Correction of manuscript (DV, UH), Supervision of Daniela Volpato (UH).

The doctoral researcher confirms that she/he has obtained permission from both the publishers and the co-authors for legal second publication.

The doctoral researcher and the primary supervisor confirm the correctness of the above mentioned assessment.

Daniela Volpato	09-12-2020	Milano	
Doctoral Researcher's Name	Date	Place	Signature
Prof. Dr.Ulrike Holzgrabe	09-12-2020	Würzburg	
Primary Supervisor's Name	Date	Place	Signature

Statement of individual author contributions to figures/tables/chapters included in the manuscripts

Publication (complete reference): Volpato D., Kauk M., Messerer R., Bermudez M., Wolber, G., Bock A., Hoffmann C.and Holzgrabe U. **The role of orthosteric building blocks of bitopic ligands for muscarinic M1 receptors** ACS Omega, 2020, 10.1021/acsomega.0c04220.

Figure	**Author Initials,** Responsibility decreasing from left to right				
Scheme 1	DV, UH	RM			
Figure 1	DV, AB, UH				
Figure 2	MK, CH	DV, AB, UH			
Figure 3	MB, GW				

Explanations (if applicable):NA

Publication (complete reference): Maspero, M.; Volpato, D.; Cirillo, D.; Yuan Chen, N.; Messerer, R.; Sotriffer, C.; Amici, M. de; Holzgrabe, U.; Dallanoce, C. **Tacrine-xanomeline and tacrine-iperoxo hybrid ligands.** *Bioorganic chemistry*, *2020*, *96*, 103633.					
Figure	**Author Initials,** Responsibility decreasing from left to right				
Scheme 1	MM, DV, CD, MDA, CD, UH	RM			
Table 1	MM, DV, CD, MDA,CD, UH	RM			
Table 2	DV, UH		MM, DC, MDA, CD		
Table 3	DV, UH		MM, DC, MDA, CD		
Figure 1	MM, DV, CD, UH				
Figure 2	DV, UH		MM, DC, MDA, CD		
Figure 3	DV, UH		MM, DC, MDA, CD		
Figure 4	DV, UH		MM, DC, MDA, CD		
Figure 5	DV, UH		MM, DC, MDA, CD		
Figure 6	NYC, CS				

Explanations (if applicable):NA

Publication (complete reference): Messerer, R.; Kauk, M.; Volpato, D.; Alonso Canizal, M.C.; Kloeckner, J.; Zabel, U.; Nuber, S.; Hoffmann, C.; Holzgrabe, U. **FRET Studies of Quinolone-Based Bitopic Ligands and their Structural Analogues at the Muscarinic M1 Receptor**. *ACS Chem. Biol.* 2017.					
Figure	**Author Initials,** Responsibility decreasing from left to right				
Scheme 1	RM, UH	JK, DV			
Scheme 2	RM, UH	JK, DV			
Figure 1	MK, CH		RM,UH	JK, DV, MCAC, UZ, SN	
Figure 2	MK, CH		RM,UH	JK, DV, MCAC, UZ, SN	
Figure 3	MK, CH		RM,UH	JK, DV, MCAC, UZ, SN	
Figure 4	MK, CH		RM,UH	JK, DV, MCAC, UZ, SN	

Explanations (if applicable):NA

Publication (complete reference): Volpato, D.; Holzgrabe, U. **Designing Hybrids Targeting the Cholinergic System by Modulating the Muscarinic and Nicotinic Receptors: A Concept to Treat Alzheimer's Disease.** *Molecules (Basel, Switzerland)* 2018, *23*.					
Figure	**Author Initials,** Responsibility decreasing from left to right				
1-26	DV, UH				

Explanations (if applicable): Figures 1,3,15,18,20 and 23 are reprinted/adapted with copyright owner's permission.

I also confirm my primary supervisor's acceptance.

Doctoral Researcher's Name Date Place Signature

D. Conference contribution

“Design, Synthesis and Pharmacological Investigation of Novel Bitopic Muscarinic Derivatives”. Oral Presentation, Retreat Receptor Dynamics, March 2018, Bayreuth.

“Bitopic Ligands and their molecular fragments for the study of the M1 Muscarinic Receptor”. Poster Presentation, DPhG Jahrestagung 2017, Saarbrücken 2017.

“Bitopic Ligands and their molecular fragments for the study of the M1 Muscarinic Receptor”. Poster Presentation, March 2017. Receptor Dynamics: Emerging Paradigms for Novel Drugs“ Institut de Génomique Fonctionnelle, Montpellier (France).

“Bitopic Ligands and their molecular fragments for the study of the M1 Muscarinic Receptor”. Poster Presentation, "Sixth European Workshop in Drug Synthesis" (VI EWDSy). May 2016. Certosa di Pontignano, Siena (Italy).

“Design, Synthesis and Pharmacological Investigation of Novel Bitopic Muscarinic Derivatives”. Poster Presentation, November 2015, Winter School at the Hebrew University/Rehovot, Israel.

“Design, Synthesis and Pharmacological Investigation of Novel Bitopic Muscarinic Derivatives”. Oral Presentation, First retreat Receptor Dynamics, March 2015, Rothenburg ob der Tauber.

E. Affidavit

I hereby confirm that my thesis entitled “Bitopic Ligands and their molecular fragments for the study of the M1 Muscarinic Receptor” is the result of my own work. I did not receive any help or support from commercial consultants. All sources and / or materials applied are listed and specified in the thesis.

Furthermore, I confirm that this thesis has not yet been submitted as part of another examination process neither in identical nor in similar form.

Place, Date Signature

Eidesstattliche Erklärung

Hiermit erkläre ich an Eides statt, die Dissertation “Bitopische Liganden und ihre Molekülfragmente für die Untersuchung des M1 Muskarinischer Rezeptor“ eigenständig, d.h. insbesondere selbständig und ohne Hilfe eines kommerziellen Promotionsberaters, angefertigt und keine anderen als die von mir angegebenen Quellen und Hilfsmittel verwendet zu haben.

Ich erkläre außerdem, dass die Dissertation weder in gleicher noch in ähnlicher Form bereits in einem anderen Prüfungsverfahren vorgelegen hat.

Ort, Datum Unterschrift